VOL. 13 NO. 1/2 JANUARY 1967
PUBLISHED MONTHLY

JOURNAL OF

ELECTROANALYTICAL CHEMISTRY

AND INTERFACIAL ELECTROCHEMISTRY

International Journal devoted to all Aspects of Electroanalytical Chemistry, Double Layer Studies, Electrokinetics, Colloid Stability, and Electrode Kinetics.

E L S E V I E R

GENERAL INFORMATION

See also Suggestions and Instructions to Authors which will be sent free, on request to the Publishers.

Types of contributions

(a) Original research work not previously published in other periodicals.
(b) Reviews on recent developments in various fields.
(c) Short communications.
(d) Bibliographical notes and book reviews.

Languages

Papers will be published in English, French or German.

Submission of papers

Papers should be sent to one of the following Editors:

Professor J. O'M. Bockris, John Harrison Laboratory of Chemistry, University of Pennsylvania, Philadelphia 4, Pa. 19104, U.S.A.
Dr. R. H. Ottewill, Department of Chemistry, The University, Bristol 8, England.
Dr. R. Parsons, Department of Chemistry, The University, Bristol 8, England. Until June 1967: Gates and Crellin Laboratories of Chemistry, California Institute of Technology, Pasadena, Calif. 91109, U.S.A.
Professor C. N. Reilley, Department of Chemistry, University of North Carolina, Chapel Hill, N.C. 27515, U.S.A.

Authors should preferably submit two copies in double-spaced typing on pages of uniform size. Legends for figures should be typed on a separate page. The figures should be in a form suitable for reproduction, drawn in Indian ink on drawing paper or tracing paper, with lettering etc. in thin pencil. The sheets of drawing or tracing paper should preferably be of the same dimensions as those on which the article is typed. Photographs should be submitted as clear black and white prints on glossy paper. Standard symbols should be used in line drawings, the following are available to the printers:

▼ ▽ ■ □ ● ◎ ▪ ◘ ⊕ ⊡ ▪ + ×

All references should be given at the end of the paper. They should be numbered and the numbers should appear in the text at the appropriate places.
A summary of 50 to 200 words should be included.

Reprints

Fifty reprints will be supplied free of charge. Additional reprints can be ordered at quoted prices. They must be ordered on order forms which are sent together with the proofs.

Publication

The *Journal of Electroanalytical Chemistry and Interfacial Electrochemistry* appears monthly and has four issues per volume and three volumes per year.

Subscription price: £ 18.18.0 or $ 51.50 or Dfl. 189.00 per year; £ 6.6.0 or $ 17.50 or Dfl. 63.00 per volume; plus postage. Additional cost for copies by air mail available on request. For advertising rates apply to the publishers.

Subscriptions

Subscriptions should be sent to:

ELSEVIER PUBLISHING COMPANY, P.O. Box 211, Amsterdam, The Netherlands.

JOURNAL OF ELECTROANALYTICAL CHEMISTRY
AND INTERFACIAL ELECTROCHEMISTRY

IMPORTANT NOTICE TO SUBSCRIBERS

The attention of our subscribers is drawn to the fact that this issue (Vol. 13, no. 1/2, January 1967) has appeared **before** the December 1966 issue (Vol. 12, no. 5/6). This has arisen because of the special preparation required by the December issue, which is dedicated to Professor M. VON STACKELBERG on the occasion of his seventieth birthday.

We earnestly request subscribers not to write to us concerning non-receipt of this special issue, since it will be despatched some weeks later than the issue which you are now reading.

We trust that early publication of Vol. 13 no. 1/2 will meet with your approval.

THE PUBLISHERS

JOURNAL OF ELECTROANALYTICAL CHEMISTRY AND INTERFACIAL ELECTROCHEMISTRY

VOL. 13 (1967)

JOURNAL
of
ELECTROANALYTICAL CHEMISTRY
and
INTERFACIAL ELECTROCHEMISTRY

AN INTERNATIONAL JOURNAL DEVOTED TO ALL ASPECTS OF ELECTROANALYTICAL CHEMISTRY, DOUBLE LAYER STUDIES, ELECTROKINETICS, COLLOID STABILITY AND ELECTRODE KINETICS

Vol. 13 1967

ELSEVIER PUBLISHING COMPANY
AMSTERDAM

PRINTED IN THE NETHERLANDS

THE ANODIC DISSOLUTION OF THIN FILMS OF COPPER METAL FROM PYROLYTIC GRAPHITE

A STUDY OF THE MULTIPLE DISSOLUTION CURRENT PEAKS

BASIL H. VASSOS AND HARRY B. MARK, JR.
Department of Chemistry, The University of Michigan, Ann Arbor, Michigan (U.S.A.)
(Received February 21st, 1966)

INTRODUCTION

When the technique of anodic stripping analysis[1-6] is employed in the determination of trace amounts (10^{-6}–10^{-10} M) of a single metal ion in solution, the resulting current–potential stripping curve very often exhibits two or more distinct dissolution peaks rather than the single peak that would be expected for the dissolution of a single species[7-11]. This effect which was often observed when solid electrodes, such as platinum[9,10], gold[9,10], and graphite[11] were used, has also been observed when mercury films on platinum are used as electrodes[8]. It has been reported, for example, for the stripping of nickel from platinum and gold electrodes[11], silver from graphite[11], and cadmium and zinc from mercury-plated platinum[8].

It has been postulated that the *extra* current peaks arising at potentials more positive than the normal dissolution potential of the metal film, represent the oxidation of the first monolayer (*first* layer of the metal on the surface of the electrode) of the metal. This suggests that the first monolayer of a deposited metal on a different solid substrate (electrode) can have a considerably larger bonding energy with this different substrate than the normal bonding or lattice energy of the metal with itself (all subsequent layers of deposited metal beyond the first monolayer)[9,11]. Thus, considerably more positive potentials are required in order to oxidize the first monolayer. In cases where more than one *extra* dissolution current peak is observed, it has been postulated that the bonding energy of the atoms of the first monolayer with different sites of the electrode substrate differ markedly[12].

NICHOLSON[9] has actually presented a theoretical treatment of the dissolution of the first monolayer, based on this model.

Several investigators have noted that the electrodeposition of carrier-free radioactive nuclides in tracer amounts occurs in measurable amounts at potentials which are several hundred millivolts more positive than the potentials observed in the deposition of macro amounts[13-29]. These results, of course, contradict those predicted by the Nernst equation which predicts a negative shift of potential with dilution. This *underpotential* with regard to deposition corresponds to the more positive dissolution peaks (to the stronger bond between the metal and the different electrode material) observed on stripping. ROGERS AND STEHNEY[30] made a careful study of the electrodeposition of carrier-free radioactive silver in free concentrations in order to determine

if the *underpotential* observed for tracer depositions corresponds to the deposition of the first monolayer and, hence, to increased bond interaction for the two different surfaces. Although the results indicated qualitatively that the amount deposited at the more negative potentials was roughly equivalent to a monolayer, they were inconclusive. First, it is difficult to estimate the true concentration of carrier-free radioactive tracer solutions because of adsorption on the surfaces of the cell; secondly and more important, it is impossible to distinguish between radioactive silver adsorbed on the electrode and actual reduced silver deposited on the electrode. Also, it is impossible to determine if this potential difference corresponds to massive deposition on certain active sites, crevices, etc. on the electrode rather than a uniform monolayer.

As previous work had not proved the existence of monolayer depositions of different interaction energy, this investigation was undertaken to try to determine the nature of the secondary more positive dissolution current peaks observed on stripping. This paper describes the results obtained from a study of the anodic dissolution of thin copper films on pyrolytic graphite electrodes. This system was chosen because of its reproducibility which made possible the deposition of surface films which correspond to the secondary or more positive *monolayer* films alone. The results of electron microprobe studies of the surfaces that correspond to deposited *monolayers* are also presented.

EXPERIMENTAL

The pyrolytic graphite electrode, electrode assembly, and electrolysis cell employed in this study were identical with those described previously[12,31–32]. The electrodeposition-potential sweep apparatus was built around Philbrick UPA-2 and P-2 operational amplifiers (G. A. Philbrick Researches, Inc., Dedham, Mass.) employing the potentiostat, sweep generator, and current follower circuits of DeFord[12,34]. In all stripping experiments the rate of the voltage sweep was 0.5 V/min. The current–potential curves were recorded by means of a Sargent Model SR recorder. The cell was thermostatted and all experiments were run at $25 \pm 0.1°$. All potentials are reported with reference to a saturated calomel electrode (S.C.E.). The electron microprobe studies of the surface composition and distribution were made with an Applied Research Laboratories X-ray microprobe. The apparent area of the electrode surface was 0.319 cm^2.

All chemicals and solvents employed were analytical or reagent grade and were further purified by massive electrolysis in the manner described previously[12,33]. All solutions were de-aerated for 2 h with nitrogen gas purified according to standard practice[35]. The water was triply distilled and then subjected to massive electrolysis.

In order to obtain reliable and reproducible i–E stripping curves, it is necessary to pre-treat each fresh pyrolytic graphite surface (all solutions, of course, must be free of surface-active agents). It was found necessary to polish the graphite surface prior to use. This was done using a metallurgical wheel with No. 600 carborumdun paper, first, followed by Whatman No. 1 filter paper. The polished electrode was then chemically cleaned and electrochemically activated. The cleaning consisted of immersing the electrode surface in 70% phosphoric acid (alkaline solutions were found to de-activate the electrode in some way) for 30–60 sec and then rinsing repeatedly. The activation was accomplished by electrochemically *cycling* the electrode in the electro-

lysis solution used throughout the study, which was 0.1×10^{-3}–$5 \cdot 10^{-5}$ M $Cu(NO_3)_2$, 0.1 M $KClO_4$, and 0.1 M $HClO_4$. The electrode was first potentiostatted at −0.40 V *vs.* S.C.E. for 100 sec (this placed a relatively thick layer of copper metal on the surface). The potential was then stepped to −0.10 V *vs.* S.C.E. (approximately the threshold of the dissolution of the copper) and the +0.50 V/min anodic potential sweep begun. When the potential reached +0.45 V *vs.* S.C.E. (all copper oxidized) the sweep was stopped and the potential stepped back to −0.40 V *vs.* S.C.E. which began another cycle (any excursion of the potential to +0.8 to +0.9 V completely deactivates the surface). After about 20–30 cycles, all subsequent i–E stripping curves obtained during the anodic sweep were reproducible and also matched those obtained for any new electrode surface (pre-treated in this manner). The reproducibility was about ±1–2%. A constant stirring rate of 200 rev./min by means of a synchronous motor was used throughout all experiments. The cyclic operation was carried out by an automated circuit which allowed for precise but variable deposition time[12].

RESULTS AND DISCUSSION

Figure 1 illustrates the typical characteristic shape of the current–potential stripping curves obtained. The electrode was plated with a thin copper-metal film by potentiostatting at −0.40 V *vs.* S.C.E. for 100 sec with a 0.1×10^{-3} M $Cu(NO_3)_2$, 0.1 M $KClO_4$, and 0.1 M $HClO_4$ solution. The i *vs.* E curve shown was recorded during the dissolution step (described above). Three distinct peaks are observed for the copper dissolution curve: peak a at +0.015 V *vs.* S.C.E., peak b at +0.15 V *vs.* S.C.E., and peak c at about +0.35 V *vs.* S.C.E. When the time of deposition (at +0.40 V *vs.*

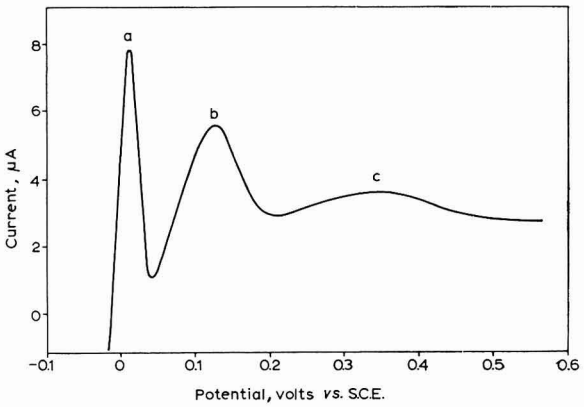

Fig. 1. Typical anodic stripping curves for a thin Cu film. Film plated from a 0.1×10^{-3} M $Cu(NO_3)_2$, 0.1 M $KClO_4$, and 0.1 M $HClO_4$ soln. at −0.40 V *vs.* S.C.E. for 100 sec. Scanning rate: 0.50 V/min.

S.C.E.) was varied, it was found that all the areas under the three peaks (and, hence, amount on surface) increase approximately proportionally with time from 0 to about 50 sec. From 50 sec upwards, peaks b and c do not increase appreciably with time, but peak a continues to increase with deposition time. This, of course, indicates that peak a represents the normal copper deposition–dissolution which presumably represents layers of copper deposited on top of a layer(s) of copper. The fact that peaks b and c

cease to grow after a certain period of time (even when the total deposition times were several thousand seconds) (see below) indicates that these peaks represent either deposition of the monolayer (with at least two distinct energies of interaction with the electrode surface) or deposition at two specific types of active site such as crevasses, or crystal lattice defects on the graphite. In either case, the deposition of the copper corresponding to peaks *b* and *c* appears to cease as some area of the electrode is covered.

An investigation was made to determine the conditions under which the *b* and *c* peaks (a *monolayer*) could be deposited alone without any *a* peak (copper on copper) being present. It was found that by depositing copper at −0.40 V *vs.* S.C.E. as described above and then stepping the potential to 0.0 V *vs.* S.C.E. and holding for a period of time (the length of this hold period is not critical, but should be greater than 100 sec), the *a* peak was missing (copper–copper layer stripped), from the subsequent stripping curves (anodic sweep carried out in same manner described above) and only the *b* and *c* peaks remain and are unchanged. A typical *i–E* curve obtained in this manner is shown in Fig. 2 which clearly shows both peaks *b* and *c*. The electrode was potentiostatted at −0.40 V *vs.* S.C.E. for 2000 sec in a solution that was 5.0×10^{-5} *M* $Cu(NO_3)_2$, 0.10 *M* $KClO_4$ and 0.10 *M* $HClO_4$. The potential was then stepped to 0.0 V *vs.* S.C.E. and potentiostatted at this potential for 250 sec before the usual anodic potential scan was applied. The *i–E* stripping curve obtained for a copper deposit made in this manner *without* the potential hold at 0.0 V *vs.* S.C.E., is shown in Fig. 3.

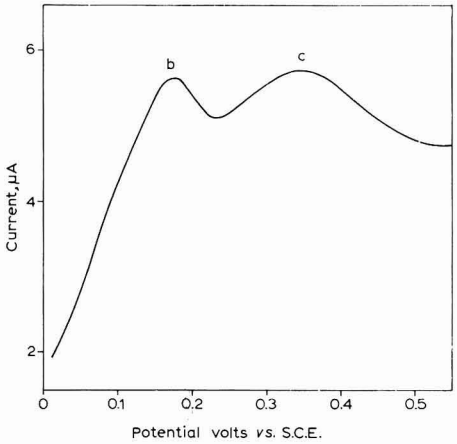

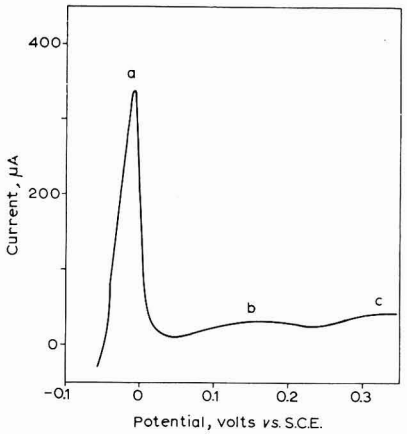

Fig. 2. Typical anodic stripping curve obtained after the *macro* Cu film was obtained by potentiostatting at 0.0 V *vs.* S.C.E. for 250 sec after deposition. Soln. was $5 \cdot 10^{-5}$ *M* $Cu(NO_3)_2$, 0.1 *M* $KClO_4$ and 0.10 *M* $HClO_4$. Scanning rate: 0.50 V/min.

Fig. 3. Typical anodic stripping curve obtained for a *macro* Cu film (deposited at −0.40 V *vs.* S.C.E. for 2000 sec using a 5.0×10^{-5} *M* $Cu(NO_3)_2$, 0.10 *M* $KClO_4$, and 0.10 *M* $HClO_4$ soln. Scanning rate: 0.50 V/min.

The large *a* peak is clearly seen and essentially obscures the *b* and *c* secondary peaks. The curves shown in Figs. 2 and 3 were reproducible to within 1–2% for subsequent runs on a single electrode surface or from electrode surface to electrode surface when the activation procedure described above was employed.

Electron microprobe[36–40] studies of pyrolytic graphite electrode surfaces con-

taining copper films prepared in exactly the same manner as described for the films that resulted in the $i-E$ stripping curves of Figs. 2 and 3, were also made. The only difference was that the electrodes were removed from the solution prior to the commencement of the anodic stripping sweep (the potential was held to 0.0 and −0.10 V, respectively, during removal). Thus, the films remained on the graphite surfaces. The surfaces were studied by two different techniques: the sample current technique (measures the electron adsorption current of the surface; the resulting oscilloscope image shows dark areas representing either holes in the surface or elements of high atomic weight and light areas representing level surfaces of low atomic weight) and the X-ray fluorescent emission technique (measures the intensity of the X-ray fluorescence at a specific wavelength emitted from the surface of the material on electron bombardment)[36-40].

Figure 4 shows a typical sample current pattern obtained for a pyrolytic graphite electrode surface having a *heavy* or *macro* copper deposit plated from a solution of $5 \cdot 10^{-5}$ M $Cu(NO_3)_2$, 0.1 M $KClO_4$ and 0.1 M $HClO_4$ potentiostatted for 2000

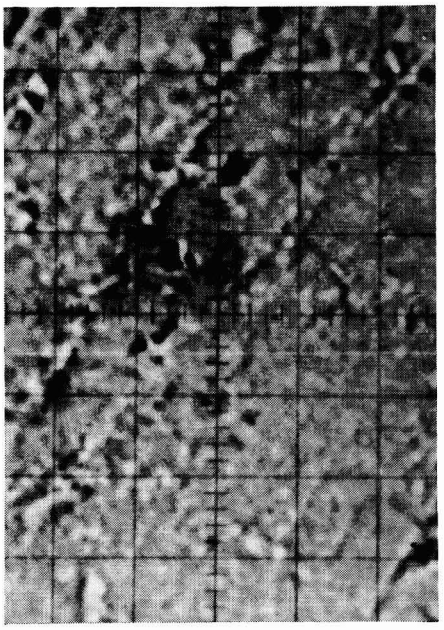

Fig. 4. Sample current pattern obtained with an electron microprobe for a Cu deposit of 1390 μC (deposited under exactly the same conditions as the film which gave the stripping curve illustrated in Fig. 3). One division on the photograph scale represents 18.5 μ.

Fig. 5. X-ray fluorescence pattern of the electrode surface of Fig. 4 (same surface area). The X-ray wavelength measured was 1.542 Å (main Cu emission line).

sec at −0.40 V *vs.* S.C.E. (the anodic stripping curve for films deposited in this manner is shown in Fig. 3 which exhibits a predominant *a* peak; the amount of copper on the electrode was 1390 μC). It shows a dark-shaded region, presumably copper, slightly to the left and above the center co-ordinant. The very dark spots and light spots probably represent scratches and other defects on the surface. The black spots

are either holes or imbedded impurities. The area under the stripping peaks of films deposited in a similar manner (see Fig. 3) indicated that the deposit was about 1390 μC of copper which would correspond to 5–6 copper layers on the surface (if the deposit was uniformly distributed).

The X-ray fluorescence microprobe scan of the same electrode surface shown in Fig. 4 is given in Fig. 5 (the X-ray monochromator of the instrument was set for the main copper emission line at 1.542 Å, as read on the instrument dial; a pure copper sample gave 36,500 counts/sec for a highly polished surface). The picture represents a 40-sec exposure. The large accumulation of light dots in the exact position of the dark-shaded area of Fig. 4 proves that this area represents a heavy copper deposit. The very centre of the cluster is estimated to be a copper deposit several microns in thickness. Thus, it appears that the main copper deposit, corresponding to the *a* peak, grows in spots and not uniformly. It was found, after examining several electrode surface areas, that the regions of heavy deposits were scarce and that the area between the heavy deposits was large but appeared to be covered with a uniform distribution of widely spaced spots (mostly copper but certainly some instrumental noise as well which could correspond to a very thin layer, one of two monolayers, uniformly distributed between the large concentrations).

Electrode surfaces deposited in the manner that gave the stripping curve of Fig. 2 (exhibits only the *b* and *c* peaks, or *mono-layer* peaks) were also studied with the electron microprobe. Figure 6 shows a sample current pattern for such an electrode surface. No dark areas are observed although several black and very light areas

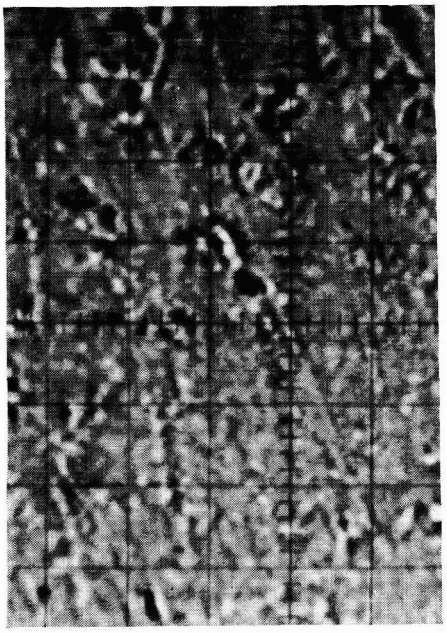

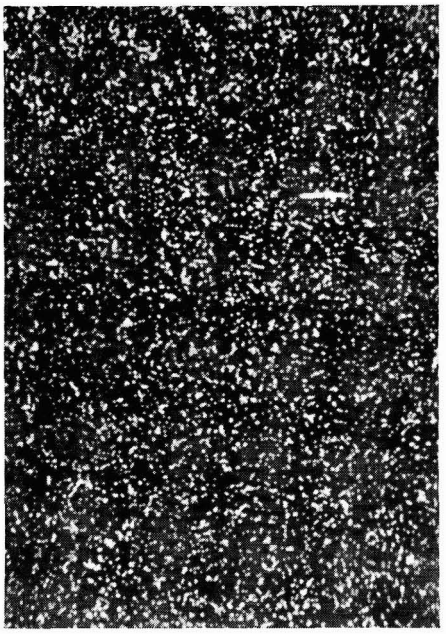

Fig. 6. Sample current pattern obtained for a *mono-layer* Cu deposit of 157 μC (deposited in the same manner as the film giving the anodic stripping curve shown in Fig. 2).

Fig. 7. X-ray fluorescence pattern of the electrode surface of Fig. 6.

representing holes and high points (or imbedded surface impurities) are observed. The X-ray fluorescence pattern obtained for the same surface (400-sec exposure), illustrated in Fig. 7, shows a uniform distribution of counts (no indication of the dark-shaded spots of Fig. 6 which are copper). The total copper on the electrode surface represents only about 157 μC (area under the stripping peaks of Fig. 2). This amount represents the lower limit of detectability of the instrument, and the counts observed contain a large background noise count as well as the smaller copper count. In order to show that this surface actually contained copper, *line reading* measurements were made of the surface (a repeated horizontal scan with no vertical motion of the electron beam, 2 μ in diameter, was made over a length of 180 μ on random areas on the surface for a period of 10 sec)[40]. The average of twelve determinations at the copper emission line of 1.532 Å was 3720 ± 55 counts/min. Moving the monochromator from the copper line in both directions yielded background counts of 3230 ± 57 and 3350 ± 56 counts/min respectively, for 12 measurements. It appears, therefore, that the surface does contain appreciable copper, and the fact that the pattern is uniform indicates that the copper is uniformly distributed (four 1-cm^2 areas were found to contain 132 ± 5 dots)[12]. Thus, the copper is not found aggregated in specific spots such as the holes and scratches observed in the sample current pictures (Figs. 4 and 6) which would give a clear heavy light dot area on the X-ray fluorescence measurement.

CONCLUSIONS

The experimental evidence obtained by means of the electron microprobe studies indicates (but does not prove, however, because of the limitations of the instrument sensitivity) that the copper remaining on the electrode surface that corresponds to the *mono-layer* peaks, *b* and *c* peaks of Fig. 3, is uniformly distributed on the surface. Calculations also showed that a monolayer of copper atoms arranged as a face-centered lattice on the surface (0.319 cm^2) would amount to 0.81×10^{-9} moles or 160 μC[12]. The areas under the *b* and *c mono-layer* peaks amounted to approximately this value, usually 150–200 μC (the area under Fig. 2 was 157 μC). Thus, the amount of copper on the surface corresponding to the *mono-layer* peaks is the right order of magnitude for a calculated monolayer. However, this result is qualitative as the roughness factor for the surface is not known. Also, the differences in surface conditions or interactions that yield the two *monolayer* peaks, *b* and *c*, is not understood.

It appears that the subsequent layers of copper on copper do grow at specific sites on the surface rather than as uniform layers. Further work is now in progress to determine the nature of these preferred sites.

It should be noted that freshly cleaved pyrolytic graphite surfaces were hard to activate in order to produce reproducible *mono-layer* peaks. Also, these peaks were generally smaller than those obtained for a polished surface. Unpolished surfaces were not studied extensively, however, as the electron microprobe requires flat, smooth surfaces and it was necessary, therefore, to polish the electrodes.

It should be noted also that as the electron microprobe sensitivity is insufficient to provide absolute proof of a uniform monolayer distribution, other methods have been examined. Autoradiography[41] and neutron activation of the electrode plus monolayer film[31,32] were much less sensitive and did not detect any surface distribution patterns. At present, a similar study of cobalt *mono-layer* films by means of Möss-

bauer spectroscopy is in progress; this technique appears to be sufficiently sensitive to detect different surface or lattice interaction[42].

ACKNOWLEDGEMENT

This research was supported in part by grants from the U.S. Army Research Office - Durham, contract No. DA-31-124-ARO-D-284 and the Michigan Memorial–Phoenix Project. We thank Drs. T. P. SCHREIBER and A. C. OLTOLINI of the General Motors Research Center, Detroit, Michigan for making the electron microprobe measurements and for their help in interpreting the results. We also thank FRANCIS J. BERLANDI for his helpful discussion of the experimental results.

SUMMARY

The anodic stripping curves of electrodeposited thin films of copper have been investigated. Three distinct current peaks were observed. The more negative peak corresponded to copper macrolayers (copper on copper); the smaller peaks, found at more positive potentials were interpreted as *mono-layer* peaks which indicates that the copper interaction with pyrolytic graphite is greater than that of the copper–copper interaction. A method for preparing the monolayer films is described. Electron-microprobe studies of the copper monolayer films indicated that the copper is uniformly distributed on the surface. These studies also showed that the *macro* layers started to grow at specific surface sites.

REFERENCES

1 T. MARPLE AND L. B. ROGERS, *Anal. Chim. Acta*, 11 (1954) 574.
2 D. ROSIE AND W. D. COOKE, *Anal. Chem.*, 27 (1955) 1360.
3 J. W. ROSS, R. D. DEMARS AND I. SHAIN, *Anal. Chem.*, 28 (1956) 1768.
4 J. G. NIKELLY AND W. D. COOKE, *Anal. Chem.*, 29 (1957) 933.
5 R. G. BALL, D. L. MANNING AND O. MENIS, *Anal. Chem.*, 32 (1960) 621.
6 R. D. DEMARS AND I. SHAIN, *Anal. Chem.*, 29 (1957) 1825.
7 S. S. LORD, R. C. O'NEILL AND L. B. ROGERS, *Anal. Chem.*, 24 (1952) 209.
8 K. GARDINER AND L. B. ROGERS, *Anal. Chem.*, 25 (1953) 1393.
9 M. M. NICHOLSON, *J. Am. Chem. Soc.*, 79 (1957) 7.
10 M. M. NICHOLSON, *Anal. Chem.*, 32 (1960) 1058.
11 S. P. PERONE, *Anal. Chem.*, 35 (1963) 2091.
12 B. H. VASSOS, Ph.D. Dissertation, University of Michigan, 1965.
13 G. VON HEVESY, *Phil. Mag.*, 32 (1912) 628.
14 G. VON HEVESY AND F. PANETH, *Wien. Ber.*, 122 (1913) 1037; 123 (1914) 1619.
15 F. JOLLIOT, *J. Chim. Phys.*, 27 (1930) 119.
16 M. HAISSINSKI AND A. COOKE, *Suppl. No. 2, J. Chem. Soc.*, (1949) 397.
17 A. COOKE, *J. Chim. Phys.*, 48 (1951) 195.
18 M. HAISSINSKI AND J. DANON, *J. Chim. Phys.*, 48 (1951) 106; 49 (1952) C 123.
19 A. S. BOSH-MAZUNDER AND M. HAISSINKSKI, *J. Chim. Phys.*, 51 (1954) 296.
20 M. A. EL GUEBELY AND M. HAISSINKSKI, *J. Chim. Phys.*, 51 (1954) 290.
21 M. H. LIETZKE AND J. C. GRIESS, JR., *J. Electrochem. Soc.*, 100 (1953) 434.
22 C. HAENY AND P. REYMOND, *Helv. Chim. Acta*, 37 (1954) 2067.
23 K. F. HERZFELD, *Physik. Z.*, 13 (1913) 29.
24 J. T. BYRNE, L. B. ROGERS AND J. C. GREISS, JR., *J. Electrochem. Soc.*, 98 (1951) 452.
25 J. T. BYRNE AND L. B. ROGERS, *J. Electrochem. Soc.*, 98 (1951) 457.
26 J. C. GREISS, JR., J. T. BYRNE AND L. B. ROGERS, *J. Electrochem. Soc.*, 99 (1952) 447.
27 J. C. GREISS JR. AND L. B. ROGERS, *J. Electrochem. Soc.*, 99 (1951) 129.
28 L. B. ROGERS, *Record Chem. Progress (Kresge-Hooker Sci. Lib.)*, 16 (1955) 197.
29 R. C. DEGEISS AND L. B. ROGERS, *J. Electrochem. Soc.*, 106 (1959) 433.

30 L. B. ROGERS AND D. F. STEHNEY, *J. Electrochem. Soc.*, 95 (1949) 25.
31 H. B. MARK, JR. AND F. J. BERLANDI, *Anal. Chem.*, 36 (1964) 2062.
32 H. B. MARK, JR., F. J. BERLANDI, B. H. VASSOS AND T. E. NEAL, *Proceedings of the 2nd International Conference on Modern Trend in Activation Analysis, College Station, Texas, 1965*, in press.
33 B. H. VASSOS, F. J. BERLANDI, T. E. NEAL AND H. B. MARK, JR., *Anal. Chem.*, 37 (1965) 1653.
34 D. D. DEFORD, Analytical Division, 133rd Meeting ACS, San Francisco, California, 1958.
35 L. MEITES, *Polarographic Techniques*, Interscience, New York, 1955, pp. 32–34.
36 I. B. BOROUSKII, *Collections of Problems in Metallurgy*, Izdatel. Akad. Nauk SSSR, Moscow, 1953, p. 135.
37 R. CASTAING AND A. GUINIER, *Proceedings of the Conference on Electron Microscopy, Delft, 1949*, Martin Nijhof, Delft, 1950.
38 J. PHILIBERT AND H. BIZONARD, *Rev. Met.*, 53 (1961) 187.
39 J. PHILIBERT, *Proceedings Second Institute Symposium on X-ray Microanalysis, Stockholm, 1960*, p. 416.
40 P. DUNCOMB AND V. E. COSLETT, *X-ray Microscopy and Microradiography*, Academic Press, New York, 1951.
41 H. J. YOGODA, *Radioactive Measurements with Nuclear Emulsions*, J. Wiley, New York, 1949.
42 F. J. BERLANDI AND H. B. MARK, JR., unpublished results, 1965.

POLAROGRAPHISCHE UNTERSUCHUNG EINIGER ARZNEILICH VERWENDETER HYDRAZINDERIVATE

L. SCHLITT, M. RINK† UND M. VON STACKELBERG

Pharmazeutisches Institut der Universität Bonn, und Institut für Physikalische Chemie der Universität Bonn

(Eingegangen am 7. Marz, 1966)

EINLEITUNG

Eine besondere Bedeutung als Arzneimittel erhielten Hydrazinderivate, als DOMAGK (1940) die tuberkulostatische Wirkung von Thiosemicarbazonen und Säurehydraziden erkannte. Eine weitere Indikation kam hinzu, nachdem einige Hydrazinderivate psychische Stimulierung und Euphorisierung zeigten, so dass heute Hydrazinabkömmlinge als Antidepressiva angewendet werden.

Es ist deshalb ausgehend von den Arbeiten von ANASTASI *et al.*[1], DUŠINSKÝ[2] und WUNDERLICH[3] untersucht worden, inwieweit die therapeutisch verwendeten Hydrazinderivate polarographische Reduktionsstufen ergeben und dadurch einer polarographischen Bestimmung zugänglich sind. Es war nicht das Ziel dieser Arbeit Analysenvorschriften im Einzelnen auszuarbeiten. Dagegen wurde versucht, die den Reduktionsstufen zugrunde liegenden Reaktionen zu ermitteln.

Neben den in Tab. 1 aufgeführten Verbindungsgruppen wurden auch einige Hydrazinsalze untersucht, bei denen die durch Hydrolyse entstehende starke Säure (H^+-Ionen) eine polarographische Bestimmung gestattet, wenn keine anderen H^+-Ionen liefernde oder verbrauchende Lösungsgenossen vorhanden sind.

EXPERIMENTELLE ANGABEN

Zur Aufnahme der Polarogramme stand ein Polarograph der Firma Kuntze, Düsseldorf, (Typ POL_3) zur Verfügung. Das Gerät arbeitet mit einem Tintenschreiber.

Als Elektrolysegefäss wurde eine H-Zelle nach LINGANE UND LAITINEN[4] benutzt, in der Kathoden- und Anodenraum durch ein Tondiaphragma getrennt sind.

Als Anode und Bezugselektrode (Gegenelektrode) diente eine gesättigte Kalomelelektrode (SCE). Die Potentialangaben sind alle auf diese Elektrode bezogen. Die Tropfkapillare hatte einen mittleren m-Wert von 1.46 mg/sec und eine mittlere Tropfzeit von $t = 4.23$ sec ohne angelegtes Potential bei einer Quecksilberbehälterhöhe von 120 cm.

Alle Proben wurden vor der Aufnahme 10 Minuten lang mit Wasserstoff entlüftet.

Die Konzentration des Hydrazinderivates wurde in weiten Grenzen variiert,

† Frau Professor Dr. MELANIE RINK ist am 24. Juli 1965 verstorben.

ebenso der pH-Wert der Lösung. Durch Verwendung von Puffern (Phthalat, Acetat, Phosphat) wurde für definierte pH-Werte gesorgt. Alle Lösungen enthielten 0.01% Gelatine. Wegen der Schwerlöslichkeit mancher Hydrazinderivate in Wasser wurden die Stammlösungen in diesem Falle mit Dimethylformamid (DMF) oder Äthanol hergestellt. Der hierdurch bedingte Gehalt der Analysenlösung an diesen Lösungsmitteln wird jeweils angegeben (Tab. 1).

Die Vermessung der Stufenhöhen erfolgte, indem die Linie des Stufenanstiegs nach oben und die Linie des Grenzstromes nach links geradlinig verlängert wurden. Die Höhe des Schnittpunktes dieser Geraden über dem Grundstrom wurde gemessen.

Wir verzichten auf eine Angabe der Diffusionsstromkonstanten, da hierdurch das Verhältnis der Stufenhöhen nur um $\pm 2\%$ verändert werden würde.

DIE BENUTZTEN PUFFERLÖSUNGEN

pH 2.6: 0.01 *N* HCl–0.1 *N* KCl

pH 3.5: Phthalatpuffer: 0.05 *M* Kaliumhydrogenphthalat mit HCl

pH 4.6: Acetatpuffer: 0.1 *N* Essigsäure–0.1 *N* Natriumacetat

pH 5.9: Phosphatpuffer: 0.1 *M* KH_2PO_4–0.01 *M* $Na_2HPO_4 \cdot 2\ H_2O$

pH 6.8: Phosphatpuffer: 0.01 *M* KH_2PO_4–0.01 *M* $Na_2HPO_4 \cdot 2\ H_2O$

pH 7.7: Phosphatpuffer: 0.005 *M* KH_2PO_4–0.05 *M* $Na_2HPO_4 \cdot 2\ H_2O$

pH 9.2: Ammoniakpuffer 0.1 *M* NH_3–0.1 *M* NH_4Cl

ERGEBNISSE

1. Hydrazinsalze:

1 Hydrazindihydrogensulfat $[NH_3–NH_3]^{2+}SO_4^{2-}$

2 Phenyläthylhydrazindihydrogensulfat (Nardil),

$[C_6H_5–CH_2–CH_2–NH_3–NH_3]^{2+}SO_4^{2-}$

In wässriger Lösung können Dihydrogenhydrazinsalze durch Hydrolyse Protonen abgeben. Gegenüber der Dissoziationskonstanten[5] für das erste Proton $K_1 = 8.5 \cdot 10^{-7}$ ist die zweite Konstante $K_2 = 8.9 \cdot 10^{-16}$ so klein, dass diese Salze in Wasser nach folgender Gleichung hydrolysieren:

$$N_2H_6^{2+} + H_2O \rightleftharpoons N_2H_5^{+} + H_3O^{+}$$

Die durch diese Hydrolyse in 0.1 *N* KCl-Lösung entstehenden Wasserstoffionen lassen sich polarographisch reduzieren. Die durch die Reduktion verbrauchten H^+-Ionen werden dabei durch Fortschreiten der Hydrolyse so schnell nachgebildet, dass die der obigen Gleichung entsprechende Protonenmenge zur Reduktion gelangt. Die Stufe ist aber kleiner als die einer freien Säure entsprechender Konzentration, da die am Hydrazin gebundenen Ionen langsamer zur Elektrode diffundieren. Das Halbstufenpotential der durch Hydrazinsulfat oder Nardil in 0.1 *N* KCl erzeugten Stufe ist identisch mit dem durch H_2SO_4-Zusatz zu 0.1 *N* KCl erhaltenen (−1.45 V)*

* Die wässrige Lösung von Nardil färbt sich in einigen Tagen durch Autoxydation gelb und gibt dann z.B. in Phosphatpuffer pH 5.9 polarographiert eine katalytische Wasserstoffstufe.

TABELLE 1

ÜBERSICHT ÜBER DIE HALBSTUFENPOTENTIALE UND HÖHEN DER REDUKTIONSSTUFEN

Depolarisatorkonzentration $4 \cdot 10^{-4}$ *M*. Gelatinegehalt 0.01%. Pufferzusammensetzung nach Tab. S. 11

	Lit.	*Halbstufenpotential (gegen SCE)*		*Grenzstrom i_g (μA) für $4 \cdot 10^{-4}$ M Lösungen*	
		Bei pH 5.9	*$dE_{\frac{1}{2}}/dpH$ (mV/pH) (pH 3.5–7.7)*	*Bei pH 5.9*	*pH-Abhängigkeit*
Säurehydrazide					
Isonicotinsäurehydrazid	1	−1.02 V	−80	6.1	Max. bei pH 4.5[a]
Nialamid, 1. Teilstufe		−0.87 V	−80	1.8 } 4.9	Max. bei pH 4.5[a]
2. Teilstufe		−1.01 V	−80	3.1 }	
Maleinsäurehydrazid		−1.33 V	−80	(1.8)[b]	
(Isonicotinsäure)	8, 9, 10	−1.10 V	−80	2.3[c]	
Thiosemicarbazone (10% DMF)					
Conteben	2	−1.05 V	1. Stufe: −45	2.3	3.1 μA bei pH 3.5[d]
Tebacyl		−1.07 V	1. Stufe: −45	2.6	3.1 μA bei pH 3.5[d]
Nicotinaldehydthiosem.		−0.96 V	−70	2.1	konst. bei pH 3.5–9.2
Isonicotinaldehydthiosem.		−0.66 V	−60	2.1	konst. bei pH 3.5–9.2
Iversal		−0.17 V	−60	2.0	2.1 (1.9) μA bei pH 3.5 (bzw 9.2)
Semicarbazone (10% DMF)					
Adrenoxyl		−0.36 V	−90	2.0	konst. bei pH 3.5–9.2
Furacin, 1. Stufe	3	−0.24 V	−60	5.3	konst. bei pH 3.5–9.2
2. Stufe		−1.28 V	−60	3.9	sinkt: 2.5 μA bei pH > 7
p-Nitrophenylhydrazin, 1. St.		−0.51 V	−60	5.9	konst. bei pH 4.6–7.7
2. St.		−1.0 V		0.8	konst. bei pH 4.6–7.7
Acetonderivate (4% Aceton)					
Hydrazin	13			ca. 4.7[b]	
Phenylhydrazin	13				
Nardil		−1.33 V	−60 (pH 4.6–7.7)	ca 2.5[b]	
Benzhydrazid			0 (pH > 7.7)		
Cyanessigsäurehydrazid					

[a] Siehe Abb. 2. [b] Der Grenzstrom geht steil in den Endanstieg über, ist daher schlecht vermessbar. Höhe annähernd pH-unabhängig. [c] Der Grenzstrom sinkt mit steigendem pH. [d] Mit steigendem pH wird diese 1. Stufe niedriger und ist bei pH 9.2 verschwunden. Dafür tritt in alkalischer Lösung eine andere Stufe bei negativerem Potential auf. Siehe Abb. 2 und 3.

2. Säurehydrazide

Die untersuchten Verbindungen:

1 Benzhydrazid, 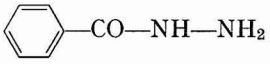

2 Kohlensäuredihydrazid(Carbohydrazid), $H_2N—NH—CO—NH—NH_2$

3 Cyanessigsäurehydrazid (Reazide), $N{\equiv}C—CH_2—CO—NH—NH_2$

4 Maleinsäurehydrazid, 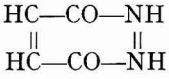

5 1-Benzyl-2-(5′-methyl-3′-isooxazolylcarbonyl)-hydrazin (Marplan),

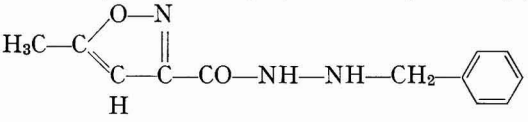

6 Isonikotinsäurehydrazid (INH), 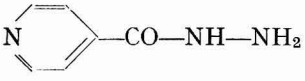

7 N′-Isonicotinyl-β-hydrazinopropionyl-benzylamid (Nialamid),

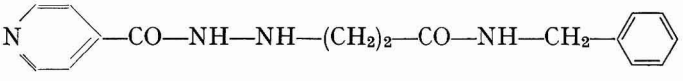

Benzhydrazid, Carbohydrazid und *Cyanessigsäurehydrazid* gaben erwartungsgemäss in sauren und in alkalischen Puffern keine polarographische Reduktionsstufe. Beim letzteren ist unter den angegebenen Bedingungen ausser der Säurehydrazidgruppe auch die —C≡N-Dreifachbindung nicht reduzierbar.

Maleinsäurehydrazid ist jedoch wegen der Konjugation zwischen den beiden C=O— und der C=C-Doppelbindung reduzierbar. Es ist anzunehmen, dass die C=C-Bindung reduziert wird (wie bei der freien Maleinsäure). Die Stufenhöhe entspricht dem Verbrauch von 2 Elektronen. Die Höhe der Stufe ist schlecht vermessbar, weil der Grenzstrom steil in den Endanstieg übergeht. Jedoch ist die Stufenhöhe annähernd pH-unabhängig.

Diese Ergebnisse entsprechen den Erfahrung, die WINKEL UND PROSKE[6] mit Säureamiden machten: Formamid, Acetamid und Benzamid sind nicht reduzierbar, wohl aber Oxamid, in dem die beiden Doppelbindungen konjugiert vorliegen. Aber auch Marplan erwies sich wider Erwarten als nicht reduzierbar.

Isonicotinsäurehydrazid (INH) und *Nialamid* (Abb. 1) sind reduzierbar und zeigen erwartungsgemäss ein sehr ähnliches polarographisches Verhalten. Das INH ist bereits früher mehrfach untersucht worden, insbesondere von ANASTASI und Mitarbeitern[1] (weitere Literaturangaben bei ZUMAN[7]). Beide Verbindungen geben eine Reduktionsstufe mit stark pH-abhängiger Höhe, deren Maximum bei pH 4 bis 5 liegt (Abb. 2). Unseren Ergebnissen in dieser Hinsicht sehr ähnlich sind die Befunde am INH von ANASTASI[1] und von VOLKE UND VOLKOVÁ[8]. Das Nialamid ergab etwas niedrigere Stufen, entsprechend einem kleineren Diffusionskoeffizienten der erheblich

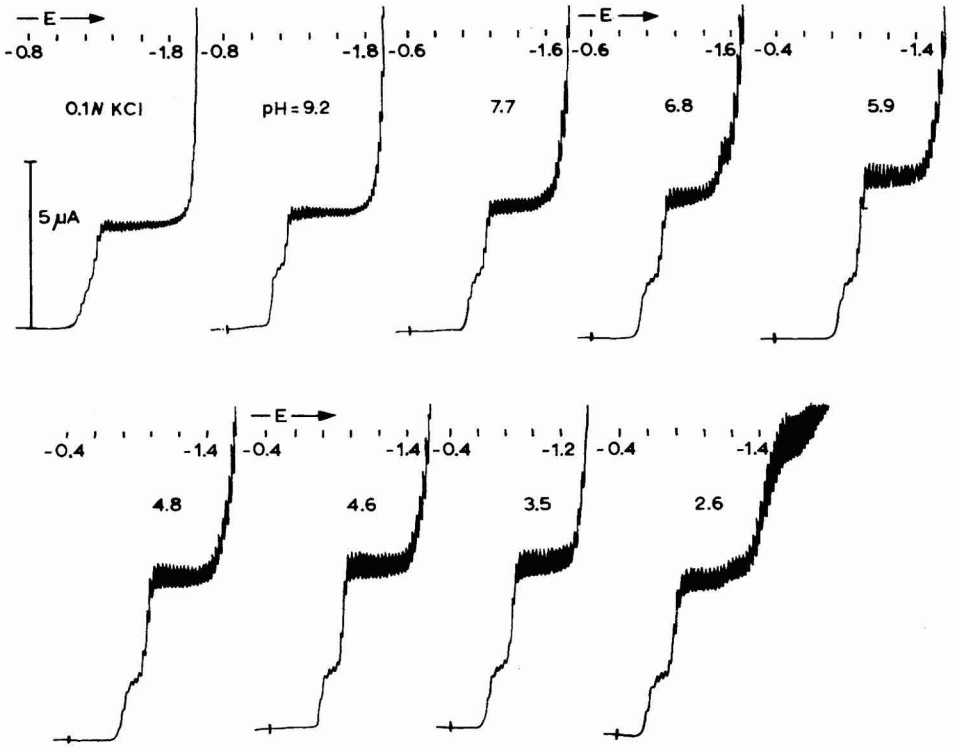

Abb. 1. Polarogramme von $4 \cdot 10^{-4}$ *M* Nialamid in Pufferlösungen (s. S. 11) mit dem angegebenen pH. Mit 0.01% Gelatine.

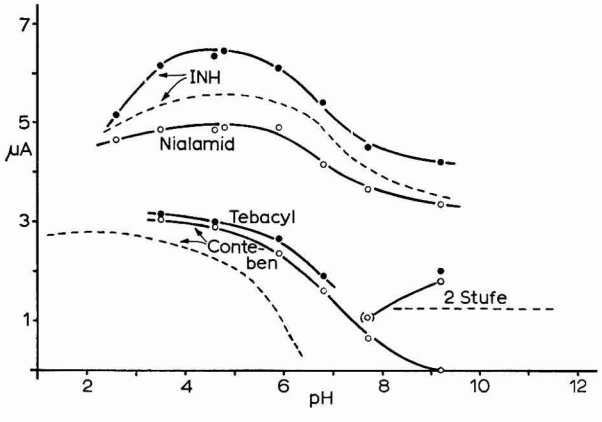

Abb. 2. pH-Abhängigkeit der Reduktionsstufenhöhen von $4 \cdot 10^{-4}$ *M* Isonicotinsäurehydrazid (INH), Nialamid, Conteben, Tebacyl. Gestrichelte INH-Kurve nach ANASTASI[1], annähernd umgerechnet auf unsere Konzentration und Kapillarenkonstante. Gestrichelte Contebenkurve nach DUŠINSKÝ[2] in Britton–Robinson-Puffer.

grösseren Molekel (und zum Teil vielleicht auch durch einen Alkoholgehalt unserer Nialamidlösung bedingt).

Bei beiden Verbindungen ist die Stufe aufgespalten in 2 Teilstufen mit nicht ganzzahligem Höhenverhältnis. Die Höhe der ersten Teilstufe nimmt mit steigendem pH nur wenig ab (beim Nialamid bei pH 2.6–9.2 von $i_d = 1.85$ auf $i_d = 1.70$ μA nach unseren Ergebnissen), während die höhere zweite Teilstufe das Maximum bei pH 4–5 zeigt, wie sich aus der Gesamtstufenhöhe nach Abb. 2 ergibt. Der Grad der Aufspaltung scheint von der Grundlösung stark abzuhängen: Mit unseren Puffern fanden wir beim Nialamid eine Differenz der Teilstufenpotentiale $\Delta E_{\frac{1}{2}} = 0.17$ V bei pH 2.6 und $\Delta E_{\frac{1}{2}} = 0.10$ V bei pH 9.2 (Abb. 1). Mit INH erhielten wir dagegen nur eine kaum feststellbare Aufspaltung (nur in saurer Lösung). Jedoch fanden ANASTASI[1] und VOLKE UND VOLKOVÁ[8] mit Britton–Robinson-Puffern bei INH eine deutliche Aufspaltung in saurer Lösung ($\Delta E_{\frac{1}{2}} = 0.15$ V)[1], die bei pH 8 nicht mehr vorhanden war. Im Hinblick auf dieses komplizierte Verhalten ist es verfrüht, Aussagen über die Reduktionsgleichung zu machen. Sicher ist, dass die Reduzierbarkeit durch den Pyridinring bedingt ist. ANASTASI[1] nimmt eine 4-Elektronenreduktion der Gruppe CO—NH—NH_2 an. Im pH-Bereich 4–5 werden aber vielleicht mehr als 4 Elektronen umgesetzt, wie ein Vergleich mit der Stufenhöhe der *Isonicotinsäure* in stark saurer Lösung (2-Elektronenreduktion[9]) vermuten lässt (Tab. 1). In Acetatpuffer (pH 4.6) wurde für INH und Nialamid die Proportionalität der Stufenhöhen mit der Konzentration im Bereich $1 \cdot 10^{-5}$ M bis $1.5 \cdot 10^{-4}$ M festgestellt, wobei mit $1 \cdot 10^{-5}$ M Lösungen noch eine Genauigkeit von etwa 10% zu erzielen war.

3. Thiosemicarbazone

1. Nicotinaldehydthiosemicarbazon, H_2N—CS—NH—N=CH— 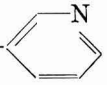

2 Isonicotinaldehydthiosemicarbazon, H_2N—CS—NH—N=CH— 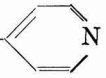

3 Benzochinonguanylhydrazon-thiosemicarbazon (Iversal),

H_2N—CS—NH—N= 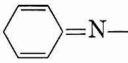 =N—NH—(C=NH)—NH_2

4 Thiosemicarbazid, H_2N—CS—NH—NH_2

5 *p*-Acetamidobenzaldehydthiosemicarbazon (Conteben),

H_2N—CS—NH—N=CH— 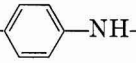 —NH—CO—CH_3

6 *p*-Äthylureidobenzaldehydthiosemicarbazon (Tebacyl),

H_2N—CS—NH—N=CH— 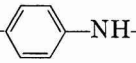 —NH—CO—NH—C_2H_5.

Ausgehend vom Conteben, dessen polarographisches Verhalten DUŠINSKÝ[2] beschreibt, sollten weitere Thiosemicarbazone untersucht werden. Die Thiosemicarba-

zone sind in Wasser nicht löslich, in Äthanol, den DUŠINSKÝ für seine Untersuchungen benutzte, nur schwer und in der Hitze. Als besseres Lösungsmittel erwies sich das Dimethylformamid (DMF). Die Stammlösungen der Thiosemicarbazone wurden daher mit DMF hergestellt. Die fertigen Analysenlösungen enthielten 10% DMF.

Bei allen untersuchten Thiosemicarbazonen zeigten die Stufen eine gute Ausbildung mit waagerechtem Grenzstrom. Beim Conteben und Tebacyl tritt bei pH > 6 eine Störung durch Ausbilding einer zweiten Stufe auf (s. weiter unten). Mit Phthalatpuffer (pH 3.5), in dem bei guter Stufenausbildung die Stufen am höchsten sind, wurde deren Konzentrationsproportionalität bei allen Verbindungen im Bereich $1 \cdot 10^{-5}$ M–$1.5 \cdot 10^{-4}$ M festgestellt. Mit $1 \cdot 10^{-5}$ M Lösungen war noch eine Genauigkeit von etwa 10% zu erzielen.

Beim *Nicotinaldehydthiosemicarbazon*, *Isonicotinaldehydthiosemicarbazon* und *Iversal* entspricht die Höhe der Reduktionsstufen im ganzen pH-Bereich einer 2-Elektronenreduktion. Bei den beiden erstgenannten Verbindungen wird es sich um die Reduktion der CH=N-Doppelbindung handeln, die durch den angrenzenden Pyridinring erleichtert ist, besonders bei der Iso-Verbindung (Tab. 1). Beim Iversal wird der chinoide Ring bei entsprechend sehr positivem Potential reduziert. Die CS-Gruppen der drei Verbindungen und die C=NH-Gruppe des Iversals sind bei den normalen polarographischen Bedingungen demnach nicht reduzierbar. Zwecks Prüfung der Reduzierbarkeit der —(C=S)-Gruppe wurde auch das *Thiosemicarbacid* polarographisch untersucht. Die Verbindung ergab in allen Pufferlösungen keine Reduktionstufe.

Conteben und *Tebacyl* (das sich nur durch einen um die Gruppe NH—CH_2-verlängerten Substituenten unterscheidet) zeigen ein sehr ähnliches polarographisches Verhalten. Die Halbstufenpotentiale sind praktisch identisch (Tab. 1). Die Stufenhöhen sind stark pH-abhängig: In stärker saurer Lösung entspricht die Höhe bei beiden Stufen einer 4-Elektronenreduktion, nimmt dann aber mit steigendem pH-Wert ab, um in alkalischer Lösung ganz zu verschwinden (Abb. 2). Dafür steigt hier eine bei negativerem Potential (−1.5 V) liegende Stufe an, die bei pH 9.2 die Höhe einer 2-Elektronenreduktion erreicht (s. Polarogramm 1 und 2 in Abb. 3). Im Prinzip das gleiche Ergebnis erhielt DUŠINSKÝ[2] beim Conteben. Auch sein Befund ist in Abb. 2 eingetragen, wobei die Umrechnung der Stromstärke auf unsere Kapillarenkonstante ($m^{2/3}t^{1/6}$) und unsere Conteben-Konzentration eine Unsicherheit bedingt. Zudem hat DUŠINSKÝ Britton–Robinson-Puffer mit 24% Äthanol benutzt. Im alkali-

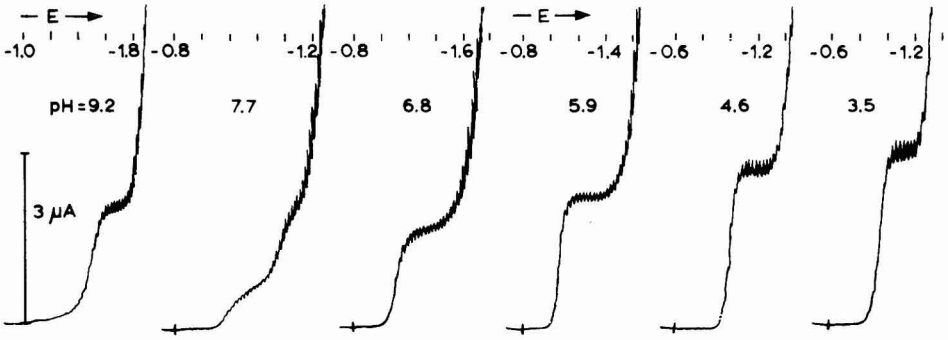

Abb. 3. Polarogramme von $4 \cdot 10^{-4}$ M Conteben in Pufferlösungen mit 10% Dimethylformamid und 0.01% Gelatine.

schen Bereich dürfte es sich um eine 2-Elektronenreduktion der CH=N-Gruppe handeln. In saurer Lösung nimmt DUŠINSKÝ eine 4-Elektronenreduktion der C=S-Gruppe an. Dies ist nicht wahrscheinlich. Wir nehmen an, dass eine zusätzliche Reduktion der CO-Gruppe stattfindet: Wenn in saurer Lösung ein Proton angelagert wird, so kann sowohl beim Conteben als auch beim Tebacyl die Anordnung

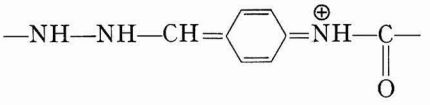

entstehen, bei der die CO-Doppelbindung eine Konjugation erhält. Die Reduktion, die bei diesem positiv geladen Ion bereits bei einem positiverem Potential erfolgt als bei der neutralen Molekel, führt dann zu

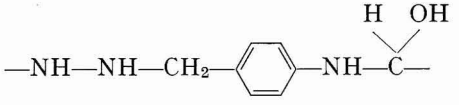

Hierfür werden 4 Elektronen und 3 H-Ionen benötigt.*
Das Problem bedarf weiterer Untersuchungen.

4. Semicarbazone

1 Adrenochrommonosemicarbazon (Adrenoxyl),

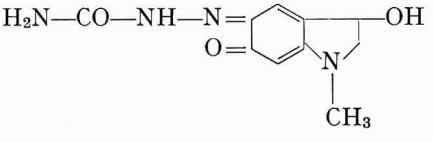

2 5-Nitro-2-furaldehydsemicarbazon (Furacin),

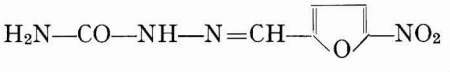

3 *p*-Nitrophenylhydrazin, $H_2N—NH—$ 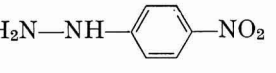

4 Semicarbazid-HCl, $H_2N—CO—NH—NH_2 \cdot HCl$

Auch hier wurden die Stammlösungen mit Dimethylformamid hergestellt, und die Analysenlösung enthielt 10% DMF.

Adrenoxyl zeigt im gesamten untersuchten pH-Bereich gut ausgebildete Stufen mit waagerechtem Grenzstrom, dessen Höhe einer 2-Elektronen-Reduktion entspricht. Die Reduktion wird sich am chinoiden Ring vollziehen. Das Potential ist etwas negativer als beim Iversal, weil es sich um einen *o*-Chinonring handelt, der zudem substituiert ist.

* Dementsprechend fanden wir bei beiden Stoffen bei der ersten Reduktionsstufe die pH-Abhängigkeit des Halbstufenpotentials $dE_{\frac{1}{2}}/dpH = -45$ mV/pH, also $\frac{3}{4}$ von 60 mV/pH, die bei gleicher Anzahl von Elektronen und Protonen zu erwarten wären. Dies gilt allerdings nur für reversible Reduktionen, bei irreversiblen ist der Betrag von $dE_{\frac{1}{2}}/dpH$ oft grösser. DUŠINSKÝ benutzte Lösungen mit 24% Alkohol. Hierdurch wird die Irreversibilität verstärkt, die Halbstufenpotentiale sind negativer. Hierauf mag es beruhen, dass DUŠINSKÝ $dE_{\frac{1}{2}}/dpH = -65$ mV/pH findet.

Furacin zeigt zwei Reduktionsstufen. Die erste, sehr positive ist der Nitrogruppe zuzuschreiben. Ihre Höhe ist praktisch pH-unabhängig. Wahrscheinlich handelt es sich um eine 4-Elektronenreduktion zur Hydroxylamingruppe. Die Höhe der zweiten Stufe entspricht in alkalischer Lösung einer 2-Elektronenreduktion und ist wohl der Carbazondoppelbindung (—N=CH—) zuzuschreiben. In saurer Lösung wird jedoch die zweite Furacinstufe erheblich höher als einer 2-Elektronenreduktion entspräche*. WUNDERLICH[3] hat nachgewiesen, dass die NO_2-Reduktionsstufe des Furacins für quantitative Bestimmungen gut geeignet ist. Er benutzte ungepufferte Lösungen.

p-Nitrophenylhydrazin ergibt eine der NO_2-Gruppe zuzuschreibende Reduktionsstufe mit pH-unabhängiger Höhe, die etwas negativer liegt als die NO_2-Stufe des Furacins (Tab. 1). Dies ist darauf zurückzuführen, dass diese Gruppe beim Nitrophenylhydrazin mit dem stabilen Benzolkern verbunden ist, beim Furacin dagegen mit dem wesentlich weniger aromatischen Furanring.

Unsere Polarogramme des Nitrophenylhydrazins zeigten noch eine zweite kleine Stufe (Tab. 1), deren Ursache ungeklärt blieb. Ihre Lage bei −1.0 V entspricht der der „Zwischenstufe" beim Furacin.

Semicarbacid ergab in allen Pufferlösungen keine Reduktionsstufe.

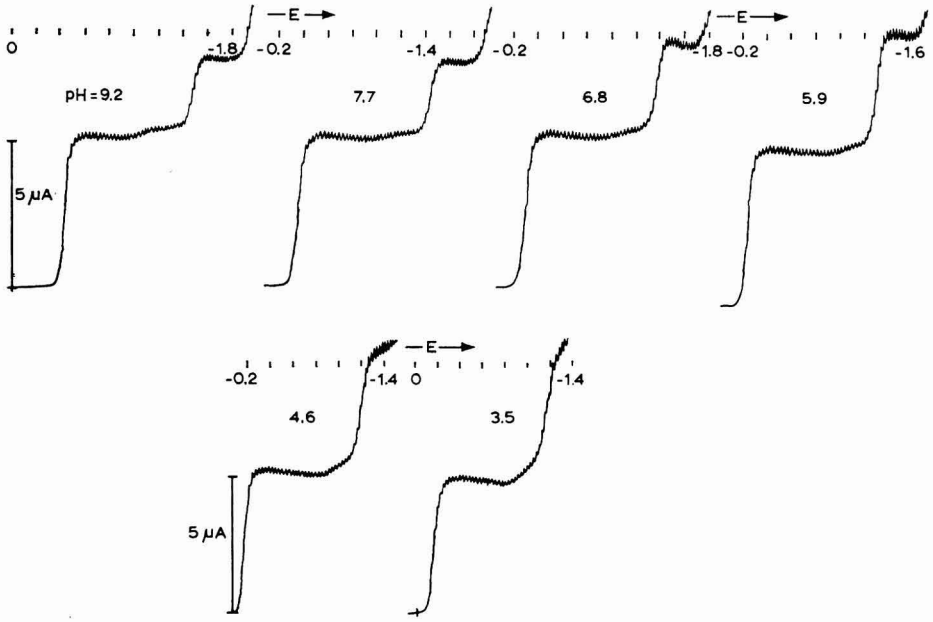

Abb. 4. Polarogramme von $4 \cdot 10^{-4}$ *M* Furacin in Pufferlösungen mit 10% DMF und 0.01% Gelatine.

* Korrigiert man die Stufenhöhen für die mit dem Potential veränderte Tropfzeit, so ergibt sich für die Diffusionsstromkonstante der 2. Stufe (einschliesslich der Zwischenstufe) bei pH 7.7 und 9.2 ein Betrag, der wenig mehr als 50% der Diffusionsstromkonstanten der 1. Stufe ausmacht. Bei pH 6.8 sind es 65% und bei pH 4.6 80%. Vielleicht erfolgt hier eine Reduktion der NO_2- zur NH_2-Gruppe. Die Polarogramme zeigen eine „Zwischenstufe" bei −1.0 V, die vielleicht den Beginn dieser Weiterreduktion der Nitrogruppe andeutet.

5. Acetonderivate

Bereits vielfach ist die Methode angewandt worden, nicht reduzierbare Ketone durch Überführung in Hydrazone polarographisch bestimmbar zu machen. Als erste haben WOLFE, HERSHBERG UND FIESER[11] sowie PRELOG UND HÄFLIGER[12] Ketosteroide mit Hilfe von Girard'schem Reagenz als Betainylhydrazone polarographisch bestimmt. In Umkehrung dieser Methode haben wir Hydrazin und nicht reduzierbare einseitig substituierte Hydrazinderivate durch Auflösen in Aceton in polarographisch bestimmbare Hydrazone übergeführt.

Die Versuche wurden mit folgenden Verbindungen durchgeführt:

1 *Hydrazin**. Da Hydrazinsulfat und Hydrazinhydrochlorid sich in Aceton nicht lösen, wurde Hydrazinhydrat benutzt.

2 *Phenylhydrazin**. Das Hydrochlorid konnte durch halbstündiges Schütteln mit Aceton in Lösung gebracht werden. Es entsteht eine hellbraune Lösung des Hydrazons.

3 *2-Phenyl-äthylhydrazindihydrogensulfat* (Nardil). In analoger Weise konnte mit dem Sulfat des Nardils eine gelblich grüne Lösung hergestellt werden.

4 *Benzhydrazid* und 5 *Cyanessigsäurehydrazid* (Reazide). Beide Säurehydrazide sind in Aceton gut löslich.

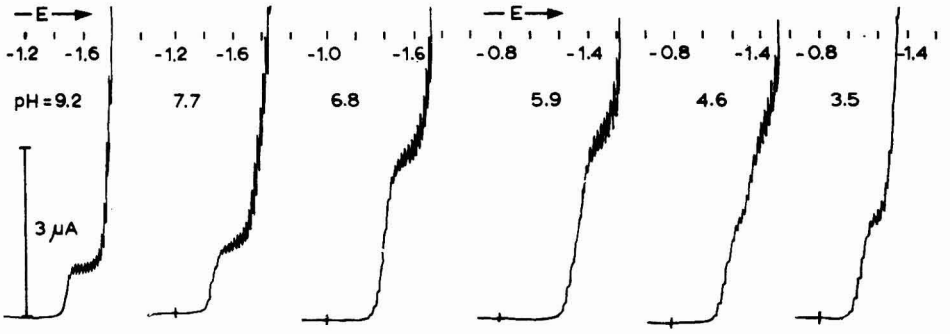

Abb. 5. Polarogramme von $4 \cdot 10^{-4}$ *M* Benzhydrazid–Acetonderivat in Pufferlösungen mit 4% Aceton und 0.01% Gelatine.

10^{-2} *M* Stammlösungen in Aceton wurden mit der Pufferlösung unter Gelatinezusatz so verdünnt, dass die Analysenlösung $4 \cdot 10^{-4}$ *M* Hydrazon, 4 Vol.% Aceton und 0.01% Gelatine enthielt. Die Polarogramme aller 5 Verbindungen sind sehr ähnlich, auch in ihrer pH-Abhängigkeit. Als Beispiel zeigt Abb. 5 die des Benzhydrazids. In alkalischen Puffern sind die Stufen niedrig. Das Maximum der Höhe wird bei pH 5 erreicht. Doch ist die Höhe hier schlecht zu vermessen, da der Grenzstrom steil in den Endanstieg übergeht. In saurer Lösung tritt eine Aufspaltung der Reduktionsstufe in 2 Teilstufen annähernd gleicher Höhe ein. Bei pH 3.5 ist in allen Fällen nur noch die erste dieser Teilstufen zu sehen, die zweite ist durch den Endanstieg verdeckt. Auch die Halbstufenpotentiale sind praktisch gleich: −1.33 V bei pH 5.9 für die Gesamtstufe. Die pH-Verschiebung beträgt −0.06 V/pH in saurem Gebiet. Im alkalischen Gebiet wird $E_{\frac{1}{2}}$ konstant: −1.48 V.

Die Stufenhöhe ist beim Hydrazinderivat, das ein Dihydrazon bilden kann, doppelt so hoch (4.7 μA bei pH 5.9) als bei den anderen Hydrazonen (2.5 μA). Es wird

* Die Acetonderivate des Hydrazins und Phenylhydrazins sind auch von BANERJEE, RIECHMANN UND BUDKE[13] polarographisch untersucht worden.

sich bei diesen um eine 2-Elektronen-, beim Hydrazinderivat um eine 4-Elektronenreduktion handeln, indem eine, bzw. zwei Hydrazongruppen (—N=C<) reduziert werden. Die CO-Gruppe der Säurehydrazide (Benzhydrazid, Cyanessigsäurehydrazid) wird nicht reduziert.

Für analytische Bestimmungen ist der steil ansteigende Grenzstrom der Reduktionsstufen ungünstig. Innerhalb der hierdurch bedingten Ungenauigkeit stellten wir bei Nardil und Cyanessigsäurehydrazid Konzentrationsproportionalität der Stufenhöhen fest ($2.5 \cdot 10^{-5}$–$2.5 \cdot 10^{-4}$ M, pH 5.9).

ZUSAMMENFASSUNG

Es wird die polarographische Reduzierbarkeit (bis zum Endanstieg des Stromes durch die Pufferlösungen) bei pharmazeutisch bedeutsamen Hydrazinderivaten untersucht. Säurehydrazide sind nur bei Konjugation der C=O-Doppelbindung mit aktiven Doppelbindungen reduzierbar. Bei Thiosemicarbazonen und Semicarbazonen ist die —N=CH-Doppelbindung reduzierbar, gegebenenfalls auch NO_2-Gruppen (Furacin) und chinoide Ringe (Adrenoxyl). Nicht reduzierbare Hydrazinderivate werden durch Herstellung der Acetonverbindungen reduzierbar gemacht. Es wird die pH-Abhängigkeit der Stufenhöhen und Halbstufenpotentiale gemessen und versucht, Aussagen über das Reduktionsprodukt zu machen. In geeigneten Pufferlösungen wird die Konzentrationsproportionalität der Stufenhöhen festgestellt, im allgemeinen bis hinab zu einer $1 \cdot 10^{-5}$ M Konzentration.

SUMMARY

The polarographic reducibility (up to the final current rise due to the buffer solution) of pharmaceutically important hydrazine derivatives was investigated. Acid hydrazides are reducible only if the C=O double bond is conjugated with active double bonds. In thiosemicarbazones and semicarbazones the —N=CH— double bond is reducible. An occasionally occuring NO_2-group (Furacin) or a quinonoid ring (Adrenoxyl) is also reducible. Non-reducible hydrazine derivatives were made reducible by preparation of the acetone compounds. The pH dependence of the wave-height and of the half-wave potential was measured and studied to provide evidence for the reaction product. It was established that the wave-height was proportional to the concentration in suitable buffer solutions, in general from a concentration of $1 \cdot 10^{-5}$ M upwards.

LITERATUR

1 A. Anastasi, E. Mecarelli und L. Novacic, *Mikrochem. Ver. Mikrochim. Acta*, 40 (1953) 113.
2 G. Dušinský, *Pharmazie*, 8 (1953) 897.
3 H. Wunderlich, *Pharmazie*, 13 (1958) 202.
4 J. J. Lingane und H. A. Laitinen, *Ind. Eng. Chem., Anal. Ed.*, 11 (1939) 504.
5 L. F. Audrieth und B. Ackerson Ogg, *The Chemistry of Hydrazine*, John Wiley, New York, 1951, S. 168.
6 A. Winkel und G. Proske, *Ber.*, 69 (1936) 1917.
7 P. Zuman, *Pharmazie*, 8 (1953) 903.
8 J. Volke und V. Volková, *Chem. Listy*, 49 (1955) 490; *Collection Czech. Chem. Commun.*, 20 (1955) 908.
9 J. Volke, *Acta Chim. Acad. Sci. Hung.*, 9 (1956) 223.
10 F. Šorm, *Chem. Obzor.*, 18 (1943) 213.
11 J. K. Wolfe, E. B. Hershberg und L. F. Fieser, *J. Biol. Chem.*, 136 (1940) 653.
12 V. Prelog und O. Häfliger, *Helv. Chim. Acta*, 32 (1949) 2088
13 D. K. Banerjee, G. C. Riechmann und C. C. Budke, *Anal. Chem.*, 36 (1964) 2220.

VOLTAMMETRIC BEHAVIOR OF SOME SELECTED METAL IONS IN ACETIC ACID

PAUL D. T. COULTER AND REYNOLD T. IWAMOTO
Department of Chemistry, University of Kansas, Lawrence, Kansas (U.S.A.)
(Received January 31st, 1966)

The polarographic behavior of electroactive species in acetic acid has been examined by a number of investigators[1-7]. BACHMAN AND ASTLE[2] report that in 0.25 *F* ammonium acetate solution, Pb^{2+}, Cd^{2+}, Zn^{2+}, Co^{2+}, Cr^{3+}, Sb^{3+}, Ni^{2+}, and Bi^{3+}, which are reduced at potentials more negative than -0.3 V *vs.* S.C.E., yield S-shaped curves. These ions are reduced at potentials 0.1–0.25 V more positive than those in water and the wave heights of their polarograms are 2/3 of those in water. Metal ions with half-wave potentials more positive than -0.3 V *vs.* S.C.E., *e.g.*, Cu^{2+}, Fe^{3+}, Hg^{2+}, and Pb^{4+}, on the other hand, yield polarograms which are "characterized by large initial slopes and by a discontinuous drop to lower levels." With increasing negative potentials, the current following the discontinuous drop again begins to increase until the potential for the reduction of hydrogen ion is reached. The magnitude of the maximum is dependent on the concentration of the electroactive species, on the supporting electrolyte, and on small amounts of water in the solution. The reduction of hydrogen ion sets the negative potential limit of 0.25 *F* ammonium acetate solution at the dropping mercury electrode at -1.4 V *vs.* S.C.E. According to BACHMAN AND ASTLE[3], "maxima in acetic acid can be explained satisfactorily on the basis of a streaming of electrolyte around the mercury drop of the type observed by ANTWEILER for aqueous solutions. The decline in current following the maximum is caused by a screening out of the reducible ions by the supporting ions, or by the neutralization of charge on the drop occurring at the electrocapillary maximum, whichever occurs first." The investigators also state that substances that undergo reduction at potentials more negative than the electrocapillary maximum, exhibit normal electrocapillary curves and give normal S-shaped polarograms. Substances that are reduced at potentials more positive than that of the electrocapillary maximum give distorted electrocapillary curves and discontinuous polarograms. ČIHALIK *et al.*[4,5], likewise concluded from their investigation of the polarographic behavior of a number of inorganic cations and anions, and of several metal ion complexes with organic ligands, that the maxima in the polarographic waves in acetic acid are due to turbulent flow.

Further examination of the polarographic features of acetic acid by HÁLA[6] revealed that the reduction of cadmium(II) and thallium(I) ions in 0.2 *M* lithium perchlorate solution was in accord with the Ilkovic equation.

The first extensive use of acetic acid as a non-aqueous solvent for the investigation of organic compounds was reported by BERGMAN AND JAMES[7]. Forty-six nitro compounds were examined by these investigators. They observed that $E_{\frac{1}{2}\,(\text{acetic acid})} = E_{\frac{1}{2}\,(\text{water})} + 0.058\,\text{pH} - 0.400$; pH is the aqueous value.

In this paper, we report the results of a study of the electrochemical behavior of metal ions in acetic acid in the absence of a complexing anion, *e.g.*, acetate. By the use of low concentrations of electroactive species and a controlled-potential polarograph, some of the difficulties previously encountered were eliminated.

EXPERIMENTAL

Reagent-grade acetic acid was purified by refluxing with chromium trioxide overnight, then distilling rapidly through a $4\frac{1}{2}$ ft., 1-in diameter glass tube packed with glass helices. The middle fraction of the distillate was treated with triacetyl borate, refluxed for several hours, and finally distilled rapidly into a glass bottle[8]. A siphon-type dispenser and a calcium chloride drying tube were attached to the bottle upon completion of the distillation. No increase in water content of the acetic acid stored and dispensed in this manner was observed. The water content was determined by gas chromatography and by the Karl Fischer method[9,10]. Both methods gave $1 \cdot 10^{-2}$ *M* for the water concentration.

Anhydrous lithium perchlorate (G. F. Smith Chemical Co.) was dried *in vacuo* at 120°. Copper(II) perchlorate hexahydrate from G. F. Smith Chemical Co. was dried by placing it in a desiccator over anhydrous magnesium perchlorate for two weeks, then in a vacuum oven for two days at room temperature and for three days at 40°. Analysis of the dried salt showed it to be $Cu_{1.00}(ClO_4)_{2.00} \cdot 4.02\ H_2O$. Cadmium perchlorate hexahydrate, a G. F. Smith Chemical Co. product, was dried in a vacuum oven for three days at 120°. The cadmium and perchlorate analyses indicated the composition of the salt to be $Cd_{1.00}(ClO_4)_{2.00} \cdot 1.94\ H_2O$. G. F. Smith Chemical Co. lead perchlorate was first dried for two months over anhydrous magnesium perchlorate, then *in vacuo* for 14 days at 70°. The salt was removed periodically, crushed, and replaced in the oven. From the lead and perchlorate analyses of this salt, the composition $Pb_{1.00}(ClO_4)_{2.02} \cdot 4.62\ H_2O$ was deduced. Thallium(I) perchlorate was obtained by gently refluxing 72% perchloric acid in contact with reagent-grade thallium metal, then cooling the reaction mixture. The precipitate of thallium(I) perchlorate was filtered off and recrystallized twice from water. Thallium(I) perchlorate does not form a hydrate; the salt, therefore, was simply dried over magnesium perchlorate. The perchlorate content of the salt was found to be 32.35%; the theoretical value is 32.28%. Nickel, cobalt, zinc and iron(II) perchlorates were dried *in vacuo* for eight days at 70°. Anhydrous silver perchlorate was dried over anhydrous magnesium perchlorate for two weeks. These latter salts, all from G. F. Smith Chemical Co., were analyzed for their perchlorate content, and the water of hydration calculated by assuming a stoichiometric proportion of metal ion to perchlorate; all gave reasonable values: silver perchlorate, 0.009; nickel perchlorate, 5.4; cobalt perchlorate, 2.4; zinc perchlorate, 2.2; and ferrous perchlorate, 4.9.

Lithium acetate, anhydrous, was prepared by the careful addition of lithium metal to acetic acid. The acetate was filtered off, recrystallized twice from acetic acid, and dried *in vacuo* for two days at 130°. The acetate analysis gave a value of 89.46% for the anion compared to the theoretical value of 89.55%. Reagent-grade anhydrous ammonium acetate was used as received.

Tris(4,7-dimethyl-1,10-phenanthroline)iron(II) perchlorate was prepared as described previously[11]. Ferrocene (Aldrich Chemical Co.) was purified by sublimation[12].

A controlled-potential polarograph, with electronic scan, similar to that of KELLEY, FISHER AND JONES[13,14] was used to obtain the current–potential curves. The reproducibility of the half-wave potential of successive runs on the same solution was better than 3 mV, and from solution to solution, better than 5 mV. A conventional polarographic H-cell was used for all the current–voltage runs, except those involving 0.25 *F* ammonium acetate solutions. A three-compartment cell with sintered glass disks separating the three compartments was used to study these solutions. A Leeds and Northrup standard 1199-31 aqueous saturated calomel reference electrode and a platinum-foil electrode, which functioned as the auxiliary electrode in a three-electrode system, were placed in one compartment of the conventional H-cell, and either a dropping mercury or a rotating platinum electrode was placed in the other. A study of the arrangement of electrodes revealed that above a 0.3–0.4 *F* concentration of lithium perchlorate, no distortion in the oxidation wave of tris(4,7-dimethyl-1,10-phenanthroline)iron(II) was observed. In the three-compartment cell, the electrodes were arranged with the working electrode in the center compartment and the reference and auxiliary electrodes in the two side compartments. With a mercury column height of 30 cm, the dropping mercury electrode on open circuit in water had a drop-time of 4.80 sec and a flow rate of 1.78 mg/sec. A platinum wire extending straight down through the bottom of a soft-glass tube rotated at *ca.* 600 rev./min with a Sargent Synchronous Rotator served as the rotating electrode. All solutions were deoxygenated for 30 min with purified nitrogen and protected from the atmosphere during a run by passing a steady stream of the gas over the surface. The nitrogen was purified by passage through two gas scrubbing towers containing a vanadium(II) solution in contact with amalgamated zinc. The deoxygenated nitrogen was dried by passing it through a tower of concentrated sulfuric acid and two towers of sodium hydroxide. Finally, before passage into the cell, the purified and dried nitrogen was pre-saturated with acetic acid.

The half-wave potentials for the oxidation of tris(4,7-dimethyl-1,10-phenanthroline)iron(II)[11], were used, as described previously, to correct the potentials in the different electrolyte solutions for differences in liquid-junction potentials between the various solutions and the saturated aqueous calomel electrode. In 1.0 *F* lithium perchlorate solution, the half-wave potential (*vs.* S.C.E.) for the oxidation of tris(4,7-dimethyl-1,10-phenanthroline)iron(II) is +0.766 V ("$0.059/n$" = 0.060) and in 0.50 *F* lithium perchlorate, +0.786 V ("$0.059/n$" = 0.060). The potential of the tris(4,7-dimethyl-1,10-phenanthroline)iron(III)/tris(4,7-dimethyl-1,10-phenanthroline)iron(II) couple in 0.25 *F* ammonium acetate solution is +0.917 V ("$0.059/n$" = 0.060). The difference between the half-wave potentials for the oxidation of ferrocene in 1.0 *F* and 0.5 *F* lithium perchlorate solutions is identical with that between the half-wave potentials for the oxidation of tris(4,7-dimethyl-1,10-phenanthroline)iron(II) in the same two solutions.

RESULTS AND DISCUSSION

Because the order of the potentials of the two copper couples, $Cu^{2+} + e \rightleftharpoons Cu^{+}$ and $Cu^{+} + e \rightleftharpoons Cu$, in a large number of nonaqueous solvents is there verse of that in water (owing to the fact that copper(I) ion is stable with respect to disproportionation in these solvents[15–18]) and because none of the previous investigators was able to ob-

tain a normal polarographic wave for copper(II) ion in acetic acid (except in the presence of fuchsine in 0.1% concentration[4]), the re-examination of the polarographic behavior of copper(II) in acetic acid was of special interest and was undertaken first.

Investigation of the discontinuity phenomenon with 0.5 F lithium perchlorate solutions of varying copper(II) perchlorate concentration revealed that, contrary to the results reported by BACHMAN AND ASTLE[2], the discontinuity potential is a function of the concentration of copper(II) perchlorate, Fig. 1 (the discontinuity potentials are reproducible to within 10 mV on scans made from either direction or on different solutions of the same composition). The relationship between the magnitude of the discontinuity phenomenon and the concentration of the reducible ion, on the other hand, was not only substantiated, but at sufficiently low concentrations of copper(II) perchlorate in 1.0 F lithium perchlorate medium, no discontinuity phenomenon was encountered. Well-developed polarographic waves were obtained. The average for the "$0.059/n$"-values, however, is 0.08, but a careful examination of the plots of log $i/(i_d-i)$ *vs.* $E_{\text{d.m.e.}}$ (see Fig. 2) reveals that the reduction wave of copper(II) is a composite of the copper(II)–copper(I), and copper(I)–copper(Hg) waves, as in

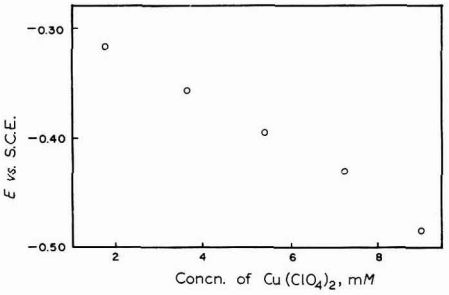

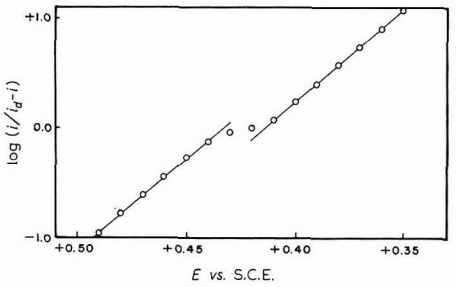

Fig. 1. Variation of discontinuity potential with $Cu(ClO_4)_2$ concn. 0.5 F $LiClO_4$.

Fig. 2. Log $i/(i_d - i)$ *vs.* $E_{\text{d.m.e.}}$ plot for the copper(II) reduction wave in 1.0 F $LiClO_4$. 0.10 mF $Cu(ClO_4)_2$.

methanol and ethanol. If it is assumed that copper(II) and copper(I) have the same diffusion coefficients and that the top and bottom sections of the wave were two separate waves one on top of the other, and if log $i/(i_d-i)$ *vs.* $E_{\text{d.m.e.}}$ is plotted for the top and the bottom halves of the wave, two separate curves are obtained. Calculations from these curves yield "$0.059/n$"-values of 0.065 for the copper(II)–copper(I) couple and 0.058 for the copper(I)–copper(Hg) couple. The potential at log $i/(i_d-i)=0$—the half-wave potential—for the copper(II)–copper(I) couple is +0.460 V *vs.* S.C.E. and for the copper(I)–copper(Hg) couple, +0.390 V. With a dropping copper amalgam electrode, a value of +0.460 V *vs.* S.C.E. was obtained for the half-wave potential of the copper(II)–copper(I) couple and +0.395 V for the copper(I)–copper(Hg) couple, both potentials being in excellent agreement with the dropping mercury electrode values. The "$0.059/n$"-value for both steps was 0.055. Because of the dependence of the potential of the copper(I)–copper step on the copper(I) concentration, the current–voltage curves for the reduction of copper(II) perchlorate at the rotating platinum electrode in 0.95 F $LiClO_4$ solution—as would be expected from the polarographic

half-wave potentials for the two copper couples—are two-step curves. Unfortunately, the two steps do not indicate that the two redox couples are reversible; the "0.059/n"-value for the copper(II)–copper(I) step is *ca.* 0.10 and that for the copper(I)–copper step is *ca.* 0.09. The half-wave potential of +0.42 V for the copper(II)–copper(I) step and the $E^{0\prime}$ value of +0.39 V for the copper(I)–copper couple, however, are in good agreement with the polarographic values and are, therefore, considered to be fairly reliable. Using the values +0.46 V for the copper(II)–copper(I) couple, and +0.39 V for the copper(I)–copper couple, we have calculated a value of *ca.* 10^{-1} for the disproportionation constant of copper(I) ion in acetic acid 1.0 F in lithium perchlorate. Unlike the situation in aqueous medium, therefore, in acetic acid 1.0 F in lithium perchlorate, copper(I) ion in concentrations less than 10^{-1} F is stable (less than 2% disproportionation). Using the half-wave potentials for the oxidation of tris(4,7-dimethyl-1,10-phenanthroline)iron(II) in (i) a 1.0 F solution of lithium perchlorate in acetic acid and (ii) in aqueous 0.1 F lithium perchlorate, we have corrected the potentials (*vs.* S.C.E.) of the copper couples in a 1.0 F solution of lithium perchlorate in acetic acid, for the difference in junction potential between this acetic acid solution *vs.* aqueous saturated calomel electrode, and aqueous 0.10 F lithium perchlorate solution *vs.* aqueous saturated calomel electrode. These potentials together with those in water[19] and those of other metal ions in acetic acid and in water[20–22] are listed in Table 1.

From the more positive values of the half-wave potentials for the reduction of copper(II), copper(I), thallium(I), cadmium(II), lead(II), and zinc(II) ions, and of the $E_{Ag(I),Ag}{}^{0\prime}$ value ($E_{\frac{1}{2}}$ corrected for concentration dependence) for Ag(I) ion in acetic acid than in water, it is clear that the solvation energy of each of these ions is lower in acetic acid than in water. In fact, because ion-association in anhydrous acetic acid is

TABLE 1

POLAROGRAPHIC BEHAVIOR OF METAL IONS IN ANHYDROUS ACETIC ACID 1.0 F IN LITHIUM PERCHLORATE AND 0.25 F IN AMMONIUM ACETATE

Couple	$E_{\frac{1}{2}(water)}$ *vs. S.C.E.*	*1.0 F $LiClO_4$*		*0.25 F $NH_4C_2H_3O_2$*	
		$E_{\frac{1}{2}}$ *vs. S.C.E.*[a]	*0.059/n*[b]	$E_{\frac{1}{2}}$ *vs. S.C.E.*[a]	*0.059/n*[b]
Cu(II), Cu(I)	−0.09[c]	+0.390	0.060		
Cu(I), Cu(Hg)	+0.15[c]	+0.320	0.056		
Tl(I), Tl(Hg)	−0.46[d]	−0.400	0.060		
Cd(II), Cd(Hg)	−0.60[d]	−0.295[g]	0.031	−0.685	0.031
Pb(II), Pb(Hg)	−0.38[d]	−0.226	0.030	−0.570	0.030
Zn(II), Zn(Hg)	−1.00[d]	−0.640	0.036	−1.085	0.040
Co(II), Co(Hg)	−1.20[d]	−0.825	0.061	−1.185	0.054
Ni(II), Ni(Hg)	−1.01[d]	−0.645	0.127	−0.975	0.086
Fe(III), Fe(II)	+0.74[e]	+0.210[h]	0.072		
Ag(I), Ag	+0.49[f]	+0.635[i]	0.060		

[a] Corrected for junction potential difference between the solvent system *vs.* aq. S.C.E. and aq. $LiClO_4$ soln. *vs.* aq. S.C.E. [b] The coefficient of the log term in the Nernst expression for the redox system. [c] Ref. 19. [d] Ref. 20. [e] Ref. 21. [f] Ref. 22. [g] No wave for the oxidation of Tl(I) was observed. [h] No wave for the reduction of Fe(II) was observed. [i] $E^{0\prime}$ (obtained with the R.P.E. and corrected for the concn. dependence of this redox system).

extensive—as evidenced by the value of $10^{5.5}$ for the formation constant of the sodium perchlorate ion-pair[23]—the solvation energy of these ions in acetic acid must be much less than in water than indicated by the reduction potentials.

As in water, the reduction of cobalt(II) and nickel(II) ions in acetic acid at the dropping mercury electrode proceeds irreversibly. The irreversible waves for these two metal ions in water, which occur at more negative potentials than the reversible standard potentials, have been attributed to the slow rate of electrochemical reduction of these ions. The more positive half-wave potentials for the reduction of cobalt(II) and nickel(II) ions at the dropping mercury electrode in acetic acid than in water, may be due either to their lower solvation energy in acetic acid than in water, or to an increase in the rate of electrochemical reduction in acetic acid over that in water, or to a combination of these two factors. A similar type of electrochemical behavior has been reported for these two metal ions in acetonitrile[15].

The markedly negative half-wave potential for the iron(III)–iron(II) couple in acetic acid is certainly surprising. High solvation energy or extensive ion-pairing of ferric ion (with perchlorate) or low solvation energy of ferrous ion, or a combination of both could account for this situation. In the absence of information on the iron(II)–iron couple, which has a potential more negative than the cathodic potential limit of acetic acid, it is difficult to account unequivocally for the relatively negative value of the iron(III)–iron(II) couple in acetic acid.

Although the strength of the interaction of solvent molecules with cations is related not only to the (ion charge)/(ion radius) values of the cations, it is interesting that the positive shifts in the potentials of thallium(I), silver(I), lead(II), cadmium(II) and zinc(II) ions in acetic acid from those in water (0.05 V, 0.15 V, 0.15 V, 0.30 V, and 0.36 V, respectively) roughly parallel the (ion charge)/(ion radius) values of these ions (0.63, 0.83, 1.6, 2.1, and 2.7). Zinc(II) ion, which is the most strongly solvated ion in water in this group of ions, as expected, shows the largest change in potential in going from an aqueous medium to acetic acid. Thallium(I) ion with a low charge and a large ionic radius (1.59 Å), on the other hand, shows the smallest change in potential, a reason for its use as a redox system to compare electrode potentials in different solvents.

In view of the stability of the acetate complexes of cadmium, lead, zinc, cobalt, and nickel ions in water[24], the negative values for the half-wave potentials of metal ions in 0.25 *F* ammonium acetate are not completely unexpected. Except for the fact that our potentials in 0.25 *F* ammonium acetate are from 0.13–0.17 V more positive than those reported by BACHMAN AND ASTLE[2] in the same medium, our electrochemical data are in good agreement with their results. Because the potentials reported by BACHMAN AND ASTLE were ". . measured against a chloranil electrode with acetic acid as solvent and were converted to the potentials corresponding to the saturated calomel electrode" and because of the constancy of the differences between our potentials and theirs, this discrepancy appears to be due to uncorrected-for junction potentials in the potentials reported by BACHMAN AND ASTLE.

ACKNOWLEDGEMENT

We wish to acknowledge the support of the Directorate of Chemical Sciences, Air Force Office of Scientific Research (Grants AFOSR 61-8 and 220-63).

SUMMARY

The polarographic behavior of copper(II), copper(I), thallium(I), cadmium(II), lead(II), zinc(II), cobalt(II), nickel(II), iron(III), and silver(I) in acetic acid 1.0 F in lithium perchlorate has been investigated. The potentials of all the couples, except the Fe(III)/Fe(II) system, are more positive than those in water. The potentials of the copper couples, unlike those in water, are in the normal order: $E_{\frac{1}{2}\mathrm{Cu(II)},\mathrm{Cu(I)}} = +0.390$ V *vs.* S.C.E. and $E_{\frac{1}{2}\mathrm{Cu(I)},\mathrm{Cu(Hg)}} = +0.320$ V *vs.* S.C.E.

REFERENCES

1 D. MacGillavry, *Trans. Faraday Soc.*, 32 (1936) 1447.
2 G. B. Bachman and M. J. Astle, *J. Am. Chem. Soc.*, 64 (1942) 1303.
3 G. B. Bachman and M. J. Astle, *ibid.*, 64 (1942) 2177.
4 J. Čihalik and J. Šimek, *Chem. Listy*, 51 (1957) 1283.
5 J. Čihalik, J. Šimek and J. Růžička, *ibid.*, 51 (1957) 1663.
6 E. Hála, *Chem. Obzor.*, 23 (1948) 145.
7 I. Bergman and J. C. James, *Trans. Faraday Soc.*, 48 (1952) 956.
8 W. C. Eichelberger and V. K. LaMer, *J. Am. Chem. Soc.*, 55 (1933) 3633.
9 J. Mitchell, Jr. and D. M. Smith, *Aquametry*, Interscience Publishers Inc., New York, 1948.
10 E. D. Peters and J. L. Jungnickel, *Anal. Chem.*, 27 (1955) 450.
11 I. V. Nelson and R. T. Iwamoto, *Anal. Chem.*, 35 (1963) 867.
12 G. Wilkinson, *Org. Syn.*, 36 (1956) 31.
13 M. T. Kelley, H. C. Jones and D. J. Fisher, *Anal. Chem.*, 31 (1959) 1475.
14 M. T. Kelley, D. J. Fisher and H. C. Jones, *Anal. Chem.*, 32 (1960) 1262.
15 I. M. Kolthoff and J. F. Coetzee, *J. Am. Chem. Soc.*, 79 (1957) 1825.
16 I. V. Nelson, R. C. Larson and R. T. Iwamoto, *J. Inorg. Nucl. Chem.*, 22 (1961) 279.
17 I. V. Nelson and R. T. Iwamoto, *Inorg. Chem.*, 1 (1962) 151.
18 K. W. Boyer and R. T. Iwamoto, *J. Electroanal. Chem.*, 7 (1964) 458.
19 I. M. Kolthoff and J. J. Lingane, *Polarography*, Interscience, New York, 2nd ed., 1952, p. 227.
20 L. Meites, *Handbook of Analytical Chemistry*, McGraw-Hill, New York, 1963, Table 5–23.
21 G. F. Smith, *Anal. Chem.*, 23 (1951) 925.
22 F. Farha, Jr. and R. T. Iwamoto, *J. Electroanal Chem.*, 8 (1964) 55.
23 I. M. Kolthoff and P. J. Elving, *Treatise on Analytical Chemistry*, Interscience, New York, 1959, p. 502.
24 L. G. Sillén and A. E. Martell, *Stability Constants of Metal-Ion Complexes*, The Chemical Society, London, 1964.

VOLTAMMETRIC BEHAVIOR OF SOME SELECTED METAL IONS IN PROPIONIC, ISOBUTYRIC AND ACRYLIC ACIDS

PAUL D. T. COULTER AND REYNOLD T. IWAMOTO
Department of Chemistry, University of Kansas, Lawrence, Kansas (U.S.A.)
(Received February 28th, 1966)

INTRODUCTION

Previous voltammetric work employing anhydrous monocarboxylic acids as solvents has been limited to acetic acid and formic acid. We report here the results of a recent examination of the electrochemical behavior of copper(II), copper(I), cadmium, lead(II), thallium(I), and silver ions in anhydrous propionic, isobutyric, and acrylic acids. Earlier, we presented some recent results on the electrochemical behavior of these and other metal ions in acetic acid[1].

EXPERIMENTAL

With the exception of the purification of solvents, the pertinent experimental details are identical with those reported previously[1].

Technical-grade propionic acid and isobutyric acid were refluxed over chromium trioxide overnight, then distilled rapidly; only the middle fraction was collected. The acids were stored in glass-stoppered bottles. Isobutyric acid showed an objectionably high background current in three days, or less, after distillation. It was necessary, therefore, to distil a fresh supply for each day's work. No change was observed in the polarographic background current of propionic acid over a two-year period. The water content of the two acids was less than 10^{-2} M, as determined by a gas chromatographic method[1].

Acrylic acid of the highest purity available (96%, practical, Matheson, Coleman and Bell) was passed slowly through a column of neutral, activated alumina. A single pass greatly reduced the polarographic background current; two additional passes caused little change. The wave form and half-wave potential for the reduction of cadmium ion were also unaffected. The purified acrylic acid still contained some of the *p*-methoxyphenol originally added to stabilize the acid, as evidenced by an anodic wave at *ca.* +0.6 V *vs.* S.C.E. The half-wave potentials of cadmium, lead(II), and thallium(I) ions evaluated in acetic acid containing *p*-methoxyphenol in concentrations similar to that in purified acrylic acid, were identical with those obtained in pure acetic acid. This indicated that the phenol had no noticeable effect on the current–voltage curves of these ions. Purified acrylic acid stored in glass bottles showed no change in background current over a four-week period.

The half-wave potentials listed below for the oxidation of tris(4,7-dimethyl-

1,10-phenanthroline)iron(II) [DMPFe] and ferrocene in 1.0 *M* lithium perchlorate solutions of the three solvents, and acetic acid, were used to estimate the differences in liquid-junction potential between the solutions and the S.C.E.

Acid	$E_{\frac{1}{2}}$ *(DMPFe)* *(V)*	*0.059/n*	$E_{\frac{1}{2}}$ *(ferrocene)* *(V)*	*0.059/n*
acetic	+0.766	0.060	+0.259	0.060
propionic	+0.764	0.061		
isobutyric	+0.685	0.061		
acrylic			+0.248	0.061
water	+0.695[a]		+0.160[b]	

[a] 0.1 *M* $LiClO_4$, ref. 2. [b] 0.1 *M* $LiClO_4$, ref. 3.

RESULTS

The half-wave potentials for the reduction of copper(II), copper(I), cadmium, lead(II), and thallium(I) ions at the dropping mercury electrode and for the reduction of silver ion at the rotating platinum electrode, in 1.0 *M* lithium perchlorate solutions of the three solvents and of acetic acid, are given in Table 1.

TABLE 1

VOLTAMMETRIC HALF-WAVE POTENTIALS[a,b]

(V *vs.* S.C.E.)

Ion[c]	*Acetic acid*		*Propionic acid*		*Isobutyric acid*		*Acrylic acid*	
	$E_{\frac{1}{2}}$	*0.059/n*	$E_{\frac{1}{2}}$	*0.059/n*	$E_{\frac{1}{2}}$	*0.059/n*	$E_{\frac{1}{2}}$	*0.059/n*
Copper(II)	+0.380	0.065	+0.365	0.033	+0.435	0.065	> +0.5	
Copper(I)	+0.320	0.058			+0.360	0.060	+0.095	0.066
Thallium(I)	−0.400	0.061	−0.405	0.058	−0.395	0.060	(insol.)	
Cadmium	−0.290	0.031	−0.270	0.029	−0.290	0.030	−0.325	0.034
Lead(II)	−0.215	0.030	−0.200	0.033	−0.200	0.034	−0.250	0.032
Silver[d]	+0.635[e]	0.060	+0.625[e]	0.065	+0.705[e]	0.065	+0.530[e]	0.063

[a] 1.0 *M* $LiClO_4$ supporting electrolyte. [b] Corrected for liquid-junction potential differences; 0.10 *M* aq. $LiClO_4$ soln. used as reference. [c] At the dropping mercury electrode. [d] At the rotating platinum electrode. [e] $E^{o\prime}$-value ($E_{\frac{1}{2}}$ corrected for concn. dependence).

DISCUSSION

The only unexpected feature of the electrochemical data is the single, two-electron polarographic wave for the reduction of copper(II) in propionic acid. The current–voltage curve was checked repeatedly, but no split wave or indication of a split wave was observed. The current–voltage curve for the reduction of copper(II) ion in propionic acid at the rotating platinum electrode, however, is a split wave. The curve, unfortunately, is too drawn out to obtain meaningful potential data. The stability of copper(I) ion in propionic acid is also indicated by the reducing power of a copper(II) solution after treatment with copper metal.

The more negative potentials for the reduction of copper(I) and silver ions in acrylic acid compared with those in the other three acids are consistent with the

expected formation of π complexes between α,β-unsaturated acids and copper(I)[4] or silver[5] ions. Also evident in the half-wave potentials of the two 1/0 couples in acrylic acid is the greater co-ordinating ability of the olefinic group with copper(I) ion than with silver ion. This is in line with the observed fact that copper(I) olefinic complexes are considerably more stable than the corresponding silver complexes[4–6].

Because of lack of information on ion-pairing of lithium perchlorate, of the supporting electrolyte, and of the metal ions with perchlorate ion in acetic acid, propionic acid, and isobutyric acid, very little can be said in discussion of the small differences in half-wave potentials of the metal ions in the three saturated acids.

ACKNOWLEDGEMENT

The authors gratefully acknowledge the support of the Directorate of Chemical Sciences, Air Force Office of Scientific Research (Grant 220-63).

SUMMARY

The polarographic behavior of copper(II), copper(I), cadmium, lead(II), and thallium(I) ions and the voltammetric behavior of silver ion at the rotating platinum electrode in 1.0 *M* lithium perchlorate solutions of anhydrous propionic acid, isobutyric acid, and acrylic acid have been examined and compared with those in anhydrous acetic acid.

REFERENCES

1 P. D. T. Coulter and R. T. Iwamoto, *J. Electroanal. Chem.*, 13 (1967) 21.
2 F. Farha, Jr. and R. T. Iwamoto, *Anal. Chem.*, 38 (1966) 143.
3 I. V. Nelson and R. T. Iwamoto, *Anal. Chem.*, 35 (1963) 867.
4 R. M. Keefer, L. J. Andrews and R. E. Kepner, *J. Am. Chem. Soc.*, 71 (1949) 2381.
5 S. Winstein and H. J. Lucas, *J. Am. Chem. Soc.*, 60 (1938) 836.
6 R. M. Keefer, L. J. Andrews and R. E. Kepner, *J. Am. Chem. Soc.*, 71 (1949) 3906.

THE INTERFACIAL TENSION OF THE MERCURY–1 *M* $HClO_4$-SOLUTION INTERFACE AT HIGH POTENTIALS; COMPARISON WITH DOUBLE-LAYER CAPACITANCE MEASUREMENTS

M. SLUYTERS-REHBACH, W. J. A. WOITTIEZ AND J. H. SLUYTERS
Laboratory of Analytical Chemistry, State University, Utrecht (Netherlands)
(Received February 3rd, 1966)

INTRODUCTION

Applying the complex plane analysis method[1] to the impedance of the Hg_2^{2+}/Hg electrode in 1 *M* $HClO_4$ solution we found that the differential double-layer capacitance increases steeply at potentials higher than +0.45 V *vs.* S.C.E.[2]. The same result was obtained with an oscilloscopic method[3].

In the potential region discussed here, the electrode reaction, $2\,Hg \rightleftarrows Hg_2^{2+} + 2e$, contributes to the cell impedance. It is essential, therefore, to make sure that the obtained capacitance values do not contain some reaction-controlled contribution that could eventually remain after subtraction of the Faraday impedance from the total cell impedance. This is possible by means of the determination of the interfacial tension, γ, which should show an abnormal decrease beyond 0.45 V in accordance with[4]

$$\frac{\partial\gamma}{\partial E} = -q(E) = -\int_0^E C_d \mathrm{d}E \qquad (1)$$

where $q(E)$ is the surface charge density and C_d the differential double-layer capacitance.

PROCEDURE AND RESULTS

Relative interfacial tension measurements were performed in an ordinary polarographic cell containing 1 *M* $HClO_4$, by means of drop-time measurements. The drop time was assumed to be proportional to the interfacial tension, without the application of further corrections[5].

Moderately low potentials of the dropping mercury electrode were adjusted externally against a mercury pool counter electrode by means of a potentiometer. Some $Hg_2(ClO_4)_2$ was added to fix the potential of the counter electrode.

At high potentials, this procedure failed owing to polarization of the mercury pool electrode. In this region, the measurements were performed at various equilibrium potentials, which were adjusted by the addition of small quantities of a saturated $Hg_2(ClO_4)_2$ solution. This procedure has no significant influence on the composition of the cell solution except at potentials beyond 0.51 V.

The potential of the dropping mercury electrode was measured against a saturated calomel electrode with a potentiometric millivolt meter.

The plot of drop time against potential (Fig. 1) closely fits to a parabola with the electrocapillary maximum at -0.525 V *vs.* S.C.E. At high potentials, the expected deviation is observed*. This follows more clearly from Fig. 2, where the drop time is plotted against $(E-0.525)^2$.

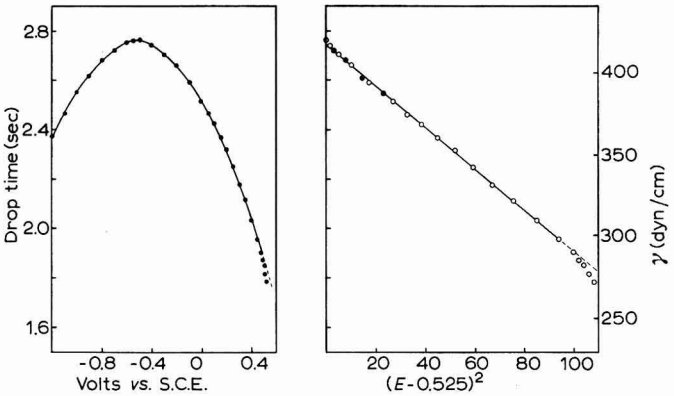

Fig. 1. Electrocapillary curve of mercury in 1 *M* $HClO_4$.

Fig. 2. Linearized electrocapillary curve of mercury in 1 *M* $HClO_4$.

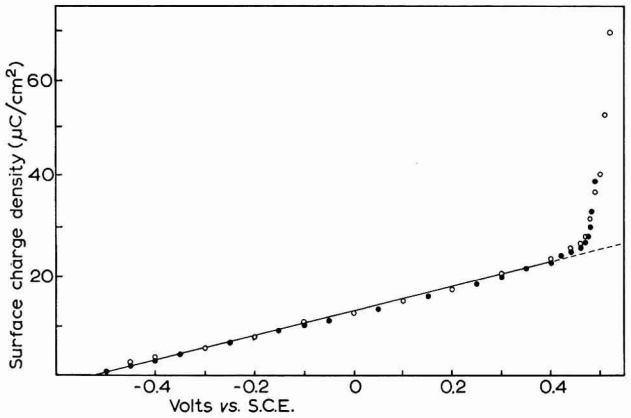

Fig. 3. Surface charge density of mercury in 1 *M* $HClO_4$: (——), calc. from Fig. 2; (○), obtained from the tangents of Fig. 1; (●), obtained by integration of capacitance data in refs. 2 and 3.

We ventured to convert the drop times to interfacial tensions, supposing the maximum value of γ to be 420 dyn cm^{-1} (see *e.g.* ref. 6). The surface-charge density was calculated as a function of potential by graphical differentiation of the curve in Fig. 1. The results are represented in Fig. 3. It is easily verified that in the potential

* In view of the accuracy of the drop-time measurements (*ca.* 0.01 sec), this deviation is significant at potentials beyond 0.45 V.

region where the interfacial tension values fit to the parabola, this plot should be a straight line, the slope of which is twice the negative slope of the line in Fig. 2.

The surface charge density was also obtained by integration of the double-layer capacitance data published previously[2,3], taking the potential of zero charge at -0.525 V. Obviously, the results are in accordance with the electrocapillary data; this provides the desired further proof of the steep increase of the double-layer capacitance at high potentials.

DISCUSSION

Dr. R. PARSONS has kindly pointed out that a thoughtless application of the Lippmann equation is not allowed if an appreciable amount of potential-determining ions is present. For in this case the electrode is not completely polarized and, if the electrode reaction is sufficiently fast, the Gibb's equation for a completely reversible electrode should be considered:

$$-\mathrm{d}\gamma = \Sigma\, \Gamma_i \mathrm{d}\mu_i + \Gamma_{Hg_2^{2+}} \mathrm{d}\mu_{Hg_2^{2+}} + \Gamma_e \mathrm{d}\mu_e$$

in which μ is the chemical potential, Γ the surface excess, and i refers to all components except Hg_2^{2+} ions and electrons[7]. The chemical potentials of these species can be related to the potential difference across the interface by

$$\mathrm{d}E = \frac{\mathrm{d}\mu_{Hg_2^{2+}}}{2F} = -\frac{\mathrm{d}\mu_e}{F}$$

Since it may be assumed that all other μ_i's are virtually independent of potential, it follows that the derivative of the electrocapillary curve gives

$$-\frac{\partial\gamma}{\partial E} = F(2\Gamma_{Hg_2^{2+}} - \Gamma_e)$$

in which $\Gamma_{Hg_2^{2+}}$ is the sum of the surface excess, $\Gamma_{Hg_2^{2+}}$ (M), on the metal side of the double layer and the surface excess, $\Gamma_{Hg_2^{2+}}$ (S), on the solution side. This means that $-\partial\gamma/\partial E$ is not equal to the charge q on the electrode, but

$$-\frac{\partial\gamma}{\partial E} = q + 2F\Gamma_{Hg_2^{2+}}(\mathrm{S})$$

If, however, the excess of Hg_2^{2+} in the solution exists only in the diffuse layer (no specific adsorption, which seems reasonable to assume as the electrode has a strongly positive charge) the correction will be negligibly small, since most of the excess of counter ions will be formed by the indifferent electrolyte, *i.e.*, H^+ and ClO_4^- ions, which are present in a much higher concentration.

These considerations are analogous to those given by OVERBEEK for a Ag/AgI electrode[7].

The question arises, whether the quantity, obtained by integrating the capacitance–potential curve in the case of a perfectly non-polarized electrode, contains a similar correction or not. In our opinion, the capacitance, measured by an a.c. method in accordance with the equivalent circuit, represents only the charge supplied to the electrode, which does not pass the interface by a faradaic process but serves to increase or decrease the surface charge of the electrode. This implies that the second equality in (1) is still correct.

Consequently, the agreement between the integrated capacitance data and differentiated electrocapillary data might suggest that, in fact, $2F\Gamma_{Hg_2^{2+}}$ (S) is negligible with respect to q in the potential region of our measurements.

SUMMARY

Interfacial tension values have been measured in order to calculate the electrical charge density as a function of potential. The results are in accordance with those obtained from double-layer capacitance data reported earlier[2,3], also at highly positive potentials.

REFERENCES

1 M. Sluyters-Rehbach and J. H. Sluyters, *Rec. Trav. Chim.*, 82 (1963) 525.
2 M. Sluyters-Rehbach and J. H. Sluyters, *Rec. Trav. Chim.*, 83 (1964) 217, 967.
3 J. H. Sluyters and R. de Leeuwe, *Rec. Trav. Chim.*, 83 (1964) 657.
4 D. C. Grahame, *Chem. Rev.*, 41 (1947) 441.
5 P. Corbusier and L. Gierst, *Anal. Chim. Acta*, 15 (1956) 254.
6 A. Frumkin, Transactions of the Symposium on Electrode Processes, Wiley, New York, 1961, p. 1.
7 J. Th. G. Overbeek, *Colloid Science*, edited by Kruyt, Elsevier, Amsterdam, 1952, ch. IV.

A STUDY OF THIOCYANATE ION ADSORPTION ON MERCURY BY CHRONOCOULOMETRY

FRED C. ANSON† AND D. A. PAYNE

Gates and Crellin Laboratories of Chemistry, California Institute of Technology, Pasadena, California 91109 (U.S.A.)*

(Received December 9th, 1965)

Chronocoulometry is a relatively new electrochemical technique that is well suited to the study of reactant adsorption[1-4]. In all previous studies, the adsorbed substance was itself reduced (or oxidized) by the electrode reaction. In this study, the adsorbed thiocyanate is investigated under conditions where it is consumed without change in oxidation state, by anodic oxidation of the mercury electrode to form the mercuric thiocyanate complex ion:

$$Hg + 2\ SCN^- = Hg(SCN)_2 + 2\ e^- \qquad (1)$$

The mercuric thiocyanate that is the product of the electrode reaction was found to be very strongly specifically adsorbed as well.

EXPERIMENTAL

The theory and practice of chronocoulometry have been described[1-4]. A schematic diagram of the circuit employed in this study is given in Fig. 1. The charge-time traces were recorded with a Tektronix Type 564 Storage Oscilloscope and the data were read with calipers directly from photographs of the traces.

Solutions were prepared from triply-distilled water (second distillation from alkaline $KMnO_4$). Reagent-grade chemicals were used without further purification except for the sodium fluoride which was recrystallized. $Hg(SCN)_2$ was recrystallized twice from hot water.

A commercially-available hanging mercury electrode was used (Brinkman Instruments, Inc.). The mercury drop extrusion experiments were performed as previously described[1] by increasing the drop area from 0.014 to 0.046 cm^2. The values of Q_{d1} obtained in this way were then applied to the chronocoulometric data which were all obtained with hanging drops having an area of 0.032 cm^2.

In order to be certain that adsorption equilibrium was maintained during the drop extrusion experiments, it was established that the measured values of the charge did not change whether or not the solution was stirred during the extrusion of the drop.

All measurements were carried out in air-free solutions. All potentials are expressed in millivolts *vs.* the saturated calomel electrode.

† Alfred P. Sloan Research Fellow.
* Contribution No. 3323.

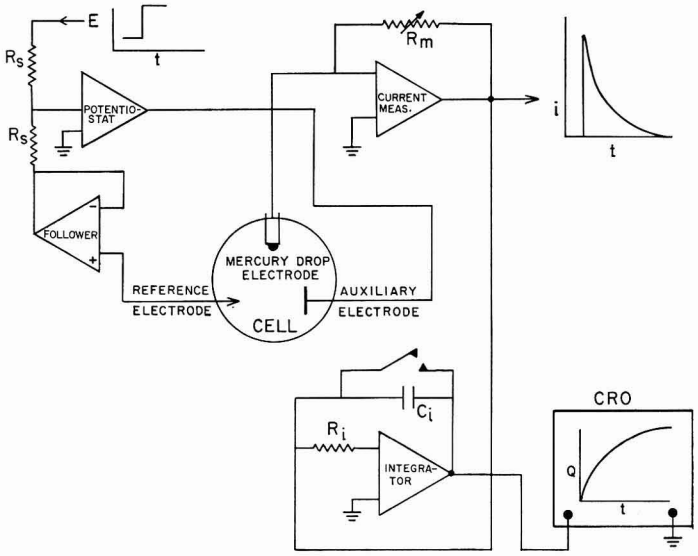

Fig. 1. Schematic diagram of apparatus for chronocoulometry. (R_s), potentiostat summing point resistors; (R_m), current measuring resistor; (R_i), integrator time constant resistor; (C_i), capacitor. The potentiostat, current measuring, and integrating amplifiers were Philbrick Type SP-656 solid-state operational amplifiers (Geo. A. Philbrick Researches, Inc., Boston, Massachusetts). The follower was a Philbrick Type P-75 solid state operational amplifier. The rise time of the potentiostat, which was the response-limiting factor, was about 75 μsec.

RESULTS AND DISCUSSION

The chronocoulometric experiments with thiocyanate were performed by stepping the potential of the mercury drop from selected initial potentials in 2-mM KSCN solution to +300 mV *vs.* S.C.E. where the diffusion-limited faradaic current resulting from reaction (1) was integrated and the resulting charge–time variation recorded. A typical plot of charge *vs.* the square root of time is shown in Fig. 2.

It has been previously shown[1,4] that the charge–time variation is given by eqn. (2):

$$Q = 2nFAC\sqrt{\frac{Dt}{\pi}} + Q_{dl} + nF\Gamma \qquad (2)$$

where Q is the total charge in coulombs measured at time t, C is the concentration of the reactant whose semi-infinite linear diffusion to the electrode of area A limits the current, Q_{dl} is the charge required to change the electrode–electrolyte double-layer capacitance from the initial to the final electrode potential, Γ is the amount of reactant (moles/cm^2) adsorbed on the electrode surface at the start of the experiment, and the other symbols have their usual significance.

In order to determine the amount of thiocyanate that is specifically adsorbed at the initial potential, it is necessary to subtract the amount of charge corresponding to the double-layer charging[1,2] from the Q-axis intercepts in plots of Q *vs.* $t^{\frac{1}{2}}$. Because the Q-axis intercept formally corresponds to the situation prevailing at $t=0$, it might appear that the correct value for Q_{dl} would be the difference between the charge in the

double layer at the final potential before any product has been produced, and the charge at the initial potential before any reactant has been consumed. In fact, this would not be the correct value of Q_{dl} to use because all the data points used in the Q–$t^{\frac{1}{2}}$ plots correspond to the absence of reactant and the presence of product at the electrode surface. The linear extrapolation of the plot, thus, does not yield a Q-intercept that corresponds to the conditions actually prevailing at $t=0$. Accordingly, the double-layer charging correction that should be applied to the intercept in Fig. 2 is the difference between the charge on the electrode at +300 mV in a thiocyanate-free, 1-mM $Hg(SCN)_2$ solution and the charge on the electrode at −200 mV in a 2-mM thiocyanate solution.

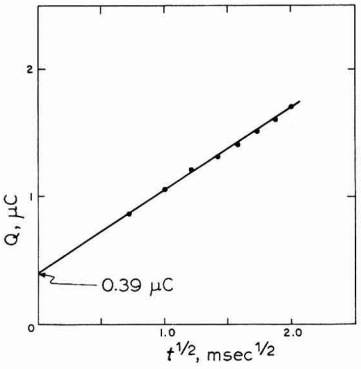

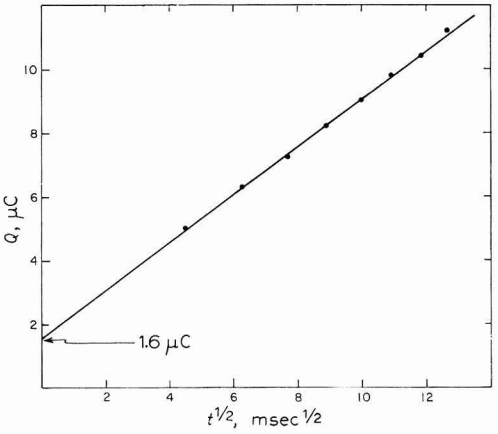

Fig. 2. Chronocoulometric plot for 2 mM KSCN soln. in 1 M $NaNO_3$. The potential was stepped from −200 to +300 mV *vs.* S.C.E. where the resulting faradaic current was integrated.

Fig. 3. Chronocoulometric plot for 1 mM $Hg(SCN)_2$ soln. in 1 M $NaNO_3$. The potential was stepped from +300 to −200 mV *vs.* S.C.E. where the resulting faradaic current was integrated.

TABLE 1

INTEGRATED CHARGE ON EXTRUDED MERCURY DROPS
Change in drop area, 0.032 cm^2

Soln. composition	*E* (*mV vs. S.C.E.*)	*Q* (*μC*)
1 F $NaNO_3$	−200	+0.32
1 F $NaNO_3$, 0.002 F KSCN	−200	+0.37
1 F $NaNO_3$	+300	+0.85
1 F $NaNO_3$, 0.001 F $Hg(SCN)_2$	+300	+0.29

The charges on the electrodes under these two sets of conditions were measured by extruding new mercury drops into the appropriate solutions and integrating the resulting charging currents. The technique has been previously described[1]. Table 1 contains the charge data obtained in this way. Two aspects of the data in Table 1 deserve comment. First, it is clear that a double-layer charging "blank" measured in pure 1 F $NaNO_3$ supporting electrolyte would seriously overcorrect the Q-intercept in

Fig. 2. Secondly, there is the unexpected result that a much smaller positive charge is on the electrode at +300 mV when $Hg(SCN)_2$ is present than when it is absent. The charge is reduced so much by the $Hg(SCN)_2$ that there is actually 0.08 μC more charge on the electrode at −200 mV in 2-mM KSCN than at +300 mV in 1-mF $Hg(SCN)_2$. If no thiocyanate were adsorbed at −200 mV, the Q *vs.* $t^{\frac{1}{2}}$ plot in Fig. 2 would have had a negative intercept of 0.08 μC. Thus, the double-layer charging blank to be applied to the Q-intercept in Fig. 2 is +0.08 μC. That is, 0.08 μC must be *added* to the uncorrected intercept to give the amount of specifically adsorbed thiocyanate.

The reason for the unexpectedly small charge at +300 mV is apparently the result of the extensive adsorption of $Hg(SCN)_2$. Figure 3 is a Q–$t^{\frac{1}{2}}$ plot for a cathodic chronocoulometric experiment with a mM $Hg(SCN)_2$ solution in 1 F KNO_3. The potential was stepped from +300 mV to −200 mV so that the double-layer charging correction to the Q-intercept is again, from Table 1, +0.08 μC. The corrected intercept amounts to 1.7 μC which correspond to very extensive adsorption of the $Hg(SCN)_2$. In fact, this adsorption is so great that it is impossible for equilibrium to be maintained with respect to $Hg(SCN)_2$ adsorption during anodic chronocoulometric experiments with the 2-mM thiocyanate solution. During the experiment that led to Fig. 2, for example, less than 1.7 μC of $Hg(SCN)_2$ were generated at the electrode.

It follows that the drop extrusion charge data in Table 1, which were obtained under equilibrium conditions, cannot provide strictly rigorous double-layer charging corrections for the chronocoulometric experiments. To overcome this difficulty we resorted to the following tactics. At sufficiently negative potentials, the amount of thiocyanate that is specifically adsorbed becomes very small. An anodic chronocoulometric experiment was performed in which the potential was stepped from −800 mV, where essentially no thiocyanate is adsorbed, to +300 mV. The Q-intercept on the resulting Q–$t^{\frac{1}{2}}$ plot was taken to be the true difference in charge on the electrode between the two potentials. In experiments where more anodic initial potentials were employed (and thiocyanate adsorption occurred) the double-layer charging correction was obtained by measuring the charge required to change the electrode potential from −800 mV to the new initial potential in 2-mM thiocyanate solution. This charge

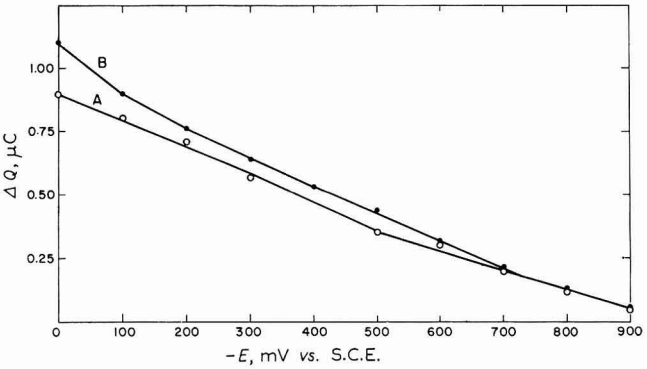

Fig. 4. Charge–potential plot for double-layer charging at mercury. Plotted as ordinate is the measured step-change in charge that resulted when the electrode potential was stepped from −1000 mV *vs.* S.C.E. to the potentials plotted as abscissas. (A), 1 M $NaNO_3$; (B), 1 M $NaNO_3$ and 2 mM KSCN.

difference was subtracted from the Q-intercept in the -800 to $+300$ mV chronocoulometric experiment, and the result was used as the new charge correction.

To facilitate the correction outlined above, data such as those in Fig. 4 were obtained. Figure 4 is a plot of ΔQ *vs.* potential for a supporting electrolyte solution with and without thiocyanate ion. Plotted as ordinates are the step-changes in charge that resulted when the potential of the electrode was stepped from -1000 mV to the potential plotted as abscissa. In no case did any faradaic current pass before or after the step, so the values of ΔQ correspond to the difference between the charge in the electrical double-layer capacitance at -1.00 V *vs.* S.C.E. and the plotted potential. The larger values of ΔQ in the presence of thiocyanate reflect the increase in double-layer capacitance produced by thiocyanate adsorption.

At potentials more negative than about -700 mV, the curves in Fig. 4 coincide because thiocyanate anion is no longer adsorbed on the negatively charged electrode from a 2-mM solution. Accordingly, the difference in ΔQ values at any potential in Fig. 4 gives the difference between the electronic charge on the electrode at those two potentials (no data is available for the thiocyanate-containing solution at potentials more anodic than 0 mV because faradaic current begins to flow at more anodic potentials). Similar data were also obtained for supporting electrolytes of 1 F NaF and 0.1 F $HClO_4$–0.9 F $NaClO_4$.

As an example, the Q-intercept obtained for the -800 to $+300$ mV chronocoulometric experiment with 2-mM thiocyanate was 0.77 μC. The Q-intercept for -200 to $+300$ mV was 0.39 μC. In Fig. 4, the difference in ΔQ between -800 and -200 mV for 2-mM KSCN solution is 0.63 μC. The charge correction for the Q-intercept in the -200 to $+300$ mV experiment is thus 0.14 μC and the amount of adsorbed thiocyanate is calculated to be 0.25 μC.

TABLE 2

SPECIFIC ADSORPTION OF THIOCYANATE ON MERCURY FROM 2-mM KSCN
Electrode area, 0.032 cm^2; final potential, $+300$ mV *vs.* S.C.E.

Initial potential (mV vs. S.C.E.)	*Corr. Q–$t^{\frac{1}{2}}$ intercepts = amount of adsorbed thiocyanate (μC)*[a] *Supporting electrolytes*		
	1 F NaF	*1 F $NaNO_3$*	*0.9 F $NaClO_4$ 0.1 F $HClO_4$*
-800	0[b]	0[b]	0[b]
-600	0.04	0.10	0
-200	0.28	0.25	0.17
0	0.58	0.61	0.50

[a] The reproducibility of the intercepts and charge measurements was approximately $\pm$ 0.05 μC. Each entry in the table carries an uncertainty of *ca.* $\pm$ 0.15 μC.
[b] Assumed equal to zero.

By repeating this process at various potentials and in various supporting electrolytes, the data in Table 2 were obtained. An increasing specific adsorption of thiocyanate anion as the electrode becomes more positively charged is observed, as expected. The changes in the amount of adsorbed thiocyanate as the supporting electrolyte is changed are within the experimental error and are probably not meas-

ures of the competition between nitrate or perchlorate and thiocyanate for adsorption sites.

Since fluoride displays the smallest tendency toward specific adsorption, the values for adsorbed thiocyanate obtained in this supporting electrolyte should match most closely the values that would occur in a pure 2-m*M* KSCN solution. WROBLOWA, KOVAC AND BOCKRIS[5] have recently published extensive tables of charge–potential data for solutions of several anions at mercury electrodes. Thiocyanate is included in this compilation although no data is supplied for concentrations below 10 m*M*. Thiocyanate appears to obey a Temkin-type isotherm[5] and extrapolation of the isotherm given by WROBLOWA *et al.*, to a concentration of 2 m*M* gives the values for adsorbed thiocyanate in the third column of Table 3. The corresponding values obtained in this study are shown in the fourth column. The agreement between the two columns is surprisingly good in view of the complete independence of the two methods that were used and the extrapolation of the isotherm that was required.

TABLE

SPECIFICALLY ADSORBED THIOCYANATE FROM 2-m*M* KSCN SOLUTION

Potential (mV vs. S.C.E.)	*Electronic[a] charge on electrode ($\mu C/cm^2$)*	*Specifically adsorbed thiocyanate ($\mu C/cm^2$)*	
		From extrapolated data of Wroblowa et al.[5] (no supporting electrolyte present)	*From this study (1 F NaF also present)*
−800	−11.0	0	0
−600	− 6.3	0	1.2 ± 3
−200	+ 9.4	4	9 ± 3
0	+23.4	18	18 ± 3

[a] The absolute values of the charge on the electrode was determined at −100 mV by drop extrusion. At other potentials, the charge was calculated from its value at −1000 mV and data such as those in Fig. 4.

Adsorption of $Hg(SCN)_2$

It was mentioned earlier that very extensive adsorption of $Hg(SCN)_2$ appears to occur at the mercury electrode at +300 mV. Equilibrium with respect to this adsorption was not reached during the anodic oxidation of the electrode in thiocyanate solutions, but by starting with solutions of $Hg(SCN)_2$, equilibrium could be established. Cathodic chronocoulometric experiments with such solutions (Fig. 3) allowed values for the adsorption of the $Hg(SCN)_2$ to be obtained. It is noteworthy that the *Q*-intercept in Fig. 3 is much larger than for the corresponding plot with 2-m*M* thiocyanate solution (potential step from −200 to +300 mV) in Fig. 2 although the slopes of the two plots are almost equal, as expected.

To obtain values for the quantity of adsorbed $Hg(SCN)_2$ from plots such as the one in Fig. 3, double-layer charging corrections were needed. These were obtained by the mercury drop extrusion technique[1]. A new drop was extruded into a stirred, 1-m*M* $Hg(SCN)_2$ solution at a selected initial potential and the charge flowing into the double-layer capacitance was measured. The process was repeated in a pure thiocyanate solution at −200 mV and the difference between the two charge values was used as the double-layer charging correction. The composition of the thiocyanate

solutions into which the mercury electrodes were extruded was adjusted to match the thiocyanate composition to which the electrode was exposed at −200 mV upon reduction of the $Hg(SCN)_2$. This was readily accomplished when the supporting electrolytes contained excess thiocyanate, but with thiocyanate-free 1-m*M* $Hg(SCN)_2$ solutions the electrode finds itself at −200 mV in a solution of thiocyanate more concentrated than 2-m*M* because of the thiocyanate produced from reduction of the adsorbed $Hg(SCN)_2$. No attempt was made to correct for this possible source of error in the double-layer charging correction. It is thus likely that the values for adsorbed $Hg(SCN)_2$ in thiocyanate-free solution are somewhat high.

Table 4 summarizes the data obtained for $Hg(SCN)_2$ adsorption. In every case but one, the double-layer charging correction was positive; that is, the observed $Q-t^{\frac{1}{2}}$ intercepts were below the value corresponding to adsorbed $Hg(SCN)_2$. This unusual circumstance, that corresponds, effectively, to a negative integral capacitance for the double-layer, arises because the adsorption of $Hg(SCN)_2$ so lowers the double-layer capacitance that there is less positive charge at the more positive potentials where $Hg(SCN)_2$ is adsorbed than at the less positive potentials where it is reduced to provide free thiocyanate ion.

The initial potentials indicated in Table 4 were the equilibrium potentials of the hanging mercury drop electrode in each solution. The $Hg-Hg(SCN)_2$ couple poises the electrode potential very strongly so it was necessary to ensure that the initial potential at which the electrode was potentiostated corresponded to its true equilibrium potential. Experiments were also performed in which the electrode was left at open circuit, where it quickly adopted its equilibrium potential. The control potential of the potentiostat was set at −200 mV and the electrode was abruptly connected to the control circuit and the resulting faradaic current was integrated. The results of these experiments were identical to those in Table 4.

The dependence of the values of Γ in Table 4 on the concentration of free thiocyanate is in accord with our assumption that it is the least soluble $Hg(SCN)_2$ species that is adsorbed from all of the solutions.

The values for adsorbed $Hg(SCN)_2$ in Table 4 are quite large and it is likely that part of the $Q-t^{\frac{1}{2}}$ intercept is due to a precipitate of $Hg_2(SCN)_2$ on the electrode rather than adsorbed $Hg(SCN)_2$, especially at lower concentrations of free thiocyanate. If equilibrium were maintained, substantial amounts of $Hg_2(SCN)_2$ should be formed. The solubility product of $Hg_2(SCN)_2$ is given[7] as $3 \cdot 10^{-20}$, the dissociation constant for[7] $Hg(SCN)_2$ is $5 \cdot 10^{-17}$, and the disproportionation constant[8] for Hg_2^{2+} is $6 \cdot 10^{-3}$. Thus, the equilibrium constant for the reaction

$$Hg + Hg(SCN)_2 = Hg_2(SCN)_2 \tag{3}$$

is $3 \cdot 10^5$ and a reaction between metallic mercury and mercuric thiocyanate is expected for $Hg(SCN)_2$ concentrations above about $3.3 \cdot 10^{-3}$ m*M*. However, the polarographic data of NYMAN AND ALBERTS[6] suggest that the rate of establishment of equilibrium for reaction (3) may be rather slow.

In solutions containing excess free thiocyanate ion, the relevant equilibrium becomes

$$Hg + Hg(SCN)_4^{2-} = Hg_2(SCN)_2 + 2\ SCN^- \tag{4}$$

The dissociation constant[7] for $Hg(SCN)_4^{2-}$ is $1 \cdot 10^{-22}$ so the equilibrium constant

TABLE 4

ADSORPTION OF $Hg(SCN)_2$ AT MERCURY

Electrode area, 0.032 cm^2

Expr. no.	*Soln. composition*	*Electronic charge on electrode*		*Potential step limits (mV)*	*Double-layer charging correction (μC)*	*$Q-t^{\frac{1}{2}}$ intercept (μC)*	*$\Gamma_{Hg(SCN)_2}$ (moles/cm^2 · 10^{10})*
		Potential (mV vs. S.C.E.)	*q (μC)*				
1	1 *M* KNO_3, 1 m*M* $Hg(SCN)_2$	+267	+0.07	+267 to −400	+0.06	2.0	3.3
	1 *M* KNO_3, 2 m*M* NaSCN	−400	+0.13	—	—	—	—
2	1 *M* KNO_3, 0.01 *M* NaSCN, 1 m*M* $Hg(SCN)_2$	+103	+0.23	+103 to −400	−0.08	2.1	3.1
	1 *M* KNO_3, 0.01 *M* NaSCN	−400	+0.15	—	—	—	—
3	0.9 *M* KNO_3, 0.1 *M* NaSCN, 1 m*M* $Hg(SCN)_2$	− 27	+0.03	−27 to −400	+0.18	1.3	2.3
	0.9 *M* KNO_3, 0.1 *M* NaSCN	−400	+0.21	—	—	—	—
4	1 *M* NaSCN, 1 m*M* $Hg(SCN)_2$	−143	+0.10	−143 to −400	+0.29	0.5	1.2
	1 *M* NaSCN	−400	+0.39	—	—	—	—

for reaction (4) is $5.5 \cdot 10^{-1}$. Thus, no formation of $Hg_2(SCN)_2$ is to be expected with millimolar $Hg(SCN)_4^{2-}$ for concentrations of thiocyanate ion greater than about 0.023 *M*.

Experiments 3 and 4 in Table 4 correspond to SCN^- concentrations greater than 0.023 *M* yet substantial adsorption of Hg(II) is observed. There is thus little doubt that $Hg(SCN)_2$ is strongly adsorbed from these solutions.

In solutions containing no free thiocyanate (experiment 1 in Table 4) some $Hg_2(SCN)_2$ formation seems likely so that the values for Γ under these conditions are probably high. It should be emphasized, however, that this uncertainty in the $Hg(SCN)_2$ data does not affect the validity of the results for SCN^- adsorption where there is no possible ambiguity about the nature of the adsorbed species, and the final procedure used to correct for double-layer charging should be valid whether the product of the electrode reaction is $Hg(SCN)_2$ or $Hg_2(SCN)_2$ or both.

CONCLUSIONS

The ability of the chronocoulometric procedure to measure rather small quantities of adsorbed anions that form mercury complexes is clearly demonstrated by the data presented here. It seems less likely that anions such as the halides that form insoluble mercurous salts will be as readily studied as thiocyanate because of the complications resulting from precipitate formation at the electrode surface, but we intend to try.

ACKNOWLEDGEMENT

This work was supported in part by the U.S. Army Research Office (Durham). The electronic apparatus was designed by GEORGE LAUER. Helpful additional experiments were performed by R. L. MYERS.

SUMMARY

The adsorption of thiocyanate anion on mercury was measured by means of a new electrochemical technique, chronocoulometry. Extensive adsorption of $Hg(SCN)_2$ was also discovered and the influence of free thiocyanate ion on this adsorption was evaluated. An interesting unexpected result of this work was the demonstration of an apparent negative integral double-layer capacitance for mercury over part of the potential range investigated.

REFERENCES

1 F. C. ANSON, *Anal. Chem.*, 38 (1966) 54.
2 F. C. ANSON, *ibid.*, 36 (1961) 932.
3 J. CHRISTIE, G. LAUER, R. A. OSTERYOUNG AND F. C. ANSON, *ibid.*, 35 (1963) 1979.
4 R. A. OSTERYOUNG AND F. C. ANSON, *ibid.*, 36 (1964) 975.
5 H. WROBLOWA, Z. KOVAC AND J. O'M. BOCKRIS, *Trans. Faraday Soc.*, 61 (1965) 1523.
6 C. J. NYMAN AND G. S. ALBERTS, *Anal. Chem.*, 32 (1960) 207.
7 *Stability Constants*, Part II, *Inorganic Ligands*, edited by J. BJERRUM, G. SCHWARZENBACH AND L. G. SILLÉN, Chem. Soc., London, 1958.
8 W. M. LATIMER, *Oxidation Potentials*, Prentice-Hall, New York, N.Y., 1952.

ANALYSE DE LA CINETIQUE DES REACTIONS AUX ELECTRODES POREUSES A GAZ PAR LES METHODES TRANSITOIRES*

M. BONNEMAY, G. BRONOËL, E. LEVART ET A. A. PILLA
Laboratoire d'Electrolyse du C.N.R.S., Bellevue, Hauts-de-Seine (France)
(Reçu le 21 janvier, 1966)

I. INTRODUCTION

Ainsi que l'ont montré de nombreux auteurs (voir entre autres réfs. 1–13) les difficultés rencontrées dans l'étude des phénomènes ayant lieu aux électrodes poreuses ou spongieuses sont dues principalement à leurs caractéristiques géométriques. Celles-ci déterminent l'existence d'un champ électrique non uniforme et sont par conséquent à l'origine des différences, parfois considérables, entre les valeurs locales de la densité de courant à l'interface métal–solution.

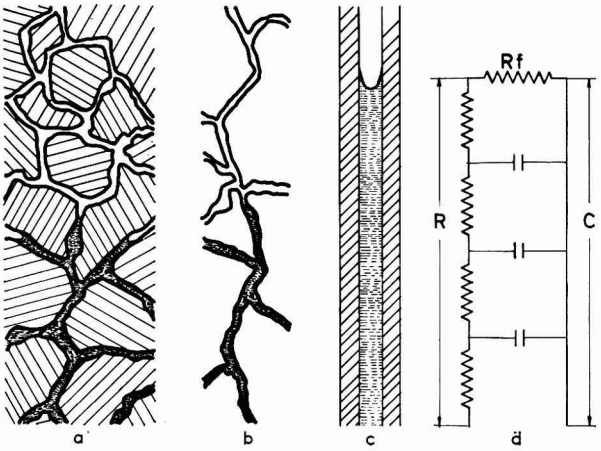

Fig. 1. Assimilation de l'électrode poreuse à gaz à une ligne de transmission. (a), Electrode poreuse; (b), motif élémentaire; (c), électrode monotubulaire; (d), ligne de transmission finie de type RC fermée sur une résistance caractéristique R_f.

Ainsi, pour les électrodes de géométrie expansée, les mesures de polarisation en régime stationnaire se révèlent d'une exploitation très délicate, surtout en ce qui concerne la correction de chute ohmique, et ne fournissent de toute façon qu'un nombre restreint d'informations.

On montrera dans cette communication que les méthodes utilisant un régime transitoire sont capables, en revanche, de donner de nombreuses indications sur les propriétés essentielles de ces électrodes.

* Présentée en partie à la 15e Réunion du C.I.T.C.E., Londres, Septembre, 1964 (abstr. 3.4).

Toutefois, l'application aux systèmes poreux des méthodes impulsionnelles ne peut être envisagée qu'après une analyse approfondie de leur structure. Le plan général de l'étude sera le suivant:

(i) Décomposition du système poreux complexe (Fig. 1a) en éléments constitutifs (pores) (Fig. 1b).

(ii) Assimilation d'un pore (élément à section variable) à une électrode monotubulaire (modèle cylindrique) (Fig. 1c).

(iii) Détermination des propriétés électrochimiques du modèle (en particulier localisation de la zone réactionnelle).

(iv) Choix d'un circuit électrique équivalent à l'électrode modèle (ligne de transmission de type RC) (Fig. 1d).

(v) Détermination des équations caractéristiques de la ligne de transmission ainsi définie, lorsqu'elle est soumise à une impulsion galvanostatique ou tensiostatique.

(vi) Vérification des équations proposées sur un système électrochimique dont les paramètres sont connus.

(vii) Analyse du comportement d'un poreux en régime transitoire.

(viii) Vérification expérimentale sur un poreux.

II. COMPORTEMENT DES ÉLECTRODES MODÈLES EN RÉGIME TRANSITOIRE

1. Etude théorique

Dans une communication précédente[14], on a développé les raisons du choix d'une électrode monotubulaire comme modèle élémentaire d'une électrode poreuse à gaz. Il s'agit d'un tube cylindrique de diamètre assez faible, de l'ordre de 0.5 mm, métallisé intérieurement et partiellement immergée dans une solution d'électrolyte. Ce modèle permet d'éviter les effets de convection (dans un poreux, l'apport des réactifs se fait essentiellement par diffusion) et, en outre, de reproduire assez fidèlement les phénomènes capillaires existant dans un pore réel.

Les expériences préliminaires effectuées sur des électrodes capillaires d'argent en présence d'oxygène et de KOH 5 *N* ont permis de constater que la zone réactionnelle efficace est limitée à une région de surface très réduite, située au-dessus du raccordement du ménisque à la paroi[15,16]. Bien entendu, cette localisation n'intervient qu'après l'épuisement du gaz dissous dans l'électrolyte contenu dans le capillaire. Sur le plan pratique, il en résulte la nécessité de prépolariser l'électrode avant de la soumettre à une impulsion.

Comme, dans ces conditions, la majeure partie du tube peut être considérée comme électrochimiquement inerte, on peut identifier cette électrode modèle à une ligne de transmission de type RC. Les éléments ohmiques, R, de cette ligne représentent la résistance de la colonne électrolytique et les éléments capacitifs, C, traduisent la capacité de double couche du système. Les éléments capacitifs sont supposés identiques sur toute la longueur, L, du tube, ce qui en toute rigueur n'est pas exact, car la tension appliquée à l'interface métal–solution varie le long du tube. Cependant, dans certaines conditions expérimentales (impulsion de faible amplitude et capacité sensiblement indépendante du potentiel), cette approximation ne conduira pas à une erreur appréciable.

La ligne RC ainsi définie est fermée à son extrémité sur une résistance R_f qui représente assez correctement l'impédance de polarisation de l'électrode, étant donné

que la composante capacitive de celle-ci peut être négligée devant la capacité totale de l'électrode. En effet, grâce à la prépolarisation et compte-tenu des dimensions de l'électrode, l'étendue de la partie électrochimiquement active (film) est très faible par rapport à la surface totale.

Les équations caractéristiques classiques, auxquelles obéissent la tension V et le courant I au point x de la ligne, sont les suivantes:

$$\frac{\partial V(x,t)}{\partial x} = -\frac{R}{L} I(x,t) \tag{1}$$

et

$$\frac{\partial I(x,t)}{\partial x} = -\frac{C}{L}\frac{\partial V(x,t)}{\partial t} \tag{2}$$

elles donnent:

$$\frac{\partial^2 V(x,t)}{\partial x^2} = \frac{RC}{L^2}\frac{\partial V(x,t)}{\partial t} \tag{3}$$

et

$$\frac{\partial^2 I(x,t)}{\partial x^2} = \frac{RC}{L^2}\frac{\partial I(x,t)}{\partial t} \tag{4}$$

(a) *Impulsion galvanostatique.* Lorsqu'une impulsion galvanostatique d'amplitude I_0 est appliquée à l'origine ($x=0$) de la ligne de longueur L, préalablement soumise à un courant stationnaire (prépolarisation) dont la valeur définit l'état de référence, les conditions aux limites peuvent être définies comme suit:

$$t=0,\ x=0:\ I=I_0 \quad \text{et} \tag{5}$$

$$x=L:\ I(L,t) = V(L,t)/R_f \tag{6}$$

L'expression explicite de la fonction $V=f(x,t)$ peut alors être obtenue à l'aide de la transformation de Laplace (avec s paramètre opérationnel). La transformée de la fonction recherchée s'écrit en effet comme suit[17]:

$$U(x,s) = \frac{I_0 R\left[\frac{R}{R_f}\operatorname{sh}\left(1-\frac{x}{L}\right)\sqrt{RCs}+RCs\operatorname{ch}\left(1-\frac{x}{L}\right)\sqrt{RCs}\right]}{s\sqrt{RCs}\left(\frac{R}{R_f}\operatorname{ch}\sqrt{RCs}+\sqrt{RCs}\operatorname{sh}\sqrt{RCs}\right)} \tag{7}$$

Plus particulièrement, pour $x=0$ (ce qui correspond au cas en pratique le plus intéressant où la tension est mesurée à l'aide d'une électrode de comparaison placée dans le plan frontal de l'électrode monotubulaire), cette équation devient:

$$U(0,s) = \frac{I_0 R\left(\frac{R}{R_f}+\sqrt{RCs}\coth\sqrt{RCs}\right)}{s\sqrt{RCs}\left(\frac{R}{R_f}\coth\sqrt{RCs}+\sqrt{RCs}\right)} \tag{8}$$

La transformation inverse de cette dernière fonction peut être effectuée grâce à l'une ou à l'autre des deux approximations suivantes:

(1) $\coth RCs = 1$, ce qui donne

$$U_1 = \frac{I_0}{s}\sqrt{\frac{R}{Cs}} \tag{9}$$

(2) $\coth\sqrt{RCs} = 1/\sqrt{RCs} + \sqrt{RCs}/3$, ce qui donne

$$U_2 = \frac{I_0 R\left[RCs + 3\left(\frac{R}{R_f}+1\right)\right]}{s\left[\left(\frac{R}{R_f}+3\right)RCs + \frac{3R}{R_f}\right]} \tag{10}$$

En retransformant les expressions (9) et (10), on obtient respectivement:

$$V(0,t) = 2I_0\sqrt{\frac{Rt}{\pi C}} \tag{11}$$

et

$$V(0, t) = I_0(R+R_f) - I_0\left[(R+R_f) - \left(\frac{RR_f}{R+3R_f}\right)\right]\exp\left[-\frac{3t}{(R+3R_f)C}\right] \tag{12}$$

Lorsque $t \to \infty$, V tend vers la valeur limite caractéristique du nouvel état stationnaire:

$$V(0, \infty) = I_0(R+R_f) \tag{13}$$

Par ailleurs, il résulte de la linéarisation de l'éqn. (12) que, pour des valeurs de R_f/R grandes (par exemple $R_f/R > 30$), une portion de la courbe expérimentale peut être assimilée avec une bonne approximation à une fonction linéaire de la forme:

$$V(0, t) = I_0\left(\frac{R}{3} + \frac{t}{C}\right) \tag{14}$$

(b) *Impulsion tensiostatique.* Dans ce cas, c'est une tension stationnaire, préalablement appliquée, qui sert d'état de référence; les conditions aux limites sont alors les suivantes:

$$t = 0,\ x = 0:\ V = V_0 \tag{15}$$

et

$$x = L:\ V(L, t) = I(L, t)R_f \tag{16}$$

Par le calcul opérationnel, on obtient la fonction transformée du courant:

$$Y(x, s) = \frac{V_0\sqrt{RCs}\left[\sqrt{RCs}\,\mathrm{sh}\left(1 - \frac{x}{L}\right)\sqrt{RCs} + \frac{R}{R_f}\,\mathrm{ch}\left(1 - \frac{x}{L}\right)\sqrt{RCs}\right]}{Rs\left(\sqrt{RCs}\,\mathrm{ch}\sqrt{RCs} + \frac{R}{R_f}\,\mathrm{sh}\sqrt{RCs}\right)}. \tag{17}$$

Cette équation devient pour $x = 0$:

$$Y(0, s) = \frac{V_0\sqrt{RCs}\left(\sqrt{RCs} + \frac{R}{R_f}\coth\sqrt{RCs}\right)}{Rs\left(\sqrt{RCs}\coth\sqrt{RCs} + \frac{R}{R_f}\right)}. \tag{18}$$

Lorsque l'approximation $\coth\sqrt{RCs} = 1$ est possible, on obtient:

$$Y_1 = \frac{V_0}{s}\sqrt{\frac{Cs}{R}}, \tag{19}$$

tandis que l'approximation $\coth\sqrt{RCs} = 1/\sqrt{RCs} + \sqrt{RCs}/3$ donne:

$$Y_2 = \frac{V_0[3(R_fCs+1)+RCs]}{s[R_fRCs+3(R+R_f)]}. \tag{20}$$

En transformant les expressions (19) et (20), on obtient respectivement:

$$I(0, t) = V_0\sqrt{\frac{C}{\pi Rt}} \tag{21}$$

et

$$I(0, t) = \frac{V_0}{R+R_f} - V_0\left(\frac{1}{R+R_f} - \frac{R+3R_f}{RR_f}\right)\exp\left[-\frac{3t(R+R_f)}{CRR_f}\right]. \tag{22}$$

Il en résulte que, pour $t \to \infty$, I tend vers la limite prévisible:

$$I(0, \infty) = \frac{V_0}{R+R_f}. \tag{23}$$

L'équation (22) peut être linéarisée pour des valeurs de R_f/R grandes, ce qui donne:

$$I(0, t) = \frac{3V_0}{R}\left(1 - \frac{3t}{RC}\right). \tag{24}$$

(c) *Discussion*. La difficulté de trouver directement la transformée inverse des fonctions (8) et (18), nous a amenés à identifier la fonction $\coth\sqrt{RSs}$ soit à 1, soit $1/\sqrt{RCs}+\sqrt{RCs}/3$. La première de ces approximations est justifiée pour des valeurs de s grandes, c'est-à-dire pour les instants initiaux, la seconde pour des valeurs petites, c'est-à-dire pour des temps proches de l'état stationnaire. On notera que l'erreur maximale, résultant de l'emploi de la meilleure de ces deux approximations, intervient pour $s \simeq 2.7/RC$. Dans les conditions les plus défavorables ($R \ll R_f$ ou $R \gg R_f$), elle peut atteindre $\pm 8\%$, mais elle est en général beaucoup plus faible, surtout lorsque le rapport R/R_f est compris entre 1 et 3.

Des vérifications effectuées sur une ligne de transmission dont le rapport R/R_f, pouvait varier de 0.1–10, nous ont permis de constater que les éqns. (11) et (21) décrivent en effet correctement la portion initiale des courbes expérimentales $V(t)$ et $I(t)$ jusqu'à un point tel ($t \simeq RC/\pi$) qu'on puisse leur substituer avantageusement les éqns. (12) et (22) qui restent à leur tour valables jusqu'à l'établissement d'un nouvel état stationnaire. En définitive, les deux approximations précitées suffisent à décrire la fonction caractéristique depuis $t = 0$ jusqu'à $t = \infty$.

De plus, si la linéarisation est possible, les éqns. (13) et (23) peuvent être utilisées dans le domaine de temps approprié. L'écart maximal observé dans ces expressions ne dépassait jamais 5%.

2. *Etude expérimentale*

Afin de justifier les hypothèses qui nous ont permis d'assimiler à une ligne de

transmission une électrode tubulaire à gaz, nous avons effectué une série d'expériences en régime d'impulsion galvanostatique à l'aide de capillaires argentés intérieurement, la réaction d'électrode étant la réduction de l'oxygène en milieu KOH 5 N.

Préalablement à l'impulsion, l'électrode est polarisée par un courant continu variant selon le cas de 10–50 μA, tandis que l'amplitude de l'impulsion ne dépasse jamais 5 μA, elle est atteinte en moins de 2 μs. Dans tous les cas, la durée de l'impulsion est limitée à l'obtention de l'état stationnaire (environ 1 s).

Ces expériences nous ont permis de calculer à partir des courbes $V=f(t)$ obtenues et à l'aide des éqns. (11), (12) et (13) les valeurs de R, C et R_f d'un certain nombre d'électrodes ayant des caractéristiques géométriques différentes.

Par ailleurs, l'examen par radiographie X permet de connaître à tout instant la hauteur de la colonne liquide et le diamètre du tube. La résistivité de l'électrolyte (1.85 Ωcm) est connue. Par ailleurs, la capacité spécifique du système (50 μF/cm^2) a été déterminée par une mesure de la pente initiale de la courbe de réponse à une impulsion galvanostatique appliquée à une électrode plane de même nature. On peut alors calculer R et C.

La confrontation des résultats obtenues par ces deux méthodes totalement indépendantes a été très concluante[18]. L'écart entre les valeurs trouvées était de l'ordre de 7% pour les résistances et de 15% pour les capacités.

III. COMPORTEMENT D'UNE ÉLECTRODE POREUSE EN RÉGIME TRANSITOIRE

1. Considérations théoriques

La prévision du comportement d'une électrode de géométrie expansée en régime impulsionnel ne peut être faite qu'en tenant compte de sa structure. Plus particulièrement, la connaissance préalable de la fonction de répartition des pores et du coefficient de tortuosité est nécessaire. La détermination de ces grandeurs caractéristiques pourra être effectuée par des méthodes classiques, telles que la porosimétrie au mercure ou la micrographie.

Considérons tout d'abord le cas d'un poreux dont la fonction de répartition $n=f(\phi)$ (où ϕ est le diamètre d'un pore) présente un maximum très prononcé situé autour d'une valeur moyenne ϕ_m (structure monomodale centrée). Cependant, tous les pores ne contiennent pas nécessairement un ménisque et ne sont donc pas électrochimiquement actifs. Seul sera étudié ici le comportement des pores efficaces. En effet, on peut montrer que le fait de ne pas considérer les pores non efficaces n'entraîne pas une erreur sur l'évaluation des paramètres que l'on se propose de déterminer. On pourra alors admettre que tous les pores efficaces, au nombre N, sont de diamètre ϕ_m.

Si le poreux est soumis à une impulsion galvanostatique d'amplitude I_0, le courant se répartira uniformément entre tous les pores efficaces, à chacun d'eux correspondra alors un courant partiel I_0/N et une tension commune $V(0, t)$. Connaissant expérimentalement la réponse en tension de l'électrode à une impulsion galvanostatique, on pourra déduire de la courbe $V=f(t)$ les valeurs des paramètres caractéristiques R, C et R_f du poreux. A l'aide de ces paramètres, il est possible de déterminer d'une part l'étendue de la partie noyée de l'électrode (x) et d'autre part celle de la zone électrochimiquement active (y).

Pour déterminer x, on se servira des deux équations suivantes:

$$RN = r = \frac{4x\varrho}{\pi\phi_m{}^2} \tag{25}$$

et

$$\frac{C}{N} = c = \pi\phi_m x\gamma \tag{26}$$

dans lesquelles R et C sont données par l'expérience. La résistivité ϱ de l'électrolyte est en général connue et on peut admettre que sa valeur moyenne dans les pores est égale à celle au sein de la solution. La valeur de la capacité spécifique, γ, peut être déterminée en effectuant une mesure classique de capacité[19] sur un élément frontal de l'électrode dont les pores ont été préalablement remplis d'une résine isolante. En effet, en divisant la valeur de la capacité ainsi déterminée par l'aire de la partie métallique de la surface frontale (surface frontale apparente moins surface des pores débouchants), on atteint la valeur de γ. Enfin, le paramètre ϕ_m (diamètre moyen d'un pore efficace) peut être déterminé par une étude texturale. La résolution du système des éqns. (25) et (26) permet donc de calculer x et N.

Si le paramètre R_f, accessible expérimentalement en même temps que R et C, n'intervient pas dans le calcul de la longueur x de la partie noyée de l'électrode, en revanche, sa connaissance est absolument indispensable pour déterminer la longueur y de la partie électrochimiquement active. De plus, des hypothèses concernant la distribution du champ dans cette région doivent pour cela être formulées. C'est ainsi que, dans le cas le plus simple, on admettra que la densité de courant est uniforme sur toute la longueur de la zone active et que, de plus, la résistante de polarisation d'un pore r_f s'identifie avec une bonne approximation à la résistance r_s caractéristique des seuls processus interfaciaux (transfert, adsorption). Dans ces conditions, on peut écrire la relation:

$$R_f N = r_f = \beta/\pi\phi_m y \tag{27}$$

où β, résistance spécifique des processus d'interface, peut être déterminée, par extrapolation à vitesse de rotation infinie, à partir des mesures de polarisation en régime stationnaire sur une électrode tournante[20]. Le nombre des pores, N, ayant été déterminé précédemment, la longueur, y, de la zone active peut être tirée de l'éqn. (27).

D'une manière plus rigoureuse, on devra tenir compte du fait que le lieu réactionnel est souvent constitué par les parties de l'électrode recouvertes d'un film de mouillage s'étendant au-delà des ménisques. Dans ces conditions, r_f ne peut plus être confondue avec r_s, mais doit être considérée comme résistance résultante d'une ligne de longueur y composée d'éléments résistifs représentant d'une part la conduction dans le film et d'autre part la cinétique des processus d'interface. Par ailleurs, il en résulte que la densité de courant dans la zone réactionnelle ne peut plus être considérée comme uniforme. Cependant, il a été montré que, même dans ces dernières conditions, la détermination de la longueur, y, reste possible[16].

Il faut cependant souligner que dans les considérations qui viennent d'être faites, on a implicitement transféré à l'électrode poreuse les propriétés particulières de l'électrode monotubulaire, qui avaient permis d'assimiler celle-ci à une ligne de transmission. En particulier, il convient de reconsidérer la notion de localisation prononcée de la zone réactionnelle. Il a bien été constaté pour les électrodes monotubulaires constituées d'un catalyseur suffisamment actif que la zone réactionnelle n'occupait pas

plus de 10% de l'aire totale de l'interface solide–liquide. Pour un pore d'un diamètre considérablement plus petit, il conviendrait donc d'apprécier la dimension maximale de la zone réactionnelle et la comparer à la longueur noyée du pore. Actuellement, notons que la couche d'arrêt (zone à petits pores) des électrodes à double porosité a le plus souvent une épaisseur de l'ordre de quelques dixièmes de millimètre, les pores ayant un diamètre compris entre 1 et 10 μ. Si le facteur de tortuosité est de l'ordre de 1.7, il conviendra donc que la longueur de la partie active soit inférieure à 100 μ pour que le schéma d'une réaction localisée puisse être encore valable. En définitive, la réponse d'une telle électrode à l'impulsion permettra de vérifier la validité des hypothèses qui peuvent être émises sur l'étendue de la zone active dans le poreux.

Le cas d'un poreux dont la courbe de répartition $n=f(\phi)$ présente plusieurs maximums (poreux polymodal) ou bien encore le cas général où la courbe de répartition est plus ou moins étalée sur un vaste domaine de diamètres doivent être examinés. Si l'on divise l'ensemble des pores en un certain nombre de familles, les membres d'une même famille se caractérisant par des sections sensiblement égales, il sera possible d'assimiler chaque groupe ainsi défini à un gros pore dont les paramètres seront respectivement

$$R_i = \frac{r_i}{n_i},\ C_i = C_i n_i \text{ et } R_{f,i} = \frac{r_{f,i}}{n_i}$$

avec n_i représentant le nombre de pores appartenant à la famille i.

Par conséquent, le poreux pourra être considéré comme constitué d'un nombre restreint d'éléments, par exemple de deux ou trois si l'on se contente d'une approximation très grossière, ayant chacun des paramètres r, c et r_f différents. En régime impulsionnel, à un instant t donné, l'impédance opérationnelle correspondante de chaque élément aura non seulement une valeur différente, mais en général aussi une forme différente. En effet, certains pores auront rapidement atteint l'état stationnaire, tandis que d'autres seront seulement au début de leur charge (partie parabolique de la courbe de réponse). Il est évident que l'analyse du comportement d'un tel poreux est difficile.

Toutefois, cette analyse peut être tentée en régime tensiostatique. Ceci puisque le courant total mesuré à chaque instant est bien la somme des courants issus de chaque pore, cette règle d'additivité n'étant pas valable pour les tensions en régime galvanostatique.

Ainsi, en divisant les pores en deux groupes dont le premier (fraction α) comprendra tous les pores se trouvant dans la région de réponse en $\sqrt{t}$ (début de charge) et le second (fraction $1-\alpha$) correspondra aux pores dont la réponse en courant aura déjà atteint la forme exponentielle (fin de charge). La fraction α dépendra évidemment de l'instant d'observation et variera progressivement de 1–0.

En se plaçant à un instant suffisamment proche du début de l'impulsion, on pourra considérer $\alpha=1$ et confronter la valeur de la pente initiale P de la courbe $I=f(t^{-\frac{1}{2}})$ avec la valeur calculable à partir de la fonction $n=f(\phi)$. En effet, P ne s'exprime alors qu'à l'aide des paramètres r_i et c_i et comme ces derniers peuvent être reliés sans ambiguité à ϕ_i et n_i, on en déduit qu'on peut calculer la valeur prévisible de P, connaissant la courbe de répartition des poreux.

Au contraire, si l'on se place à un instant suffisamment proche de l'état stationnaire, on peut considérer que $\alpha=0$, c'est-à-dire que l'évolution du courant dans

chaque pore, quel que soit son diamètre, peut être décrite par une expression de forme exponentielle[22]. Celle-ci comprend, en plus des paramètres r_i et c_i, le paramètre faradique $r_{f,i}$ qui, contrairement aux précédents, ne peut être calculé en tenant compte des seuls facteurs structuraux de l'électrode; cependant, des théories développées par ailleurs[21], permettent d'évaluer correctement la résistance faradique $r_{f,i}$.

Le calcul du courant global produit durant cette période reste possible, point par point, mais il n'est pas possible d'obtenir une formule générale exprimant ce courant.

2. Etude expérimentale

Il résulte des considérations développées dans les chapitres précédents que l'analyse des courbes de réponse obtenues en régime transitoire constitue une méthode très intéressante d'étude des électrodes poreuses et permet en particulier de mettre en évidence des facteurs texturaux. En effet, la courbe de réponse à une impulsion galvanostatique ne peut être correctement décrite par les équations approchées (11) et (12) que si l'électrode se caractérise par un spectre de porosité monomodal centré. De plus, pour que cette courbe puisse présenter une portion rectiligne, le rapport R_f/R doit être suffisamment élevé.

Afin de vérifier ces conclusions, on a réalisé deux électrodes de texture très différente. L'une était caractérisée par le fait que tous ses pores avaient des diamètres sensiblement égaux; l'autre électrode présentait au contraire un spectre de porosité très étalé. Dans les deux cas, l'activité électrochimique de l'électrode était telle que, dans les conditions choisies de fonctionnement, la résistance globale d'interface R_f était nettement plus élévée que la résistance R de la phase électrolytique. Le montage utilisé pour les mesures était celui de l'impulsion galvanostatique[26]. Les courbes obtenues en régime galvanostatique ont bien montré que seulement pour l'électrode à répartition monomodale centrée, une partie rectiligne était visible. Le calcul des paramètres R, C et R_f, effectué pour cette dernière électrode, a permis de trouver des valeurs en bon accord avec celles que sa structure permettait par ailleurs de prévoir.

En ce qui concerne l'électrode se caractérisant par un spectre étalé de porosité, la détermination de ses paramètres électrochimiques pourrait être tentée, comme nous l'avons vu, en interprêtant les résultats des mesures effectuées en régime tensiostatique. Cependant, comme il est généralement admis que les caractéristiques électrochimiques de telles électrodes sont bien moins bonnes que celles des électrodes à porosité uniforme, il nous a paru peu judicieux d'effectuer une analyse, d'ailleurs assez délicate, sur un système dont l'intérêt n'est pas évident. En revanche, nous montrerons à quels résultats permet d'aboutir la méthode d'analyse proposée dans le cas d'une électrode poreuse de conception industrielle.

Les électrodes utilisées pour cette étude nous ont été obligeamment fournies par le Centre de Recherches de Marcoussis de la Compagnie Générale d'Electricité. Il s'agit d'électrodes frittées qui ont été depuis plus de deux ans employées pour la construction des piles O_2/H_2 fonctionnant à basse température. Les études texturales effectuées sur ces électrodes avaient permis de préciser que la majeure partie des pores avait des diamètres voisins de 0.5 μ.

Un échantillon d'environ 10 mm^2 de surface frontale a été découpé et placé dans une cellule où les conditions habituelles de fonctionnement lui ont été imposées. Le gaz utilisé était l'oxygène, sa surpression était maintenue de 10 g/cm^2 inférieure à celle

de début de bullage. L'électrolyte, KOH 5 N, était maintenu à la température constant de 25°.

L'électrode a été polarisée cathodiquement de 25, 100, 150 et 200 mV et, le régime stationnaire ayant été atteint, une impulsion galvanostatique a été appliquée. Son amplitude était telle que la surtension maximale qui pouvait en résulter restait toujours inférieure à 10% de la polarisation permanente. Il a été constaté que, bien qu'il ne fût pas possible de décéler une portion rectiligne sur les courbes observées, celle-ci pouvaient être convenablement décrites par les éqns. (11) et (12) définies précédemment.

De ces observations, on peut formuler une première conclusion concernant les caractéristiques des électrodes étudiées. Il se confirme que leur spectre de porosité est très centré autour d'une valeur moyenne, puisque les équations établies pour l'électrode monotubulaire restent valables. Par ailleurs, la composante purement ohmique de la polarisation globale n'est visiblement pas négligeable devant la composante faradique. Les valeurs de R, C et R_f ont été calculées à l'aide des éqns. (11), (12) et (13) pour les différentes polarisations permanentes appliquées (voir tableau). Pour cela, le début de la courbe $V=f(t)$ a été retracé en fonction de $\sqrt{t}$, Fig. 2, et tout le reste sous la forme de log $((V_\infty - V)/V_\infty)=f(t)$, Fig. 3.

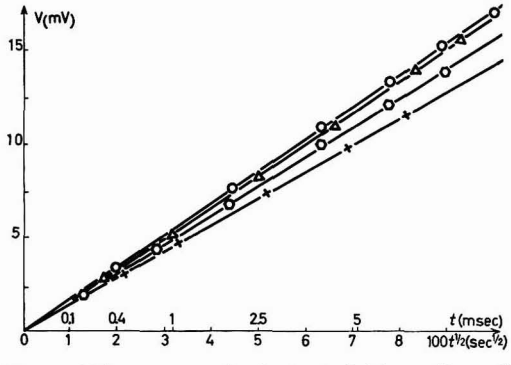

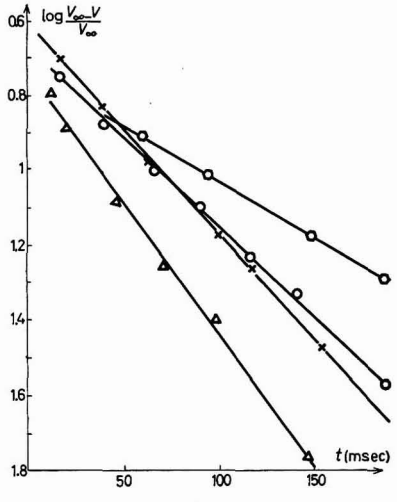

Fig. 2. Réponse pour les instants initiaux d'une électrode poreuse industrielle à une impulsion galvanostatique. Courbe $V = f(\sqrt{t})$. (⬡), 25; (○), 100; (×) 150; (△), 200 mV.

Fig. 3. Réponse pour les instants proches de l'état stationnaire de la même électrode. Courbe log $V_\infty - V/V_\infty = f(t)$. (⬡), 25; (○), 100; (×), 150; (△), 200 mV.

Les calculs effectués ensuite ont permis de déterminer d'une part à l'aide des éqns. (25) et (26) la longueur développée des canaux noyés, x, et d'autre part à l'aide de l'éqn. (27) la longueur de la région active, y. En divisant x par 1.7 (valeur estimée du coefficient de tortuosité), on atteint l'épaisseur de la partie noyée de l'électrode.

La valeur de la capacité spécifique γ (50 μF/cm²) avait préalablement été déterminée par la mesure de la pente initiale de la courbe de réponse à une impulsion galva-

nostatique, effectuée en milieu KOH 5 N sous atmosphère inerte. La résistance spécifique, β, (250 Ωcm^2) avait été déterminée en mesurant, dans le même milieu, mais en présence d'oxygène, le courant limite s'établissant pour une polarisation stationnaire donnée (25–200 mV) à une électrode tournante. Les deux séries d'expériences avaient été effectuées sur le même échantillon dont seule la surface frontale pouvait entrer en contact avec l'électrolyte, les pores ayant été remplies d'araldite.

L'ensemble des résultats obtenus est présenté sur le tableau suivant.

TABLEAU 1

Prépolarisation (mV)	R (Ω)[1]	C (F)[1]	R_f (Ω)[1]	x (μ)[2]	y (μ)[3]	δ (μ)[4]	N ($\cdot 10^8$)[2]
− 25	0.63	0.090	1.40	870	86	520	1.3
−100	0.47	0.060	1.38	600	87	350	1.2
−150	0.31	0.051	1.43	480	84	280	1.4
−200	0.27	0.034	1.75	340	69	200	1.2

[1] Valeurs rapportées à 1 cm^2 de surface frontale.
[2] Valeurs calculées en prenant $\gamma = 5 \cdot 10^{-5}$ Fcm^{-2}, $\varrho = 1.85$ Ωcm et $\phi_m = 0.5$ μ.
[3] Valeurs calculées en prenant $\beta = 250$ Ωcm^2 et $\phi_m = 0.5$ μ.
[4] Valeurs corrigées compte-tenu du coefficient de tortuosité $\tau = 1.7$.

L'examen des valeurs de R, C, x et δ obtenues fait apparaître une nette décroissance de l'étendue de la partie noyée de l'électrode en fonction de la prépolarisation appliquée. Ce résultat apporte une précision relative à la texture de l'électrode étudiée qui ne comporterait donc pas de couche d'arrêt bien définie comme celle qui caractérise les électrodes de type Bacon. En accord avec les observations précédemment effectuées sur des électrodes capillaires d'argent[15], le déplacement observé de la position moyenne des ménisques peut s'expliquer par une variation de la tension interfaciale en fonction de la prépolarisation.

En revanche, on constate que la longueur y de la zone réactionnelle est pratiquement indépendante de la prépolarisation. Rappelons que des constatations analogues ont été faites dans une étude de la distribution du champ à une électrode monotubulaire à gaz[21]. Il en résulte que les propriétés mises en évidence sur les électrodes modèles (localisation de la zone active dans un film de mouillage, indépendance de la cinétique des processus d'interface du potentiel) doivent également caractériser les électrodes poreuses étudiées.

En définitive, la zone remplie d'électrolyte aurait, pour une pression inférieure de 10 g/cm^2 à la pression de bullage, une épaisseur variant de 0.5–0.2 mm, cette dernière valeur étant celle obtenue lors des conditions habituelles de fonctionnement (200 mV de polarisation), tandis que la longueur de la zone électrochimiquement active serait dans les mêmes conditions de l'ordre de 70 μ. On peut en conclure qu'il serait possible de réduire jusqu'à 0.1 mm l'épaisseur de l'électrode sans en diminuer les performances.

Par ailleurs, la comparaison des valeurs des résistances obtenues permet d'aboutir à des conclusions analogues. En effet, comme à la température des essais (25°) la résistance R représente déjà 15–30% de la résistance globale observée, et qu'il est par ailleurs connu que l'élévation de température modifie peu la conductibilité de l'élec-

trolyte mais, en revanche, diminue considérablement la valeur du terme d'interface, on peut prévoir qu'à 70° la polarisation d'origine ohmique représentera 90% de la polarisation globale. Il en résulte que pour améliorer ces électrodes, il sera de loin plus intéressant de tenter de diminuer la chute ohmique dans leurs parties noyées que d'essayer d'accroître l'activité électrochimique du catalyseur.

Il semble bien que les données récentes concernant de nouvelles structures d'électrode[23–25] justifient cette orientation.

CONCLUSIONS

L'étude du comportement en régime transitoire des électrodes à géométrie expansée apporte de précieuses informations tant sur les phénomènes essentiels dont sont le siège les électrodes de puissance pour piles à combustible que sur la signification de certaines mesures électriques effectuées sur les systèmes électrochimiques à champ non uniforme.

En ce qui concerne la compréhension des phénomènes intervenant lors du fonctionnement des électrodes poreuses utilisées dans les piles à combustible, leur étude en régime transitoire permet non seulement de mieux connaître leur structure, mais encore de préciser la distribution du courant. Il a en effet été montré que l'analyse des courbes de réponse à une impulsion galvanostatique permet de différencier une structure à porosité monomodale centrée d'une texture à pores de diamètres très différents. Par ailleurs, il semble que l'analyse de l'écart obtenu entre la courbe de réponse de l'électrode et les courbes données par les équations caractéristiques (11) et (12) peut permettre de déterminer la fonction de distribution des pores. Par ailleurs, cette analyse permet de démontrer si l'électrode considérée comporte une zone réactionnelle de dimensions faibles par rapport à celle de la région noyée et dans ce cas de déterminer leurs longueurs respectives.

En ce qui concerne la signification des mesures électriques effectuées sur les systèmes à champ non uniforme, les considérations suivantes peuvent être formulées:

Il est évident que la réponse à une impulsion se traduit par un phénomène continu dans le temps. Ainsi, en régime galvanostatique, on ne peut trouver de discontinuité sur la courbe $V=f(t)$ d'un système à champ non uniforme puisque celui-ci est équivalent à un circuit électrique à paramètres distribués. La mesure de la chute ohmique sur un tel système ne peut donc se faire comme pour les systèmes à champ uniforme par observation d'un saut à l'enclanchement ou au déclanchement galvanostatique.

Pour les mêmes raisons, liées à la propagation progressive de l'impulsion dans la ligne, la valeur de la capacité mesurée en régime impulsionnel ou alternatif, dépendra de l'instant de l'observation ou de la fréquence du signal alternatif utilisé. En toute rigueur, une mesure directe ne pourra jamais être représentative de la totalité de l'interface solide–liquide.

A basse fréquence (ou aux temps assez grands), des effets faradiques se superposent aux effets purement capacitifs et à haute fréquence, la pénétration du signal dans le poreux ne sera que très faible, à la limite ($f\rightarrow\infty$) les régions frontales seront seules intéressées.

En revanche, l'analyse du comportement électrochimique des systèmes à champ non uniforme est rendue possible par l'emploi d'une méthode, telle celle que

nous avons décrite, qui consiste à représenter le système électrochimique sous la forme d'un circuit électrique équivalent à paramètres distribués.

Il apparaît donc qu'il est intéressant de tenter de rendre compte de l'influence de la structure des électrodes sur leurs propriétés électrochimiques en les assimilant à une série de mailles réparties selon un axe qui s'identifie à une des directions privilégiées de la structure.

REMERCIEMENTS

Les auteurs tiennent à exprimer leurs remerciements à MM. G. PESLERBE et J. SARRADIN pour l'aide qu'ils ont apporté dans la réalisation de la partie expérimentale de ce travail. De plus, ils remercient la Délégation Générale à la Recherche Scientifique et Technique pour l'aide financière apportée dans le cadre de la Convention No. 61 FR 075.

RÉSUMÉ

En assimilant à une ligne de transmission finie de type RC une électrode monotubulaire à triple contact, on obtient des équations permettant de prévoir sa réponse à une perturbation impulsionnelle, galvanostatique ou tensiostatique. La validité de ces équations a pu être vérifiée d'une part sur des lignes composées d'éléments connus et d'autre part sur des électrodes modèles de caractéristiques connues.

Dans la deuxième partie du travail, la théorie est étendue aux électrodes poreuses réelles, ceci grâce à l'hypothèse que ces dernières peuvent être considérées comme constituées de motifs ayant pour modèle l'électrode monotubulaire précédemment définie. Il en résulte que l'analyse du comportement d'un poreux en régime impulsionnel permet d'étudier sa texture et d'en déterminer les paramètres. Ces conclusions, appliquées à l'étude d'électrodes de conception industrielle, permettent de dégager les caractéristiques essentielles de l'électrode en fonctionnement et par conséquent de définir les conditions qui doivent être établies pour l'amélioration de ces électrodes.

SUMMARY

By simulating a monotubular electrode with triple contacts by a finite transmission line of type RC, equations enabling the prediction of its response to a galvanostatic or tensiostatic impulse, may be obtained. The validity of these equations has been verified for lines of known elements and electrode models of known characteristics.

In the second part of this work, the theory is extended to real porous electrodes on the basis of the hypothesis that the latter can be considered as composed of units having as model the monotubular electrode defined previously. As a result, the analysis of the behaviour of a porous electrode under impulse conditions enables its texture to be studied and the parameters determined. These conclusions applied to a study of commercial electrodes reveal the essential characteristics of the electrode in action and, consequently, define the conditions that should improve their performance.

BIBLIOGRAPHIE

1 J. J. COLEMAN, *Trans. Electrochem. Soc.*, 90 (1946) 545.
2 J. EULER ET W. NONNENMACHER, *Electrochim. Acta*, 2 (1960) 268.
3 R. K. BURSHTEIN, A. G. PSHENICHNIKOV ET N. A. SHUMILOVA, *Dokl. Akad. Nauk. SSSR*, 143 (1962) 1409.
4 O. S. KSENZHEK, *Russ. J. Phys. Chem.*, 36 (1962) 121.
5 A. WINSEL, *Z. Elektrochem.*, 66 (1962) 287.
6 H. B. URBACH, *Fuel Cells*, Vol. 2, G. J. YOUNG (Ed.), Reinhold, New York, 1960, p. 7.
7 F. G. WILL, *J. Electrochem. Soc.*, 110 (1963) 145, 152.
8 N. GUILLOU ET R. BUVET, *Electrochim. Acta*, 8 (1963) 489.
9 G. FEUILLADE, *Compt. Rend.*, 256 (1963) 2786.
10 E. A. GRENS ET C. W. TOBIAS, *Ber. Bunsenges. Physik. Chem.*, 68 (1964) 236.
11 L. G. AUSTIN ET H. LERNER, *Electrochim. Acta*, 9 (1964) 1469.
12 R. DE LEVIE, *Electrochim. Acta*, 8 (1963) 751.
13 F. A. POSEY, *J. Electrochem. Soc.*, 111 (1964) 1173.
14 M. BONNEMAY, G. BRONOËL ET E. LEVART, *Compt. Rend.*, 257 (1963) 3394.
15 M. BONNEMAY, G. BRONOËL ET E. LEVART, *Electrochim. Acta*, 9 (1964) 727.
16 M. BONNEMAY, G. BRONOËL, E. LEVART, A. A. PILLA ET E. NAKACHE, *Compt. Rend.*, 262c (1966) 63.
17 M. BONNEMAY, G. BRONOËL, E. LEVART, A. A. PILLA ET E. POIRIER D'ANGÉ D'ORSAY, *Compt. Rend.*, 258 (1964) 4256.
18 M. BONNEMAY, G. BRONOËL, E. LEVART, A. A. PILLA ET E. POIRIER D'ANGÉ D'ORSAY, *Compt. Rend.*, 258 (1964) 6139.
19 R. PARSONS, *Modern Aspects of Electrochemistry*, Vol. 1, edited by J. O'M. BOCKRIS, Butterworths, Londres, 1954, p. 141.
20 V. G. LEVICH, *Physicochemical Hydrodynamics*, Prentice Hall, New Jersey, 1962, p. 286.
21 M. BONNEMAY, G. BRONOËL, E. LEVART ET A. A. PILLA, *Communication No. 34 présentée à la Réunion de l'Electrochemical Society, Washington, Octobre, 1964.*
22 M. BONNEMAY, G. BRONOËL, E. LEVART ET G. PESLERBE, *J. Electrochem. Soc.*, 111 (1964) 265.
23 R. G. HALDEMAN, W. P. COLEMAN, S. H. LANGER ET W. A. BARBER, *Advances in Chemistry Series*, 47 (1965) 106.
24 H. A. LIEBHAFSKY, *Communication présentée au Symposium International sur les Piles à Combustible, Paris, Février, 1965.*
25 C. KORDESCH, *Communication présentée au Symposium International sur les Piles à Combustible, Paris, Février, 1965.*
26 M. BONNEMAY, *Les Piles à Combustible*, (Ouvrage collectif publié sous le patronage de la D.G.R.S.T.) Technip, Paris, 1965, ch. 1.4.

ETUDE DE LA DISTRIBUTION DU CHAMP ELECTRIQUE RESULTANT D'UNE ANISOTROPIE DANS LE TRANSPORT DES REACTIFS ET DES CHARGES*

M. BONNEMAY, G. BRONOËL, E. LEVART ET A. A. PILLA
Laboratoire d'Électrolyse du C.N.R.S., Bellevue, Hauts-de-Seine (France)
(Reçu le 21 janvier, 1966)

ÉTUDE THÉORIQUE—NOTION DE CHAMP PRIMAIRE DE DIFFUSION

La distribution des courants à une électrode est fonction des conditions dans lesquelles s'effectue le transport de charges et de matière dans la cellule électrolytique et des caractéristiques cinétiques des processus d'interface. En ce qui concerne le transport d'une espèce active i, il est connu[1,2] que le flux local, q_i, de matière arrivant à l'électrode peut être donné par l'équation générale:

$$q_i = -D_i \operatorname{grad} c_i + c_i \mu_i \operatorname{grad} \varphi + v c_i \tag{1}$$

avec

D_i = coefficient de diffusion de l'espèce i,
c_i = concentration de l'espèce i,
μ_i = mobilité de l'espèce i,
φ = potentiel électrique,
v = champ vectoriel de vitesse hydrodynamique.

Dans cette équation, le premier terme du membre de droite représente l'apport de l'espèce i par diffusion, le deuxième son apport par migration et le troisième par convection.

En ce qui concerne la consommation électrochimique du flux de matière en un point de l'électrode de coordonnées (x, y, z), on pourra écrire pour la densité locale de courant l'équation suivante:

$$i(x,y,z) = nF \sum_1^i q_i(x,y,z) = f\left[\varphi(x,y,z),\ \sum_1^i c_i(x\,y,z)\right] \tag{2}$$

qui représente une des conditions aux limites nécessaires à la résolution de eqn. (1).

De plus, les espèces j produites par la réaction s'éloignent de l'interface réactionnelle suivant un mode de transport dont l'expression est analogue à (1). Notons que le flux des espèces i arrivant à un point donné de l'interface est toujours égal au flux correspondant j des espèces produites par la réaction, ce qui définit une condition supplémentaire aux limites. La détermination de la densité locale de courant $i(x,y,z)$ nécessitera de donner une forme explicite à la fonction caractéristique des processus d'interface $f(\varphi,c)$. C'est ainsi que pour le cas où seulement deux espèces Ox

* Présentée en partie à la 15e Réunion du C.I.T.C.E., à Londres, Septembre, 1964 (abstr. 4.6).

et Red interviennent dans la réaction d'interface, considérée dans ce cas comme un simple transfert de n charges, l'expression (2) prendra la forme[3-5]:

$$i(x,y,z) = \boldsymbol{k}c_{\mathrm{Red}}(x,y,z) \exp\left[\frac{\alpha nF}{RT}\varphi(x,y,z)\right] - \boldsymbol{k}c_{\mathrm{Ox}}(x,y,z) \exp\left[-\frac{(1-\alpha)nF}{RT}\varphi(x,y,z)\right]. \quad (3)$$

Dans la plupart des systèmes électrochimiques, la présence d'un électrolyte support conduit à ce que le transport des charges dans l'électrolyte par l'espèce électroactive est négligeable[2]. On peut donc poser dans l'éqn. (1) $c_i\mu_i \operatorname{grad} \varphi = 0$. De même, le terme de convection, vc_i, dans (1) peut souvent être rendu négligeable par le choix de conditions expérimentales adéquates. Ceci est réalisé en particulier dans les pores des électrodes de géométrie expansée[6,7]. Il en résulte que l'équation de transport des espèces actives pourra s'écrire, pour la plupart des systèmes étudiés, sous la forme:

$$q_i = q_i^d = -D_i \operatorname{grad} c_i\,, \quad (4)$$

avec comme condition aux limites:

$$i(x,y,z) = nF \sum_1^i q_i^d(x,y,z) = f\left[\varphi, \sum_1^i c_i(x,y,z)\right]. \quad (5)$$

Dans les mêmes conditions, des équations analogues pourront s'écrire pour le transport des espèces j produites par la réaction

$$q_j = q_j^d = -D_j \operatorname{grad} c_j \quad (4')$$

$$i(x,y,z) = nF \sum_1^j q_j^d(x,y,z) = f\left[\varphi, \sum_1^j c_j(x,y,z)\right]. \quad (5')$$

Aux limites, les deux flux opposés sont égaux, on a donc:

$$q_i^d(x,y,z,) = q_j^d(x,y,z,)\,. \quad (6)$$

En ce qui concerne l'évacuation des charges* à travers la solution électrolytique considérée (avec un électrolyte support), le flux de charges identifiable ici à un flux de porteurs ioniques p est exprimé par:

$$q_p^m = c_p\mu_p \operatorname{grad} \varphi \quad (7)$$

et aux limites:

$$i(x,y,z) = nF \sum_1^p q_p^m(x\,y,z) = f\left[\varphi, \sum_1^i c_i(x,y,z)\right]. \quad (8)$$

Pour décrire le transport dans le système considéré ici, on dispose donc des éqns. (4), (4') et (7) avec leurs conditions aux limites respectives (5), (5'), (6) et (8) qui montrent qu'il y a couplage par la variable φ entre le transport de la matière et l'évacuation des charges[20,21]. De ce fait, dans tout le volume électrolytique, il y a influence mutuelle des flux locaux de diffusion et de migration, c'est-à-dire que la distribution spatiale de chacun d'eux dépend de la distribution spatiale de l'autre.

* Le problème de la conduction électronique de l'interface d'une électrode vers celle de l'autre à travers le circuit extérieur ne sera pas traité ici.

Toutefois, cette influence mutuelle dans l'espace n'existe pas si le système électrochimique est tel que l'apport des réactifs est uniforme pour toute l'interface et que, de plus, le champ primaire de conduction y est également uniforme, car le champ secondaire résultant est alors uniforme. Bien que le couplage aux limites subsiste dans ce cas, une solution analytique des éqns. (4) et (4') devient possible, même pour une expression relativement complexe de la cinétique d'interface[8]. L'équation (7), qui décrit la chute ohmique dans l'électrolyte, n'intervient alors que par son influence uniforme, pour toute l'interface, sur la variable φ.

Pour tenter la résolution du problème dans le cas le plus général où les éqns. (4), (4') et (7) doivent être considérées, il est utile de caractériser les systèmes étudiés non seulement par leur champ électrique primaire, qui est une notion bien connue[9], mais encore par leur champ primaire de diffusion. Ce dernier peut être représenté par les profils de concentration qui existeraient pour un milieu électrolytique de résistivité nulle, si les réactions d'interface se déroulaient à une vitesse infiniment grande. Ainsi défini, le champ primaire de diffusion a les mêmes propriétés que le champ primaire électrique, en effet, il ne dépend que des caractéristiques géométriques du système. D'une façon générale, la distribution du courant à l'électrode résultera de l'interaction entre le champ primaire de diffusion et le champ primaire électrique, compte-tenu de leur couplage aux limites avec l'expression appropriée de la cinétique d'interface. Quelques exemples de systèmes où il y a des interactions de ce type sont montré sur la Fig. 1.

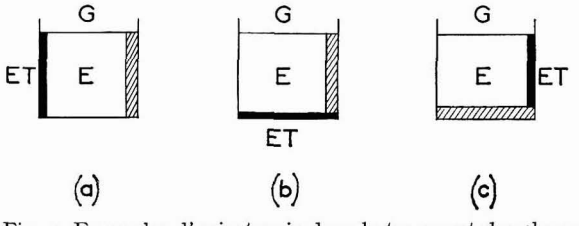

Fig. 1. Exemples d'anisotropie dans le transport des charges et des réactifs. (G), Espèce active à l'état gazeux; (E), électrolyte; (ET), électrode étudiée. (a), Champ primaire électrique uniforme, champ primaire de diffusion non uniforme; (b), champ primaire électrique non uniforme, champ primaire de diffusion uniforme; (c), champ primaire électrique non uniforme; champ primaire de diffusion non uniforme.

Pour les cas les plus complexes où la géométrie de l'ensemble est telle que les expressions tridimensionnelles des gradients de φ et de c doivent être considérées, la détermination analytique de la distribution du courant présente des difficultés quasi-insurmontables. C'est ainsi que pour une électrode à gaz, on s'est souvent limité à ne considérer que le phénomène d'apport du réactif, couplé aux limites avec l'expression de la cinétique d'interface, et on a été conduit à négliger le gradient du potentiel. Notons, que par ailleurs on a réduit l'expression de grad c à une ou deux composantes et, de plus, on a donné à la fonction d'interface $i = f(c,\varphi)$ une forme simplifiée[10-12]; d'autres études, tenant compte d'un couplage entre grad c et grad φ, ont été limitées à des systèmes monodimensionnels. Pour des expressions non linéaires de la cinétique d'interface, la résolution n'a pu être effectuée que par des méthodes numériques[13-17].

On se propose dans cet article de résoudre le problème général, c'est-à-dire de déterminer la fonction de distribution du courant en se basant sur le fait que cette

distribution ne dépend que de trois grandeurs élémentaires: champ primaire électrique, champ primaire de diffusion, cinétique des processus d'interface.

Le champ primaire électrique peut, quelle que soit la géométrie de la cellule, être déterminé par une méthode numérique[18] ou plus aisément par une analyse rhéographique[19]. La fonction $f(\varphi,c)$, représentant la cinétique d'interface, peut être déterminée par le tracé de la courbe de polarisation stationnaire, corrigée du terme de diffusion, sur une électrode soumise à un champ électrique uniforme.

En ce qui concerne le champ primaire de diffusion, sa détermination analytique est possible pour des systèmes où la diffusion s'effectue suivant un mode linéaire, cylindrique ou sphérique. En effet, les solutions de l'équation de diffusion, obtenues par ailleurs[1], décrivent directement le champ primaire ainsi défini. Pour des systèmes de géométrie plus complexe, il ne semble pas que de telles solutions aient été obtenues jusqu'à présent (voir toutefois[20]).

L'analogie formelle[22,23] existant entre un champ électrique primaire et un champ primaire de diffusion ($\nabla^2\varphi$ analogue à $\nabla^2 c$) nous conduit à préconiser l'emploi d'une solution analogique pour la détermination des flux locaux de diffusion. Les surfaces d'isoconcentration sont, en effet, analogues aux surfaces équipotentielles. L'une des surfaces équipotentielles limites sera représentative de la surface à concentration maximale, c_0, de l'espèce réagissante. L'autre limite représentera la surface de préélectrode qui aura, d'après la définition donnée au champ primaire, une concentration nulle. En fait, pour la détermination des courants locaux à l'électrode, il suffit de déterminer la répartition de la concentration sur une surface S située à une distance δ de l'interface, suffisamment petite pour que le flux de diffusion puisse être considéré avec une bonne approximation comme normal à l'interface.

Il pourra être procédé d'une façon analogue pour déterminer la répartition des potentiels correspondant au champ électrique primaire sur cette même surface.

Ainsi pour un point de coordonnées (x,y,z) de l'interface correspondra un point sur la surface S qui aura comme coordonnées x',y',z'. Il s'agit alors, connaissant en outre la forme de la cinétique des processus d'interface, de déterminer le courant local résultant des phénomènes considérés. Connaissant pour un point de coordonnées x',y',z' la concentration $c(x',y',z')$, il est possible de définir le courant local affectant le point correspondant de l'interface.

En effet, on peut écrire pour une seule espèce participant à la réaction:

$$i_d(x,y,z) = i_d(x',y',z') = nFD \operatorname{grad} c(x',y',z') = nFD\frac{\mathrm{d}c(x',y',z')}{\mathrm{d}w} \tag{9}$$

où w est toujours pris normal à l'interface. Cette équation monodimensionnelle et ponctuelle peut être résolue compte-tenu des conditions aux limites: $w = 0$, $c = 0$ et $w = \delta$, $c = c(x',y',z')$. On obtient:

$$i_d(x',y',z') = nF\frac{D}{\delta}c(x',y',z')\,. \tag{10}$$

Au même point est affectée une surtension de diffusion dont la valeur est donnée par:

$$|\eta_d(x',y',z')| = \frac{RT}{nF}[\log c_0 - \log c(x',y',z')] \tag{11}$$

Il en résulte qu'il est possible de définir une résistance locale caractéristique du champ primaire de diffusion au point considéré:

$$R_d(x,y,z) = R_d(x',y',z') = \eta_d/i_d \tag{12}$$

Par ailleurs, l'analyse rhéographique du champ électrique primaire, effectuée pour le même point (x',y',z'), permet d'écrire l'équation suivante:

$$i_\Omega(x,y,z) = i_\Omega(x',y',z') = c_p\mu_p \operatorname{grad} \varphi(x',y',z') = c_p\mu_p \frac{\mathrm{d}\varphi(x',y',z')}{\mathrm{d}w} \tag{13}$$

qui a comme conditions aux limites $w = 0$, $\varphi = 0$ et $w = \delta$, $\varphi = \varphi(x',y',z')$. Ceci permet de définir la résistance ohmique R_Ω caractéristique de chaque point de l'interface.

Envisageons tout d'abord le cas d'un système dont la cinétique des processus d'interface est infiniment rapide ($R_f = 0$). Comme à chaque point de l'interface est affectée une résistance R_Ω, on pourra représenter le champ éléctrique primaire par le schéma de la Fig. 2a où, pour une tension V_0 appliquée aux bornes du système, les résistances r sont choisies telles que $r(x,y,z) = R_\Omega(x,y,z) \times [V_0 - \varphi(x',y',z')]/\varphi(x',y',z')$.

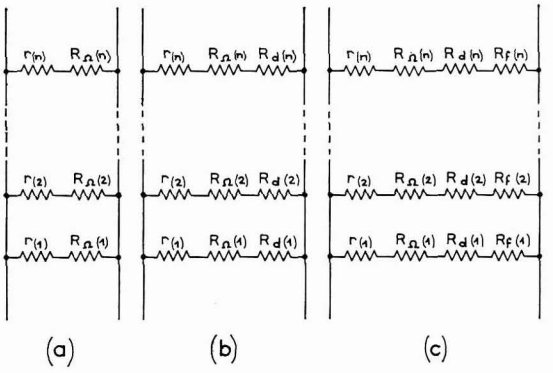

Fig. 2. Circuits électriques utilisés pour la détermination de la distribution du courant à une électrode.

Pour effectuer le couplage du champ primaire électrique avec celui de diffusion, il suffit alors d'ajouter, ainsi qu'il est montré sur la Fig. 2b, en série avec chaque résistance R_Ω, une résistance R_d dont la valeur est définie par (12). La distribution du courant résultant peut alors être évaluée à l'aide de l'équation suivante:

$$i(x,y,z) = \frac{V_0}{R_\Omega(x,y,z) + R_d(x,y,z) + r(x,y,z)} = \frac{\varphi(x',y',z')}{R_\Omega(x\,y,z) + R_d(x\,y,z)} \tag{14}$$

Notons que l'interface réactionnelle est décrite comme une fonction de points, seule la localisation de chacun de ces points sur l'électrode nécessitant un recours aux coordonnées. Le problème prend ainsi un caractère purement monodimensionnel.

Dans le cas où les processus d'interface ont une vitesse finie et participent donc au contrôle de la réaction d'électrode, il convient, pour déterminer la distribution du courant, de recourir à un procédé analogue, la solution ne pouvant toutefois être obtenue que par des itérations successives.

Dans une première phase, on posera arbitrairement $R_f = 0$ pour toute interface,

ce qui permettra, en procédant comme dans l'exemple précédant, d'effectuer un premier couplage entre le champ éléctrique primaire et celui de diffusion. On obtiendra ainsi une première série de valeurs de $\varphi(x',y',z')$. Connaissant par ailleurs les valeurs correspondantes de $c(x',y',z')$ et la fonction $R_f = f(\varphi,c)$, on pourra attribuer ensuite à chaque point de l'interface une valeur appropriée de R_f qui s'ajoutera en série avec les résistances R_Ω et R_d précédemment déterminées. Cette addition provoquera un changement des valeurs locales du potentiel sur la surface S, qui passeront de $\varphi(x',y',z')$ à $\varphi'(x',y',z')$ (voir Fig. 2c).

Il s'agit alors de déterminer, par une nouvelle opération analogique, les concentrations $c'(x',y',z')$ qui existeraient à une distance δ de l'interface si à cette dernière étaient affectées les concentrations $c(x',y',z')$ initialement déterminées pour S. La réalisation d'une cuve rhéographique, nécessaire à cette détermination, comportant une électrode non-équipotentielle, ne présente pas de difficultés particulières. Les valeurs de c' ainsi obtenues permettront de calculer pour chaque point de l'interface suivant (12) les résistances correspondantes R_d'.

Dans une opération suivante, il sera constitué, pour chaque point de l'interface, un circuit comportant en série R_d', R_Ω, R_f et r. Il en résultera que les tensions existantes aux points (x',y',z') passeront de la valeur φ' à la valeur φ''. Il conviendra alors de calculer une nouvelle série de valeurs de la résistance interfaciale (R_f') telles qu'elles soient compatibles avec les valeurs correspondantes de φ'' et de c'.

Cette itération pourra être poursuivie jusqu'à ce que les valeurs obtenues soient suffisamment près de leur convergence. Le nombre d'itérations nécessaire dépendra essentiellement de la forme de la fonction $R_f = f(\varphi,c)$ et de la valeur du rapport $\lim R_f/(R_\Omega + \lim R_d)$.

En définitive, cette méthode permet donc d'atteindre la distribution du courant à l'électrode lorsqu'il existe un couplage entre diffusion, conduction électrolytique et cinétique des processus d'interface, ceci quelle que soit en principe la géométrie de la cellule ou la forme des cinétiques impliquées.

VÉRIFICATIONS EXPÉRIMENTALES

Afin de vérifier la validité de cette méthode de détermination de la distribution du courant à une électrode dans des conditions de couplage entre les processus d'apport d'un réactif et le mode d'évacuation des charges, il a été procédé à une série d'expériences. Celles-ci ont été choisies de telle façon, que les processus d'interface puissent être considérés, compte-tenu du mode d'apport des réactifs et de la conduction du milieu, comme ayant une vitesse infiniment grande. Le système étudié est schématisé Fig. 3.

L'électrode de travail est constitué par un tube de graphite dont le diamètre interne est de 2.75 mm et dont la surface interne est parfaitement polie et propre. La longueur du tube est de 70 mm.

L'une de ses extrémités est fermée par une paroi poreuse qui sépare ainsi l'électrolyte support, contenu initialement dans le tube, d'un compartiment constituant la source de l'espèce électroactive.

Le rôle de la paroi poreuse est, d'une part, de déterminer un plan bien défini à concentration constante c_0 et, d'autre part, d'empêcher les effets de convection dans la région terminale du tube.

A l'autre extrémité de l'électrode et dans une position symétrique à celle du poreux est disposée la contre-électrode.

Les ions Cu^{2+} ($CuSO_4$) ont été choisi comme espèce électroactive, en raison de la faible surtension d'activation qui caractérise leur dépôt sur la surface étudiée[19].

L'électrolyte support était K_2SO_4. On a fait en sorte que la conductibilité de la solution soit toujours indépendante de la concentration en Cu^{2+} (la concentration maximale en Cu^{2+} était toujours très faible devant la concentration des espèces de l'électrolyte support).

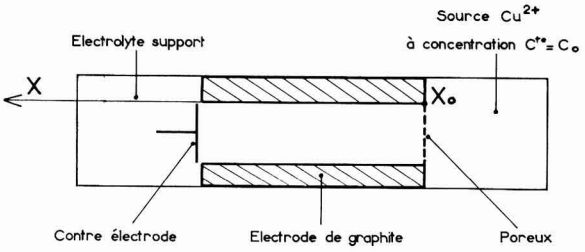

Fig. 3. Dispositif utilisé pour la vérification de la validité de la méthode.

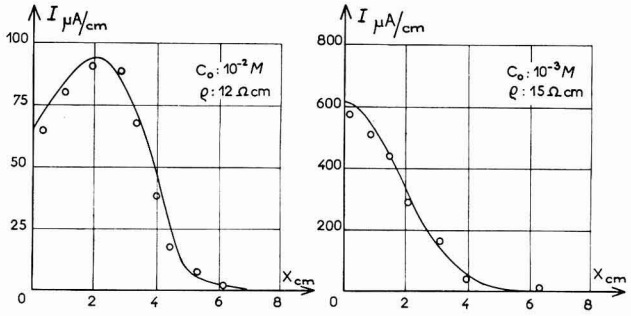

Fig. 4. Confrontation des valeurs des courants locaux obtenus: (○), expérimentalement; (—), avec les prévisions théoriques.

Un potentiostat assure l'application de la tension V_0 entre l'électrode de travail et la contre-électrode. Le courant global d'électrolyse est mesuré.

A l'issue d'une expérience, on découpe soigneusement le tube suivant son axe afin d'examiner la répartition du dépôt de cuivre sur les parois (mesure de l'épaisseur locale).

Des expériences ont été effectuées avec différentes concentrations c_0 en cuivre (10^{-1}–10^{-4} M) et des résistivités variables de l'électrolyte (10–20 Ωcm).

La détermination du champ primaire et du champ de diffusion est effectuée sur une cuve rhéographique classique[19]. Soulignons que les dimensions de la cuve pouvaient être considérablement plus grandes que celles de l'électrode étudiée puisque les mesures de tension dans un milieu homogène ne sont pas affectées par les effets de convection.

La Fig. 4 donne à titre d'exemple les résultats de deux expériences. Sur cette figure, il a été tracé les points déterminés expérimentalement et ceux calculés suivant la méthode décrite ici. On constate que dans les deux cas les points expérimentaux ne s'écartent jamais de plus de 15% de la courbe théorique. Ainsi il s'avère que la métho-

de proposée permet non seulement de donner l'allure de la répartition du courant à l'électrode, mais encore d'évaluer avec une bonne approximation les valeurs réelles des courants locaux.

CONCLUSION

L'introduction de la notion de "champ primaire de diffusion" permet de jeter les bases d'une méthode relativement simple de détermination de la distribution du courant à une électrode pour un système où les phénomènes d'apport, de consommation électrochimique et d'évacuation des charges sont couplés. Ce couplage résulte en définitive de la disposition géométrique des phases dans la cellule, celle-ci créant des conditions anisotropiques de transport des charges et des masses.

L'utilisation de procédés rhéographiques pour la détermination des profils de concentration et des profils de potentiels rend cette méthode plus aisément utilisable que les méthodes numériques qui pourraient aussi être adoptées.

Cette méthode de caractère général permet de prévoir, connaissant la géométrie d'une cellule, les différents profils possibles de la distribution du courant en fonction de la forme de la cinétique d'interface envisagée. En définitive, il sera possible, pour un système donné, de calculer l'importance relative de termes de transport, de conduction et de réaction d'interface. De telles études s'avèreront prometteuses lorsqu'elles concerneront les électrodes expansées utilisées dans les générateurs électrochimiques. De plus, la méthode décrite ici pourra être avantageusement adoptée pour l'étude de la distribution du courant dans toutes les opérations telles que, par exemple, électro-déposition ou corrosion où les transports de charge et de masse sont déterminants.

REMERCIEMENTS

Les auteurs tiennent à exprimer leurs remerciements à Mme. G. PICQ pour l'aide qu'elle a apporté dans la réalisation de la partie expérimentale de ce travail. De plus, ils remercient la Délégation Générale à la Recherche Scientifique et Technique pour l'aide financière apportée dans le cadre de la Convention No. 61 FR 075.

RÉSUMÉ

Après avoir défini la notion de champ primaire de diffusion, on propose une méthode de détermination de la distribution du courant à une électrode lorsque cette distribution résulte du couplage entre les processus d'interface, de diffusion et de conduction électrolytique. Cette méthode, qui fait appel à l'analogie formelle existant entre un champ de diffusion et un champ électrique, consiste à déterminer par rhéographie, et à l'aide d'itérations successives, pour chaque point de la surface de l'électrode, une série de résistances représentatives de l'apport de réactifs, de l'évacuation de charges et des processus d'interface. Elle permet d'atteindre la distribution du courant quelle que soit la géométrie de la cellule ou la forme des cinétiques impliquées.

SUMMARY

The concept of a primary diffusion field having been defined, a method is

proposed for the determination of the current distribution at an electrode when this distribution results from a combination of the processes at the interface, of diffusion and of electrolytic conduction.

This method, which depends upon the formal analogy between a diffusion field and an electric field, consists in determining repeatedly, for each point on the electrode surface, a series of resistances representing the bringing together of the reactants, the discharge of the ions and the interface processes.

It permits investigation of the current distribution whatever the cell geometry or the form of kinetics involved.

BIBLIOGRAPHIE

1 V. G. LEVICH, *Physicochemical Hydrodynamics*, Prentice Hall, Englewood Cliffs, 1962, pp. 39–53.
2 C. W. TOBIAS, M. EISENBERG ET C. R. WILKE, *J. Electrochem. Soc.*, 99 (1952) 359.
3 R. AUDUBERT, *J. Chim. Phys.*, 21 (1924) 351.
4 T. ERDEY-GRUZ ET M. VOLMER, *Z. Physik. Chem.*, A 150 (1930) 203.
5 A. N. FRUMKIN, *Z. Physik. Chem.*, A 164 (1933) 121.
6 N. IBL ET R. H. MULLER, *J. Electrochem. Soc.*, 105 (1958) 346.
7 A. M. BATICLE, *J. Electroanal. Chem.*, 8 (1964) 13.
8 P. DELAHAY, *Double Layer and Electrode Kinetics*, Interscience, Londres, 1965, pp. 167–195.
9 H. E. HARING ET W. BLUM, *Trans. Am. Electrochem. Soc.*, 44 (1923) 313.
10 L. G. AUSTIN ET H. LERNER, *Electrochim. Acta*, 9 (1964) 1469.
11 L. G. AUSTIN, *Trans. Faraday Soc.*, 60 (1964) 1319.
12 R. DARBY, *Advan. Energy Conversion*, 5 (1965) 43.
13 J. S. NEWMAN ET C. W. TOBIAS, *J. Electrochem. Soc.*, 109 (1962) 1183.
14 E. A. GRENS ET C. W. TOBIAS, *Ber. Bunsenges. Physik. Chem.*, 68 (1964) 236.
15 E. A. GRENS, R. M. TURNER ET T. KATAN, *Advan. Energy Conversion*, 4 (1964) 109.
16 E. A. GRENS ET C. W. TOBIAS, *Electrochim. Acta*, 10 (1965) 761.
17 F. G. WILL, *J. Electrochem. Soc.*, 110 (1963) 152.
18 J. A. KLINGERT, S. LYNN ET C. W. TOBIAS, *Electrochim. Acta*, 9 (1964) 297.
19 R. H. ROUSSELOT, *Répartition du Potentiel et du Courant dans les Électrolytes*, Dunod, Paris, 1959.
20 M. GUILLOU, Thèse, Paris, 1963.
21 R. BUVET, *Les Piles à Combustible*, (Ouvrage collectif publié sous le patronage de la D.G.R.S.T.) Technip, Paris, 1965, ch. 1.3.
22 W. C. ELMORE, *J. Appl. Phys.*, 10 (1939) 724.
23 A. BORUCKA, *Communication présentée à la 13ème Réunion du C.I.T.C.E., Rome, 1963.*

A MULTI-PURPOSE RECORDING pH-METER

PIETRO LANZA
Istituto Chimico "G. Ciamician" dell'Università, Bologna (Italy)
(Received January 5th, 1966)

In the course of research on the complexes of silver ions with gelatin and with synthetic polymers, it became necessary to add certain quantities of silver nitrate at definite intervals, maintaining the pH at a constant value. Under some conditions, when either the systems are slow in reaching equilibrium at the desired pH-value, or the silver electrode only attains the equilibrium potential slowly, the experiment is very tedious. The operation has, therefore, been made automatic. The apparatus prepared for this experiment proved to be very versatile and also useful for other purposes (*e.g.*, kinetic measurements, automatic titrations, etc.).

DESCRIPTION OF THE APPARATUS

The apparatus, illustrated in the block diagram (Fig. 1), is composed of the following basic elements:

(A) pH-meter Knick model pH35, adapted for pH or e.m.f. measurements (scale division at the highest sensitivity 0.01 pH-unit or 1 mV).

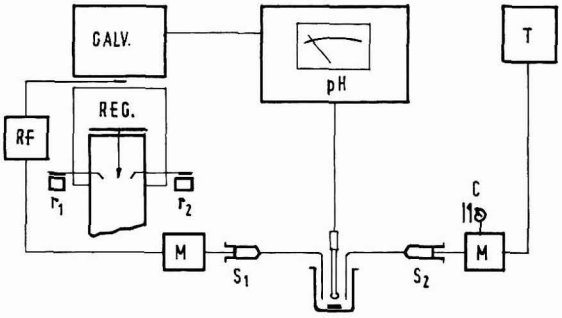

Fig. 1. Block diagram of the apparatus.

(B) Galvanometer Lange model Multiflex MG2, sensitivity $4 \cdot 10^{-9}$ A/division, connected with a recorder Lange model 2. A device is attached to the recorder in order that records may be taken on 88-mm or 218-mm paper-tape. Two relays (r_1, r_2), each moving a ball pen, are connected to the recorder for marking the traces on the paper tape.

(C) Time-relay composed of two elements, Schleicher model MZ51. This device enables an electrical circuit to be closed for variable periods of time from 0.3 sec to 6 h. The ratio between the time of the closed circuit and the opened circuit is

independently variable, because the duration of the impulse does not affect the length of the interval.

(D) Two motor-driven syringe-microburettes (s_1, s_2, Fig. 2). The plungers of the syringes are driven by a synchronous motor Crouzet, type 832, with a ferrite rotor. A characteristic of this motor is that it comes to a sudden stop when the current is cut off; there is, therefore, no possibility that the inertia of the motor will release an excess of the reactant. The speed of displacement of the plunger can be varied from 1.59 mm/min to 25.4 mm/min by means of interchangeable gears. The microburettes are fitted with syringes type S2YP (capacity 2 ml) and type S110Y (capacity 10 ml) made by the Micrometric Instrument Co. The volumetric error of the syringe microburettes was measured by weighing the water expelled and was found to be

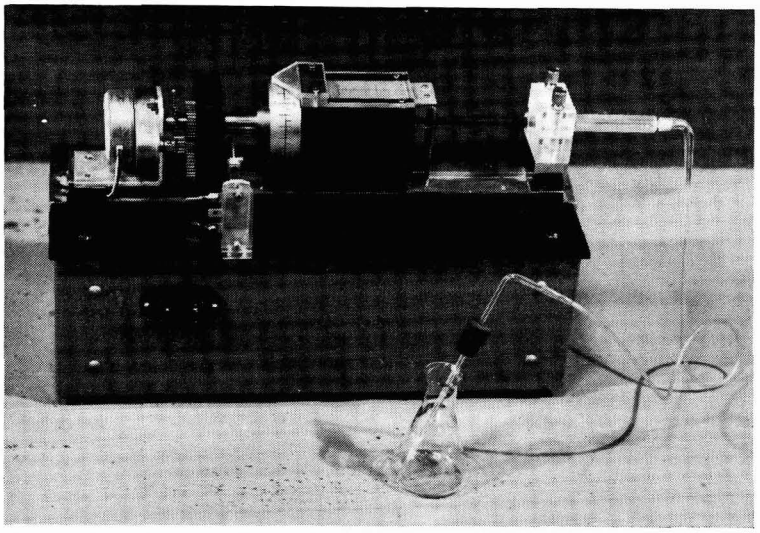

Fig. 2. Motor-driven syringe microburette.

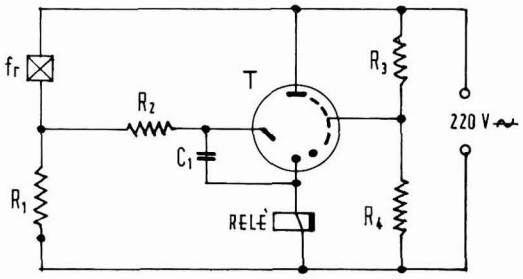

Fig. 3. Circuit of the relay with photoresistor. (fr), photoresistor PTW L29-00; (T), cold cathode tube Cerberus GR16; (Relé), relay Schrach RN 215901; (C_1), 200 pF; (R_1), 1 MΩ, 0.5 W; (R_2), 1 MΩ, 0.5 W; (R_3), 1 MΩ, 0.5 W; (R_4), 0.33 MΩ, 0.5 W.

less than 0.5%. The flow of reactant from these syringes can be varied from 0.0625 ml/min to 1000 ml/min and from 0.3125 ml/min to 5000 ml/min, respectively. A micro-switch driven by cams allows the volume delivered to be recorded on the paper-

tape by means of the relay r_1 or r_2. The motors of the syringes are operated by the time-relays or by the pH-meter through an electronic device.

(E) Relay with photo-resistor. This device, which operates the syringe microburette if the pH changes, has the following circuit (Fig. 3). The photoresistor is fixed in a slot of a plate of plexiglass, which may take the place of the graduated scale of the galvanometer. It is connected in the circuit in such a way that when the light of the galvanometer falls upon the photoconducting surface, the cold cathode tube strikes and the relay is energized, thus stopping the electrical supply to the syringe. When, as a result of a pH change, the photoresistor is not illuminated, the relay is released and the syringe starts.

FUNCTIONS OF THE APPARATUS

With the apparatus described it is possible to record three variables simultaneously.

(i) Recording of pH or e.m.f. by the continuous action of the recorder connected with the galvanometer.

(ii) Recording of time by marking on the paper-tape the signals of r_1 or r_2 energized by the time-relay.

(iii) Recording of the volume of reactant added by marking on the tape the signals of r_1 or r_2 energized by a dry-battery through the micro-switch with cams C.

APPLICATIONS

1. Keeping the pH of a system at a constant value (pH-stat)

The solution contained in the cell is brought to the desired pH by the addition of a suitable reagent. The light spot of the galvanometer is brought into the scale by regulating the mechanical "zero" of the instrument, and the sensitivity is adjusted on the basis of the foreseeable pH change and of the admissable pH variation. The syringe is filled with the reactant, the concentration of which is chosen by considering the volume of the solution and its buffering capacity. The photoresistor is put in such a position that its sensitive surface is situated just at the boundary of the light spot so that the smallest displacement causes the release of the relay, and the setting in motion of the syringe.

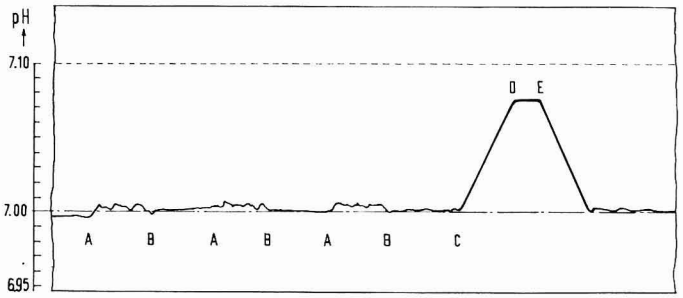

Fig. 4. Recording using the apparatus as a pH-stat with slow displacements of the pH.

The apparatus was checked by injecting at intervals at the lowest speed, by means of the syringe S_2 and the time relay, 0.100 ml of 1 *N* NaOH into 50 ml of phosphate buffer pH 7.00 at a constant temperature of 25° ± 0.2. The syringe, S_1, filled with 1 *N* HCl, and which is set in motion at every pH displacement, maintains the system at the desired pH-value. Under the conditions of the experiment, a single addition of the base should increase the pH by 0.07 units. The automatic addition of the acid keeps the pH at the desired value within ± 0.01 units. The recording is shown in Fig. 4. In the diagram, the letters A and B indicate, respectively, the beginning and the end of the NaOH addition, automatically neutralized. The line CD corresponds to an addition of 0.100 ml of NaOH without the automatic addition of HCl. At the point E, the automatic regulation was put into action again. Figure 5 shows the functioning of the apparatus under the same conditions, when the pH has been altered by instantaneous additions of 0.100 ml of NaOH at time intervals.

2. Preparation of gelatin solutions at a desired pH-value

In experiments with photographic gelatins, it was necessary to make a series of measurements at a determined and constant pH-value. When a solution of gelatin is brought to a pH-value different from the isoionic pH by the addition of some acid or base, a slow but continuous change of pH tends to bring the system back to the initial pH. This phenomenon is particularly evident on the alkaline side. This necessitates in practice, the addition of successive small quantities of acid or base until the system reaches the desired pH. This procedure has been made automatic with the

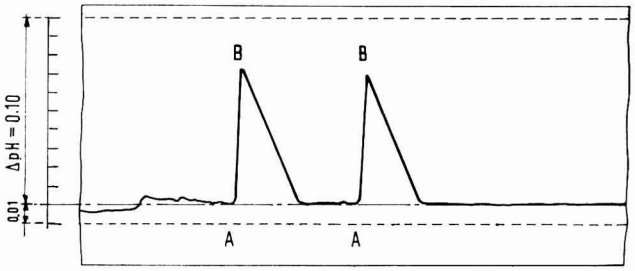

Fig. 5. Recording using the apparatus as pH-stat with fast displacements of the pH.

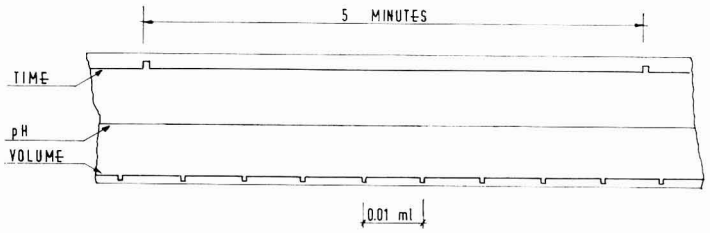

Fig. 6. Recording of kinetic measurements.

apparatus described. First, the gelatin solution is brought to the desired pH-value

by adding base (or acid). The pH is then maintained constant at the established point by automatic additions of suitable reagents until equilibrium is attained in the course of several hours. It is possible and convenient to use the apparatus overnight.

3. Applications to measurements in chemical kinetics

The equipment described has found useful applications in the kinetic study of the hydrolysis of esters at established and constant pH-values. For this purpose the apparatus is arranged with the relay, r_2, operated by the time-relay, so that the time may be recorded on the paper-tape. The relay, r_1, driven by the micro-switch with the cams of the syringe, marks the volume of the base injected into the system. The syringe becomes operative owing to the small pH displacement. The time, the pH, and the volume of the base used for controlling occasional shifts of pH from the desired value, are marked on the tape (Fig. 6). This figure represents an experiment on the hydrolysis of acetylglycolic acid at pH 9 and 60°. In order to avoid excessive use of the paper tape, the motion of the tape is synchronized with the motion of the syringe. The length of the tape thus corresponds approximately to the consumption of base.

4. Recording of the quantity of H^+ displaced in the complexation of silver ion with gelatin at established pH-values

If complexes are formed during the addition of silver ions to a solution of protein, there is an appreciable lowering of the pH due to the displacement of H^+ ions from basic groups complexed with metallic cations. The quantity of base needed for maintaining the pH constant at each silver ions addition is related to the amount of the displaced H^+ ions. In order to apply automation in this case, the apparatus is arranged so that the motor-syringe injects into the system, at determined intervals, suitable quantities of $AgNO_3$. The volume of this reagent is determined by the duration of the motion of the motor, which is operated by the time-relay. The device

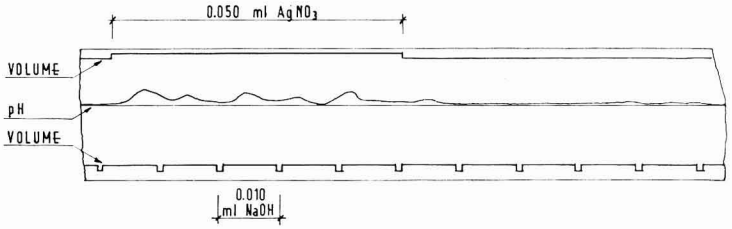

Fig. 7. Recording of the volume of base used, as a function of the Ag^+ added to a gelatin solution.

keeps the pH constant by automatic additions of NaOH. The volumes of NaOH and $AgNO_3$, as well as the pH, are recorded on the tape. It is possible, therefore, to determine the quantity of the H^+ ions displaced/single addition of $AgNO_3$.

Figure 7 shows part of the recording of an experiment made under the following conditions: 50 ml of 1% gelatin in 0.2 *N* KNO_3 were brought to pH 7, using the apparatus overnight. Then 0.05-ml additions of 0.01 *N* $AgNO_3$ were injected by the syringe at 5-min intervals. The pH was kept constant with 0.01 *N* NaOH.

5. Recording of a potentiometric titration curve

The apparatus records the pH and the volume of titrant used. Figure 8 shows a curve obtained by titrating 10 ml of 0.01 N H_3PO_4 with 0.1 N NaOH. Each mark on the recording corresponds to 0.010 ml. The derivative of the same curve is recorded in Fig. 9. This was obtained by fitting a 800-μF condenser and a 8-kΩ resistor to the galvanometric recorder input.

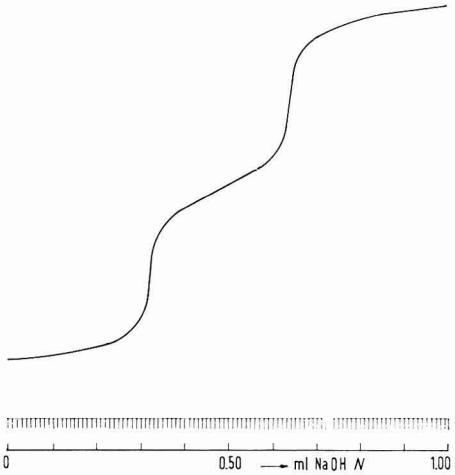

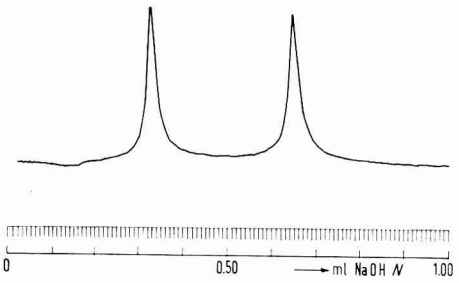

Fig. 8. Recording of a potentiometric titration curve.

Fig. 9. Recording of the derivative titration curve.

ACKNOWLEDGEMENT

This research was supported by a financial contribution from the C.N.R.

SUMMARY

An apparatus has been described that can record three variables, pH, volume and time, simultaneously. Various functions of the apparatus have also been described: its use as pH-stat; some applications in the kinetic study of the hydrolysis of esters at constant pH; the automatic recording of potentiometric titration curves.

THE RECORDING OF A POLAROGRAPHIC "REDOX-WAVE" ON A STATIONARY ELECTRODE BY THE CYCLIC VOLTAMMETRIC METHOD

G. FARSANG AND L. TOMCSÁNYI*
Institute of Inorganic and Analytical Chemistry, L. Eötvös University, Budapest (Hungary)
(Received December 14th, 1965)

A well-known phenomenon in polarography using the dropping-mercury electrode is the so called "redox-wave". This is the only polarographic wave obtained when both components, oxidized and reduced forms, of a polarographically-reversible redox system are present[1]. The intersection of this wave with the base line of the galvanometer yields the actual formal redox-potential value of the given reversible redox system. The values of the cathodic and anodic diffusion-limiting currents are proportional, respectively, to the concentrations of the oxidized and reduced form of the system. Thus, the quantitative measurement of the two components is possible when their concentrations have a similar order of magnitude in the mixture investigated.

The use of a slow (0.1–2 V/min) polarization rate for recording such systems on a stationary electrode by cyclic polarization is apparently unknown (cyclic voltage sweep chronoamperometry)[2].

The use of stationary electrodes with polarographic methods has increased in recent years and systems that contain both forms of the system may frequently be investigated. In this case, a special recording method only can be used and this is essentially identical with the cyclic polarization method suggested by KEMULA AND KUBLIK[3] and by CERMAK[4] but is different in its application from that given by these authors. Differences in the methods are due to the fact that on a given electrode in a solution containing both components of the redox system exhibiting reversible properties, there is only one electrode potential in the polarization range, where no current is measured in the cell, and this is the actual redox-potential of the respective redox system. At any other potential there is current in the system effecting a change in the electrode surface concentrations. As a result, the simple relation with the concentration of the solution and the reproducibility of the i–V curves recorded by the usual cyclic polarization method, are lost. This paper describes the development of a special cycl polarization method by which stationary electrodes can be used for the voltammetric investigation of systems of this type.

EXPERIMENTAL

We used a version of the carbon-paste electrode[5] suggested by ADAMS and modified by one of us. Spectrally-pure graphite and a methyl silicon polymer of molecular weight about 60,000 were used. The electrolysis cell is shown in Fig. 1.

* Present address: Research Institute for non-ferrous metals, Budapest (Hungary)

Voltammetric and potentiometric measurements were carried out on a platinum plate electrode 0.16 cm^2 in area which was pre-treated for voltammetric measurements as described by KUBLIK[7]. The reference electrode was a saturated calomel electrode of area 3.15 cm^2. The salt bridge was filled by the solution to be investigated and the end joined to the calomel electrode was sealed by a plug rolled from filter paper strips.

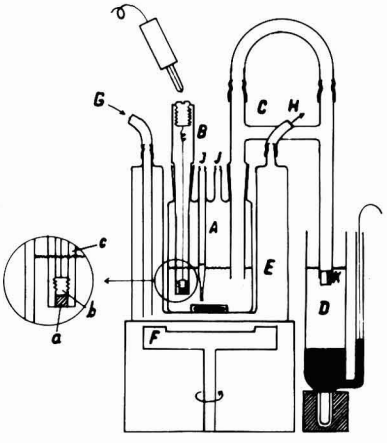

Fig. 1. Arrangement of voltammetric cell. (A), Electrolytic vessel; (B), carbon-paste electrode; (C), salt bridge; (D), saturated calomel electrode; (E), red copper thermostatting case; (F), magnetic stirrer; (G), inlet of water from thermostat; (H), water outlet; (I), gas entrance pipe; (J), gas outlet; (K), filter paper plug; (a), carbon-paste; (b), copper block; (c), plexiglass bar.

Cyclic current–voltage curves were recorded by a "Radelkisz OH-102" type polarograph with a polarization rate of 1.33 V/min, unless otherwise specified. Potentiometric measurements were made with a "Radelkisz OP-205" type pH-meter. $K_3Fe(CN)_6$ and $K_4Fe(CN)_6$ used for the investigations were of "Merck p.a." quality. Solutions of these substances were prepared by dissolving weighed amounts (measured with an accuracy of 0.1 mg) in the 1 *M* KCl used as the base electrolyte. The base electrolyte was prepared by dissolving in double-distilled water the necessary quantity of "Reanal p.a." KCl purified by recrystallization and measured with an accuracy of 0.1 mg.

All measurements were carried out in a thermostatted cell at $25.0 \pm 0.2°$.

METHOD OF RECORDING "REDOX WAVE" ON A STATIONARY ELECTRODE

Cyclic polarization is set from the polarization voltage corresponding to the redox-potential. This value can be determined potentiometrically or prior to polarization, by connecting the cell into the polarization circuit and with constant mixing of the solution, locating the polarization voltage where there is no current in the cell. The stirring of the solution is necessary to remove continually the diffusion layer formed on the surface of electrode during electrolysis.

Commencing from this polarization voltage, and polarizing the electrode in the positive direction, the oxidation current of the reduced form of the redox system in the solution is obtained, yielding a peak-type curve which is usual on stationary

electrodes. After the current peak is formed, the direction of polarization is reversed and we return to the value of the initial polarization voltage; then, by stirring for 30–40 sec, the diffusion layer formed on the surface of the elctrode during the oxidation half-cycle is removed. When stirring is stopped, about half a minute is necessary for the turbulence of the solution to cease. Now, by polarizing the electrode in the negative direction, the cathodic polarization curve can be recorded. This yields the reduction current of the oxidized form in solution. When the cathodic current peak has been recorded, by reversing the polarization direction and returning to the initial potential, the polarization cycle is completed. Now there is an anodic current

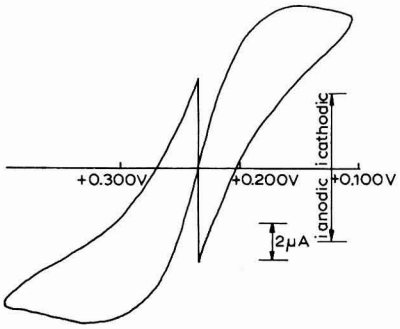

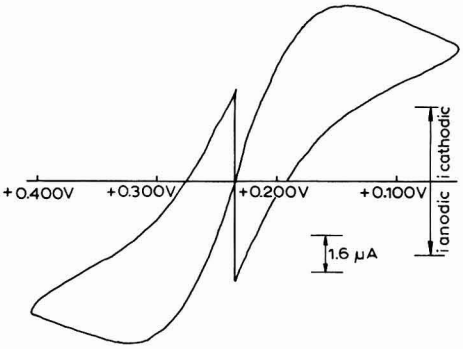

Fig. 2. "Redox wave" recorded on platinum electrode in 1 M KCl base soln. containing $1 \cdot 10^{-3}$ M Fe(II)–Fe(III) cyanide. Polarisation rate, 0.375 V/min.

Fig. 3. "Redox wave" recorded on carbon-paste electrode in 1 M KCl base soln. containing $1 \cdot 10^{-3}$ M Fe(II)–Fe(III) cyanide. Polarisation rate, 0.375 V/min.

at this potential, for the ox/red ratio on the surface of the electrode during the reduction half-cycle has become smaller. Consequently, the actual redox-potential on the surface of the electrode has a more negative value than that corresponding to the bulk of the solution, so that an anodic process must occur on the electrode. By mixing the solution, the diffusion layer is removed and the anodic current drops to zero. Cyclic voltage curves recorded on platinum and carbon-paste electrodes in an equimolar mixture ($1 \cdot 10^{-3}$ M), of potassium ferrocyanide and potassium ferricyanide in 1 M KCl base solution are shown in Figs. 2 and 3 respectively.

RESULTS

To investigate whether the method is applicable to quantitative analysis the following measurements were made.

The anodic and cathodic peak heights were measured as functions of the corresponding concentrations by changing the concentration ratio ox/red of the two components of the redox system investigated over the range 0.2–5. Measurements were done on the carbon-paste electrode in the concentration ranges 10^{-4}–10^{-5} M and 10^{-3}–10^{-4} M. On the platinum electrode, measurements were carried out only in the 10^{-3}–10^{-4} M concentration range, as the residual current of the electrode, because of the chemisorption of oxygen, made measurements in the lower concentration range

TABLE 1

INVESTIGATION OF THE Fe(II)–Fe(III) CYANIDE REDOX SYSTEM ON A CARBON-PASTE ELECTRODE

$K_4Fe(CN)_6$ C (mol/l)	$K_3Fe(CN)_6$ C (mol/l)	$i_{pA} \cdot 10^6$ A	$i_{pC} \cdot 10^6$ A	$i_{pA} \cdot 10^2/C_{K_4Fe(CN)_6}$	$i_{pC} \cdot 10^2/C_{K_3Fe(CN)_6}$
$2 \cdot 10^{-4}$	$1 \cdot 10^{-3}$	2.28	10.7	1.14	1.07
$4 \cdot 10^{-4}$	$1 \cdot 10^{-3}$	4.32	10.7	1.08	1.07
$6 \cdot 10^{-4}$	$1 \cdot 10^{-3}$	6.24	10.6	1.04	1.06
$8 \cdot 10^{-4}$	$1 \cdot 10^{-3}$	8.04	10.3	1.00	1.03
$1 \cdot 10^{-3}$	$1 \cdot 10^{-3}$	9.96	10.3	1.01	1.03
$1 \cdot 10^{-3}$	$8 \cdot 10^{-4}$	10.1	8.28	1.01	1.04
$1 \cdot 10^{-3}$	$6 \cdot 10^{-4}$	10.1	6.13	1.01	1.02
$1 \cdot 10^{-3}$	$4 \cdot 10^{-4}$	10.2	4.20	1.02	1.05
$1 \cdot 10^{-3}$	$2 \cdot 10^{-4}$	10.2	2.28	1.02	1.14
				Average value $\bar{K} = 1.04 \pm 0.04$	1.06 ± 0.04

TABLE 2

INVESTIGATION OF THE Fe(II)–Fe(III) CYANIDE REDOX SYSTEM ON A CARBON-PASTE ELECTRODE

$K_4Fe(CN)_6$ C (mol/l)	$K_3Fe(CN)_6$ C (mol/l)	$i_{pA} \cdot 10^7$ A	$i_{pC} \cdot 10^7$ A	$i_{pA} \cdot 10^2/C_{K_4Fe(CN)_6}$	$i_{pC} \cdot 10^2/C_{K_3Fe(CN)_6}$
$2 \cdot 10^{-5}$	$1 \cdot 10^{-4}$	2.52	10.1	1.26	1.01
$4 \cdot 10^{-5}$	$1 \cdot 10^{-4}$	4.32	10.1	1.08	1.01
$6 \cdot 10^{-5}$	$1 \cdot 10^{-4}$	6.36	10.1	1.06	1.01
$8 \cdot 10^{-5}$	$1 \cdot 10^{-4}$	8.28	10.2	1.04	1.02
$1 \cdot 10^{-4}$	$1 \cdot 10^{-4}$	9.60	10.3	0.96	1.03
$1 \cdot 10^{-4}$	$8 \cdot 10^{-5}$	9.60	8.04	0.96	1.00
$1 \cdot 10^{-4}$	$6 \cdot 10^{-5}$	9.72	6.24	0.97	1.04
$1 \cdot 10^{-4}$	$4 \cdot 10^{-5}$	9.72	4.44	0.97	1.11
$1 \cdot 10^{-4}$	$2 \cdot 10^{-5}$	10.1	2.52	1.01	1.26
				Average value: $\bar{K} = 1.03 \pm 0.09$	1.06 ± 0.08

TABLE 3

INVESTIGATION OF THE Fe(II)–Fe(III) CYANIDE REDOX SYSTEM ON A PLATINUM ELECTRODE

$K_4Fe(CN)_6$ C (mol/l)	$K_3Fe(CN)_6$ C (mol/l)	$i_{pA} \cdot 10^6$ A	$i_{pC} \cdot 10^6$ A	$i_{pA} \cdot 10^2/C_{K_4Fe(CN)_6}$	$i_{pC} \cdot 10^2/C_{K_3Fe(CN)_6}$
$2 \cdot 10^{-4}$	$1 \cdot 10^{-3}$	4.96	18.6	2.48	1.86
$4 \cdot 10^{-4}$	$1 \cdot 10^{-3}$	8.80	18.6	2.20	1.86
$6 \cdot 10^{-4}$	$1 \cdot 10^{-3}$	13.1	18.9	2.18	1.89
$8 \cdot 10^{-4}$	$1 \cdot 10^{-3}$	15.7	19.7	1.96	1.97
$1 \cdot 10^{-3}$	$1 \cdot 10^{-3}$	19.7	20.6	1.97	2.06
$1 \cdot 10^{-3}$	$8 \cdot 10^{-4}$	19.2	16.7	1.92	2.09
$1 \cdot 10^{-3}$	$6 \cdot 10^{-4}$	20.2	13.1	2.02	2.18
$1 \cdot 10^{-3}$	$4 \cdot 10^{-4}$	18.9	9.28	1.89	2.35
$1 \cdot 10^{-3}$	$2 \cdot 10^{-4}$	17.4	4.48	1.74	2.24
				Average value: $\bar{K} = 2.0 \pm 0.2$	2.0 ± 0.2

impossible. This gives the analytical accuracy of the simultaneous measurement of the two components of the redox system. The results obtained are summarized in Tables 1, 2 and 3.

The values of the anodic (i_{pA}) and cathodic (i_{pC}) current peaks, the concentrations and also the ratios obtained by dividing the current values by the respective concentrations are indicated in the tables. The ratio values so obtained were used to

calculate the data characteristic of the analytical accuracy of the method. At a given electrode reaction (n, D) and recording conditions (A, V) the following simple relation is obtained for the peak current:

$$i_p = k \cdot C \tag{1}$$

where

$$k = 2.72 \cdot 10^5 n^{\frac{3}{2}} A D^{\frac{1}{2}} V^{\frac{1}{2}} \tag{2}$$

according to the Randles–Sevčik theory[8]. The validity of the Randles–Sevčik equation for the application of slow polarization was proved by ADAMS and co-workers[9]. It is reasonable to assume the validity of the Randles–Sevčik equation for our method, because the setting of polarization from the redox-potential creates nearly identical conditions in the presence of both components of the redox system, to those when only one of the two is present in the solution. When the Randles–Sevčik equation is valid, the scatter of the values obtained by dividing the i_p values measured in the different depolarizer concentrations by the respective concentrations is characteristic of the analytical accuracy that can be achieved by the method.

A comparison of the data of Tables 1, 2 and 3 shows that the most favourable conditions are assured in the 10^{-3}–10^{-4} M concentration range and with the carbon-paste electrode.

In Table 2, in the 10^{-4}–10^{-5} M concentration range the lower accuracy is due to the disturbing effect of the residual current. The correction of residual current would, in this case, make measurement difficult, as for each ox/red ratio the polarization is set from different potentials, so that the curve of the residual current should be recorded for each ratio in order to correct the given peak currrents. However, it can be seen from Table 2 that even without this cumbersome correction, the accuracy of the method is not much less than the usual accuracy of voltammetric methods.

Table 3 contains the data obtained using a platinum electrode, and clearly demonstrates that even in a concentration range of one order of magnitude higher, the error is greater than that found with the carbon-paste electrode.

Measurements were carried out by the potentiometric method in order to in-

TABLE 4

REDOX-POTENTIAL VALUES OF THE Fe(II)–Fe(III) CYANIDE REDOX SYSTEM MEASURED IN 1 M KCl SOLUTION ON PLATINUM AND CARBON-PASTE ELECTRODES

$K_3Fe(CN)_6$ C (mol/l)	$K_4Fe(CN)_6$ C (mol/l)	$C_{K_3Fe(CN)_6}/C_{K_4Fe(CN)_6}$	E (mV vs. N.H.E.)			mV	
			Measured value		Calculated value	Pt	C.P.
			On PtE.	On C.P.E.			
$2 \cdot 10^{-4}$	$1 \cdot 10^{-3}$	0.20	421	414	421	0	−7
$4 \cdot 10^{-4}$	$1 \cdot 10^{-3}$	0.40	438	433	439	−1	−6
$6 \cdot 10^{-4}$	$1 \cdot 10^{-3}$	0.60	449	448	450	−1	−2
$8 \cdot 10^{-4}$	$1 \cdot 10^{-3}$	0.80	458	456	457	+1	−1
$1 \cdot 10^{-3}$	$1 \cdot 10^{-3}$	1.00	463	464			+1
$1 \cdot 10^{-3}$	$8 \cdot 10^{-4}$	1.25	468	470	469	−1	+1
$1 \cdot 10^{-3}$	$6 \cdot 10^{-4}$	1.67	474	478	476	−2	+2
$1 \cdot 10^{-3}$	$4 \cdot 10^{-4}$	2.50	485	494	587	−2	+7
$1 \cdot 10^{-3}$	$2 \cdot 10^{-4}$	5.00	508	513	505	+3	+8

vestigate the agreement of the equilibrium redox-potential values that can be measured on carbon-paste electrode with the redox-potential values measured on the platinum electrode and calculated by the Nernst–Peters equation. Measurements were taken in the 10^{-3}–10^{-4} M concentration range, for ox/red ratios ranging from 0.2 to 5.0 in a 1 M KCl base solution. In the calculation the redox-potential measured at 25.0° on the platinum electrode in a 1 M KCl solution containing $1 \cdot 10^{-3}$ M ferri- and ferrocyanides was accepted as the formal redox-potential.

The data summarized in Table 4 show that redox-potentials measured on platinum and carbon-paste electrodes by the potentiometric method agree within the limit of error with the calculated values. In this case, the redox-potential could be measured just as simply and accurately by the carbon-paste electrode as by the platinum electrode. On the carbon-paste electrode, the potential-determining equilibrium established in 8–10 sec. This measurement is the base of the procedure used by us in which the redox-potential is determined by the potentiometric method prior to cyclic polarization, the potentiometer of the polarograph then being adjusted to this value as the intial polarization voltage.

From these measurements it follows that for voltammetric titrations, the carbon-paste electrode can be conveniently used as indicator electrode. In many cases it is more advantageous than platinum, owing to its lower residual current.

SUMMARY

The application of the cyclic voltammetric method (cyclic voltage sweep chronoamperometry) for a special case was investigated. The method of recording the type of current known in polarography as "redox-wave", on a stationary electrode was developed by cyclic polarization. Analytical applications of the method were investigated.

The validity of redox-potential values measured on a carbon-paste electrode was proved by potentiometric measurements. The results obtained suggest that a carbon-paste electrode is a suitable indicator electrode in voltammetric and potentiometric end-point methods.

REFERENCES

1 I. M. Kolthoff and J. J. Lingane, *Polarography*, Vol. I., Interscience Publishers Inc., New York, 2nd ed., 1952, p. 205.
2 P. Delahay, G. Charlot and H. A. Laitinen, *Anal. Chem.*, 32 (1960) 103 A.
3 W. Kemula and Z. Kublik, *Nature*, 182 (1958) 799.
4 V. Cermak, *Collection Czech. Chem. Commun.*, 24 (1959) 831.
5 R. N. Adams, *Anal. Chem.*, 30 (1958) 1576.
6 G. Farsang, *Acta Chim. Acad. Sci. Hung.*, 45 (1965) 163.
7 Z. Kublik, *J. Electroanal. Chem.*, 5 (1963) 450.
8 P. Delahay, *New Instrumental Methods in Electrochemistry*, Interscience Publishers Inc., New York, 1954.
9 T. R. Mueller and R. N. Adams, *Anal. Chim. Acta*, 25 (1961) 482.

THE APPLICATION OF DOUBLE POTENTIAL-STEP CHRONOCOULOMETRY TO THE STUDY OF CHEMICAL REACTIONS FOLLOWING THE ELECTRODE REACTION. THEORY

JOSEPH H. CHRISTIE

Gates and Crellin Laboratories of Chemistry, California Institute of Technology, Pasadena, California 91109 (U.S.A.)*

and

North American Aviation Science Center, Thousand Oaks, California 91360 (U.S.A.)

(Received February 14th, 1966)

Chronopotentiometry with current reversal[1-4] has been used to study the kinetics of a chemical reaction following an electrode reaction, but application to fast chemical reactions is severely limited by the fact that a significant fraction of the constant current passed is consumed by double-layer charging. This means that the experimental system does not fit the theoretical model that assumes a constant faradaic current; furthermore, the transition time observed is extremely poorly defined because of the large fraction of the current going into double-layer charging near the transition time.

SCHWARZ AND SHAIN[5] have recently presented a double potential-step technique in which the faradaic and charging currents are easily separated. In this technique, for which the name *double potential-step chronoamperometry* seems appropriate, the potential is switched from a potential, E_0, at which no current flows, to a potential, E_1, at which the reaction $O + ne \rightarrow R$ occurs; after a time, τ, the potential is switched to E_2 at which the direction of the electrode reaction is reversed: $R \rightarrow O + ne$. Since the double-layer charging current decays more rapidly than does the faradaic current, the current measured after about 100 μsec is purely faradaic.

SCHWARZ AND SHAIN[5] have derived the limiting-current response of an electrode reaction coupled with a following chemical reaction to give a non-electroactive product

$$\begin{aligned} &O + ne = R \\ &R \overset{k}{\rightarrow} Z \end{aligned} \qquad (1)$$

for the condition that E_1 and E_2 are such that $C_O\,(0, t \leq \tau) = 0$ and $C_R\,(0, t > \tau) = 0$.

Recent papers[6,7] have pointed out that the total charge passed during a controlled-potential experiment can also be separated into *diffusing* and *non-diffusing* charge since the *non-diffusing* (double layer, adsorption, electrode film) charge appears as a step-function at the time at which the potential step is applied.

This paper presents the theoretical relations for the Q–t response to a double potential step for simple chemical reactions following a simple electrode reaction. This

* Contribution No. 3342.

technique, in which charge rather than current is measured, can best be called *double potential-step chronocoulometry*.

We shall assume in the following that: (a) Fick's law is applicable to each species independently, (b) convection and migration effects are negligible, (c) diffusion is linear, (d) each reacting species is soluble in the solution or in the electrode phase and all chemical reactions are homogeneous, (e) there exist two potentials E_1 and E_2 such that $C_O(0, t) = 0$ for $E = E_1$ and $C_R(0, t) = 0$ for $E = E_2$, (f) adsorption effects are negligible, and (g) double-layer effects on the rate of the chemical reaction are negligible.

The initial and boundary conditions on the partial differential equations for mass transfer in all cases considered are

$$t = 0: \quad C_O(x, 0) = {}^*C_O; \; C_R(x, 0) = 0 \tag{2}$$

$$x \to \infty: \quad \lim_{x\to\infty} C_O(x, t) = {}^*C_O; \; \lim_{x\to\infty} C_R(x, t) = 0 \tag{3}$$

$$x = 0: \quad D_O\left(\frac{\partial C_O}{\partial x}\right)_{x=0} = -D_R\left(\frac{\partial C_R}{\partial x}\right)_{x=0} = \frac{I}{nF} \tag{4}$$

$$C_O(0, t) = 0, \; t < \tau \tag{5}$$

$$C_R(0, t) = 0, \; t > \tau \tag{6}$$

(Symbols are defined in Appendix I).

No chemical reaction

For comparison with the results obtained below for cases in which there is a coupled chemical reaction, we first consider the case in which there is no chemical reaction. For this case the mass transfer equations are

$$\frac{\partial C_O}{\partial t} = D_O \frac{\partial^2 C_O}{\partial x^2} \tag{7}$$

$$\frac{\partial C_R}{\partial t} = D_R \frac{\partial^2 C_R}{\partial x^2} \tag{8}$$

The solution for the Q–t behaviour in this case may be obtained from integration of the expression for the I–t behaviour derived by KAMBARA[8], but it will be worked out here in order to illustrate the method to be used when coupled chemical reactions are considered. This method is patterned after that used by SCHWARTZ AND SHAIN and allows direct calculation of the Q–t behaviour, without recourse to integration of the expression for the I–t behaviour, the procedure used previously in the derivation of chronocoulometric equations[6,7].

Taking Laplace transforms of the mass transfer eqns. (7) and (8) and solving in the usual way, using the initial and boundary conditions (2), (3), (4), we obtain for the Laplace transform of the current,

$$\bar{I} = nF\sqrt{D_R}\sqrt{s}\bar{C}_R(0, s) \tag{9}$$

This equation is merely the Laplace transform of the familiar equation given by

application of Duhamel's theorem[9]

$$C_R(0, t) = \frac{1}{nF\sqrt{\pi D_R}} \int_0^t \frac{I(\theta)\,d\theta}{\sqrt{t-\theta}} \tag{10}$$

Since, by definition,

$$Q(t) = \int_0^t I(\theta)\,d\theta \tag{11}$$

we have

$$\bar{Q}(s) = \frac{1}{s}\bar{I}(s) \tag{12}$$

and by eqn. (9)

$$\bar{Q}(s) = \frac{nF\sqrt{D_R}}{\sqrt{s}}\bar{C}_R(0, s) \tag{13}$$

Taking inverse transforms and applying the convolution theorem, we obtain the general result

$$Q(t) = \frac{nF\sqrt{D_R}}{\sqrt{\pi}} \int_0^t \frac{C_R(0, \theta)}{\sqrt{t-\theta}}\,d\theta \tag{14}$$

In the present case, we have assumed that the surface concentration of R is zero for $t > \tau$ and eqn. (14) becomes:

$$Q(t \leq \tau) = \frac{nF\sqrt{D_R}}{\sqrt{\pi}} \int_0^t \frac{C_R(0, \theta)}{\sqrt{t-\theta}}\,d\theta \tag{15a}$$

$$Q(t > \tau) = \frac{nF\sqrt{D_R}}{\sqrt{\pi}} \int_0^\tau \frac{C_R(0, \theta)}{\sqrt{t-\theta}}\,d\theta \tag{15b}$$

Since $C_O(0, t \leq \tau) = 0$, the surface concentration is given by[10]

$$C_R(0, t \leq \tau) = \sqrt{\frac{D_O}{D_R}} * C_O \tag{16}$$

Substituting into eqns. (15a) and (15b), and performing the integrations we obtain

$$Q(t \leq \tau) = \frac{2\,nF\sqrt{D_O} * C_O}{\sqrt{\pi}}\sqrt{t} \tag{17}$$

$$Q(t > \tau) = \frac{2\,nF\sqrt{D_O} * C_O}{\sqrt{\pi}}\left[\sqrt{t} - \sqrt{t-\tau}\right] \tag{18}$$

The same results may be obtained by the equivalent procedure of calculating

$$\bar{C}_R(0, s) = \int_0^\tau e^{-st} C_R(0, t)\,dt\,,$$

substituting into eqn. (13), and taking the inverse transform. In the present case, performing the integrations is easier.

Dividing eqns. (17) and (18) by the Cottrell charge

$$Q_C = \frac{2\,nF\sqrt{D_O}\,{}^*C_O}{\sqrt{\pi}}\sqrt{\tau} \tag{19}$$

gives the dimensionless equations

$$\frac{Q\,(t \leq \tau)}{Q_C} = \sqrt{\frac{t}{\tau}} \tag{20}$$

$$\frac{Q\,(t > \tau)}{Q_C} = \sqrt{\frac{t}{\tau}} - \sqrt{\frac{t}{\tau} - 1} \tag{21}$$

Figure 1 shows $Q(t)/Q_C$ as a function of t/τ. As in chronopotentiometry with current reversal, a convenient parameter for analysis of double potential-step chronocoulometric results is the ratio of the charge passed in the reverse process to that passed in the forward process. Whereas chronopotentiometry with current reversal

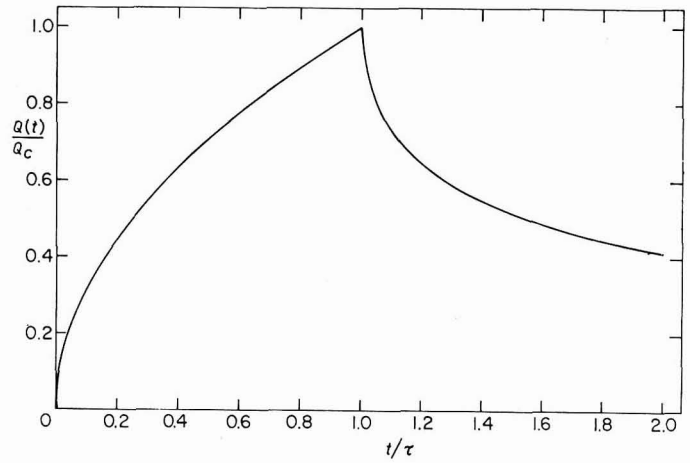

Fig. 1. $Q(t)/Q_C$ *vs.* t/τ for a simple electrode reaction; calc. from eqns. (20) and (21).

has two characteristic times, the forward generation time and the reverse transition time, double potential-step techniques have only one, the forward generation time, τ; the second characteristic time must be chosen arbitrarily. An experimentally and mathematically convenient choice is $t = 2\tau$. The ratio

$$\left|\frac{Q_b}{Q_f}\right| = \left|\frac{Q(2\tau) - Q(\tau)}{Q(\tau)}\right| = 2 - \sqrt{2} = 0.5858 \tag{22}$$

is therefore the characteristic ratio for double potential-step chronocoulometry. This ratio, corresponding to equal forward and reverse times, is the double potential-step chronocoulometric analog of the chronopotentiometric transition time ratio of 1/3, corresponding to equal forward and reverse currents.

An observed deviation from the ratio $|Q_b/Q_f| = 2 - \sqrt{2}$ indicates that the system under study does not fit the simple model described here. We consider below the effect of following chemical reactions on this ratio.

Catalytic reaction

For the irreversible catalytic regeneration of O by reaction of R in solution

$$\begin{aligned} &O + ne \rightarrow R \\ &R + Z \xrightarrow{k_c} O \end{aligned} \tag{23}$$

the mass transfer equations are

$$\frac{\partial C_O}{\partial t} = D\frac{\partial^2 C_O}{\partial x^2} + \beta^2 C_R \tag{24}$$

$$\frac{\partial C_R}{\partial t} = D\frac{\partial^2 C_R}{\partial x^2} - \beta^2 C_R \tag{25}$$

where $\beta^2 = k_c C_Z$. It has been assumed that $D_O = D_R = D$; this approximation results in a great simplification in the mathematics. It has also been assumed that C_Z is sufficiently large that it does not change during the course of the experiment; β^2 is then a pseudo-first-order rate constant. The initial and boundary conditions on C_O and C_R are given in eqns. (2–6).

The analogs of eqns. (13) and (15a, b) for this mass transfer problem are

$$\frac{\bar{Q}}{nF\sqrt{D}} = \frac{\sqrt{s+\beta^2}}{s}\bar{C}_R(0, s) \tag{26}$$

and

$$Q(t \leq \tau) = nF\sqrt{D}\int_0^t \left[\frac{e^{-\beta^2(t-\theta)}}{\sqrt{\pi}\sqrt{t-\theta}} + \beta \operatorname{erf}\beta\sqrt{t-\theta}\right] C_R(0, \theta)\, d\theta \tag{27a}$$

$$Q(t > \tau) = nF\sqrt{D}\int_0^\tau \left[\frac{e^{-\beta^2(t-\theta)}}{\sqrt{\pi}\sqrt{t-\theta}} + \beta \operatorname{erf}\beta\sqrt{t-\theta}\right] C_R(0, \theta)\, d\theta \tag{27b}$$

The forward ($t < \tau$) process corresponds to the problem treated by DELAHAY AND STIEHL[11]; it can be shown from their results that $C_R(0, t \leq \tau) = {}^*C_O$.

Substituting this value into eqns. (27a) and (27b) and performing the integrations gives

$$Q(t \leq \tau) = \frac{nF\sqrt{D}\,{}^*C_O}{\beta}\left\{(\beta^2 t + \tfrac{1}{2})\operatorname{erf}\beta t^{\frac{1}{2}} + \frac{\beta t^{\frac{1}{2}}}{\sqrt{\pi}}e^{-\beta^2 t}\right\} \tag{28}$$

$$\begin{aligned} Q(t > \tau) = \frac{nF\sqrt{D}\,{}^*C_O}{\beta}\Big\{&(\beta^2 t + \tfrac{1}{2})\operatorname{erf}\beta t^{\frac{1}{2}} + \frac{\beta t^{\frac{1}{2}}}{\sqrt{\pi}}e^{-\beta^2 t} \\ &- [\beta^2(t-\tau) + \tfrac{1}{2}]\operatorname{erf}\beta(t-\tau)^{\frac{1}{2}} - \frac{\beta(t-\tau)^{\frac{1}{2}}}{\sqrt{\pi}}e^{-\beta^2(t-\tau)}\Big\} \end{aligned} \tag{29}$$

The currents I ($t \leq \tau$) and I ($t > \tau$) may be obtained by differentiation of eqns. (28) and (29), respectively.

The desired parameter is $|Q_b/Q_f|$, which we obtain by setting $t = \tau$ and $t = 2\tau$ in eqns. (28) and (29), respectively.

$$\left|\frac{Q_b}{Q_f}\right| = \left|\frac{Q(2\tau)-Q(\tau)}{Q(\tau)}\right| = 2 - \frac{(2\beta^2\tau+\frac{1}{2})\,\mathrm{erf}\sqrt{2\beta^2\tau}+\sqrt{\frac{2\beta^2\tau}{\pi}}\,\mathrm{e}^{-2\beta^2\tau}}{(\beta^2\tau+\frac{1}{2})\,\mathrm{erf}\sqrt{\beta^2\tau}+\sqrt{\frac{\beta^2\tau}{\pi}}\,\mathrm{e}^{-\beta^2\tau}} \tag{30}$$

Figure 2 shows a plot of the ratio $|Q_b/Q_f|$ *vs.* $\sqrt{\beta^2\tau}$. Two limiting cases can be seen in eqn. (30) and Fig. 2. As $\beta^2\tau \to 0$, $|Q_b/Q_f| \to 2-\sqrt{2}$; *i.e.*, as the rate of the catalytic reaction decreases, the behaviour becomes simply diffusion limited. As $\beta^2\tau \to \infty$,

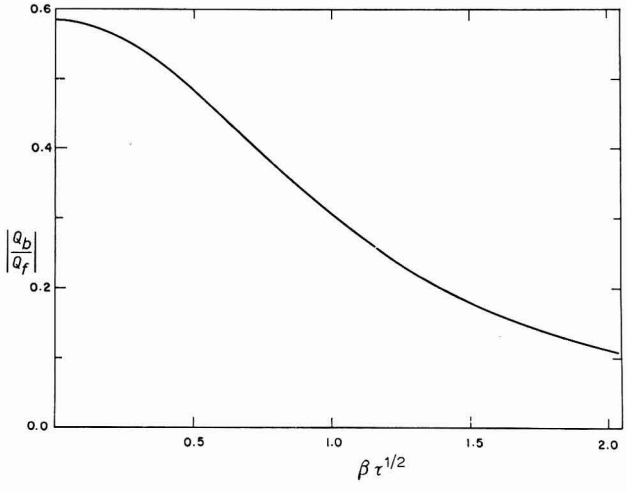

Fig. 2. $|Q_b/Q_f|$ *vs.* $\beta\tau^{\frac{1}{2}}$ for catalytic reaction; calc. from eqn. (30).

$|Q_b/Q_f| \to 0$; *i.e.*, if the catalytic reaction is very fast, essentially all the R formed during the forward process is consumed by the chemical reaction and none is left to react at the electrode during the reverse process.

Following chemical reaction

The double potential-step chronoamperometric equations for an irreversible chemical reaction following the electrode reaction (reaction 1) have been derived by SCHWARZ AND SHAIN[5]. The analogous chronocoulometric equations may be derived either by a procedure similar to that used above or by simple integration of the $I-t$ equations given by SCHWARZ AND SHAIN. The latter procedure is more straight-forward and will be used here.

The current–time equations are[5]:

$$I\,(t \leq \tau) = \frac{nF\sqrt{D_O}\,{}^*C_O}{\sqrt{\pi t}} \tag{31}$$

$$I\,(t > \tau) = -\frac{nF\sqrt{D_O}\,{}^*C_O}{\sqrt{\pi}}\left[\frac{\varphi(k,t,\tau)}{\sqrt{t-\tau}} - \frac{1}{\sqrt{t}}\right] \tag{32}$$

where

$$\varphi(k, t, \tau) = e^{-kt}{}_1F_1(\tfrac{1}{2}, 1, k\tau) + \sum_{n=1}^{\infty} \frac{e^{-kt}[k(t-\tau)]^n}{n!}\, {}_1F_1(n+\tfrac{1}{2}, n+1, k\tau) \tag{33}$$

where ${}_1F_1(a, b, z)$ is Kummer's confluent hypergeometric function, sometimes denoted by $M(a, b, z)$ or $\Phi(a, b, z)$, and defined by the relation

$${}_1F_1(a, b, z) = 1 + \frac{az}{b} + \frac{a(a+1)}{b(b+1)}\frac{z^2}{2!} + \ldots + \frac{a(a+1)\ldots(a+n-1)}{b(b+1)\ldots(b+n-1)}\frac{z^n}{n!} + \ldots \tag{34}$$

The chronocoulometric equations are then:

$$Q(t \leq \tau) = \frac{nF\sqrt{D_O}\,{}^*C_O}{\sqrt{\pi}} \int_0^t \frac{d\theta}{\sqrt{\theta}} = \frac{2\,nF\sqrt{D_O}\,{}^*C_O\sqrt{t}}{\sqrt{\pi}} \tag{35}$$

$$Q(t > \tau) = \frac{nF\sqrt{D_O}\,{}^*C_O}{\sqrt{\pi}} \left\{\int_0^\tau \frac{d\theta}{\sqrt{\theta}} - \int_\tau^t \frac{\varphi(k, \theta, \tau)}{\sqrt{\theta-\tau}}\, d\theta - \int_\tau^t \frac{d\theta}{\sqrt{\theta}}\right\} \tag{36}$$

The evaluation of the integrals contained in eqn. (36) is carried out in Appendix II. The result is

$$Q(t > \tau) = \frac{2nF\sqrt{D_O}\,{}^*C_O}{\sqrt{\pi}} [\sqrt{t} - \Psi\sqrt{t-\tau}] \tag{37}$$

where

$$\begin{aligned}\Psi(t, k\tau) = {} & \frac{\sqrt{\pi}}{2}\frac{\operatorname{erf}[k(t-\tau)]^{\frac{1}{2}}}{\sqrt{k(t-\tau)}}\, e^{-k\tau}\Big\{{}_1F_1(\tfrac{1}{2}, 1, k\tau) \\ & + \sum_{n=1}^{\infty} \frac{{}_1F_1(n+\frac{1}{2}, n+1, k\tau)}{2^n(n!)}(2n-1)!!\Big\} - e^{-kt}\sum_{n=1}^{\infty} \frac{{}_1F_1(n+\frac{1}{2}, n+1, k\tau)}{n!} \\ & \cdot \left[\frac{[k(t-\tau)]^{n-1}}{2} + \sum_{i=1}^{n-1} \frac{[k(t-\tau)]^{n-i-1}}{2^{i+1}} \frac{(2n-1)!!}{(2n-2i-1)!!}\right]\end{aligned} \tag{38}$$

Equation (35) for $Q(t \leq \tau)$ is identical with eqn. (17) for the case in which there is no coupled chemical reaction, since the charge passed in the forward process is independent of the following chemical reaction. Equation (38) for $Q(t > \tau)$ differs from eqn. (18) only by the occurrence of the factor Ψ. The magnitude of Ψ is a measure of the rate of the following chemical reaction.

The desired parameter is again the ratio of the charge passed in the reverse process to that passed during the forward process.

$$\left|\frac{Q_b}{Q_f}\right| = 1 - \sqrt{2} + \Psi(2\tau, k\tau) \tag{39}$$

where the value of $\Psi(t, k\tau)$ for $t = 2\,\tau$ is given by

$$\begin{aligned}\Psi(2\tau, k\tau) = {} & -e^{-2k\tau}\Big\{\sum_{n=1}^{\infty} \frac{{}_1F_1(n+\frac{1}{2}, n+1, k\tau)}{n!} \times \\ & \left[\frac{(k\tau)^{n-1}}{2} + \sum_{i=1}^{n-1} \frac{(k\tau)^{n-i-1}}{2^{i+1}} \frac{(2n-1)!!}{(2n-2i-1)!!}\right]\Big\} \\ & + \frac{\sqrt{\pi}}{2}\frac{\operatorname{erf}\sqrt{k\tau}}{\sqrt{k\tau}}\, e^{-k\tau}\sum_{n=1}^{\infty} \frac{{}_1F_1(n+\frac{1}{2}, n+1, k\tau)}{2^n n!}(2n-1)!!\end{aligned} \tag{40}$$

By making use of the identity

$$\frac{\sqrt{\pi}}{2}\frac{\operatorname{erf} x}{x} = e^{-x^2}\,{}_1F_1(1, \tfrac{3}{2}, x^2)$$

eqn. (40) may be rewritten

$$\Psi(2\tau, k\tau) = e^{-2k\tau}\left\{\sum_{n=1}^{\infty}\frac{{}_1F_1(n+\frac{1}{2}, n+1, k\tau)}{2^n n!}\left[(2n-1)!!\,{}_1F_1(\tfrac{1}{2}, \tfrac{3}{2}, k\tau) - (k\tau)^{n-1}\right.\right.$$
$$\left.\left. - (2n-1)!!\sum_{i=1}^{n-1}\frac{2^i(k\tau)^{n-i-1}}{(2n-2i-1)!!}\right] + {}_1F_1(\tfrac{1}{2}, \tfrac{3}{2}, k\tau)\,{}_1F_1(\tfrac{1}{2}, 1, k\tau)\right\} \quad (41)$$

This equation converges much more rapidly than eqn. (40) and was employed for the calculation of Ψ. The values of ${}_1F_1(a, b, z)$ were calculated directly from the definition, eqn. (34).

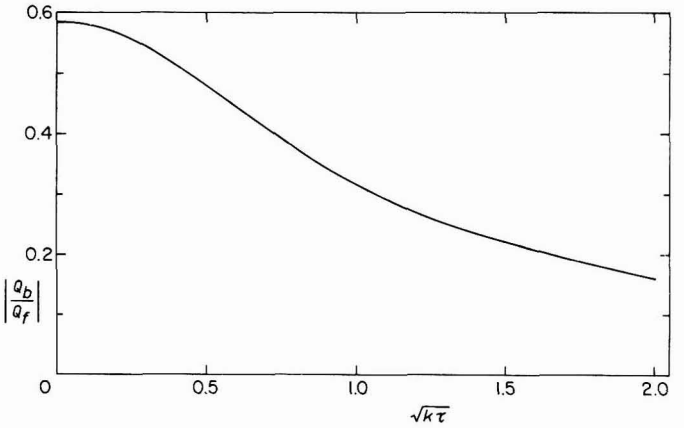

Fig. 3. $|Q_b/Q_f|$ *vs.* $\sqrt{k\tau}$ for following reaction; calc. from eqns. (39) and (41).

Figure 3 shows a plot of $|Q_b/Q_f|$ *vs.* $\sqrt{k\tau}$. As in the catalytic case, two limits can be seen in Fig. 3. If the reaction is very slow, essentially none of the R formed in the forward process is removed by the chemical reaction and $|Q_b/Q_f| \rightarrow 2-\sqrt{2}$, the diffusion-limited value; if the chemical reaction is very fast, essentially all of the R formed is consumed by the chemical reaction and $|Q_b/Q_f| \rightarrow 0$.

DISCUSSION

For both the catalytic and the following reaction cases, the region around $\sqrt{\beta^2\tau}$ or $\sqrt{k\tau} = 1$ offers the most precision for the determination of β^2 or k, since it is in this region that the maximum slope of the $|Q_b/Q_f|$ *vs.* $\sqrt{\beta^2\tau}$ or $\sqrt{k\tau}$ plot occurs. Since τ can be made smaller than 10 msec, (pseudo-)first-order rate constants greater than 100 sec^{-1} can probably be determined by this method. A lower limit on the rate constants that can be determined is set by the requirement that the diffusion remains linear.

A striking advantage of this technique over controlled-current techniques is

that an approximate correction for double-layer charging can easily be made. In this case, it is sufficient to subtract the double-layer charge measured in a separate experiment in the absence of the faradaic reaction; such a simple procedure is not possible in a controlled-current method.

Double potential-step chronocoulometry and chronoamperometry are analogous to techniques, such as reverse-current chronopotentiometry, in which the product of the electrode reaction is formed at a known rate, allowed to diffuse and react for a known time and the solution near the electrode then analyzed by changing the electrode condition (current or potential). The amount of product remaining is a measure of the rate of the chemical reaction. The results of the double potential-step technique should be more reliable, however, since the imprecision inherent in the transition time determination is eliminated and a better correction for double-layer charging may be made.

Under optimum conditions, the precision of the double potential-step chronocoulometric and chronoamperometric methods is essentially the same and the two techniques should necessarily give the same result.

The double potential-step chronocoulometric method offers promise for the quantitative study of simple chemical reactions following an electrode reaction. The following paper[12] demonstrates the advantages of this technique for the study of a well-known catalytic reaction.

ACKNOWLEDGEMENTS

This work was carried out under the direction of Professor FRED C. ANSON and Dr. ROBERT A. OSTERYOUNG, both of whom have made helpful comments and criticisms during the course of this work.

The author is especially indebted to PETER JAMES LINGANE for his invaluable assistance in the preparation of the working curves and for his continuing interest in the development of this work.

This work was supported, in part, by the Office of Army Research (Durham).

SUMMARY

The theoretical relations for the study of following and catalytic chemical reactions by the new technique of double potential-step chronocoulometry have been developed. Working curves for the evaluation of (pseudo-)first-order rate constants are presented. It is suggested that this technique will compare favorably with other electrochemical techniques for the study of chemical reactions coupled with the electrode reaction.

REFERENCES

1 A. C. TESTA AND W. H. REINMUTH, *Anal. Chem.*, 32 (1960) 1512.
2 C. FURLANI AND G. MORPURGO, *J. Electroanal. Chem.*, 1 (1960) 351.
3 H. B. HERMAN AND A. J. BARD, *Anal. Chem.*, 36 (1964) 510.
4 J. H. CHRISTIE AND G. LAUER, *Anal. Chem.*, 36 (1964) 2037.
5 W. M. SCHWARZ AND I. SHAIN, *J. Phys. Chem.*, 69 (1965) 30.
6 J. H. CHRISTIE, G. LAUER, R. A. OSTERYOUNG AND F. C. ANSON, *Anal. Chem.*, 35 (1963) 1979.
7 J. H. CHRISTIE, G. LAUER AND R. A. OSTERYOUNG, *J. Electroanal. Chem.*, 7 (1964) 60.

8 T. KAMBARA, *Bull. Chem. Soc. Japan*, 27 (1954) 523, 527, 529.
9 W. H. REINMUTH, *Anal. Chem.*, 34 (1962) 1446.
10 P. DELAHAY, *New Instrumental Methods in Electrochemistry*, Interscience, New York, 1954, p. 53.
11 P. DELAHAY AND G. L. STIEHL, *J. Am. Chem. Soc.*, 74 (1952) 3500.
12 P. J. LINGANE AND J. H. CHRISTIE, *J. Electroanal. Chem.*, 13 (1967) 227.

APPENDIX I

Symbols used

$^*C_O$	= bulk concentration of the oxidant;
C_O, C_R	= concentration of the oxidant and reductant, respectively;
D_O, D_R	= diffusion coefficients of the oxidant and reductant, respectively;
n	= number of electrons in the charge transfer reaction;
F	= the Faraday (96,487 C);
E	= electrode potential;
t	= time;
τ	= time at which the potential is stepped from E_1 to E_2;
I	= current density;
x	= distance from the electrode surface;
Q	= charge/unit area [see eqn. (11)];
$\bar{I}$, $\bar{C}_R$, $\bar{Q}$	= Laplace transforms of I, C_R, Q, respectively;
s	= Laplace transformation variable;
θ	= dummy time variable (for integration);
k	= first-order rate constant for following reaction;
k_c	= rate constant for catalytic reaction;
β^2	= pseudo-first-order rate constant for catalytic reaction;
${}_1F_1(a, b, z)$	= Kummer's confluent hypergeometric function (see eqn. 34);
$(2n-1)!!$	$= 1\times 3\times 5\times \ldots \times(2n-3)\times(2n-1)$.

APPENDIX II

Making the substitution $\xi=\theta-\tau$ in the second integral in eqn. (36) and integrating by parts

$$\int_0^{t-\tau}\frac{\varphi(k,\xi+\tau,\tau)}{\sqrt{\xi}}\,\mathrm{d}\xi = 2\,\varphi(k,t,\tau)\sqrt{t-\tau} - 2\int_0^{t-\tau}\sqrt{\xi}\left(\frac{\mathrm{d}\varphi}{\mathrm{d}\xi}\right)\mathrm{d}\xi \qquad \text{(AII-1)}$$

Since

$$\frac{\mathrm{d}\varphi}{\mathrm{d}\xi} = \mathrm{e}^{-k\tau}\left\{-k\mathrm{e}^{-k\xi}{}_1F_1(\tfrac{1}{2},1,k\tau) + \sum_{n=1}^{\infty}\frac{{}_1F_1(n+\tfrac{1}{2},n+1,k\tau)}{n!}\left[-k\mathrm{e}^{-k\xi}(k\xi)^n + nk\mathrm{e}^{-k\xi}(k\xi)^{n-1}\right]\right\} \qquad \text{(AII-2)}$$

we have

$$-\int_0^{t-\tau}\sqrt{\xi}\left(\frac{\mathrm{d}\varphi}{\mathrm{d}\xi}\right)\mathrm{d}\xi = \frac{2}{\sqrt{k}}\mathrm{e}^{-k\tau}\left\{{}_1F_1(\tfrac{1}{2},1,k\tau)\int_0^{\sqrt{k(t-\tau)}}y^2\mathrm{e}^{-y^2}\mathrm{d}y + \sum_{n=1}^{\infty}{}_1F_1(n+\tfrac{1}{2},n+1,k\tau)\left[\int_0^{\sqrt{k(t-\tau)}}\frac{y^{2n+2}\mathrm{e}^{-y^2}}{n!}\mathrm{d}y - \int_0^{\sqrt{k(t-\tau)}}\frac{y^{2n}\mathrm{e}^{-y^2}}{(n-1)!}\mathrm{d}y\right]\right\} \qquad \text{(AII-3)}$$

where the substitution $y^2=k\xi$ has been made.

Since

$$\int_0^{\sqrt{k(t-\tau)}} y^{2n+2} e^{-y^2} dy = -\tfrac{1}{2}[k(t-\tau)]^{n+\frac{1}{2}} e^{-k(t-\tau)} + \frac{2n+1}{2} \int_0^{\sqrt{k(t-\tau)}} y^{2n} e^{-y^2} dy \tag{AII-4}$$

the last two integrals may be combined to give

$$\begin{aligned} -\int_0^{t-\tau} \sqrt{\xi}\left(\frac{d\varphi}{d\xi}\right) d\xi = \frac{2e^{-k\tau}}{\sqrt{k}} \Bigg\{ {}_1F_1(\tfrac{1}{2}, 1, k\tau) \int_0^{\sqrt{k(t-\tau)}} y^2 e^{-y^2} dy \\ + \sum_{n=1}^{\infty} {}_1F_1(n+\tfrac{1}{2}, n+1, k\tau) \Bigg[- \frac{[k(t-\tau)]^{n+\frac{1}{2}} e^{-k(t-\tau)}}{2(n!)} \\ + \int_0^{\sqrt{k(t-\tau)}} \frac{y^{2n} e^{-y^2}}{2(n!)} dy \Bigg] \Bigg\} \end{aligned} \tag{AII-5}$$

in which we have used the identity

$$\frac{2n+1}{2(n!)} - \frac{1}{(n-1)!} = \frac{1}{2(n!)}$$

Observing that, as can be shown by repeated integrations by parts,

$$\begin{aligned} \int_0^z y^{2n} e^{-y^2} dy = -e^{-z^2} \left\{ \frac{z^{2n-1}}{2} + \sum_{i=1}^{n-1} \frac{z^{2(n-i)-1}}{2^{i+1}} \frac{(2n-1)!!}{(2n-2i-1)!!} \right\} \\ + \frac{\sqrt{\pi}}{2^{n+2}} \operatorname{erf} z[(2n-1)!!] \end{aligned} \tag{AII-6}$$

we can evaluate all the integrals in eqn. (AII-5). The result is

$$\begin{aligned} -\int_0^{t-\tau} \sqrt{\xi}\left(\frac{d\varphi}{d\xi}\right) d\xi = \frac{e^{-k\tau}}{\sqrt{k}} \Bigg\{ {}_1F_1(\tfrac{1}{2}, 1, k\tau) \left[z e^{-z^2} - \frac{\sqrt{\pi}}{2} \operatorname{erf} z \right] \\ + \sum_{n=1}^{\infty} \frac{{}_1F_1(n+\frac{1}{2}, n+1, k\tau)}{n!} e^{-z^2} \Bigg[z^{2n+1} + \frac{z^{2n-1}}{2} \\ + \sum_{i=0}^{n-1} \frac{z^{2(n-i)-1}}{2^{i+1}} \frac{(2n-1)!!}{(2n-2i-1)!!} \Bigg] \\ - \sum_{n=1}^{\infty} \frac{{}_1F_1(n+\frac{1}{2}, n+1, k\tau)}{n!} \frac{\sqrt{\pi}}{2^{n+1}} \operatorname{erf}(z)\, (2n-1)!! \Bigg\} \end{aligned} \tag{AII-7}$$

where $z^2 = k(t-\tau)$.

Substituting (AII-7) into (AII-1) and hence into (36) and performing the first and third integrals in (36), which are straight forward, gives eqn. (37).

COULO-POTENTIOMETRIC ACID-BASE TITRATIONS EMPLOYING TWIN MERCURY ELECTRODES

II. CHARACTERIZATION OF THE MERCURY ELECTRODE, ITS PREPARATION AND TREATMENT*

M. ARIEL AND E. KIROWA-EISNER

Laboratory of Analytical Chemistry, Department of Chemistry, Israel Institute of Technology, Haifa (Israel)

(Received December 2nd, 1965)

INTRODUCTION

The successful analytical application of the twin mercury electrodes indicating system can be realized only when the titration end-point is marked unequivocally by a sharp PDP (potential difference peak)[1]; this, in turn, depends on the proper functioning of the electrodes. A partial solution of this problem has been described[1]. The electrode characterization, including its sensitivity and rate of response, the criterion by which its functioning may be judged and the interferences encountered are dealt with in this paper. Finally, methods for electrode preparation and pre-treatment are discussed and a method recommended.

ELECTRODE CHARACTERIZATION: SENSITIVITY AND RATE OF RESPONSE

The sensitivity of the electrode is partly determined by the relative values of the residual current, i_r, and the limiting current at the start of the titration, $i_{1,0}$. The discrepancy between the equivalent point and the end-point (%), due to the residual current, is given by $i_r/i_{1,0} \cdot 100$ (as a result of the residual current, the potential-current curve is distorted; at the equivalent point, the system appears to have passed beyond it). The experimental value of the residual current at a potential of +0.1 V, was $1.5 \cdot 10^{-3}$ μA; this measurement was carried out in a stirred 5% KNO_3 solution in the absence of dissolved oxygen and mercury ions at a hanging drop electrode. Under the same conditions, in the presence of $5 \cdot 10^{-4}$ N acid, the limiting current was 15 μA, *i.e.*, at this acid concentration, the residual current is only 0.01% of the limiting current. The reproducibility of the residual current is better than 10%. The low value of the residual current and its good reproducibility, allow the titration of very dilute solutions (down to $3 \cdot 10^{-6}$ N); this cannot be achieved with any other known electrode.

Mercury-coated silver electrodes, prepared and treated as described below, have a rapid response rate; at the end-point the potential attains 95% of its final value within 10 sec. They are, therefore, eminently suitable for the titration of dilute solutions.

* Part of a D.Sc. thesis presented by E.K.E. to the Senate of the Technion.

CRITERION FOR THE PROPER FUNCTIONING OF THE ELECTRODES

"S"-shaped titration curves do not lend themselves readily to visual inspection for possible distortion. The peaked shape, on the other hand, provides a convenient means for judging the state of the electrode—the half-peak width under standard conditions. Proper functioning under normal working conditions is ensured by specifying the half-peak width (determined on the basis of a suitable number of experiments) for the most severe conditions (dilute solutions).

INTERFERENCES AND PROBABLE REASONS FOR ELECTRODE FAILURE

In addition to the interferences previously mentioned[1], the effect of dissolved oxygen, causing the dissolution of mercury and the appearance of mercuric ions in the solution[2], and the deleterious effect of surface-active substances on the electrode surfaces, must be taken into account.

The reasons for electrode failure have not been investigated. It may be assumed that the malfunction of an electrode is partly due to the gradual adsorption of contaminants on the surface. The failure of freshly prepared electrodes could be attributed to the presence of silver oxides on the silver wire (preventing proper mercury coating). Malfunction of the electrodes distorts the titration curves and changes their slope. With automatic recording of the titration curve (and constant rate of titrant addition) a lag in the end-point, resulting from the delayed response of the impaired electrode, becomes apparent.

ELECTRODE PREPARATION AND TREATMENT

Various mechanical, chemical and electrochemical methods of coating the silver wire with mercury were tried in order to produce electrodes fulfilling the requirements set out above; these included polishing the silver wire to remove oxide layers, electropolishing and electroplating[1]. The ideal method for producing a reliable electrode was by passing alternate positive and negative current pulses through the impaired electrode. This treatment, described in detail below, is rapid, does not require a special electroplating solution and invariably gives satisfactory results. Under optimum conditions, up to 50 titrations have been recorded at an electrode before it needed regeneration, although the number is usually somewhat lower depending on the solutions in which the electrode is used.

During the positive pulse, the potential of the electrode *vs.* the solution is positive and some of the mercury coating dissolves. A fresh mercury surface is produced and various contaminants, previously adsorbed and probably largely responsible for its malfunction, are removed from the electrode surface and pass into solution. Short dissolution periods (of the order of milli- or microseconds) will not suffice, since the quantity of mercury dissolved will be too small. With considerably increased current densities, short pulses should also be effective. Current pulses exceeding 1 sec tend to produce mercuric oxide on the electrode—this is undesirable.

The negative pulse, following the positive, ensures the removal of oxidized substances from the electrode surface; the hydrogen gas evolved probably cleans the

electrode mechanically. The treatment is concluded with a negative pulse, to reduce any mercuric oxide present.

The application of a considerable number of alternating positive and negative pulses thoroughly cleans the electrode surface and provides a convenient, rapid and reliable method of electrode regeneration.

Recommended method for electrode preparation and regeneration

The end (1–2 cm) of a clean silver wire, 2 mm in diameter and of length depending on the dimensions of the titration cell, is dipped into pure mercury. If the coating appears uneven, the mercury may be spread evenly by rubbing the area to be coated with a soft paper tissue. The electrode is transferred into a 50-ml beaker, containing a 1% KNO_3–10^{-4} N HNO_3 solution. The electrode is connected through a double-pole double-throw switch to a current supply, with a platinum wire serving as auxiliary electrode. Alternating negative and positive pulses, of 20 mA and 1 sec duration each, are passed between the electrodes for a total treatment period of 1 min. The last pulse is negative (*i.e.*, the mercury electrode is negative) and is prolonged for 3–5 sec. The electrode polarity is reversed by manual switching and the duration of the pulses measured by means of a stop-watch. Throughout the treatment, the solution in which the electrodes are dipped is stirred with a magnetic stirrer. The process, starting with the dipping of the electrode into mercury, should then be repeated. Two electrodes (connected to each other) may be prepared simultaneously by this method.

The regeneration of impaired electrodes is carried out as above after wiping the electrode dry with tissue paper; in this case the treatment need only be performed once.

CRITERION FOR ELECTRODE FUNCTIONING. EXPERIMENTAL DETAILS

About 60 ml of a 10% KNO_3 solution were introduced into a coulometric cell and acid generated coulometrically by passing a 20-mA generating current for about 20 sec. This acid was then titrated coulometrically with a 3 mA generating current and with the two mercury electrodes under test serving as indicating system. The titration curve was recorded and the half-peak (PDP) width measured. A half-peak width smaller than 15 sec indicates that the electrodes are functioning correctly.

The sensitivity of the electrode was determined as described above using a Radiometer Polariter, Type PO4d.

SUMMARY

The preparation, pretreatment and regeneration of the mercury-coated silver electrode, employed in the twin mercury electrodes acid–base indicating system, is described. Methods for determining electrode sensitivity, rate of response and the criterion for correct electrode performance are given. Possible interferences are mentioned.

REFERENCES

1 M. Ariel and E. Kirowa-Eisner, *J. Electroanal. Chem.*, 10 (1965) 319.
2 S. E. S. El Wakkad and T. M. Salem, *J. Phys. Chem.*, 54 (1950) 1371.

THE ELECTRO-OXIDATION OF POLYCYCLIC AROMATIC HYDROCARBONS IN ACETONITRILE STUDIED BY CYCLIC VOLTAMMETRY

M. E. PEOVER AND B. S. WHITE*

Formerly of the National Chemical Laboratory, now with Division of Molecular Science, National Physical Laboratory, Teddington, Middlesex (Great Britain)

(Received February 11th, 1966)

INTRODUCTION

In an earlier paper GOUGH AND PEOVER described the application of slow-sweep cyclic voltammetry to the study of the oxidation of some aromatic compounds at a platinum electrode in acetonitrile[1]. It was found that, in general, and for polycyclic aromatic hydrocarbons in particular, electron-transfer is coupled with a rapid irreversible chemical reaction. The unsubstituted hydrocarbons apparently undergo a multi-electron oxidation, but when electron-donating substituents are present in suitable positions, a one-electron wave results. Here we present the results of work with rapid-sweep cyclic voltammetry designed to determine the nature of the primary electrode process and the consequences of the coupled chemical reactions for some polycyclic aromatic hydrocarbons, and thence to attempt to evaluate the one-electron oxidation redox potentials.

EXPERIMENTAL

Conventional polarograms were obtained at a rotating platinum electrode (RPE) (rotation 500 rev/min., surface area approx. 0.25 mm^2) and a Cambridge Instruments polarograph. A.c. polarograms were obtained with a Univector polarograph operating at 35 c/sec with a superimposed voltage of 26.5 mV. A three-electrode cell with iR-compensator was employed.

The triangular-wave polarograph was constructed from a Hewlett-Packard wave-form generator 202A, with associated bias and amplitude controls. Current–voltage curves were displayed on a Solartron oscilloscope or Hewlett-Packard 140A and photographed employing Polaroid film. It was found necessary to employ frequencies up to 1 kc/sec in order to eliminate the chemical processes in the systems under study, and a differential cell was used to reduce the base current from the charging of the electrode double-layer. A three-compartment cell, separated by 4-porosity sinters had a coil of silver wire (2 m) immersed in 10^{-2} M $AgClO_4$, 10^{-1} M NEt_4ClO_4 in the centre compartment, as a common counter-electrode. Two closely similar platinum micro-electrodes, formed by sealing a length of platinum wire into a glass tube and

* Present address: Department of Chemical Engineering, Manchester College of Science and Technology.

grinding the end flat, served as the differential indicator electrodes. The electrodes were balanced for the small difference in surface area immersed in the supporting electrolyte at the frequencies to be used, and the same ratio of correction settings maintained in subsequent measurements with one electrode in the test solution. A region of 0.4–0.5 V was normally scanned. The test solution contained 0.1 *M* NEt_4ClO_4 and was purged of oxygen with nitrogen. After an initial treatment with concentrated nitric acid followed by acidic ferrous ammonium sulphate, the micro-electrodes were wiped with fine emery paper before a set of readings. The surface conditions were sufficiently reproducible using this procedure. Corrections for *iR*-drop were necessary at the higher frequencies. The cell resistance was determined by bridge measurements at several frequencies and at a bias potential such that the resistance was independent of frequency.

RESULTS

The seven polycyclic aromatic hydrocarbons studied are listed in Table 1. It is convenient to consider first the behaviour of 9,10-diphenylanthracene which may be regarded as a model compound, since even at the slow rates of voltage-sweep used in conventional polarography the compound undergoes reversible oxidation to the free-radical cation, the latter having a lifetime which is long compared with the rate of diffusion. Thus at the RPE two well-defined one-electron oxidation waves are found,

TABLE 1

OXIDATION POTENTIALS OF SOME POLYCYCLIC AROMATIC HYDROCARBONS IN ACETONITRILE AT A PLATINUM MICRO-ELECTRODE AT 25°

Reference electrode Ag/0.01 *M* $AgClO_4$, 0.1 *M* Et_4NClO_4 (CH_3CN) which is +0.30 V *vs.* S.C.E.

Compound	$E_{\frac{1}{2}}$	E_s	$E_0{}^1$	*Compound*	$E_{\frac{1}{2}}$	E_s	$E_0{}^1$
9,10-Diphenylanthracene	0.92	0.92	0.92	Chrysene	1.22	1.27	1.29
Anthracene	0.91	0.99	0.99	Phenanthrene	1.28	1.36	1.45
1,2-Benzanthracene	1.00	1.09	1.07	Triphenylene	1.46*	1.55*	1.50
Pyrene	1.06*	1.24*	1.12				

$E_{\frac{1}{2}}$, half-wave potential at a rotating platinum electrode, 500 rev/min, 0.3 V min^{-1}. E_s, summit potential of a.c. polarogram, 35 c/sec, 26.5 mV. $E_0{}^1$, limiting potential at sweep rates 100–500 V sec^{-1}. $E_0{}^1 = E_p - 0.03$ V.

* Insoluble deposits finally cover the electrode.

the first being associated with a reproducible well-defined a.c. polarogram of height and half-peak width appropriate for rapid transfer of one electron[2], Fig. 1. A comparison with the *reduction* behaviour at the DME, also shown in Fig. 1, shows clearly the symmetry of the two processes. The cyclic voltammograms show one-electron oxidation to stable products and their subsequent reduction, and illustrate the advantage of differential methods at high frequencies, Figs. 2–4.

The separation in anodic and cathodic peak potentials is about 60 mV, as required for rapid one-electron transfer, up to about 30 V/sec. Above this value the separation increases, indicating departure from ideal behaviour. At high scan-rates, the uncertainties in the potentials due to *iR*-drop become more serious, nevertheless it is worth noting that the peak separations found at 50 V/sec (63 mV) and at 500 V/sec (72 mV) correspond to values of the standard rate constant of 1.75 cm sec^{-1} and

1.6 cm sec^{-1}, respectively, following the treatment of NICHOLSON[3]. The order of magnitude thus appears to be significant. The peak anodic current function, $ip/\sqrt{v}$, is essentially independent of scan-rate, Fig. 5. The slow-sweep cyclic voltammetry of diphenylanthracene in acetonitrile has also been described by VISCO AND CHANDROSS[4] with essentially the same results.

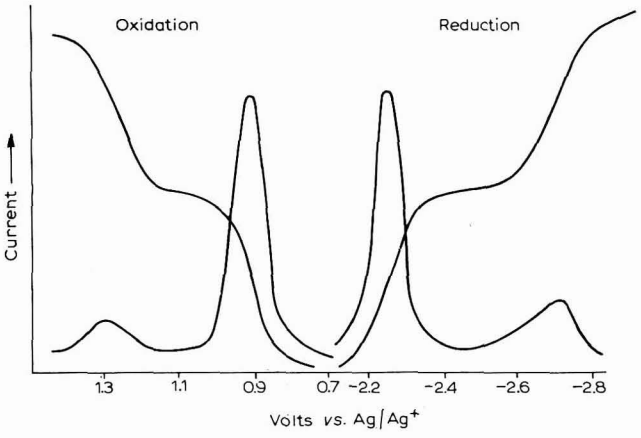

Fig. 1. Reduction and oxidation polarograms of 9,10-diphenylanthracene in acetonitrile–0.1 M NEt_4ClO_4 at DME and RPE; a.c. frequency: 35 c/sec; 26.5 mV.

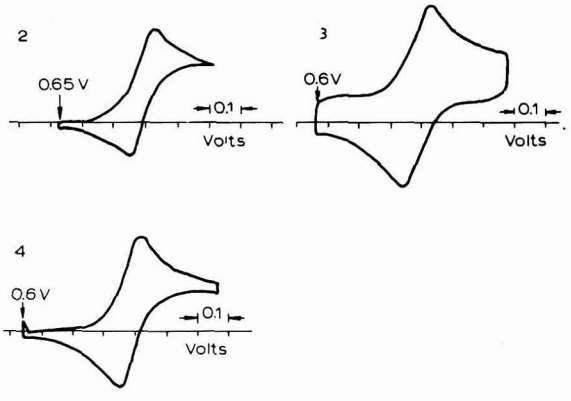

Figs. 2–3. Cyclic voltammogram of the oxidation of 9,10-diphenylanthracene in acetonitrile at: (2) 0.1 V sec^{-1}; (3) 50 V sec^{-1}.

Fig. 4. Differential cyclic voltammogram of the oxidation of 9,10-diphenylanthracene in acetonitrile at 50 V sec^{-1}.

Of the unsubstituted hydrocarbons, 1,2-benzanthracene shows the simplest behaviour. Figure 6 illustrates the complete lack of cathodic trace in the cyclic voltammogram at low sweep-rates due to the coupled chemical changes, while at high sweep-rates the cathodic trace is well-developed, approaching equality with the anodic current, Fig. 7. The latter is a steady-state trace, the current–voltage curves in the first 0.1 sec showing considerable reduction in the anodic peak-current, Fig. 8. The

anodic–cathodic peak separations are 80–90 mV in the range 20–200 V/sec, somewhat larger than for diphenylanthracene.

Chrysene, pyrene, and anthracene show poorly-developed cathodic currents at high sweep-rates in that order of decreasing stability of the cation radicals. The formation of an insulating film on the electrode with pyrene can be prevented by limiting

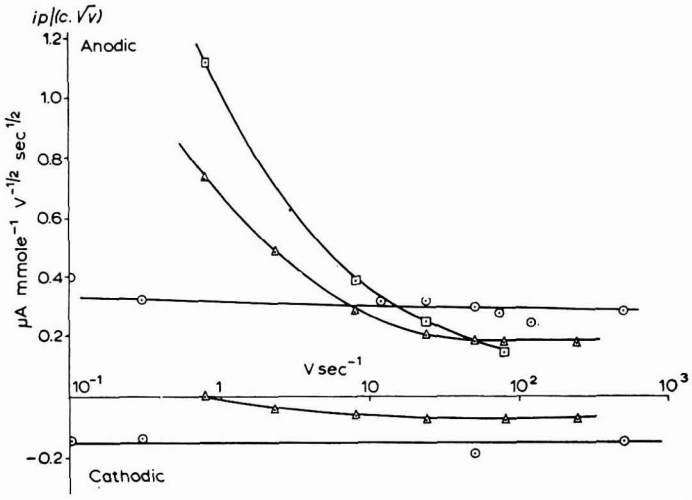

Fig. 5. Dependence of peak anodic and cathodic current functions $ip/\sqrt{v}$ on scan-rate for the electro-oxidation of aromatic hydrocarbons in acetonitrile–0.1 *M* NEt_4ClO_4. (The cathodic current function is measured to the background current as zero rather than the current at the reversal potential). (○), 9,10-diphenylanthracene; (△), 1,2-benzanthracene; (□), chrysene.

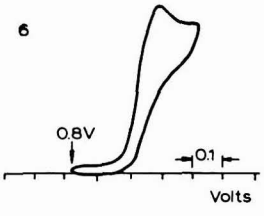

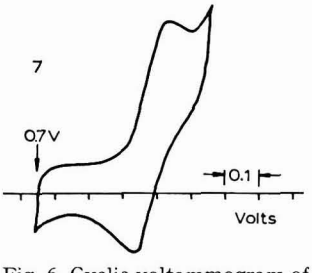

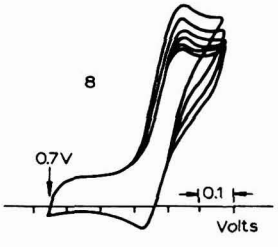

Fig. 6. Cyclic voltammogram of the oxidation of 1,2-benzanthracene in acetonitrile at 0.8 V sec^{-1}.

Figs. 7–8. Differential cyclic voltammogram of the oxidation of 1,2-benzanthracene in acetonitrile at 40 V sec^{-1}: (7) steady state; (8) on a fresh electrode, 0.1 sec exposure.

the sweep to just beyond the peak potential. No cathodic portion is discernible with triphenylene and an insulating film forms on the electrode within a few seconds.

The potential of the anodic peak is shown as a function of scan-rate in Fig. 9. The value is independent of scan-rate for 9,10-diphenylanthracene indicating negligible overvoltage up to at least 30 V/sec; at higher scan-rates, a small positive shift in peak potential is observed. For the other compounds, the peak potential is dependent on scan-rate for lower values, becoming virtually independent at higher values.

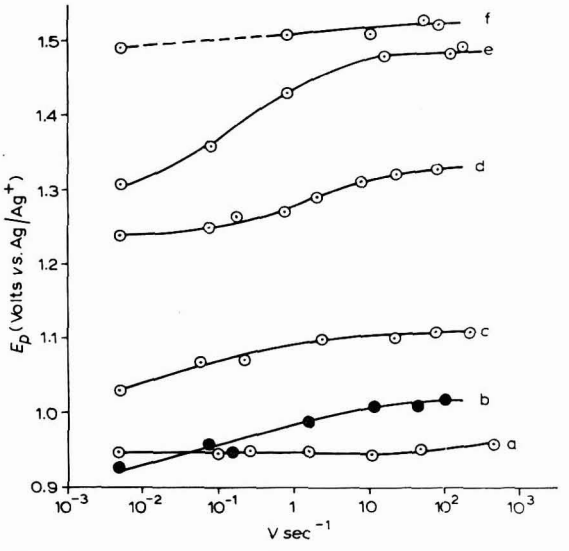

Fig. 9. Dependence of anodic peak potentials on scan-rate for oxidation in acetonitrile: (a), 9,10-diphenylanthracene; (b), anthracene; (c), 1,2-benzanthracene; (d), chrysene; (e), phenanthrene; (f), triphenylene.

The steady-state peak anodic currents are shown in Fig. 5 for three of the compounds. Virtually ideal behaviour is shown with 9,10-diphenylanthracene but this is approached only at higher frequencies with the unsubstituted compounds.

The current–voltage curves at a RPE in acetonitrile for these compounds have been described by GOUGH AND PEOVER[1]. We now find that well-developed a.c. polarograms are obtained, the summit potentials being somewhat more positive than the half-wave potentials, in contrast to the diphenylanthracene case. The values of the half-wave and summit potentials are listed in Table 1.

DISCUSSION

The results for 9,10-diphenylanthracene make it clear that in this case, electro-oxidation in acetonitrile at all scan-rates employed, occurs by removal of two electrons in *successive* one-electron steps separated by about 0.5 V, the first charge-transfer having an apparent standard rate constant of the order 1 cm sec^{-1} at a platinum electrode. The results for the unsubstituted compounds are more complex and the following discussion is based on the theoretical analysis of cyclic voltammetric curves given by NICHOLSON AND SHAIN[5,6].

At high rates of voltage scan, the results can be treated in terms of the process

$$A \overset{-e}{\rightleftarrows} A^+ \overset{k_f}{\rightarrow} B \overset{-e}{\rightarrow} C \qquad (1)$$

When k_f/v becomes vanishingly small (v is the rate of voltage change), the limiting behaviour is that of the system

$$A \overset{-e}{\rightleftarrows} A^+ \qquad (2)$$

Thus for 1,2-benzanthracene, the limiting behaviour can be regarded as approaching process (2). The data in Figs. 5 and 9 bear out this contention. It was noted that the separation in anodic and cathodic peak potentials is 80–90 mV, *i.e.*, some 20 mV greater than with diphenylanthracene. It is possible that the products of the coupled chemical reactions poison the electrode surface, leading to lower apparent rates of electron-transfer. Alternatively, even in regions of low values of k_f/v it is possible for the cathodic current observed to be almost entirely due to the process $C \rightarrow B$, provided the standard potentials of the $A \rightleftharpoons A^+$, $B \rightleftharpoons C$ couples are very close (see Fig. 5 of ref. 6). The separation in anodic and cathodic peak potentials is then a complex function of the properties of the $A \rightleftharpoons A^+$ and $B \rightleftharpoons C$ couples. The differentiation between process (2) and that discussed above is too slight for a distinction to be drawn from the precision of the present experimental data. Nevertheless, in both cases the anodic currents and peak potentials are determined primarily by process (2). We are therefore justified in regarding the limiting anodic peak potentials, Fig. 9, as characteristic of process (2), whence the formal redox potential can readily be obtained. As the scan-rate is reduced, the anodic peak potentials become more cathodic and the anodic current increases to a value corresponding to the transfer of several electrons/molecule. We must conclude that process (1) becomes modified by additional chemical reactions leading to the possibility of further electro-oxidation without change of potential. Again, the standard potentials must be close to that of process (2) and the chemical reactions must be irreversible since no other electrochemical changes are observed at more negative potentials.

From the general similarity in behaviour of all the polycyclic aromatic hydrocarbons studied, it can be concluded that the above discussion is applicable to these others also. In particular, the limiting peak potentials in Fig. 9 have been used to obtain the redox potentials listed in Table 1. The uncertainties introduced by the ambiguities in interpretation of peak separations and electron-transfer rates about 10–15 mV. The values of the redox potentials are on the whole more positive than the a.c. summit potentials obtained with a small amplitude superimposed frequency of 35 c/sec. The magnitude of the alternating current associated with fast charge-transfer in the presence of an irreversible coupled chemical reaction is much reduced as a result of half-wave rectification, but the summit potential is much less affected. The latter lies between the d.c. half-wave potential and the limiting values at high sweep-rates and close to the limiting values provided no filming of the electrode occurs. The redox potentials obtained in this work have been used in a study of the surface potential of acetonitrile[7].

Finally, attention should be drawn to the variation in the values of half-wave potentials for the oxidation of aromatic hydrocarbons reported in the literature[1,8–10]. It can now be seen that since all these values were obtained at rates of voltage change where the coupled chemical reactions are dominant, the resulting half-wave potentials

are therefore strongly dependent on the scan-rate employed. We also find that the values are strongly dependent on concentration under these conditions.

ACKNOWLEDGEMENTS

We thank Mr. J. D. DAVIES for the preliminary work and Mr. J. S. POWELL for technical assistance. The paper is published by permission of the Director of the National Physical Laboratory.

SUMMARY

The electro-oxidation of 9,10-diphenylanthracene results in a relatively stable radical-cation with a rate of charge-transfer of the order 1 cm sec^{-1} at a platinum electrode in acetonitrile. 1,2-Benzanthracene exhibits behaviour approaching that of diphenylanthracene at high rates of voltage change (500 V sec^{-1}). At lower sweep-rates, irreversible chemical reactions intervene leading to further oxidation, the standard potentials of subsequent steps being close to that for the first charge-transfer. Anthracene, pyrene, phenanthrene and triphenylene exhibit similar limiting behaviour of anodic currents and peak potentials at high scan-rates, which is identified with the formation of radical cations: the cations of these hydrocarbons have a lifetime of a few milliseconds. The common supposition that the primary electrode process involves the formation of the dipositive ion is thus incorrect. Moreover, conventional polarographic oxidation potentials of the unsubstituted compounds are controlled by chemical reaction. The reversible oxidation potentials for the charge-transfer step have been evaluated from the data at high rates of voltage sweep.

REFERENCES

1 T. A. GOUGH AND M. E. PEOVER, *Proc. 3rd International Polarography Congress, Southampton, 1965*, Macmillan, London, 1966, p. 1017.
2 V. A. KIR'YANOV AND V. YU. FILINOVSKII, *Zh. Fiz. Khim.*, 37 (1963) 2122.
3 R. S. NICHOLSON, *Anal. Chem.*, 37 (1965) 1351.
4 R. E. VISCO AND E. A. CHANDROSS, *J. Am. Chem. Soc.*, 86 (1964) 5350.
5 R. S. NICHOLSON AND I. SHAIN, *Anal. Chem.*, 36 (1964) 706
6 R. S. NICHOLSON AND I. SHAIN, *Anal. Chem.*, 37 (1965) 178.
7 B. CASE, N. S. HUSH, R. PARSONS AND M. E. PEOVER, *J. Electroanal. Chem.*, 10 (1965) 320.
8 H. LUND, *Acta. Chem. Scand.*, 11 (1957) 1323.
9 J. W. LOVELAND AND G. R. DIMELER, *Anal. Chem.*, 33 (1961) 1196.
10 E. S. PYSH AND N. C. YANG, *J. Am. Chem.*, 85 (1963) 2124.

ANODIC BEHAVIOUR OF PHOSPHITES AND HYPOPHOSPHITES

A. HICKLING AND D. JOHNSON
Donnan Laboratories, University of Liverpool (England)
(Received December 15th, 1965)

INTRODUCTION

Calculations from available thermodynamic data give the following standard redox potentials on the hydrogen scale:

$$H_3PO_3 + H_2O \rightleftharpoons H_3PO_4 + 2\,H^+ + 2\,e \quad -0.275\ V$$

$$H_2PO_3^- + H_2O \rightleftharpoons H_2PO_4^- + 2\,H^+ + 2\,e \quad -0.265$$

$$HPO_3^{2-} + H_2O \rightleftharpoons HPO_4^{2-} + 2\,H^+ + 2\,e \quad -0.234$$

$$H_3PO_2 + H_2O \rightleftharpoons H_3PO_3 + 2\,H^+ + 2\,e \quad -0.499$$

$$H_2PO_2^- + H_2O \rightleftharpoons H_2PO_3^- + 2\,H^+ + 2\,e \quad -0.506$$

Purely on energy grounds it might thus be expected that phosphites and hypophosphites in acid and neutral solutions would be oxidised very readily at an anode. Since no information could be found in the literature[1] on this subject, it has now been investigated experimentally, and the surprising result has emerged that both phosphites and hypophosphites are relatively inert towards anodic oxidation even at potentials of +2 V when oxygen is being freely evolved. Hypophosphites can, however, be oxidised anodically at surfaces such as palladium that bring about their catalytic decomposition, and the mechanism of this unusual reaction has been explored.

EXPERIMENTAL

Electrolyses were mainly carried out in 0.1 *M* KH_2PO_4 + 0.1 *M* Na_2HPO_4 buffer of approximately pH 7, as medium; supplementary experiments with 0.1 *N* H_2SO_4 and 0.1 *N* NaOH showed the effects of acidity and alkalinity. Phosphite and hypophosphite solutions were made up by weight from commercially available specimens of $Na_2HPO_3 \cdot 5\,H_2O$ and NaH_2PO_2, both of which analysed better than 98% pure. The cell was an open beaker, usually thermostatted at 25°, provided with stirrer, thermometer, and a tubular cathode compartment closed at the lower end by a porous plug. Sheet anodes of total apparent area 10 or 2 cm^2 were used according to the current density (CD) required, and these were sealed into glass holders, either directly, or by Araldite cement; the cathode was a spiral of platinum wire. Anodes of smooth platinum, palladium, graphite, lead, and nickel have been employed, each being appropriately cleaned before use; in addition, platinised platinum (ptPt), plati-

num coated with finely divided palladium by electrodeposition (pdPt), and lead coated with lead dioxide by anodic treatment in sulphuric acid (PbO_2) have also been tried.

After much preliminary work, a volumetric method of analysis for phosphite and hypophosphite was devised. To estimate phosphite the sample was buffered at pH 7 with phosphate buffer and excess iodine added; the mixture was then left for 1 h and back-titrated with sodium thiosulphate. Under these conditions phosphite is quantitatively oxidised but hypophosphite is unaffected. To estimate hypophosphite, the sample was acidified with 9 *N* sulphuric acid and excess ceric ammonium sulphate added; the mixture was then heated for $2\frac{1}{2}$ h at 35°, cooled and back-titrated with ferrous ammonium sulphate using ferroin as indicator. Under these conditions the hypophosphite is quantitatively oxidised to phosphite which is itself unaffected.

RESULTS

Phosphite

Table 1 gives the current efficiencies (CE's) of oxidation observed with 100 ml of 0.1 *M* Na_2HPO_3 in phosphate buffer of pH 7 at 25° using a variety of anodes, each of 2 cm^2 area; the CD was 0.05 A cm^{-2}, the actual current 0.1 A, and 0.01 F was passed, theoretically sufficient for half the phosphite present to be oxidised to phosphate.

TABLE 1

Anode	Pt	ptPt	pdPt	Pd	C	Pb	Ni	PbO_2
CE %	0	0	0	1	2	2	5	6

Oxidation in nearly all cases was nil or trivial. The experimental conditions were then varied. The Pt anode was used in the same solution with CD's varying from 0.01–0.05 A cm^{-2}, and the phosphite concentration varying from 0.02–0.2 *M*; in no experiment was a CE greater than 2% recorded. When the medium was changed from the phosphate buffer to 0.1 *N* H_2SO_4 or 0.1 *N* NaOH, there was, again, no oxidation. If potassium iodide was added to the electrolyte, so that iodine could be liberated at the anode, phosphite was readily oxidised. Thus, 0.08 *M* Na_2HPO_3 + 0.1 *M* KI in phosphate buffer electrolysed under the conditions used in Table 1, gave a CE of phosphite oxidation of 66%. It seems, therefore, that oxidation can occur *via* a chemical oxidant formed at the anode if it can persist for some time. Observations with a PbO_2 anode seem to support this. A small CE was observed at this electrode in neutral solution possibly due to formation of a higher oxide. The CE was perceptibly increased in 0.1 *N* H_2SO_4 medium and by lowering the CD to 0.01 A cm^{-2}, values as high as 50% were obtained.

The potentials of the working anodes were measured during electrolysis and CD–potential curves were studied. The static potential of a Pt electrode in 0.1 *M* Na_2HPO_3 in phosphate buffer was about +0.3 V. It rose at once to that of oxygen evolution (*i.e.*, in the range +1.4–2.0 V depending upon CD) when current was passed and, unexpectedly, this potential was generally higher with phosphite present than in

its absence. This effect of phosphite in raising the potential of oxygen evolution was consistently observed in all solutions.

Hypophosphite

Table 2 gives the CE's of oxidation of hypophosphite assuming oxidation to phosphite, and those of phosphite formation actually observed with an electrolyte of 0.1 *M* NaH_2PO_2 in phosphate buffer under the experimental conditions quoted for Table 1.

TABLE 2

Anode	*Pt*	*ptPt*	*pdPt*	*Pd*	*C*	*Pb*	*Ni*	*PbO_2*
CE oxidation %	2	4	45	28	15	7	4	10
CE phosphite % formation	2	3	40	30	6	2	3	3

Oxidation was generally small except at Pd and, particularly, pdPt, at which it was substantial; it is noteworthy that, in general, more hypophosphite was oxidised than appeared as phosphite in the final electrolyte implying that some direct oxidation to phosphate probably occurs.

Attempts to increase the trivial oxidation at a Pt electrode by varying the experimental conditions, *e.g.* by lowering the CD to 0.1 A cm^{-2}, by increasing the concentration to 0.2 *M*, and by raising the temperature to 40°, were all unsuccessful. Potential measurements also indicated the absence of any genuine reaction; in the presence of hypophosphite, the rest potential of Pt was about +0.3 V, but, as with phosphite, it rose immediately on passing current to a value appreciably higher than that for oxygen evolution in phosphate buffer alone.

Reaction at palladium anodes

Since oxidation did occur at Pd anodes, this reaction was particularly studied. It was found that the most reproducible results could be obtained using pdPt, the electrodeposition being carried out under standardised conditions from a 2% solution of $PdCl_2$ in *N* HCl to give about 2 mg of Pd cm^{-2}. When such an electrode was dipped into 0.1 *M* NaH_2PO_2 in phosphate buffer, hydrogen gas was evolved and a potential of about −0.45 V was set up. In confirmation of the earlier work of NYLÉN[2], this potential was found to vary approximately linearly with log [NaH_2PO_2] and pH, the slopes of the two graphs being −0.032 and −0.058, respectively; the addition of phosphite to the solution did not affect the potential. When current was passed to make the metal anodic, the electrode could sustain quite a high CD before the potential was markedly displaced. The voltammetry of the system was investigated both galvanostatically and potentiostatically, and some of the potentiostatic curves, which are particularly interesting, are shown in Fig. 1, A and B. Under the usual conditions of electrolysis in stirred solution, polarisation was slight up to a CD of about 0.008 A cm^{-2}; it then gradually increased and the CD reached a peak value of about 0.02 A cm^{-2} when the anode potential was in the region of 0 V. With further increase of anode potential, the CD decreased rapidly and somewhat irregularly and then remained low

until the onset of oxygen evolution at a high positive potential. If the solution was unstirred, a definite limiting current was observed in the first step at 0.008 A cm^{-2}, but the peak was unaffected and subsequent behaviour was much the same. In Fig. 1B is shown the influence of hypophosphite concentration in stirred solutions. With *M* NaH_2PO_2 the peak was not reached even at a CD of 0.03 A cm^{-2}; with 0.01 *M* NaH_2PO_2 a limiting CD was observed at 0.003 A cm^{-2} and the peak was lowered to 0.006 A cm^{-2}; subsequent behaviour was much the same as in 0.1 *M* NaH_2PO_2. Change of pH had a marked effect on the shape and height of the peak. Rise of pH moved the initial section of the curve to more negative potentials, but the peak itself still occurred at about 0 V and its height was very much increased. Increase in temperature, likewise raised the peak CD considerably.

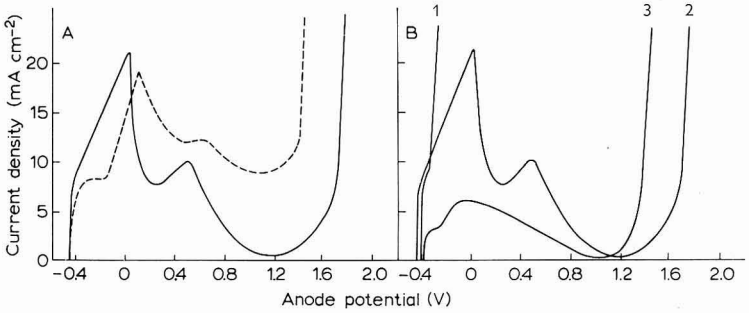

Fig. 1. Potentiostatic current density–potential curves for a palladium-black anode in sodium hypophosphite solns. A: (——), stirred; (---), unstirred. B: (1), 1.0; (2), 0.1; (3), 0.01 *M*.

TABLE 3

Potential (V)	*F/mole hypophosphite used*	*F/mole phosphite formed*
−0.3	1.16	1.57
−0.15	1.25	1.80

It is thus evident that hypophosphite can undergo some low potential oxidation at a Pd surface. To establish its nature, potentiostatic electrolyses were carried out at selected potentials on the curve using 0.1 *M* NaH_2PO_2 in phosphate buffer, and the number of faradays involved in the reaction was found. For potentials on the ascending branch of the curve, reasonably reproducible results were obtained independent of size of anode or duration of electrolysis; mean values are summarised in Table 3.

Attempts to obtain corresponding values at the peak potential itself, and on the descending part of the curve, gave erratic results, sometimes of the same order of magnitude but often tending towards higher values.

DISCUSSION

At first sight, the failure to oxidise phosphite and hypophosphite at most

anodes, even with an overpotential of over 2 V, seems to constitute an electrochemical paradox. It follows, however, quite simply from the views currently held on the structures of these substances. As first suggested by MITCHELL[3], each of the acids (and presumably the corresponding anions) can exist in tautomeric forms which may be represented as

$$HPO(OH)_2 \rightleftharpoons P(OH)_3$$

$$H_2PO(OH) \rightleftharpoons HP(OH)_2$$

and it is probably only the 3-valent phosphorus compounds that can be readily oxidised. Now, the concentration of these active forms at equilibrium is extremely small[4], and their rate of reaction at an electrode must be correspondingly low. Since the conversion of the inactive to the active forms does not involve charge transfer, it is unlikely to be accelerated by the field at the anode–solution interface, and hence no supply of extra electrical energy can bring about the oxidation. If, however, electrolysis liberates a chemical oxidising agent at the anode which can persist in the solution, then oxidation can occur at a rate dependent on the conversion of the inactive to the active forms, a process which is acid-catalysed. Thus, the behaviour found experimentally is what would be expected although it is an extreme example of thermodynamic considerations being completely outweighed by structural and kinetic factors.

The static potentials observed with finely divided Pd electrodes in hypophosphite solutions suggest that an electrochemical reaction can occur involving 2 electrons in which 2 hydrogen ions are produced from each hypophosphite molecule, but phosphite itself is not an immediate product of the oxidation. This can readily be formulated as adsorption of the hypophosphorous acid molecule or anion on Pd *via* the covalently-bound hydrogen atoms, followed by ionisation of these and formation of metaphosphorous acid which is left attached to the surface by the lone pair of electrons of the phosphorus, *e.g.*,

$$Pd + H_2PO(OH) \rightleftharpoons Pd\text{---}H_2PO(OH) \rightleftharpoons Pd\text{—}PO(OH) + 2\,H^+ + 2\,e$$

or

$$Pd + H_2POO^- \rightleftharpoons Pd\text{---}H_2POO^- \rightleftharpoons Pd\text{—}POO^- + 2\,H^+ + 2\,e$$

If the surface concentration of the metaphosphite is constant under a given set of experimental conditions, the static potential would be given by

$$\pi = \pi' + \frac{RT}{F}\ln[H^+] - \frac{RT}{2F}\ln[NaH_2PO_2]$$

$$= \pi' - 0.059\ \mathrm{pH} - 0.03\ \log_{10}[NaH_2PO_2] \text{ at } 25^\circ$$

which is in good agreement with the value found. Since hydrogen can be catalytically evolved at Pd, it is apparent that the hydrogen atoms may separate as an H_2 molecule instead of being ionised, and this process may compete with the electrochemical reaction. Thus, we can draw up a possible scheme for the reactions at a Pd anode as follows.

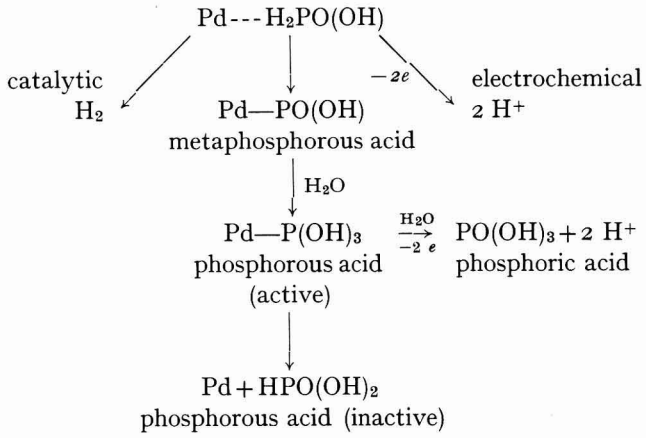

For the hypophosphite ion an exactly analogous set of reactions can be postulated.

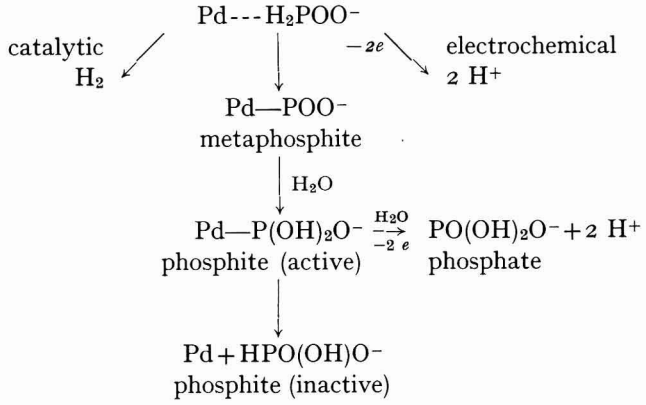

Because of the competition of the catalytic and electrochemical decompositions at the beginning, one would expect the oxidation of each mole of hypophosphite to require rather less than 2 faradays, tending towards this value as the potential becomes more positive and the rate of the electrochemical reaction is accelerated; this agrees with what has been observed. The whole process is somewhat analogous to the anodic oxidation of the borohydride ion[5] where a competition between chemical and electrolytic steps can occur, although in this case Pt is the active surface. At a later stage in the anodic reaction of hypophosphite at Pd, the active form of phosphite is an essential intermediate, and hence one would expect some oxidation of this to phosphate to occur, as is found in practice.

The general form of the oxidation step at Pd observed in the voltammetric studies, also permits of reasonable interpretation on the present view. The step starts at the static potential for the system, which varies of course with the pH value, and the reaction initially proceeds with only slight displacement of potential. At high CD's, some concentration polarisation is apparent, and in unstirred solutions or in stirred solutions at low hypophosphite concentrations, a limiting CD of the order of magni-

tude expected for diffusion of hypophosphite ions to the anode is manifested. In the absence of any limit of this kind, the rate of reaction increases with rise of potential up to a peak value at about 0 V; above this the CD declines abruptly, and it seems likely that when the surface is sufficiently positive, repulsion of the hydrogen atoms prevents the essential initial adsorption step occurring. The influence of temperature and hypophosphite concentration on the peak CD is qualitatively as expected; the experimental results also indicate that the rate of the reaction must increase with rise of pH.

Sodium hypophosphite is used as reducing agent in the electroless deposition of nickel[6] which can only be initiated at certain catalytically-active surfaces of which Pd is a notable example. It has generally been supposed that the deposition is a chemical reduction brought about by atomic hydrogen, but the present work suggests an alternative explanation. At such an active surface, the hypophosphite is oxidised electrochemically setting free electrons which may discharge nickel ions. The deposition of nickel would then be an electrolytic process occurring *via* numerous local cells on the metal surface. It is usually found that the ratio, H_2 evolved/Ni deposited, is constant for a given set of experimental conditions and decreases with rise of pH. This would be expected on the present view since both products will arise from the same adsorption complex, and the ratio will depend on the relative velocities of the catalytic and electrochemical decompositions; any acceleration of the electrochemical reaction as, for example, by rise of pH, should be reflected in a decrease of the ratio. Nickel itself catalyses the electroless deposition process and hence might be expected to be a good anode for the electrolytic oxidation of hypophosphite. To test this, finely divided nickel was electrolytically deposited on a smooth Pt electrode. When this electrode was immersed in 0.1 *M* NaH_2PO_2 in phosphate buffer at 25° the potential was about +0.05 V and no catalytic decomposition was apparent; on anodic polarisation no appreciable current passed until oxygen evolution set in. When the temperature was raised, however, a marked change occurred above 50°. The static potential swung negative to about −0.5 V and gas was evolved from the nickel surface; when current was passed, there was now a very clear low-potential oxidation step similar, qualitatively, to that observed with finely divided Pd but with the peak CD at a rather more negative potential. It thus appears that the oxidation can occur at nickel although it is not so effective a surface as Pd. In contrast to this, tests of a ptPt anode showed no activity up to the highest temperature used of 70°.

ACKNOWLEDGEMENT

We thank the Science Research Council for a studentship awarded to one of us (D.J.).

REFERENCES

1 *Gmelins Handbuch der anorganische Chemie*, 8th ed., *Phosphorus*, 16C (1965) 99, 125.
2 P. Nylén, *Arkiv Kemi*, 11B (1934) No. 29.
3 A. D. Mitchell, *J. Chem. Soc.*, 117 (1920) 1322; 119 (1921) 1266; 121 (1922) 1626; 123 (1923) 629, 2241.
4 Ref. 1, *loc. cit*: pp. 101, 126.
5 J. P. Elder and A. Hickling, *Trans. Faraday Soc.*, 58 (1962) 1852.
6 G. Gutzeit, *Trans. Inst. Metal Finishing*, 33 (1956) 383.

POLAROGRAPHISCHE UNTERSUCHUNGEN AN PHOSPHORORGANISCHEN VERBINDUNGEN

II. DIE pH-ABHÄNGIGKEIT DER INHIBITION*

H. SOHR UND KH. LOHS

Institut für Verfahrenstechnik der organischen Chemie, Leipzig, der Deutschen Akademie der Wissenschaften zu Berlin, Forschungsgemeinschaft

(Eingegangen am 13. Dezember, 1965)

Die Reaktivität der tetraetrisch konfigurierten phosphororganischen Verbindungen vom Typ der Trialkyl- und Triarylphosphate sowie der entsprechenden Thiophosphate, Phosphon- und Phosphinsäureester, Phosphinoxide und der analogen Thioverbindungen hängt insbesondere von der Polarität und der Polarisierbarkeit der jeweiligen Phosphoryl- bzw. Thiophosphorylgruppierung ab[1]. Polarität und Polarisierbarkeit sind ihrerseits wiederum vom Einfluss der Substituenten sowie den durch sie bedingten sterischen Faktoren abhängig, wobei die Thiophosphorylgruppierung im allgemeinen stärker polarisierbar ist, als die Phosphorylgruppierung.

Wesentlich ist nun, dass sowohl in der Phosphoryl- als auch in der Thiophosphorylgruppierung der koordinative Charakter des Moleküls seinen Ausdruck findet, was durch eine Neigung zur Komplexbildung (einschliesslich der Anlagerung von H^+-Ionen) und durch die Ausbildung von Wasserstoffbrückenbindungen mit geeigneten protonenaktiven Verbindungen deutlich wird[2,3]. Die Komplexbildungstendenz wird vor allem für die Extraktion von Schwermetallionen, insbesondere von Lanthaniden und Aktiniden technisch und analytisch genutzt. Die Nucleophilität der Thiophosphorylgruppe ist gegenüber der Phosphorylgruppe grösser, die Protonenaffinität und damit auch die Tendenz zur Ausbildung von Wasserstoffbrückenbindungen geringer[4].

In diesem Zusammenhang war es für uns von Interesse, inwieweit Oberflächenaktivität und Inhibitorwirkung solcher phosphororganischen Verbindungen mit der Komplexbildungstendenz verknüpft bzw. die genannten Faktoren von gegenseitigem Einfluss sind.

EXPERIMENTELLES

Die polarographischen i–E-Kurven wurden mit einem Heyrovský-Polarographen vom Typ LP55A aufgenommen. Als Hg-Elektrode diente eine stumpfe Jenaer Kapillare mit einer Ausflussgeschwindigkeit von 1.18 mg sec^{-1} und einer Tropfzeit (t) von 5.5 sec bei 70 cm Quecksilberhöhe und als Gegenelektrode eine gesättigte Kalomelelektrode. Die Messtemperatur in der Zelle betrug $25 \pm 0.2°$. Die phosphororganischen Verbindungen wurden nach allgemein bekannten Methoden hergestellt und destillativ gereinigt. Als Reinheitskriterium diente der Brechungsindex; Triphenylphosphinoxid ist durch mehrfache Umkristallisation gereinigt worden. Wenn

* Für 1. Mitteilung sehe *J. Electroanal. Chem.*, 11 (1966) 188.

nicht anders angegeben, betrug die Tropfzeit $t=6.5$ sec und die Empfindlichkeit des Galvanometers $E=1/70$. Als Depolarisator diente Cu(II) als Aquo- und Äthylendiamintetraessigsäure-Komplex (Cu-Konzentration $3 \cdot 10^{-3}$ M; EDTA-Konzentration $6 \cdot 10^{-3}$ M). Die untersuchten Lösungen enthielten 0.1 N Na_2SO_4 als Grundelektrolyt in bidest. Wasser. Die Einstellung des jeweiligen pH-Wertes erfolgte mittels eines Autotitrators (Radiometer Kopenhagen, Typ TTT1a) und entsprechend verdünnter H_2SO_4- bzw. NaOH-Lösung.

ERGEBNISSE UND DISKUSSION

a) Zur Komplexbildung in der Lösung

In unserer ersten Mitteilung[5] findet sich der Hinweis, dass die Abscheidung des mit einem pK_a-Wert von 18.3 sehr stabilen Cu(II)–EDTA-Komplexes (pH 3.5) an der Hg-Elektrode durch phosphororganische Verbindungen wesentlich stärker inhibiert wird, als dies bei der Abscheidung des vergleichsweise schwachen Cu(II)–Aquo-Komplexes (pH 4.1) der Fall ist.

Die eingehendere Bearbeitung zeigte, dass diese Inhibition des Cu(II)–Aquo-Komplexes stark pH-abhängig ist. Unter der Voraussetzung, dass der Elektrodenprozess bei der Abscheidung des Aquo-Komplexes im pH-Bereich 1–5 unverändert bleibt (wobei die bei pH 5 auftretenden geringen Konzentrationen des Cu(II)–Hydroxo–Aquo-Komplexes neben dem Cu(II)–Aquo-Komplex keine wesentliche Änderung des Elektrodenprozesses zur Folge hat), gibt es für die Ursache dieser pH-Abhängigkeit zwei Erklärungen. Entweder liegt eine Änderung der Oberflächenaktivität und damit eine Änderung des Adsorptions- bzw. Assoziationsgleichgewichtes vor oder es treten Wechselwirkungen zwischen dem phosphororganischen Inhibitor und dem Depolarisator auf. Auf Grund tensametrischer Aufnahmen stellten wir fest, dass sich die Oberflächenaktivität der verwendeten phosphororganischen Substanzen im angegebenen pH-Bereich in Abwesenheit der genannten Depolarisatoren nicht ändert. Andere Autoren gelangten bei einer Vielzahl oberflächenaktiver Substanzen zu analogen Ergebnissen[6]. Somit ist die oben geäusserte Annahme einer pH-Abhängigkeit der Inhibition infolge Wechselwirkung zwischen dem Inhibitor und dem Depolarisator berechtigt. Eine solche Erklärung wird vor allem auch durch die erwähnte Komplexbildungstendenz dieser phosphororganischen Verbindungen nahegelegt. Bei der Komplexbildung in der Lösung und im Bereich der an der Elektrode adsorbierten Molekeln ist allerdings zu berücksichtigen, dass in der Zwischenphase die Konzentration der phosphororganischen Molekeln bei völliger Bedeckung der Hg-Oberfläche maximal ist, während sie in der wässrigen Phase den jeweils angegebenen Konzentrationswert besitzt.

Da die Einstellung der Gleichgewichte zwischen den phosphororganischen Verbindungen und den H_3O^+-Ionen bzw. den Cu(II)–Aquo-Komplex-Ionen in der Lösung vor allem bei schwerlöslichen Substanzen eine gewisse Zeit erfordert, wurde erst polarographiert, nachdem die jeweiligen Lösungen zwei Stunden gestanden hatten. Daneben spielt auch die Tropfzeit sowie das Konzentrationsverhältnis der phosphororganischen Verbindungen zur Konzentration der H_3O^+-Ionen und der Cu(II)-Komplex-Ionen in der Lösung eine Rolle. Über die Konstitution und genauen Zusammensetzungen der Komplexe, welche in der Lösung entstehen, ihre Beständigkeitskonstanten usw. finden sich in der Literatur, die sich nahezu ausschliesslich auf die Ver-

hältnisse bei der Schwermetallextraktion aus wässrig-organischer Phase bezieht, keine Angaben.

In wässriger Lösung konkurrieren die Wassermoleküle und die Moleküle der jeweiligen phosphororganischen Verbindungen um die Koordinationsstellen am Cu(II)-Zentralatom. Unter diesen Bedingungen ist das Gleichgewicht infolge der relativ schwachen Komplexbildungstendenz der phosphororganischen Verbindungen vom eingangs erwähnten Typ stark nach der Seite des Aquo-Komplexes verschoben, da die H_2O-Konzentration unvergleichlich grösser als die der phosphororganischen Verbindungen ist.

b) Zur Komplexbildung an der Hg-Elektrode

Anders verhält es sich jedoch, was die Komplexbildung in der Zwischenphase zwischen Hg-Elektrode und Lösung anbelangt. In diesem Bereich verschiebt sich das Komplexgleichgewicht jenachdem ob die Cu(II)-Aquo-Komplex- oder die H_3O^+-Konzentration dominiert; es wird dann der jeweilige Komplex mit der betreffenden phosphororganischen Verbindung gebildet (Gl. 1 und 2). Hier bietet sich eine Parallele zu den Ergebnissen der Extraktion von Schwermetallionen oder Säuren aus wässriger Lösung, wobei sich die phosphororganischen Verbindungen (z.B. Tri-*n*-butylphosphat) in der organischen Phase befinden und die Phosphorylgruppen nach der wässrigen Phase hin gerichtet sind. Über die Zusammensetzung der Komplexe, die dabei entstehen, wurde in der Literatur mehrfach berichtet[7-14]. Je nach der Art der extrahierbaren Kationen werden Komplexe mit 1, 2 oder 3 Molekülen der als Extraktionsmittel dienenden phosphororganischen Verbindungen gebildet.

Bei pH 1 kann man annehmen, dass die an der Hg-Elektrode adsorbierten phosphororganischen Verbindungen, deren Phosphorylgruppen ebenfalls in die Lösung hineinragen, vorrangig mit H^+-Ionen abgesättigt werden (Gl. 1):

$$\left[\begin{matrix} R_1 \diagdown \\ R_2 — P \rightarrow O \\ R_3 \diagup \end{matrix}\right]_{ads.} + H_3O^+ \rightleftharpoons \left[\begin{matrix} R_1 \diagdown \\ R_2 — P \rightarrow OH^+ \\ R_3 \diagup \end{matrix}\right]_{ads.} + H_2O \qquad (1)$$

(R_1, R_2 und R_3 können sowohl gleiche oder unterschiedliche Alkyl-, Aryl-, Alkoxi- und Aryloxigruppen darstellen. Die Phosphorylgruppe kann möglicherweise durch eine Thiophosphorylgruppe ersetzt sein.)

Dies hat zur Folge, dass die Koordinationsstellen für die andiffundierenden Cu(II)-Aquo-Komplex-Ionen blockiert sind. Möglicherweise spielen hier im Hinblick auf die Durchtrittsreaktion Coulombsche Kräfte (ψ_1-Effekte) noch eine Rolle[15,16]. Erhöht man den pH-Wert der Lösungen auf 3, so konkurrieren die H_3O^+-Ionen und die Cu(II)-Aquo-Komplex-Ionen nach Gl. 1 und 2 um die Koordinationsstellen.

$$\left[\begin{matrix} R_1 \diagdown \\ R_2 — P \rightarrow O \\ R_3 \diagup \end{matrix}\right]^{-}_{ads.} + \left[Cu(H_2O)_6\right]^{2+} \rightleftharpoons \left[Cu(H_2O)_{6-n} \left(\begin{matrix} R_1 \diagdown \\ R_2 — P \rightarrow O \\ R_3 \diagup \end{matrix}\right)_n\right]_{ads.} + n\,H_2O \qquad (2)$$

Die Substitution der H_2O-Moleküle im Cu(II)-Aquo-Komplex durch die adsorbierten Phosphorsäureestermoleküle nach Gl. 2 führt infolge einer kurzzeitigen Komplexbildung zu einer wesentlichen Verringerung des Abstandes der Cu-Ionen zur Hg-Oberfläche, wodurch die Geschwindigkeit der Durchtrittsreaktion erhöht und die Inhibition verringert wird. Bei pH 5 verläuft die Reaktion vorrangig nach Gl. 2, was

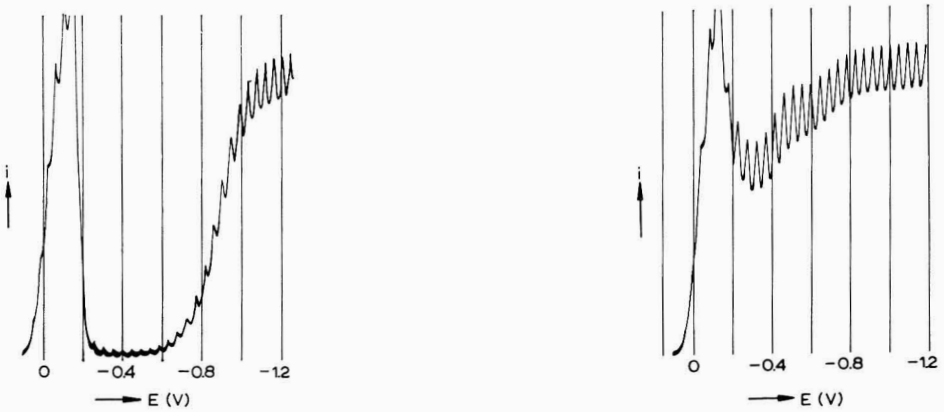

Abb. 1–2. Polarogramme des Cu(II)–Aquo-Komplexes ($3 \cdot 10^{-3}$ M) in Gegenwart von $2 \cdot 10^{-4}$ M Triisobutylphosphat. (1), pH 1; (2), pH 5.

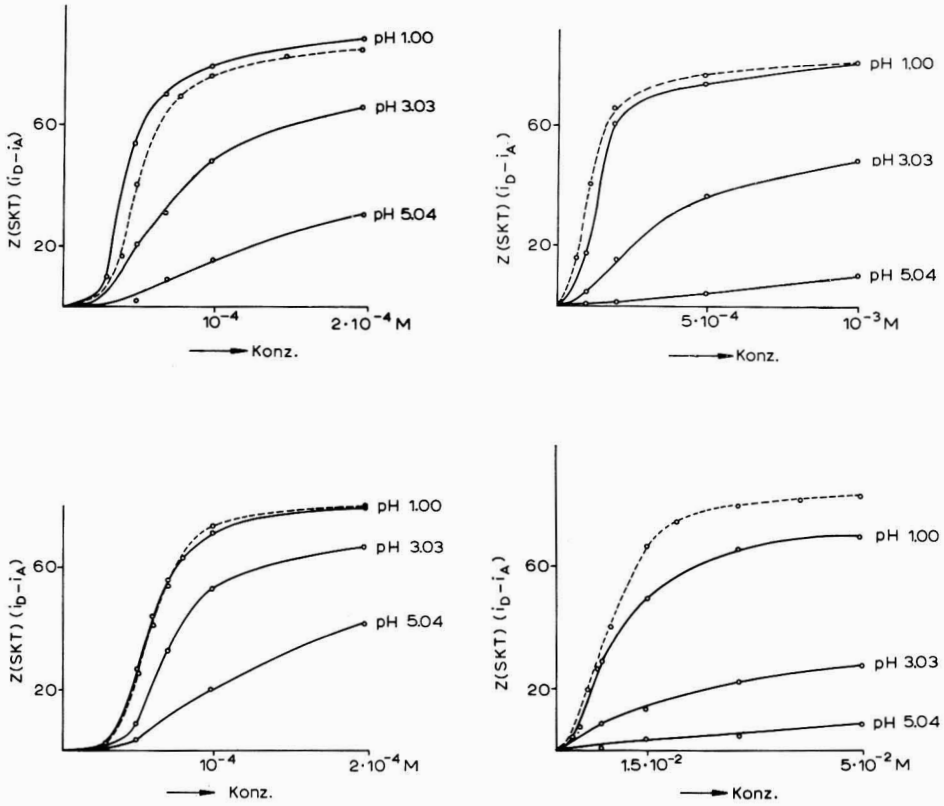

Abb. 3–6. pH-Abhängigkeit der Inhibition des Cu(II)–Aquo-Komplexes ($3 \cdot 10^{-3}$ M) in Gegenwart von: (3), Triisobutylphosphat; (4), Tripropylphosphat; (5), Triphenylphosphinoxid; (6), Triäthylphosphat. (-----), Inhibition des Cu(II)–EDTA-Komplexes (Cu(II), $3 \cdot 10^{-3}$ M; EDTA, $6 \cdot 10^{-3}$ M; pH, 3.5).

an Hand der Abb. 1 und 2 demonstriert wird. Setzt man an Stelle des Cu(II)–Aquo-Komplexes den Cu(II)–EDTA-Komplex als Depolarisator ein, so findet auf Grund der hohen Komplexstabilität im Bereich der Hg-Elektrode keine oder nur eine sehr geringe Substitution der Koordinationssphäre des Cu(II)-Zentralatoms nach Gleichung 2 statt.

Die Abbildungen 3–6 geben die pH-Abhängigkeit der Inhibition einzelner phosphororganischer Verbindungen wieder. Als Mass für die Inhibition gilt der Abstand zwischen der Diffusionsstromstärke (i_D) der Grundlösung und dem Kurvenminimum (i_A), gemessen in Skt. Die ($i_D - i_A$)-Werte vom Cu–EDTA-Komplex wurden mit dem Quotienten i_D-Aquo-Komplex/i_D-EDTA-Komplex multipliziert, da sich die Diffusionskoeffizienten beider Komplexe unterscheiden.

c) Vergleich der Inhibitionseffekte des Cu(II)–Aquo- und Cu(II)–EDTA-Komplexes

Die Feststellung, dass sich die i_A-Werte des Cu(II)–Aquo-Komplexes bei pH 1 und die des Cu(II)–EDTA-Komplexes bei pH 3.5 in Gegenwart von Tripropylphosphat, Triisobutylphosphat und Triphenylphosphinoxid vor allem bei höheren Konzentrationen dieser Verbindungen (Abb. 3–5) sehr ähnlich sind, ist zunächst überraschend. Triäthylphosphat (Abb. 6) weicht stark von diesen Ergebnissen ab. Die Inhibitionseffekte sind hier für den Cu(II)–Aquo-Komplex selbst bei pH 1 schwächer. Die Ursache dafür ist wahrscheinlich in der grösseren Komplexbildungstendenz des Triäthylphosphates zu sehen. Auch der verringerte Abstand zwischen den einzelnen Phosphorylgruppen der adsorbierten Triäthylphosphatmoleküle kann in Betracht gezogen werden. Ausserdem verringert sich mit Abnahme der Länge der Alkylgruppen auch die Dicke der Adsorptionsschicht.

Was die Breite des Potentialbereiches der Inhibition anbelangt, so unterscheiden sie sich für den Cu(II)–Aquo-Komplex bei pH 1 und dem Cu(II)–EDTA-Komplex bei pH 3 ebenfalls. Der Potentialbereich der Inhibition ist im Falle des Cu(II)–Aquo-Komplexes breiter (Abb. 7). Hierbei ist zu berücksichtigen, dass beim Cu(II)–EDTA-Komplex ein Überschuss an EDTA vorliegt und diese selbst oberflächenaktiv ist[17], ohne dass jedoch die Differentialkapazität der Doppelschicht bei dieser Konzentration in 0.1 N Na_2SO_4-Lösung wesentlich beeinflusst wird.

Je nach pH-Wert der Lösung kann die EDTA als Anion bzw. Betain oder sogar Doppelbetain vorliegen[18,19], weshalb es erforderlich ist, dass bei Inhibitionsmessungen in Gegenwart von EDTA-Komplexen der pH-Wert der Lösung angegeben werden muss.

Es konkurrieren demnach derartigen Anionen bzw. Betaine mit der betreffenden phosphororganischen Verbindung um die Adsorptionsstellen, jedoch ohne einen Inhibitionseffekt zu verursachen. Bei höheren Konzentrationen phosphororganischer Verbindungen (vor allem, wenn sie stark oberflächenaktiv sind) dominieren diese Verbindungen und somit ähneln solche Polarogramme denen des Cu(II)–Aquo-Komplexes in saurer Lösung (pH 1) unter sonst gleichen Bedingungen.

Triphenylphosphinoxid, das infolge seines aromatischen Charakters im positiven Potentialbereich (bezogen auf das Potential des elektrokapillaren Maximums) sehr adsorptionsaktiv ist, dominiert deshalb auch bei niedrigen Konzentrationen. Das gleiche, was die Breite des Potentialbereiches anbelangt, gilt auch für die Tiefe der Einschnitte (i_A-Werte). Überführt man die Lösungen des Cu–EDTA-Komplexes in stark saures Milieu (pH 1), wobei der Cu(II)–EDTA-Komplex abgebaut und ein

Doppelbetain gebildet wird, so tritt der oben dargestellte Sachverhalt noch deutlicher in Erscheinung (Abb. 8). Im negativen Potentialbereich (bezogen auf das Potential des elektrokapillaren Maximums) wird die Inhibition fast völlig aufgehoben und die Inhibitionsintensität verringert (Zunahme der i_A-Werte). In diesem Zusammenhang wurde auch die Inhibition von Cu(II)-Ionen in Gegenwart von 1 M KCl geprüft. Unter diesen Bedingungen wird der Elektrodenprozess bekanntlich durch die zweistufige Reduktion des $[CuCl_4]^{2-}$-Komplexes an der Elektrode charakterisiert[20,21].

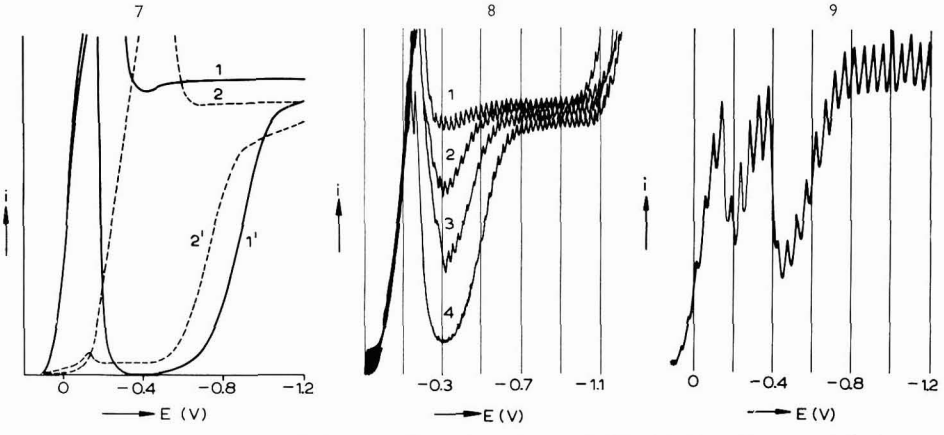

Abb. 7. Polarogramme des Cu(II)–Aquo-Komplexes ($3 \cdot 10^{-3}$ M): (1), Grundlösung; (1′), Grundlösung + $2 \cdot 10^{-4}$ M Triisobutylphosphat; und des Cu(II)–EDTA-Komplexes (pH, 3; Cu(II), $3 \cdot 10^{-3}$ M; EDTA, $6 \cdot 10^{-3}$ M): (2), Grundlösung; (2′), Grundlösung + $2 \cdot 10^{-4}$ M Triisobutylphosphat.

Abb. 8. Polarogramme des Cu(II)–EDTA-Komplexes (Cu(II), $3 \cdot 10^{-3}$ M; EDTA, $3.2 \cdot 10^{-3}$ M; pH, 1) in Gegenwart von Triisobutylphosphat: (1), $5 \cdot 10^{-5}$ M; (2), $7.5 \cdot 10^{-5}$ M; (3), $1 \cdot 10^{-4}$ M; (4), $3 \cdot 10^{-4}$ M. $E = 1/100$; $t = 3.0$ sec.

Abb. 9. Polarogramm des Cu(II)–Aquo-Komplexes ($3 \cdot 10^{-3}$ M) in 0.1 M H_2SO_4 in Gegenwart von $1.5 \cdot 10^{-2}$ M Trimethylthiophosphat.

Wir stellten dabei fest, dass im pH-Bereich 1–5 die Inhibition geringer ist, als die des Cu(II)–EDTA-Komplexes bei pH 3 in 0.1 N Na_2SO_4-Lösung und des Cu(II)–Aquo-Komplexes bei pH 1 in 0.1 N Na_2SO_4-Lösung und ferner, dass sie nahezu unabhängig vom pH-Wert der Lösung angegeben werden kann.

d) Zum Verhalten der Thiophosphorsäureester

Die Inhibitionswirkungen der Thiophosphorsäureester sind auf dem positiven Potentialbereich (bezogen auf das Potential des elektrokapillaren Maximums) beschränkt und weniger ausgeprägt als bei den analogen Phosphorsäureestern[5].

Wir stellten fest, dass in stark saurer Lösung erstaunlicherweise grundsätzlich andere Inhibitionswirkungen auftreten (Abb. 9). Gleichartige Polarogramme konnten wir auch mit Tributylthiophosphat in wässr.–methanolischer Lösung sowie mit dem gut wasserlöslichen Dimethoat (O,O-Dimethyl-S-(N-methyl)carbamyl-methyldithiophosphat) erhalten.

Wie eingangs erwähnt, ist die Nucleophilität der Thiophosphorsäureester grösser als die der analogen Phosphorsäureester, während es sich mit der Protonen-

affinität gerade umgekehrt verhält. Nach den bisher vorliegenden Ergebnissen scheint an der Hg-Elektrode eine Umlagerung der Thiophosphorsäureestermoleküle unter dem Einfluss der H^+-Ionen vor sich zu gehen. Während im Bereich des ersten Minimums die Thiophosphorylgruppe der Hg-Elektrode zugerichtet ist, liegen möglicherweise beim zweiten Minimum die Alkylgruppe an der Hg-Oberfläche an.

Je nach H^+-Ionenkonzentration verschwinden beide Einschnitte mit der Zeit, da die Anlagerung der Cu^{2+}-Ionen an die Thiophosphorsäureestermoleküle überwiegt. Hierüber soll in einer der folgenden Mitteilungen eingehend berichtet werden.

Frau B. MOTHES und Herrn J. LUNGWITZ gilt unser Dank für ihre fleissige und gewissenhafte Mitarbeit.

Herrn Dr. JEHRING, Institut für physikalische Chemie der D.A.d.W. zu Berlin, danken wir für die Unterstützung bei der Aufnahme tensametrischer Polarogramme.

ZUSAMMENFASSUNG

Es wird gezeigt, dass die Inhibition der Abscheidung von Cu(II)–Aquo-Komplex-Ionen durch einige phosphororganische Verbindungen in starkem Masse vom pH-Wert der Lösung abhängt. Die Ursache hierfür ist in der Komplexbildungstendenz und der Protonenaffinität der Phosphoryl- bzw. Thiophosphorylgruppe zu sehen. Bei pH 1 ist die Inhibition der Abscheidung von Cu(II)–Aquo-Komplex-Ionen mit der Inhibition der Abscheidung von Cu(II)–EDTA-Komplexe vergleichbar.

Besonders charakteristische Polarogramme erhält man in Anwesenheit von Thiophosphorsäureestern in der Lösung. Es treten dabei zwei nebeneinanderliegende Minima auf.

LITERATUR

1 I. R. VAN WAZER, *Phosphorus and its Compounds*, Volume I, Interscience, New York, 1958.
2 L. PAULING, *J. Phys. Chem.*, 56 (1952) 361.
3 R. G. GILLIS, J. F. HORWOOD UND G. L. WHITE, *J. Am. Chem. Soc.*, 80 (1958) 2999.
4 H. TEICHMANN, *Dissertation*, Humboldt-Universität, Berlin, 1962.
5 H. SOHR, *J. Elektroanal. Chem.*, 34 (1966) 188.
6 S. L. GUPTA UND S. K. SHARMA, *J. Indian. Chem. Soc.*, 41 (1964) 384.
7 K. ALCOCK, F. C. BEDFORD, W. H. HARDWICK UND H. A. C. MCKAY, *J. Inorg. Nucl. Chem.*, 4 (1957) 100.
8 D. SARGILL, K. ALCOCK, J. M. FLETSCHER, E. HESFORD UND H. A. C. MCKAY, *J. Inorg. Nucl. Chem.*, 4 (1957) 304.
9 G. F. BEST, H. A. C. MCKAY UND P. R. WOODGATE, *J. Inorg. Nucl. Chem.*, 4 (1957) 315.
10 D. F. PEPPARD, W. J. DRISCOLL, R. J. SIRONEN UND S. MCCARTY, *J. Inorg. Nucl. Chem.*, 4 (1957) 326.
11 K. ALCOCK, G. F. BEST, E. HESFORD UND H. A. C. MCKAY, *J. Inorg. Nucl. Chem.*, 6 (1958) 328.
12 E. HESFORD, E. E. JACKSON UND H. A. C. MCKAY, *J. Inorg. Nucl. Chem.*, 9 (1959) 193.
13 E. HESFORD UND H. A. C. MCKAY, *J. Inorg. Nucl. Chem.*, 13 (1960) 156.
14 H. SPECKER, *Z. Anorg. Allg. Chem.*, 333 (1964) 18.
15 L. E. GIERST, *Z. Elektrochem.*, 59 (1955) 784.
16 I. M. KOLTHOFF UND Y. OKINAKA, *J. Am. Chem. Soc.*, 82 (1959) 2296.
17 C.-S. TZA, S. L. SHIA UND G.-T. SAR, *Hua Hsueh Hsueh Pao*, 29 (1963) 379.
18 G. SCHWARZENBACH UND H. ACKERMANN, *Helv. Chim. Acta*, 30 (1947) 1799.
19 R. L. PECSOK, *J. Chem. Educ.*, 29 (1952) 579.
20 J. J. LINGANE, *Ind. Eng. Chem., Anal. Ed.*, 15 (1943) 583.
21 Cambridge Instrument Co., List No. 109.

POLAROGRAPHISCHE UNTERSUCHUNGEN AN PHOSPHORORGANISCHEN VERBINDUNGEN

III. DIE KOMPLEXBILDUNGSTENDENZ IN DER ADSORPTIONSSCHICHT

H. SOHR UND KH. LOHS

Institut für Verfahrenstechnik der organischen Chemie, Leipzig, der Deutschen Akademie der Wissenschaften zu Berlin, Forschungsgemeinschaft

(Eingegangen am 7. März, 1966)

In der vorangegangenen Mitteilung[1] konnten wir zeigen, dass für phosphororganische Verbindungen des Typs:

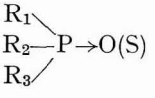

(R_1, R_2 und R_3 = Alkyl-, Aryl-, Alkoxy-, Aryloxygruppen) zwischen ihren Extraktionseigenschaften gegenüber Schwermetallionen sowie Mineralsäuren und den polarographischen Inhibitionseffekten Parallelbeziehungen bestehen. Für die Komplexbildung dieser phosphororganischen Verbindungen mit Schwermetall- und H^+-Ionen kommt als Koordinationsstelle nur die Phosphoryl- bzw. Thiophosphorylgruppierung in Frage[2-6].

Eine derartige Komplexbildung ist ferner für eine Reihe von Schwermetallkomplexen im Hinblick auf die katalytische Beschleunigung der hydrolytischen Spaltung hochtoxischer Phosphorsäure- und Phosphonsäureester durch solche Komplexe interessant geworden[7-10]. Allerdings ist hierbei zu berücksichtigen, dass sich die phosphororganischen Verbindungen, die durch Metallkomplexe beschleunigt hydrolytisch gespalten werden und jene, die als Extraktionsmittel Verwendung finden, hinsichtlich ihrer Struktur und der Elektronendichteverteilung der Phosphoryl- bzw. Thiophosphorylgruppe unterscheiden. Ausserdem nimmt die Komplexbildung an der Phasengrenze bei der Extraktion bzw. in der Adsorptionsschicht der Hg-Elektrode sowie in der Lösung einen unterschiedlichen Verlauf. Daher ist es verständlich, dass nur die Komplexbildungstendenz unter den vorgenannten Bedingungen vergleichbar ist.

Wie schon in der vorangegangenen Mitteilung[1] angedeutet wurde, ist die Konzentration der betreffenden phosphororganischen Verbindung in der Adsorptionsschicht bei völliger Bedeckung der Elektrode maximal, wenn man die Ausdehnung dieser Schicht modellmässig auf die Zwischenphase beschränkt. Somit besteht ein erhebliches Konzentrationsgefälle der oberflächenaktiven Substanz zwischen der Adsorptionsschicht und der angrenzenden Lösungsphase, was die Ursache für die bevorzugte Komplexbildung zwischen den in der Lösung vorhandenen Depolarisatoren und den oberflächenaktiven Molekülen in der Adsorptionsschicht darstellt.

EXPERIMENTELLES

Die polarographischen *i–E*-Kurven wurden mit einem Heyrovský-Polarographen vom Typ LP 55 A aufgenommen. Als Hg-Elektrode diente eine stumpfe Jenaer Kapillare mit einer Ausflussgeschwindigkeit von 4.22 mg sec^{-1} und einer Tropfzeit (t) von 2.8 sec bei 50 cm Quecksilberhöhe (h) und als Gegenelektrode eine gesättigte Kalomelelektrode. Die Temperatur in der Messzelle betrug 25 ± 0.2°. Als Grundelektrolyt wurde eine 0.1 N Na_2SO_4-Lösung verwendet (bidest. Wasser). Die zu polarographierenden Lösungen wurden 3 Std. vorher angesetzt.

ERGEBNISSE UND DISKUSSION

(*a*) *Penetrationsströme*

Das Auftreten kinetischer Ströme an der Hg-Elektrode ist immer ein Zeichen dafür, dass ein mit geringerer Stromstärke verlaufender und demzufolge langsamerer Prozess als die Andiffusion des Depolarisators zur Elektrode geschwindigkeitsbestimmend ist. Wenn Ströme solcher Art bei Adsorptionsvorgängen im Potentialbereich vollständiger Bedeckung der Hg-Oberfläche mit einer oberflächenaktiven Substanz auftreten, spricht man allgemein von Penetrationsströmen[11–14]. Danach wäre unter solchen Bedingungen das Eindringen des Depolarisators in die Adsorptionsschicht geschwindigkeitsbestimmend.

KOLTHOFF UND OKINAKA stellten bei der Untersuchung der Inhibition von Cu^{2+}-Ionen in Gegenwart von X 100 und ähnlichen oberflächenaktiven Substanzen fest, dass ebenfalls eine kinetische Vorstufe gebildet wird. Nach ihrer Meinung han-

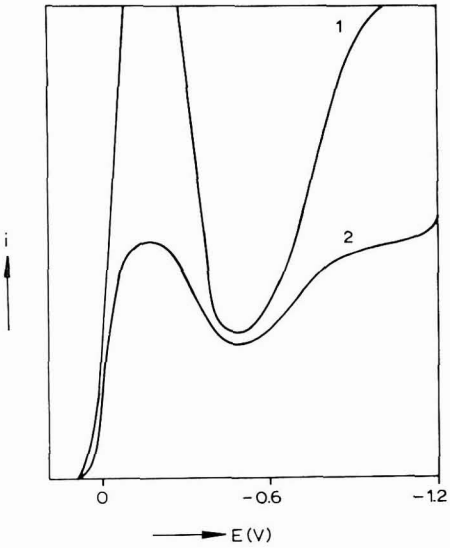

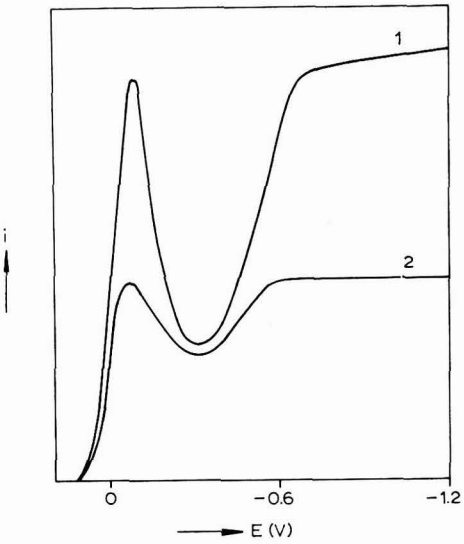

Abb. 1. Polarogramme von Cu^{2+} ($2 \cdot 10^{-3}$ M) in Gegenwart von Triäthylphosphat ($5 \cdot 10^{-3}$ M), pH 1, E = 1/100; (1) h = 69 cm, t = 1.7 sec; (2) h = 15 cm, t = 7.5 sec.

Abb. 2. Polarogramme von Cu^{2+} ($5 \cdot 10^{-4}$ M) in Gegenwart von Tripropylphosphat ($5 \cdot 10^{-3}$ M), pH 5, E = 1/30; (1) h = 69 cm, t = 1.7 sec; (2) h = 15 cm, t = 7.5 sec.

delt es sich dabei um einen kinetischen Strom, der durch das Gleichgewicht

$$Cu^{2+} + OH^- \rightleftharpoons CuOH^+ \qquad (1)$$

bedingt ist. Ursache dieser Annahme ist die Abhängigkeit der Höhe dieser Vorstufe von der Konzentration der OH-Ionen[15]. Diese Interpretation lässt sich auf unsere Ergebnisse offenbar nicht anwenden, obgleich wir auch eine Abhängigkeit der Stufenhöhe des Penetrationsstromes von der Konzentration der OH-Ionen feststellten. So erhielten wir z.B. beim Triäthylphosphat selbst bei pH 1 noch einen gut ausgebildeten kinetischen Strom (Abb. 1). Abb. 2–4 zeigen bei unterschiedlichen Bedingungen weitere derartige Penetrationsströme im Adsorptionsgebiet. Da die Adsorptionspotentiale der verwendeten Inhibitoren negativer liegen als das Halbstufenpotential vom Cu^{2+} in 0.1 *N* Na_2SO_4–Lsg., treten diese kinetischen Ströme nicht als Vorstufen, sondern als Minima der polarographischen Wellen in Erscheinung.

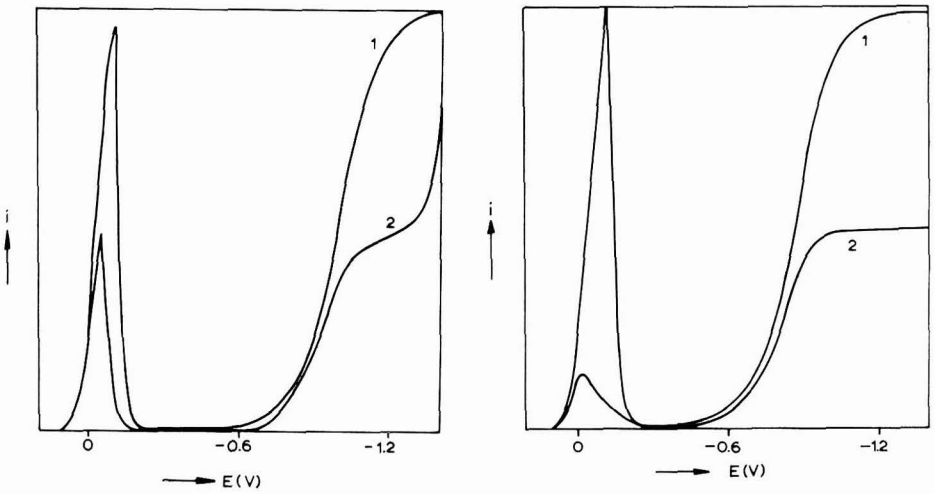

Abb. 3-4. Polarogramme von Cu^{2+} ($3 \cdot 10^{-3}$ *M*) in Gegenwart von Tributylphosphat ($5 \cdot 10^{-4}$ *M*). $E = 1/150$; (1) $h = 69$ cm, $t = 1.7$ sec; (2) $h = 15$ cm, $t = 7.5$ sec. Abb. 3, pH 1; Abb. 4, pH 3.

Nach unserer Auffassung sind in Übereinstimmung mit den Ergebnissen unserer vorangegangenen Mitteilung[1] diese kinetischen Ströme durch folgende Gleichung bedingt:

$$\left[\begin{matrix} R_1 \diagdown \\ R_2 — P \rightarrow O \\ R_3 \diagup \end{matrix}\right]_{ads.} + \left[M(H_2O)_x\right]^{Z+} \rightleftharpoons \left[M(H_2O)_{x-y}\left(\begin{matrix} R_1 \diagdown \\ R_2 — P \rightarrow O \\ R_3 \diagup \end{matrix}\right)_y\right]^{Z+}_{ads.} + (H_2O)_y \qquad (2)$$

M = Schwermetall- bzw. H^+-Ionen, x und y = Ligandenzahlen, Z = Zahl der Ladungen.

Anstelle von H_2O können auch andere Liganden stehen; z.B. treten auch bei der Abscheidung von $CuCl_4^{2-}$-Ionen in Gegenwart geeigneter phosphororganischer Verbindungen derartige kinetische Ströme auf. Voraussetzung für die Gültigkeit von Gl. (2) ist allerdings, dass die Liganden des Depolarisators in der Adsorptionsschicht substituierbar sind.

Für das Studium kinetischer Ströme ist es ausserdem wichtig, die I–t-Kurven der oberflächenaktiven Substanzen zu kennen. Bekanntlich ist es bei stark oberflächenaktiven Substanzen mit verhältnismässig kleinen Diffusionskoeffizienten möglich, dass die Inhibitionseffekte bei sehr kurzen Tropfzeiten wegfallen oder zumindest stark verringert sein können. Bei den phosphororganischen Verbindungen lagen bereits entsprechende Messungen vor[16].

(*b*) *Inhibitionseffekte in Gegenwart von Fremdkationen*

Wenn in einer Lösung mehrere Kationen vorhanden sind, die sich nach Gl. (2) in dieser Adsorptionsschicht einlagern können, so ist es zunächst wichtig, bei

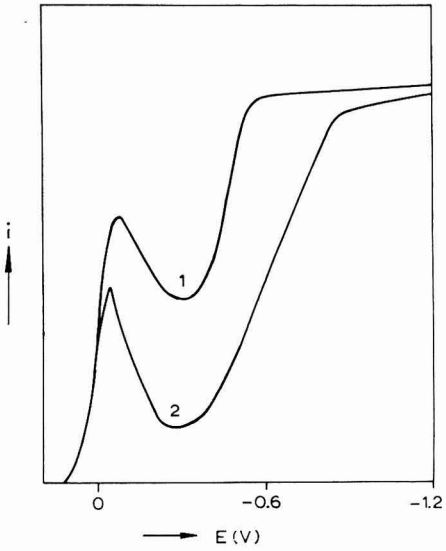

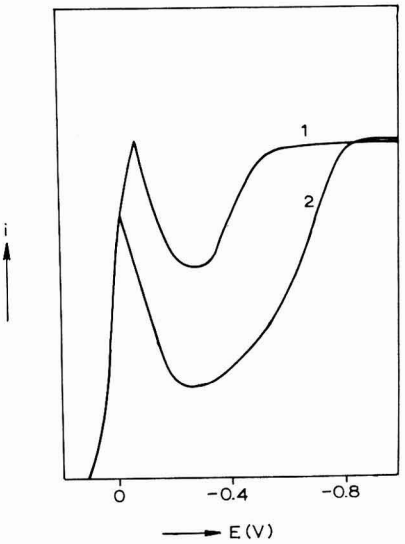

Abb. 5. Polarogramme von Cu^{2+} ($5 \cdot 10^{-4}$ M) in Gegenwart von Tributylphosphat ($5 \cdot 10^{-4}$ M), pH 5, $E = 1/15$; $t = 6.5$ sec. (1) 0; (2) $5 \cdot 10^{-5}$ M $ZrOCl_2$.

Abb. 6. Polarogramme von Cu^{2+} ($5 \cdot 10^{-4}$ M) in Gegenwart von Tripropylphosphat ($5 \cdot 10^{-3}$ M), pH 5, $E = 1/20$; $t = 6.5$ sec. (1) 0; (2) $5 \cdot 10^{-4}$ M $Th(NO_3)_4$.

welchem Potential deren Abscheidung an der Hg-Elektrode erfolgt. Liegen neben $[Cu(H_2O)_2]^{2+}$-Ionen H^+-Ionen in der Lösung vor, die bei wesentlich negativeren Potentialen abgeschieden werden, so werden die Inhibitionseffekte verstärkt[1]. Wenn Gl. (2) qualitativ die Verhältnisse an der Hg-Elektrode richtig wiederspiegelt, dann muss in Gegenwart von Kationen, die leicht mit phosphororganischen Verbindungen extrahierbar sind und somit Gl. (2) genügen und deren Halbstufenpotentiale wesentlich negativer als das des $[Cu(H_2O)_6]^{2+}$ liegen, allgemein eine Vergrösserung der Inhibitionseffekte bei der Abscheidung des $[Cu(H_2O)_6]^{2+}$, des $[Cd(H_2O)_6]^{2+}$ und anderer Schwermetallionen auftreten. Abb. 5 und 6 zeigen eindeutig, dass diese Annahme berechtigt ist. Auffällig ist dabei vor allem, dass die ZrO^{2+}-Ionen einen sehr grossen Einfluss im Hinblick auf eine Vergrösserung der Inhibition ausüben, was im Einklang mit der ausgeprägten Tendenz der Extrahierbarkeit aus wässriger Lösung und demzufolge der Komplexbildung im Einklang steht[17]. Auch beim Th^{4+} ist die Vergrösse-

rung der Inhibition noch beträchtlich, während wir beim La^{3+} unter diesen Bedingungen keinen Einfluss auf die Cu-Welle feststellen konnten. Offensichtlich ist die Komplexbildungstendenz beim $[Cu(H_2O)_6]^{2+}$ in der Adsorptionsschicht nach Gl. (2) grösser als die vom La^{3+}, so dass die freien Koordinationsstellen durch Cu-Ionen besetzt werden. Interessant ist in diesem Zusammenhang, dass im Gegensatz zur Abscheidung von $[Cu(H_2O)_6]^{2+}$ die La^{3+}-Ionen die Inhibition bei der Abscheidung von $[Cd(H_2O)_6]^{2+}$ vergrössern (Abb. 7). Somit ist die Komplexbildungstendenz der $[Cd(H_2O)_6]^{2+}$ nach Gl. (2) geringer als beim $[Cu(H_2O)_6]^{2+}$, was auch schon durch den grossen Inhibitionseffekt in Abwesenheit von Fremdkationen bei pH 5 zum Ausdruck kommt. Diese Feststellung ist wiederum in guter Übereinstimmung mit der ungleich

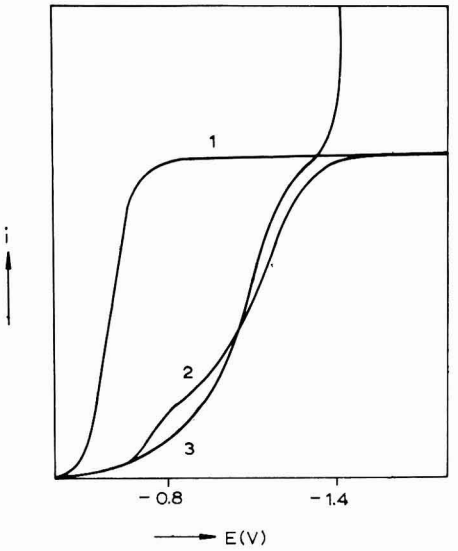

Abb. 7. Polarogramme von Cd^{2+} ($5 \cdot 10^{-4}$ M), pH 5, $E = 1/20$; $t = 6.5$ sec. (1) 0; (2) Tripropylphosphat ($5 \cdot 10^{-3}$ M); (3) Tripropylphosphat ($5 \cdot 10^{-3}$ M) + $La(NO_3)_3$ (10^{-3} M).

geringeren katalytischen Aktivität des $[Cd(H_2O)_6]^{2+}$ bei der Hydrolyse bestimmter phosphororganischer Verbindungen im Gegensatz zum $[Cu(H_2O)_6]^{2+}$. Somit ist die Annahme einer Parallelbeziehung zwischen der Inhibitionsaktivität der genannten Kationen und der katalytischen Aktivität bei der hydrolytischen Spaltung bestimmter phosphororganischer Verbindungen gerechtfertigt, denn die Abstufungen sind in beiden Fällen die gleichen:

$$Cu^{2+} \geqslant ZrO^{2+} > Th^{4+} > La^{3+} \gg Cd^{2+}$$

Einen weiteren Beweis für die Gültigkeit von Gl. (2) konnten wir dadurch erbringen, indem wir durch Anreicherung bestimmter Kationen in dieser Adsorptionsschicht an der Kemula-Elektrode bei der nachfolgenden Abscheidung eine wesentlich höhere Empfindlichkeit erreichten, als das bei der klassischen Polarographie der Fall ist[18].

ZUSAMMENFASSUNG

Oberflächenaktive Substanzen vom Typ phosphororganischer Verbindungen

neigen in der Adsorptionsschicht zur Komplexbildung mit in der Lösung vorhandenen Kationen. Kationen dieser Art zeichnen sich allgemein dadurch aus, dass sie mit phosphororganischen Verbindungen mehr oder weniger leicht aus wässriger Lösung extrahierbar sind. In Gegenwart von $[Cu(H_2O)_6]^{2+}$ und $[Cd(H_2O)_6]^{2+}$-Ionen lässt sich das vorgelagerte Gleichgewicht zwischen diesen Depolarisatoren und den adsorbierten phosphororganischen Verbindungen an Hand der auftretenden kinetischen Ströme nachweisen. Die Verstärkung der Inhibitionseffekte in Gegenwart bestimmter Fremdkationen ist auch dahingehend erklärbar.

SUMMARY

Surface active substances like the phosphororganic compounds tend to form complexes in the adsorption layer with cations present in the solution. Cations of this type are in general more or less readily extracted from aqueous solution with phosphororganic compounds. In the presence of $[Cu(H_2O)_6]^{2+}$ and $[Cd(H_2O)_6]^{2+}$ ions the preceding equilibrium between these depolarizers and the adsorbed phosphororganic compounds can be detected by the resulting kinetic current. The increase of the inhibition effect in the presence of certain foreign cations is also explained in this way.

LITERATUR

1 H. Sohr und Kh. Lohs, *J. Electroanal. Chem.*, 13 (1967) 107.
2 F. J. Collopy und J. R. Blum, *J. Phys. Chem.*, 64 (1960) 1324.
3 A. W. Nikolajew und Ss. M. Schubina, *Zh. Neorgan. Khim.*, 6 (1961) 799.
4 J. R. Feraro und D. F. Peppard, *Nucl. Sci. Eng.*, 16 (1963) 389.
5 G. Günzler und P. Mühl, *J. Prakt. Chem.*, [4] 23 (1964) 71.
6 G. Hilgetag und H. Teichmann, *Angew. Chem.*, 77 (1965) 1001.
7 T. Wagner-Jauregg, B. E. Hackley Jr., T. A. Lies, O. O. Owens und R. Proper, *J. Am. Chem. Soc.*, 77 (1955) 922.
8 K. B. Augustinsson und G. Heimbürger, *Acta Chem. Scand.*, 9 (1955) 383.
9 R. C. Courtney, R. L. Gustafson, S. J. Westerback, H. Hyytiainen, S. C. Chaberek Jr. und A. E. Martell, *J. Am. Chem. Soc.*, 79 (1957) 3030.
10 R. L. Gustafson und E. Martell, *J. Am. Chem. Soc.*, 84 (1962) 2309.
11 M. A. Loschkarew und A. A. Krjukowa, *Zh. Fiz. Khim.*, 23 (1949) 209.
12 M. A. Loschkarew, *Dokl. Akad. Nauk SSSR*, 72 (1950) 729.
13 W. W. Losew, *Dokl. Akad. Nauk SSSR*, 107 (1956) 432; 111 (1956) 626.
14 A. N. Frumkin, *Nova Acta Leopoldina*, 19 (1957) 1.
15 J. M. Kolthoff und Y. Okinaka, *J. Am. Chem. Soc.*, 81 (1959) 2296.
16 H. Sohr, *Dissertation*, TH Merseburg, 1964.
17 K. Alcock, F. C. Bedford, W. H. Hardwick und H. A. C. McKay, *J. Inorg. Nucl. Chem.*, 4 (1957) 100.
18 H. Sohr und L. Liebetrau, *Z. Anal. Chem.*, im Druck.

ELECTROCHEMICAL MEASUREMENTS ON THIN LAYERS OF NICKEL OXIDE

M. L. KRONENBERG

Research Laboratory, Union Carbide Consumer Products Company, Division of Union Carbide Corporation, Parma 30, Ohio (U.S.A.)

(Received February 7th, 1966)

Most studies of the nickel oxide electrode have been made on "thick" porous surfaces where it is especially difficult to define the physical and chemical state of the system. In addition to the difficulty associated with an unknown surface area which is a general problem for porous electrodes, the powdered nickel oxide electrode has a significant potential gradient within the bulk of the electrode and an inherent instability because the higher oxidation state is discharged *via* a corrosion couple with oxygen evolution on nickelous hydroxide[1]. Thus, upon charging or discharging the electrode, the bulk oxide apparently lags behind the surface oxide in degree of oxidation or reduction. One cannot say with certainty whether the potential measured at any state of charge or discharge is characteristic of the surface oxidation state or a state somewhere between the bulk and the surface. In addition, it is well known that when the charging or discharging current is interrupted, the potential of the nickel oxide electrode changes with time and the rate of change is dependent on the concentration of electrolyte. This change in electrode potential then, is attributed to corrosion reactions and adjustments between the surface and bulk oxides. Meaningful polarization curves and potentials characteristic of a specific oxidation state are, therefore, difficult to obtain.

In the work reported here the oxides were formed on 40-mil nickel wire (99.8% pure, Driver-Harris, Co., Harrison, New Jersey). The controlled electrochemical oxidation of a well defined surface at low current density permitted the formation of a reproducible, thin layer of the higher nickel oxide (approximately 1–2 molecular layers of oxide) avoiding a significant potential gradient within the oxide. A study of this electrochemically formed oxide also yielded important information regarding the nickel oxide–oxygen corrosion couple, oxygen evolution on nickel oxide and the electrochemical properties of the oxide films.

Constant current (10 μA/cm^2) charging curves for nickel wire at 23° for KOH solutions of varying concentrations are shown in Fig. 1. The horizontal steady-state lines are attributed to oxygen evolution, and the curved portion preceding this to a mixed potential involving simultaneous nickel oxide (2+) oxidation and oxygen evolution. This is believed to be the case because the coulombic capacity of a thin nickelic oxide layer is essentially independent of charging time after several minutes charging at a given current density. Also, it has been shown recently by other workers[2] that nickel metal is oxidized to the 2+ state almost immediately in air- or oxygen-containing alkaline solutions. The data in Fig. 1 show that the oxygen evolution potential

and Ni^{2+} oxidation potential increase significantly with decreasing KOH concentration. Potential values are relative to the Hg/HgO/KOH (9 *N*) electrode.

In order to study the Ni^{2+}–Ni^{3+} charging and discharging reaction for these electrodes, it was necessary to observe these reactions at sweep times slightly faster than a pen recorder (5 sec/cm). Oscilloscopic pictures were taken of the complete constant current charge and discharge curves for this electrode to obtain the electrochemical capacities and potential associated with the oxide layer. In Fig. 2 is shown an oscilloscope trace of a complete discharge and charging curve for nickelic oxide electrochemically formed on 40-mil nickel wire in a 9 *N*-KOH solution. Here "a" represents the steady-state oxygen evolution potential of 0.579 V *vs.* a Hg/HgO/KOH (9 *N*) reference electrode at a current density of 30 $\mu A/cm^2$. Section "b" represents primarily the discharge of the higher nickel oxide to nickel oxide (2+). This appears to be a continuous curve and there is no significant capacity attributed to more than one discrete discharge step. That is, it appears to be $Ni^{(3+x)+} \rightarrow Ni^{2+}$, rather than $Ni^{(3+x)+} \rightarrow Ni^{3+} \rightarrow Ni^{2+}$. Of course, x may be zero or a fraction. Curve "b" represents a coulombic capacity of approximately 0.5 mC/cm^2. In 1 *N* KOH solutions, capacities up to 1.3 mC/cm^2 were observed, which corresponds to approximately 1.2 $Å^2$ apparent area/surface nickel atom. Since the area of a nickel atom is almost twice this amount, this implies that 1–2 layers of oxide are formed assuming a roughness factor somewhere between

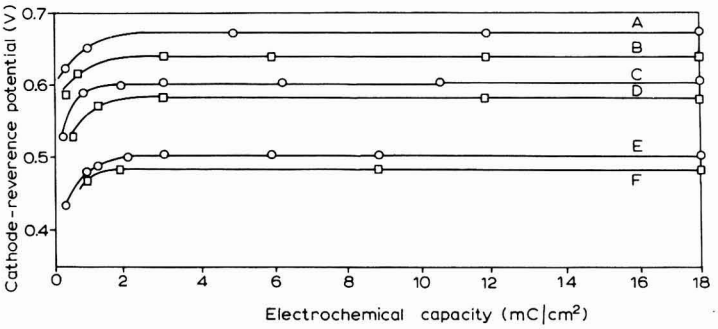

Fig. 1. Constant current charging curves for nickel wire in KOH solns: (A), 0.1; (B), 0.5; (C), 1.0; (D), 3.0; (E), 9.0*N*; (F) satd.

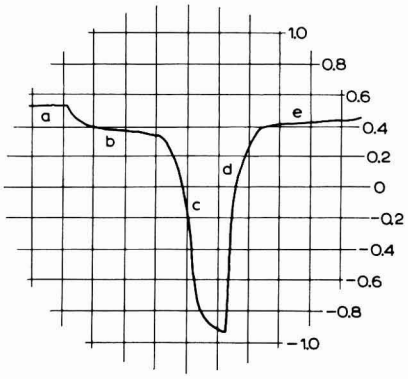

Fig. 2. Oscilloscope trace of complete discharge and charging curve for nickelic oxide electrochemically formed on nickel wire.

1 and 2. HICKLING AND SPICE[3] in a study of the anodic behavior of nickel in alkaline solutions, formed the oxide in 1 *N* NaOH and Na_2CO_3 solutions. They too concluded that an oxide layer 1–2 molecules thick was formed assuming a roughness factor between 3 and 4 for the nickel substrate they used.

Curve "c" represents the potential decrease to the hydrogen evolution potential. Apparently, the reduction of Ni^{2+} to metal occurs below the hydrogen evolution potential under these conditions, since there is no significant arrest that can be attributed to this reaction. At "d", the current was reversed to a charging current and "e" represents the electrochemical oxidation of $Ni^{2+} \rightarrow Ni^{(3+x)+}$.

It was possible, by examining charging data, to estimate an upper limit to the reversible potential of the nickel oxide electrode. The final charging potential was independent of charging time after several coulombs/cm^2 were passed, and electrochemical capacity was found to be essentially independent of charging time after several minutes at the final charging potential, so only oxygen evolution occurs here. This, however, presents an apparently paradoxical situation since the final charging potential should be above the nickel oxide potential because the higher oxide has already been produced and should continue to be produced. One possible explanation is that the reversible potential for formation of the higher oxide shifts anodically as the degree of oxidation increases. Another possible explanation is that a very high polarization is associated with nickelic oxide formation relative to oxygen evolution when the surface becomes completely covered with the higher oxide, and the electrode soon appears to be passivated relative to further oxidation of the lower nickel oxide. This would result in a high coulombic efficiency for oxygen evolution and would account for the apparent lack of dependence of electrochemical capacity on charging time. According to this reasoning then, on the basis of the data presented in Table 1, the reversible potential would have to be equal to or less than 0.447 V *vs.* a Hg/HgO/KOH (1 *N*) electrode. This is consistent with the results reported by CONWAY AND GILEADI[4] who obtained a value of approximately 0.425 V in 1 *N* KOH solutions, for "thick" nickel oxide electrodes with a degree of charge of 20–50%, by extrapolating anodic and cathodic e.m.f. decay lines plotted logarithmically with time.

Several potentiostatic experiments were run in 1 *N* KOH solutions. In these experiments, the potential of an initially charged nickel wire was decreased several millivolts at a time and the corresponding current was measured. Although the current recovered to small positive values down to 0.4V, the first swings in a negative direction were at 0.430 ± 0.004V. Since the system is complicated by the presence of mixed oxides and a corrosion couple, it is difficult to attach any real significance to this potential.

In order to study the corrosion associated with the Ni^{3+}–O_2 couple, open circuit

TABLE 1

Final charging potential	*Current density ($\mu A/cm^2$)*
0.447	1.2
0.484	2.5
0.511	4.6
0.516	5.0
0.543	10.0

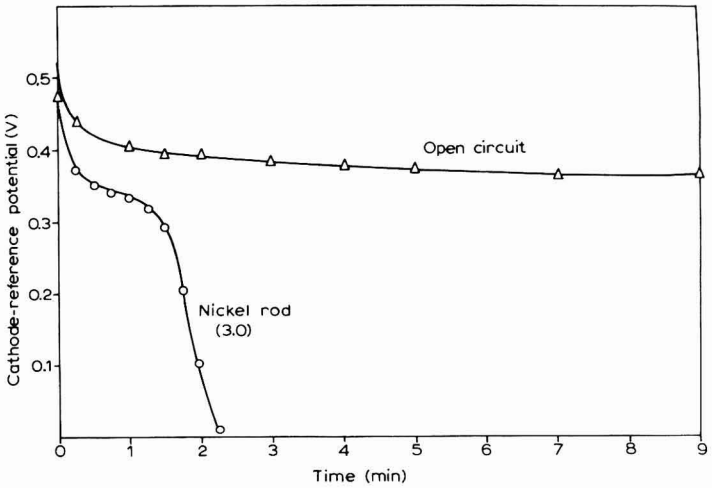

Fig. 3. Corrosion rate of electrochemically formed nickelic oxide.

decay rates of charged electrodes were obtained. The influence of an auxiliary electrode on the corrosion rate was determined by connecting the charged nickel oxide electrode (1 cm^2 in area) to another nickel electrode (10 cm^2) through a precision resistor and measuring the corrosion current as shown in Fig. 3. In this figure, the bracketed number represents the peak corrosion current in microamps for the auxiliary nickel electrode through a 400-kΩ resistor. The corrosion current measured through the precision resistor does not represent the total corrosion rate since oxygen evolution continues at the corroding electrode in competition with that occurring at the auxiliary electrode. However, by comparing the discharge time with and without an auxiliary electrode, it was possible to estimate the normal corrosion rate for nickel oxide from the data and this was estimated to be approximately 1 $\mu A/cm^2$.

ACKNOWLEDGEMENT

The author wishes to acknowledge the helpful suggestions of Drs. R. F. SCARR and R. A. POWERS and the assistance of G. R. TUCHOLSKI who made many of the experimental measurements.

REFERENCES

1 P. L. BOURGAULT, *The Electrochemical Behavior of the Nickel Oxide Electrode*, Thesis, University of Ottawa, 1961.
2 J. WEINIGER AND M. BREITER, General Electric Research Report No. 62-RL-(3144 M), October, 1962.
3 A. HICKLING AND J. E. SPICE, *Trans. Faraday Soc.*, 43 (1947) 762.
4 B. E. CONWAY AND E. GILEADI, *Can. J. Chem.*, 40 (1962) 1933.

THEORETICAL AND EXPERIMENTAL STUDY OF ANODIC STRIPPING VOLTAMMETRY WITH MERCURY-PLATED GRAPHITE ELECTRODES

S. P. PERONE AND ANN BRUMFIELD
Department of Chemistry, Purdue University, Lafayette, Indiana (U.S.A.)
(Received February 3rd, 1966)

Attention has been directed recently to the preparation and application of thin-film mercury electrodes[1-6]. This has been prompted by two primary considerations. First, a thin-film mercury electrode can be prepared on a substrate of any required geometry, thereby furnishing an electrode with the characteristics of mercury but with none of the geometrical limitations of a liquid. Second, stripping voltammetry with thin-film amalgams leads to considerably enhanced sensitivity and resolution compared to a hanging drop or mercury pool[4].

Some recent work in this laboratory has been directed towards the preparation, application, and evaluation of thin-film mercury electrodes for reduction processes[6]. A mercury-plated planar graphite surface was used, with film thicknesses of the order of 0.5–10 μ. These were evaluated using chronopotentiometry and voltammetry, and the results compared to theoretical predictions. The use of mercury-plated graphite electrodes for anodic stripping voltammetry has recently been reported by MATSON, ROE AND CARRITT[5]. However, no comparison with theoretical predictions was made.

The primary objective of the work reported here was to provide a quantitative evaluation of the mercury-plated graphite electrode for application to anodic stripping analysis. This evaluation was based on comparison of anodic stripping current–potential–time characteristics with theoretical predictions for diffusion-controlled processes in thin-film electrodes. Stripping with constant current and with linearly varying potential were investigated using Cd(II).

EXPERIMENTAL

Apparatus

The operational amplifier circuitry used for voltammetric experiments has been described previously[7]. Modifications for chronopotentiometry were made readily according to circuitry discussed by SCHWARZ AND SHAIN[8]. A change could be made instantaneously from a controlled-potential to a controlled-current mode simply by throwing a single switch. The instrument used for recording current–voltage and potential–time curves was an Esterline-Angus S601S, 1/8-sec, variable speed, variable range recorder.

Cells and electrodes

The cells, salt-bridge arrangements, reference electrodes, and counter electrodes

used in this study have been described previously[9]. The preparation of the mercury-plated electrodes from wax-impregnated graphite electrodes has been described previously[6]. The exposed surface was circular and planar with a geometrical surface area of 0.32 cm^2. Electrode thicknesses were computed from plating currents observed and the atomic radius of mercury. Thicknesses employed in this study varied from 0.5–5 μ. The 1.0-μ plate was used for most applications.

Reproducible constant stirring was achieved by a synchronous rotator equipped with a magnet attachment. Electrodeposition of Cd(II) was carried out at −1.00 V *vs.* S.C.E.

Materials and solutions

Chemicals used were of reagent grade; no further purification was attempted. Solutions were prepared with water purified by distillation and passage through a mixed-bed cation–anion exchange resin. Mercury(II) solutions for plating purposes were prepared as described previously[6]. Cadmium(II) solutions were prepared in 0.1 *M* KCl. All experiments were performed at ambient temperatures between 23° and 25°. Sample solutions were de-aerated for at least 15 min with high-purity nitrogen.

RESULTS AND DISCUSSION

Stripping with constant current

Theory. The concentration gradient in the thin-film amalgam during stripping with constant current can be derived from the following boundary-value problem:

Assume Fick's Law governing linear diffusion holds for substance R dissolved in the mercury film:

$$0 < x < l, \quad dC_R/dt = D_R(d^2C_R/dx^2) \tag{1}$$

Initial conditions:

$$t = 0, \quad 0 < x < l, \quad C_R = C_R^* \tag{2}$$

Boundary conditions:

$$t > 0, \quad |i/nFA| = \lambda = \text{constant} \tag{3}$$

$$t > 0, \quad x = l, \quad D_R(dC_R/dx) = -\lambda \tag{4}$$

$$t > 0, \quad x = 0, \quad D_R(dC_R/dx) = 0 \tag{5}$$

where x is the linear distance from the graphite–mercury interface, and l is the mercury-film thickness. Other terms have their usual significance. Note that anodic current is conventionally considered as negative in sign.

The initial condition states that the initial concentration of the reduced species within the mercury film is constant. The first boundary condition indicates that a constant anodic current is imposed on the electrolysis cell. The second boundary condition indicates that the imposed current describes the outward flux of substance R at the electrode surface. The third boundary condition indicates that the diffusion is not semi-infinite, but is limited to the thickness of the mercury film.

This boundary-value problem is similar to one in heat conduction considered by CARSLAW AND JAEGER[10] and is similar to a problem describing electrolysis in a thin-layer of solution[11]. The solution can be obtained by conventional Laplace trans-

form techniques. Solving for the concentration of substance R at the electrode surface one obtains:

$$C_R(x=l) = C_R^* - \frac{2\lambda t^{\frac{1}{2}}}{(\pi D_R)^{\frac{1}{2}}} \left\{ \sum_{n=0}^{\infty} \exp(-n^2y^2)[1+\exp(-2ny^2-y^2)] - 2(\pi)^{\frac{1}{2}} y \sum_{n=1}^{\infty} (n) \operatorname{erfc}(ny) \right\} \quad (6)$$

where,

$$y = l/(D_R t)^{\frac{1}{2}} \quad (7)$$

For values of y greater than 4.6, the terms in brackets in eqn. (6) reduce to unity, and eqn. (6) reduces to the expression for semi-infinite linear diffusion[12]. For values of y less than 0.6, the bracketed terms in eqn. (6) reduce to $(\pi)^{\frac{1}{2}}/2y$. Therefore, for small values of y, eqn. (6) becomes:

$$C_R(x=l) = C_R^* - \lambda t/l \quad (8)$$

Equation (8) is identical to that obtained by CHRISTENSEN AND ANSON[11] for the analogous case in thin-layer electrolysis.

When t is equal to the transition time, τ, $C_R(x=l) = 0$.

$$\tau = lC_R^*/\lambda \quad (9)$$

From eqn. (9) it is seen that τ is directly proportional to C_R^* and hence should form the basis of a stripping analysis method. Furthermore, the quantity $i\tau$ should be a constant. In addition,

$$C_R^* = Q/nFAl \quad (10)$$

where Q is the number of coulombs of reduction current required to form the amalgam of concentration C_R^*. Therefore, from eqns. (3), (9) and (10)

$$i\tau = Q \quad (11)$$

indicating that all reduced material is removed from the mercury film at the transition. This means that successive stripping transitions should be free of any cumulative effects of preceding oxidations, a distinct advantage over the case with bulk mercury electrodes.

The potential–time behavior for a reversible stripping process can be obtained by substitution into the Nernst equation of the appropriate time-dependent expressions for the oxidized and reduced forms at the electrode surface, $C_O(x=l)$ and $C_R(x=l)$. $C_R(x=l)$ is defined by eqn. (8); $C_O(x=l)$ is given by the previously derived[12] expression for a product formed under constant flux, as long as $C_O(x=l) \gg C_O^*$. This last condition is ordinarily achieved early in the stripping step, if any of the desired gain in sensitivity is to be obtained. Thus, eqn. (12) may be derived:

$$E = E^0 + (0.059/n)\log\frac{C_O(x=l)}{C_R(x=l)} = E^0 + (0.059/n)\log\frac{[2\lambda(t/\pi D_O)^{\frac{1}{2}}]}{[C_R^* - \lambda t/l]} \quad (12)$$

Substituting for C_R^* from eqn. (9) and rearranging one obtains:

$$E = E^0 + (0.059/n)\log[2l/(\pi D_O)^{\frac{1}{2}}] + (0.059/n)\log[t^{\frac{1}{2}}/(\tau - t)] \quad (13)$$

Experimental correlations. Several experimental studies might be carried out to verify that the electrode process corresponds to the above theory. The quantity, $i\tau$, should be proportional to C_R^*. Also, with any given value of C_R^*, variation of the

stripping current should result in a constant product, $i\tau$. In addition, τ is proportional to lC_R^*, and for a given pre-reduction period with constant stirring, C_R^* is proportional to $1/l$. Therefore, τ should be constant regardless of the electrode thickness, l, as long as the same quantity of material is reduced in the pre-reduction step (of course, the requirement that $l/(D_R t)^{\frac{1}{2}}$ be less than 0.6 must still be met).

From eqn. (13), two further correlations are obvious. First, a plot of potential *vs.* $\log t^{\frac{1}{2}}/(\tau - t)$ should be linear with a slope of $0.059/n$ V. Second, the potential at any given point on the curve ($E_{\frac{1}{4}}$ for convenience), should shift $0.059/n$ V for every 10-fold change in l.

Experimental results. Using a $5 \cdot 10^{-5}$ *M* Cd(II) solution, the value of C_R^* was varied by varying the pre-reduction time from 5–20 min in 5 steps. In the corresponding stripping steps the product, $i\tau$, was proportional to the length of pre-reduction time, and hence to the value of C_R^*. These data are shown in Table 1.

TABLE 1

DEPENDENCE OF $i\tau$ ON AMALGAM CONCENTRATION*

Pre-redn. time, t_e (min)	*Current, i ($A \cdot 10^{-6}$)*	*Transition time, τ (sec)*	*$i\tau$ (A sec $\cdot 10^3$)*	*$i\tau/t_e$*
5	160	15.5	2.48	0.496
10	320	15.3	4.90	0.490
12.5	400	15.2	6.08	0.486
15	480	15.2	7.29	0.486
20	640	15.1	9.65	0.483

* 1.0-μ electrode, $5 \cdot 10^{-5}$ *M* Cd(II).

TABLE 2

DEPENDENCE OF $i\tau$ ON STRIPPING CURRENT*

Current, i ($A \cdot 10^6$)	*Transition time, τ (sec)*	*$i\tau$ (A sec $\cdot 10^3$)*
62.5	38.0	2.38
70.0	36.5	2.56
80.0	32.0	2.56
90.0	30.0	2.70
100	26.7	2.67
110	23.5	2.68
120	21.2	2.55
130	19.1	2.48
140	17.3	2.42

* $5 \cdot 10^{-5}$ *M* Cd(II), 5-min pre-reduction time, 1.0-μ electrode.

Table 2 summarizes the stripping data obtained when C_R^* was maintained constant and the stripping current was varied from 62.5–140 μA. The value of $i\tau$ remained virtually constant, varying only between $2.4–2.7 \cdot 10^{-3}$ A sec.

To illustrate that the stripping transition time was independent of electrode thickness, the electrode thickness was varied from 0.5–5.0 μ, and the same quantity of amalgamating material was deposited for each thickness. That is, a $5 \cdot 10^{-5}$ *M* Cd(II) solution was electrolyzed with constant stirring for 5 min to prepare the amalgam in

each case. Table 3 summarizes the stripping data obtained. As predicted, τ remained virtually constant regardless of the electrode thickness.

The theoretical shape of the potential–time curve for constant current stripping from a thin-film electrode is compared in Fig. 1 to the theoretical shape of the potential–time curve for an infinitely thick electrode (*e.g.*, a hanging drop or mercury pool). The stripping curve with a thin-film electrode undergoes a slightly more sharply defined transition. Thus, slightly better resolution should be obtainable with thin-film electrodes in the stripping analysis of mixtures.

TABLE 3

EFFECT OF MERCURY FILM THICKNESS ON τ*

Mercury film thickness (μ)	*Transition time, τ (sec)*
0.5	15.0
1.0	15.0
2.0	15.0
5.0	15.2

* $5 \cdot 10^{-5}$ *M* Cd(II), 5-min pre-reduction time, stripping current 160 μA.

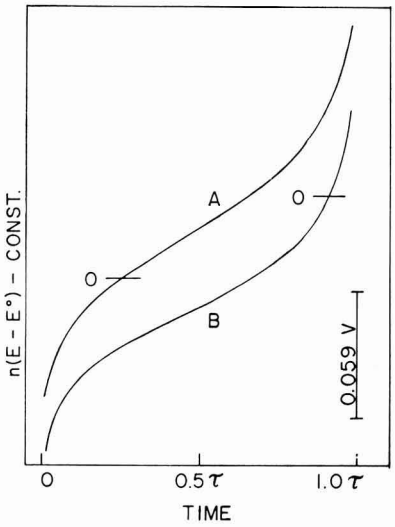

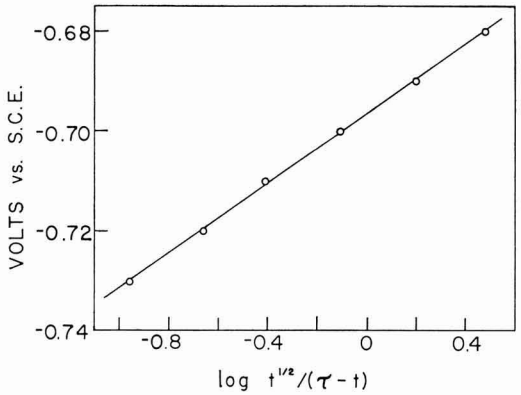

Fig. 1. Theoretical shapes of potential–time stripping curves. (A), For infinitely thick mercury electrode with uniform initial amalgam concn.: constant = 0, for $D_O = D_R$. (B), For mercury-film electrode, where $y < 0.6$; constant = $0.059/n \log 2l/(\pi D_O)^{\frac{1}{2}}$

Fig. 2. Experimental log plot of potential–time stripping curve. $5 \cdot 10^{-5}$ *M* Cd(II), 5 min pre-reduction time, 1.0-μ mercury-film electrode.

Figure 2 shows an experimental plot of E *vs.* $\log t^{\frac{1}{2}}/(\tau - t)$ for the stripping of Cd from a 1.0-μ mercury-film electrode. The straight line plot predicted from eqn. (13) is obtained. The slope is 0.034 V, in good agreement with the predicted value of 0.030 V. In addition, when the mercury-film thickness was varied from 0.5–5.0 μ, $E_{\frac{1}{4}}$ shifted from -0.659 to -0.625 V *vs.* S.C.E. Thus, a shift of $+0.034$ V was observed for a 10-

fold increase in electrode thickness, again in good agreement with the dependence predicted from eqn. (13).

Stripping by electrolysis with linearly varying potential

To characterize further the thin-film electrodes, comparison of stripping curves obtained with linearly varying potential to recently-developed theory[4] was made.

ROE AND TONI[4] developed the theory for stripping with linearly varying potential (LVP) under non-stationary conditions, *i.e.*, with convection removing oxidized material from the electrode surface. Three important characteristics of stripping current–voltage curves predicted under these conditions are: very sharp stripping peaks, a linear dependence of the peak height on amalgam concentration, and a linear dependence of peak height on scan rate. They verified these predictions experimentally using a mercury-coated nickel wire electrode. In the work reported here, comparison with these predictions was made by carrying out experiments using the thin-film mercury-plated graphite electrode. The shape of stripping curves was compared to theory and the dependence of peak height on amalgam concentration and on scan rate was investigated.

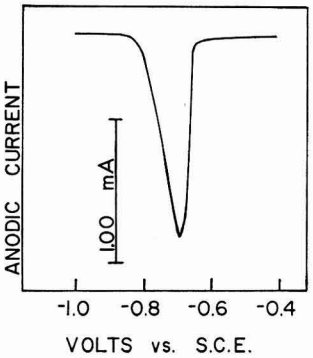

Fig. 3. Experimental current–voltage stripping with linearly varying potential. $5 \cdot 10^{-5}$ *M* Cd(II), 15-min pre-reduction time, 1.0-μ mercury-film electrode, scan rate 18.6 mV/sec.

Figure 3 shows a typical current–voltage curve for the stripping of Cd with LVP. In these experiments, stirring was continued through the stripping step in accordance with the conditions under which the theory was derived[4]. The stripping curve is sharp as predicted, but a quantitative correlation is not obtained. For example, the predicted peak height for the curve in Fig. 3 is 2.43 mA, whereas the observed peak height is 1.42 mA.

Table 4 shows the experimental dependence of peak height and peak area on amalgam concentration where the pre-reduction time was varied from 5–27 min. Table 5 shows the experimental dependence of peak height on scan rate obtained by varying the scan rate from 4.8–76 mV/sec. Although peak areas are linearly proportional to amalgam concentration, the expected linear relationship between peak height and amalgam concentration is not observed, nor is the predicted linear dependence of peak height on scan rate observed.

The significance of the relatively poor correlation between experimental and theoretical behavior for stripping with linearly varying potential is difficult to eval-

uate, particularly since the chronopotentiometric correlation appears excellent. Furthermore, experimental conditions used for the LVP stripping experiments were very similar to those used by ROE AND TONI[4] when they obtained good correlation at a mercury-coated nickel wire electrode.

Perhaps the explanation for the poor correlation with LVP stripping theory obtained here, lies in the fact that the mercury-plated graphite electrode simply does not correspond well to the theoretical model developed by ROE AND TONI. For example,

TABLE 4

DEPENDENCE OF STRIPPING PEAK HEIGHT AND PEAK AREA ON AMALGAM CONCENTRATION*

Pre-redn. time, t_e (min)	*Peak current, i_p ($A \cdot 10^3$)*	*Peak area, q (arbitrary units)*	i_p/t_e	q/t_e
5.0	0.700	56	0.140	11.2
7.5	0.940	81	0.125	10.8
10	1.08	112	0.108	11.2
15	1.42	154	0.095	10.3
27	2.10	295	0.078	10.9

* $5 \cdot 10^{-5}$ *M* Cd(II), 1.0-μ electrode, scan rate 18.6 mV/sec.

TABLE 5

DEPENDENCE OF STRIPPING PEAK HEIGHT ON SCAN RATE*

Scan rate, v (mV/sec)	*Peak current, i_p ($A \cdot 10^3$)*	i_p/v
4.8	0.32	0.066
9.3	0.50	0.054
18.6	0.76	0.040
36.8	1.20	0.033
76.0	1.90	0.025

* $5 \cdot 10^{-5}$ *M* Cd(II), 1.0-μ electrode, 5-min pre-reduction time.

one of the simplifying assumptions made by those authors was that a well-defined diffusion layer of constant thickness be set up at the solution–electrode interface. This was to be accomplished experimentally by constant reproducible stirring of the solution. Examination of the surface of a mercury-plated graphite electrode with a magnifying glass or microscope demonstrates that the film is really a composite of many tiny mercury droplets[5,6]. Thus, since the actual diffusion layer with stirring is considered to be of the order of only about 1-μ thick[13], a well-defined diffusion layer probably cannot be set up as required for the LVP theory to hold. On the other hand, with chronopotentiometry, for transition times greater than about 1 sec, not only is the diffusion layer more drawn-out ($>10\ \mu$) but the flux at the interface is controlled; therefore, the effects of surface roughness are minimized and better correlation with theory should be expected.

SUMMARY

The application of mercury-plated graphite electrodes to stripping analysis has

been evaluated. Theoretical relationships for chronopotentiometric stripping were derived. Excellent correlation between experimental and theoretical behavior was obtained using mercury films from 0.5–5.0 μ thick. Transition times are linearly related to amalgam concentration and reflect the complete removal of reduced species from the mercury film.

Stripping with linearly varying potential was also investigated, and results were compared to previously derived theory. Correlation was not so good as for chronopotentiometry, although analytical data could be obtained from peak areas. It is suggested that the poor correlation in the case of stripping with linearly varying potential is due to surface roughness effects.

REFERENCES

1 W. T. de Vries and E. van Dalen, *J. Electroanal. Chem.*, 8 (1964) 366.
2 S. A. Moros, *Anal. Chem.*, 34 (1962) 1584.
3 L. Ramaley, R. L. Brubaker and C. G. Enke, *Anal. Chem.*, 35 (1963) 1088.
4 D. K Roe and J. E. A. Toni, *Anal. Chem.*, 37 (1965) 1503.
5 W. K. Matson, D. K. Roe and D. E. Carritt, *Anal. Chem.*, 37 (1965) 1594.
6 S. P. Perone and K. K. Davenport, *J. Electroanal. Chem.*, 12 (1966) 269.
7 S. P. Perone and T. R. Mueller, *Anal. Chem.*, 37 (1965) 2.
8 W. M. Schwarz and I. Shain, *Anal. Chem.*, 35 (1963) 1770.
9 S. P. Perone and W. J. Kretlow, *Anal. Chem.*, 37 (1965) 968.
10 H. S. Carslaw and J. C. Jaeger, *Conduction of Heat in Solids*, Oxford Univ. Press, London, 2nd ed., 1959, p. 112.
11 C. R. Christensen and F. C. Anson, *Anal. Chem.*, 35 (1963) 205.
12 P. Delahay, *New Instrumental Methods in Electrochemistry*, Interscience, New York, 2nd ed., 1954, p. 180.
13 *Ibid.*, p. 226.

SPHERICAL-, SHIELDING-, AND STREAMING EFFECTS IN CURRENT-REVERSAL CHRONOPOTENTIOMETRY AT THE HANGING MERCURY DROP ELECTRODE

ROYCE W. MURRAY AND DONALD J. GROSS*
Department of Chemistry, University of North Carolina, Chapel Hill, N. C. 27515 (U.S.A.)
(Received February 15th, 1966)

The usual form of current-reversal chronopotentiometry consists of a step change in the sign of the applied current at a time t_f prior to the transition time of the forward electrode reaction. In the case of linear diffusional mass transport control, the relation of the reverse transition time, τ_b, measured from t_f, is the well known[2] $t_f = 3\tau_b$. Current-reversal experiments at the hanging mercury drop electrode (HMDE) yield this ratio in simple diffusional systems provided that the time span of the experiment is sufficiently short to approximate closely linear diffusion to the electrode. If the experimental times employed are long, the spherical nature of the hanging drop electrode causes an increase and a decrease in the ratio $t_f/\tau_b = 3.00$ for the cases of the electrode reaction product (during t_f) being soluble in the solution and mercury phase, respectively. The theory for the effect of spherical diffusion in the former case is described by the relationship

$$1 + \exp[D(\tau_b + t_f)/r_o^2]\,\mathrm{erfc}\,[D^{\frac{1}{2}}(\tau_b + t_f)^{\frac{1}{2}}/r_o] = 2\,\exp[D\tau_b/r_o^2]\,\mathrm{erfc}\,[D^{\frac{1}{2}}\tau_b^{\frac{1}{2}}/r_o] \qquad (1)$$

where r_o is the spherical electrode radius in centimetres and D is the diffusion coefficient of the species reacting during τ_b. This equation was recently obtained[6] by application of the response function additivity principle, but its validity has not yet been experimentally confirmed.

The present report represents an investigation of eqn. (1) using as a model system the oxidation of mercury from a HMDE into perchloric acid medium followed by reduction of the (solution soluble) mercury(I) product upon anodic → cathodic current reversal. In the course of this theoretical examination, certain effects were noted which could be attributed to streaming at the electrode surface and shielding of the upper portion of the mercury drop by the supporting glass capillary; these effects have been characterized.

EXPERIMENTAL

The cell assembly, operational amplifier instrument and associated automatic current-reversal circuit, and recording equipment employed were the same as noted in a previous report[5]. The S.C.E. reference electrode was isolated from the test solution to avoid the undesirable introduction of chloride ion.

Two Pt tip electrodes were used to support the hanging mercury drop. One

* Present address: U.S. Army Nuclear Defence Laboratory, Edgewood Arsenal, Maryland.

consisted of a Pt wire sealed into soft-glass tubing with the end polished flat so that the Pt wire tip was flush with the flat glass surface. This will be referred to below as the *blunt* electrode. The other, *pointed* electrode was prepared in the same manner and then ground and polished as close to a point as possible without materially disturbing the flat Pt tip and its surrounding glass sleeve. The diameter of the remaining flat surface (Pt tip plus surrounding glass) was about 0.07 cm.

RESULTS AND DISCUSSION

It is apparent from an inspection of eqn. (1) that both an increase in the value of t_f or a decrease in the value of r_o have the effect of magnifying the spherical contribution to the diffusion of mercury(I) and will increase the value of t_f/τ_b. The magnitude of the applied current has no predicted effect on t_f/τ_b.

The experimental variation of t_f/τ_b over a broad range of t_f at an electrode of radius 0.0616 cm is shown in Fig. 1 for the blunt and pointed electrodes. Theoretical curves[4] computed from eqn. (1) for mercury(I), $D = 0.91 \times 10^{-5}$ cm²/sec, are shown

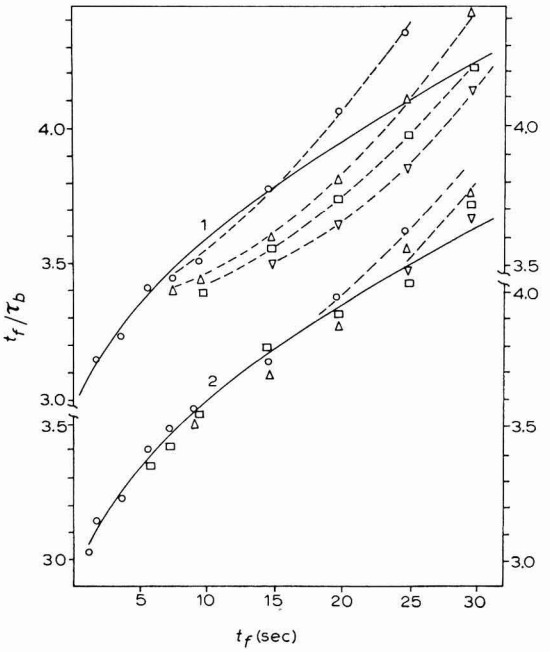

Fig. 1. Dependency of chronopotentiometric current-reversal ratio, t_f/τ_b, on the time, t_f, of anodic current application to a HMDE of radius 0.0616 cm in 1 M $HClO_4$. Solid curve is theoretical for $D_{Hg(I)} = 0.91 \cdot 10^{-5}$ cm²/sec. (○), 0.344; (△), 0.172; (□), 0.0688; (▽), 0.0344 mA cm⁻².

for comparison. The t_f/τ_b data taken at the pointed electrode display a close agreement with the theoretical curve, and the expected independence of the applied current is obtained up to a t_f-value of about 15 sec. At $t_f > 15$ sec, however, appreciable positive deviation from theory is apparent with the pointed electrode. The data taken at the blunt electrode, Fig. 1, exhibit both negative and positive deviations from theory and also a pronounced dependency on the applied current.

Figure 2 shows data taken with the two electrodes for a smaller electrode radius of 0.0489 cm. These data exhibit characteristics similar to those of Fig. 1 except that the deviations from theory appear at somewhat shorter t_f-values.

Figures 1 and 2 show that at least two factors must be combining to produce the deviations from theoretical behavior; one factor produces a lengthening of τ_b (the negative deviation in t_f/τ_b) and the other a decrease in τ_b (the positive deviation in t_f/τ_b). The severity of their effects is enhanced in the blunt-end electrode as compared to the pointed electrode and, to a smaller degree, by a decrease in the electrode radius.

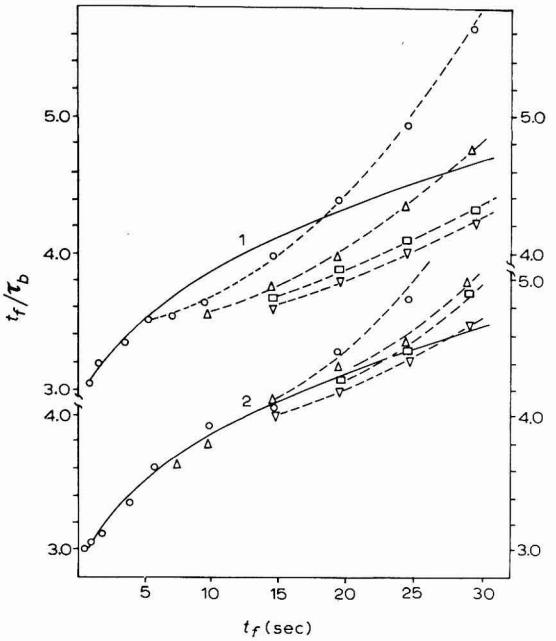

Fig. 2. Dependency of chronopotentiometric current-reversal ratio, t_f/τ_b, on the time, t_f, of anodic current application to a HMDE of radius 0.0489 cm in 1 M $HClO_4$. Solid curve is theoretical for $D_{Hg(I)} = 0.91 \cdot 10^{-5}$ cm²/sec. (○), 0.344; (△), 0.172; (□), 0.0688; (▽), 0.0344 mA cm^{-2}.

It is reasonable to assume that the negative deviation of t_f/τ_b from theory arises from shielding of the electrode by the glass surface immediately above it. Reflection of the diffusion layer around the electrode neck from the glass surface results in an effective retention of mercury(I) species near the electrode surface and a lengthening of τ_b. The expectations that this effect should be lessened in the pointed electrode compared to the blunt electrode and by a larger-radius electrode, appear to be confirmed by the data of Figs. 1 and 2. Further confirmation of this explanation of the negative deviation in t_f/τ_b is provided by cathodic current chronopotentiometry of mercury(I) at long transition times, data for which is given in Table 1. The values of $i\tau^{\frac{1}{2}}$ are lower for the blunt electrode owing to a more severe impingement of the depleted mercury(I) diffusion layer on the glass surface in that case. Shielding effects have also been directly observed by SHAIN AND MARTIN[8] in long-time experiments in chronoamperometry with the HMDE; the expected increase in the magnitude of the shielding effect with increased electrolysis time was not observed in the chrono-

amperometric data but is apparent in the increasing difference between the blunt and pointed electrode data of Table 1. A computation of a theoretical $i\tau^{\frac{1}{2}}$ from the equation for spherical diffusion in forward current chronopotentiometry[3] yields values of $i\tau^{\frac{1}{2}}=158$ and 166 μA sec$^{\frac{1}{2}}$ for $\tau=9.0$ and 16.0 sec, respectively, indicating the presence of some residual shielding effect even with the pointed electrode.

It is interesting that the shielding effect can produce an apparent constancy of $i\tau^{\frac{1}{2}}$ in cathodic current chronopotentiometry to longer transition times, than predicted

TABLE 1

Cathodic current chronopotentiometry of 1 mM mercury(I) in 1.2 M $HClO_4$ at a hanging mercury drop electrode of radius 0.0443 cm.

Current (μA)	τ_{pt}[a] *(sec)*	$i\tau_{pt}^{\frac{1}{2}}$ *(μA sec$^{\frac{1}{2}}$)*	τ_{bt}[b] *(sec)*	$i\tau_{bt}^{\frac{1}{2}}$ *(μA sec$^{\frac{1}{2}}$)*
40.0	0.116	136	0.117	136.5
25.0	0.300	137	0.305	138
10.0	2.06	143.5	2.04	143
6.67	4.96	148	4.84	146
5.00	9.60	155	8.75	148
4.00	16.0	160	14.4	152
3.64	20.6	166	18.7	157
3.33	26.5	172	23.9	162

[a] Transition time at pointed electrode.
[b] Transition time at blunt electrode.

by the theoretical spherical relation. This suggests that the design of a badly shielded electrode can allow application of the hanging drop form of electrode—with its virtues of ease of renewal, etc.—to chronopotentiometric quantitative analysis at transition times longer than those conventionally supposed to represent upper limits for maintaining constant $i\tau^{\frac{1}{2}}$.

The positive deviations of t_f/τ_b from theory can be attributed to convective mass transfer of mercury(I) away from the electrode surface, shortening τ_b. One source of the convective disturbance can be a downward streaming of solution from the electrode initiated by the gradient in solution density formed by the mercury(I) diffusion profile. This effect should be enhanced by larger applied currents, which produce steeper density gradients, and should also be more pronounced at longer experimental transition times. The positive variations of t_f/τ_b in Figs. 1 and 2 are in accord with both these expectations, and it can be concluded that the density effect constitutes a major source of the convective motion. No convective effects were observed in the cathodic current chronopotentiometry of mercury(I), indicating that a lowered surface solution density does not initiate as severe a convective motion as a raised surface solution density for this redox system in the hanging drop electrode geometry. BARD[1] also has demonstrated that chronopotentiometric transition times can be strongly affected by density gradient stirring and that such effects can be markedly dependent on the orientation and direction of the density gradient with respect to the solution.

It is significant that both the positive deviation in t_f/τ_b and the current dependency of that ratio are lessened for the pointed electrode compared to the blunt electrode, which suggests the presence of an additional aspect of the convective disturbance inasmuch as these two electrodes differ considerably in their shielding charac-

teristics, some connection of this additional factor with shielding seems likely. It is quite possible that the higher solution density at the neck of the drop in the more highly shielded blunt electrode simply produces a more pronounced density streaming effect. An additional possibility is that some solution streaming may be initiated by the unequal current density between the shielded neck and the unshielded bottom of the drop. The arguments for this type of streaming, which would be more severe for the blunt electrode, are essentially the same as those advanced for anodic and cathodic maxima in polarography[7,9]. A measure of the relative extents of the contribution of these two factors does not seem possible with the present data, however.

It should be noted that externally-supplied vibrations are not a significant source of the convective effects observed. This has been ascertained by favorable experience with mercury pool electrodes at long transition times in the same cushioned-cell arrangement used in the present study.

ACKNOWLEDGEMENT

This research—taken from the Ph.D. thesis of DONALD J. GROSS, University of North Carolina, 1965—was supported in part by Advanced Research Projects Agency under Contract SD-100. Presented at the Division of Analytical Chemistry, 152nd National Meeting, ACS, New York, September 1966.

SUMMARY

The theoretical expression for spherical diffusion effects in current-reversal chronopotentiometry (solution-soluble products) has been experimentally tested by the anodic production of mercury(I) from a hanging mercury drop electrode into 1.2 M $HClO_4$ followed by current reversal. Satisfactory agreement with the theory was obtained under conditions of minimal shielding of the drop by the glass–platinum contact. Negative deviations from theoretical t_f/τ_b can result from severe shielding, and positive deviations can arise from convective disturbances under certain conditions.

REFERENCES

1 A. J. BARD, *Anal. Chem.*, 33 (1961) 11.
2 T. BERZINS AND P. DELAHAY, *J. Am. Chem. Soc.*, 75 (1953) 4205.
3 P. DELAHAY AND G. MAMANTOV, *J. Am. Chem. Soc.*, 76 (1954) 5319.
4 H. MATSUDA, S. OKA AND P. DELAHAY, *J. Am. Chem. Soc.*, 81 (1959) 5077.
5 R. W. MURRAY AND D. J. GROSS, *Anal. Chem.*, 38 (1966) 392.
6 R. W. MURRAY AND C. N. REILLEY, *J. Electroanal. Chem.*, 3 (1962) 182.
7 Y. OKINAKA, I. M. KOLTHOFF AND T. MURAYAMA, *J. Am. Chem. Soc.*, 87 (1965) 423.
8 I. SHAIN AND K. J. MARTIN, *J. Phys. Chem.*, 65 (1961) 254.
9 M. V. STACKELBERG AND R. DOPPELFELD, *Advances in Polarography*, Vol. I, edited by I. S. LONGMUIR, Pergamon Press, New York, 1960, p. 68.

AN APPLICATION OF CURRENT-CESSATION CHRONOPOTENTIOMETRY TO QUANTITATIVE ANALYSIS

W. A. ALEXANDER AND D. J. BARCLAY
Department of Pure and Applied Chemistry, University of Strathclyde, Glasgow, C. 1 (Scotland)
(Received December 13th, 1965)

INTRODUCTION

Current-cessation chronopotentiometry has been considered for multi-component systems by ROUSE[1], TESTA AND REINMUTH[2], and PALKE, RUSSELL AND ANSON[3]. The present study, which is the result of investigations into the decay of the potential of the working electrode in coulometric titrations[4], considers an extended technique as an analytical tool. The appraisal given, is based on preliminary investigations and no statistical tests have yet been applied to the usefulness of the method.

PRINCIPLE OF THE METHOD

Consider a solution containing red_1 and red_2 where $[red_2] \gg [red_1]$, the square brackets representing concentrations. These species are related by the reactions:

$$red_1 + n_1e \rightarrow ox_1 \quad \text{(i)}$$

$$red_2 + n_2e \rightarrow ox_2 \quad \text{(ii)}$$

$$n_2red_1 + n_1ox_2 \rightarrow n_2ox_1 + n_1red_2 \quad \text{(iii)}$$

The above conditions are precisely those necessary for the coulometric titration of

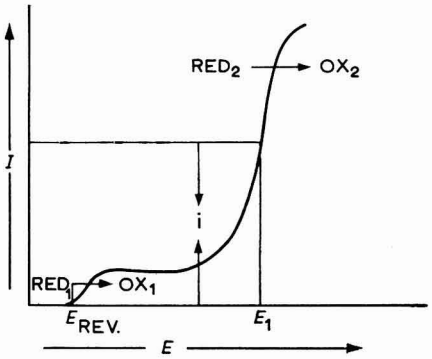

Fig. 1. Current–potential curves for a system containing red_1 and red_2.

red_1 by ox_2. The current–potential curves for this system are shown in Fig. 1 which illustrates current values at the start of current pulse. In the technique described in this paper, a pulse of current of intensity, i, and duration, t, is passed through a

platinum electrode immersed in this solution. If the current, i, is greater than the limiting-diffusion current of red_1, then the potential of this polarised electrode will be E_1 (Fig. 1). On interrupting the current, the potential will decay from E_1 to E_{rev}, the equilibrium potential of the system. It has previously been shown that if $[red_1] \sim [red_2]$ and if the current is switched off at τ_2—the transition time of red_2—then a third transition time, τ_3, is observed. τ_3 was given as[3]:

$$\tau_3 = \frac{\tau_2^2}{4\tau_1} \tag{1}$$

where τ_1 is the transition time of red_1 and it is assumed that the diffusion coefficients of red_1 and ox_2 are equal, and that the rate of reaction (iii) is rapid at the surface of the electrode or in the bulk of the solution. It will be shown that a similar expression holds if the current is switched off before τ_2.

Consider that at the end of the pulse an amount, s, of ox_2 is concentrated in the immediate vicinity of the electrode of area 1 cm^2. It is assumed that s is given by:

$$s = \frac{it}{n_2 F} \tag{2}$$

Ox_2 will now diffuse from the electrode—the solution is unstirred—and assuming linear diffusion, the concentration of ox_2 at a time, t', after the current has been interrupted, and at a distance, x, from the electrode, is given by:

$$[ox_2]_{x,t'} = \frac{s}{(\pi D_2 t')^{\frac{1}{2}}} e^{-x^2/(4D_2 t')} \tag{3a}$$

and at the electrode:

$$[ox_2]_{0,t'} = s(\pi \cdot D_2 t')^{-\frac{1}{2}} \tag{3b}$$

This, of course, ignores the presence of red_1. If the concentration of red_1 at the electrode be the same as the bulk concentration, one has, if reaction(iii) is instantaneous:

$$[ox_2]_{0,t'} = s(\pi D_2 t')^{-\frac{1}{2}} - \frac{n_1}{n_2}[red_1] \tag{4}$$

The equilibrium potential at any time after interrupting the current is given by the Nernst equation using surface concentrations of ox_2 and red_2. *i.e.*,

$$E = E^{\circ\prime} + \frac{RT}{n_2 F} \ln \frac{s(\pi D_2 t')^{-\frac{1}{2}} - \frac{n_1}{n_2}[red_1]}{[red_2]} \tag{5}$$

where $E^{\circ\prime}$ is the formal potential of reaction (ii) and it has been assumed again that the surface concentration of red_2 is the same as the bulk concentration. It is readily seen that the electrode potential is decreasing with time, and that the maximum rate of change is given when:

$$[red_1] = \frac{n_2}{n_1} s(\pi D_2 t_{max}')^{-\frac{1}{2}} \tag{6}$$

This equation is equivalent to (1) as can be seen by substituting from constant-

current chronopotentiometry[5]:

$$[\mathrm{red}_1] = \frac{2i\tau_1^{\frac{1}{2}}}{(\pi D_1)^{\frac{1}{2}} n_1 F}$$

and putting $s = it/nF$,

$$t_{\max}' = \frac{t^2}{4\tau_1} \tag{7a}$$

If the diffusion coefficients are not equal

$$t_{\max}' = \frac{t^2 D_1}{4\tau_1 D_2} \tag{7b}$$

To be more exact, t should be replaced by $(t-\tau_1)$, but τ_1 will be negligible in comparison to t.

The important result analytically is eqn. (6) which indicates that a plot of the concentration of red_1 *vs.* $t_{\max}'^{-\frac{1}{2}}$ is linear. It also suggests that a wide range of concentrations of red_1 could be studied as s is very easily varied.

The above treatment would also apply to systems containing originally, ox_1 and ox_2. It will be seen later that this simple derivation is not wholly adequate but that the general principles involved are sound.

EXPERIMENTAL

All reagents were of analytical grade; solutions were prepared in de-oxygenated distilled water and investigations were carried out where necessary in a nitrogen atmosphere. The temperature was maintained constant to within 0.1°.

The circuit is shown in Fig. 2. The current was accurately measured by observing the potential drop over a standard resistance. The time of electrolysis was measured on an electric stop-clock controlled by S1.

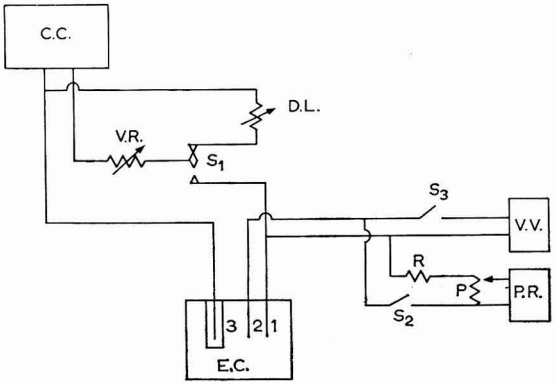

Fig. 2. The circuit diagram. The current measuring device is not shown (see text). (C.C.), electronic source of constant current; (V.R.), 0–200 kΩ variable resistor; (D.L.), dummy load, 0–10 kΩ variable resistor; (S1), relay contacts which also operate electric clock; (S2, S3), on-off switches; (R), 500 kΩ resistor; (P), 0–100 kΩ potentiometer; (V.V.), Pye Dynacap pH-meter (used on the mV scale); (P.R.), Honeywell-Brown pen recorder, 10-mV full-scale deflection; (E.C.), electrolysis cell; (1), working electrode; (2), reference electrode—calomel or platinum; (3), auxiliary electrode.

The electrolysis cell was a 150-ml beaker. The electrode assembly, mounted in a rubber bung, consisted of two similar platinum wires (length 2 cm, 22 s.w.g.), an auxiliary electrode in an isolated compartment, and a saturated KCl calomel reference electrode. The cell was mounted in a thermostatically controlled water bath.

The systems studied are listed in Table 1 together with details of the composition of the generating electrolyte.

Operation

An aliquot of red_1 (or ox_1) was transferred to the generating electrolyte, the electrode assembly was immersed in the solution (the generating electrode was washed with distilled water and wiped with a tissue between readings) and the solution allowed to come to rest—5 min was found to be adequate. S1 was operated to send a pulse of intensity, i, for a time, t, through the solution. The values of i, selected by means of the variable resistor VR, and t were chosen to give transition times between 30 and 200 sec. In this range, an average deviation of 1.4% in t_{max}' was found.

TABLE 1

SYSTEMS STUDIED BY THE TECHNIQUE DESCRIBED IN THE TEXT

Red_1	*Red_2*	*Ox_1*	*Ox_2*	*Composition of generating electrolyte*
Fe(II)	Ce(III)			Satd. $Ce_2(SO_4)_3$, 2 *M* H_2SO_4
Fe(II)	Cl^-			1 *M* HCl
		H^+	H_2O	1 *M* Na_2SO_4
		Fe(III)	W(VI)	0.1 *M* Sodium tungstate, Conc. HCl

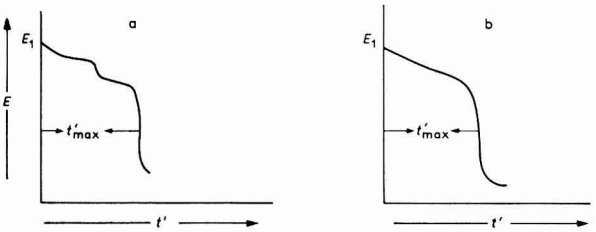

Fig. 3. Examples of decay chronopotentiograms (see text for difference).

The decay of the potential of the electrode, measured against the calomel or the unpolarised platinum electrode, was recorded (or observed on the Pye Dynacap pH-meter) and curves of the type shown in Fig. 3, a and b, obtained. The shape of the curve appeared to vary with the state of the working electrode. A new electrode tended to give curves of the type shown in 3a, while an electrode which had been in use for some time gave curves of the shape shown in 3b.

The decay times, t_{max}', were measured at various concentrations of red_1 and then $[red_1]$ was plotted against $t_{max}'^{-\frac{1}{2}}$. Straight lines were obtained for all the systems listed in Table 1, but did not, as might be predicted from eqn. (6), intersect at the origin. Typical results for the Fe(II)–Cl^- system are given in Table 2, and Fig. 4 shows the lines obtained for this system for different values of s.

TABLE 2

TYPICAL RESULTS FOR THE REACTION BETWEEN Fe(II) AND CHLORINE

Fe(II) concn. (10^{-4} M)	*i (mA)*	*t (sec)*	t_{max}'	$t_{max}'^{-\frac{1}{2}}$
1	1	5	215	0.0680
2	1	5	186	0.0733
3	1	5	168	0.0780
4	1	5	146	0.0828
10	5	5	227	0.066
15	5	5	136	0.086
20	5	5	93.6	0.103
25	5	5	66.0	0.123
30	5	5	50.0	0.142

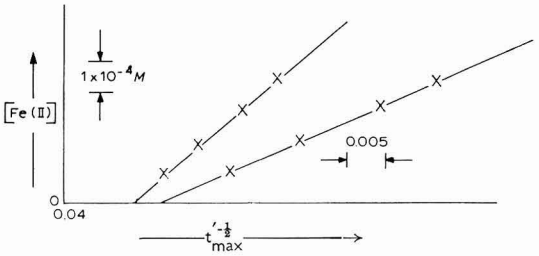

Fig. 4. Plots of [red$_1$] *vs.* $t_{max}'^{-\frac{1}{2}}$ illustrating the different slopes for different values of *s*.

TABLE 3

COMPARISON OF THE THEORETICAL AND EXPERIMENTAL SLOPES OF THE PLOT OF [ox$_1$] OR [red$_1$] *vs.* $t_{max}'^{-\frac{1}{2}}$. D_2 WAS TAKEN AS 10^{-5} cm/sec IN ALL CASES

System	*i*	*t*	*Concn. range (M)*	*Theoretical slope* $\times 10^5$	*Actual slope* $\times 10^5$
Fe(II)–Ce(III)	5	5	10^{-3}–10^{-2}	4.6	2.7
Fe(II)–Cl^-	5	5	10^{-3}–10^{-2}	4.6	2.9
H^+–H_2O	10	5	10^{-3}–10^{-2}	9.2	1.75

TABLE 4

THE EFFECT OF VARYING THE AREA OF THE ELECTRODE

Area of electrode (cm^2)	t_{max}' *(sec)*
1.505	119
1.26	106
0.84	89
0.35	80

The slopes of the lines were calculated and compared with the theoretical value given by eqn. (6). The results of this were always smaller than the theoretical value as can be seen from Table 3.

The effect of temperature variation on t_{max}' was studied for the system Fe(II)–

Cl^- at an iron concentration of 10^{-3} M. At room temperature, a temperature coefficient of 8 sec/degree was found. This illustrates the necessity of precise temperature control in this technique.

Table 4 gives some results on the same system, of reducing the apparent area of the electrode.

The concentration range studied was 10^{-4}–10^{-2} M.

DISCUSSION

The experimental results show that there are some obvious defects in the theory outlined above. These arise from the apparent failure to explain the finite intercept, the low experimental values of the slope, the anomalous variation in t_{max}' with area, and the complex shape of the decay curve.

It was assumed that the amount s of red_1 was deposited instantaneously. This is clearly an oversimplification and the low experimental slope could be due to the diffusion of ox_2 during the pulse; s in eqn. (6) would then have to be replaced by $s-f(it)$, where this latter term is some function of the current and electrolysis time and would be dependent on the diffusion coefficient of ox_2.

Again, for an electrode of area A, eqn. (6) becomes:

$$[red_1] = \frac{S}{A}(\pi D_2 t_{max}')^{-\frac{1}{2}}$$

and t_{max}' should decrease with increasing area. This is contrary to the experimental results and may be explicable on the basis that more ox_2 will diffuse during the pulse at an electrode of small area than would for a larger electrode.

Ideally, the length of the pulse should be very short, but with the instrumentation available it was considered that any value of t smaller than 2 sec could not be measured with sufficient accuracy to yield valid results.

The finite intercept on the $t'^{-\frac{1}{2}}$ axis can be understood by considering the effect of applying a pulse of electricity to a solution containing only red_2. The potential of this electrode when the solution is homogeneous is given by the Nernst equation using bulk concentrations of ox_2 and red_2. The ratio ox_2:red_2 will be very small—say 10^{-6}—and the potential can then decay by as much as $0.059 \log[ox_2]/[red_2]$, *i.e.*, 0.36 V. That is, even without red_1 being present, the potential of the electrode can pass through the inflection potential. This, in fact, was observed experimentally but the decay times were too long to permit accurate measurement. They were, however, of the correct order to account for the intercept.

A hypothesis is presented to account for the presence of two inflections in the decay curve. If we allow that at the end of the pulse the potential-determining couple is ox_2–red_2 (Fig. 5a), and that when the solution is homogeneous the potential-determining couple is ox_1–red_1 (Fig. 5b), we have the possibility that at some time during the decay a transition to a mixture potential (Fig. 5c), determined by both couples, will be observed. This transition would then correspond to the observed inflection.

In general, no kinetic information could be obtained about reaction (iii) by this method, since as has been shown by SPIRO AND RAVNO[6], the platinum surface acts as a heterogeneous catalyst. This aspect, however, should enable a variety of redox

reactions, that normally would be too slow for coulometric or volumetric titrations, to be carried out by this technique.

Further work will be concerned with designing more sophisticated instrumentation and with the study of slow redox reactions.

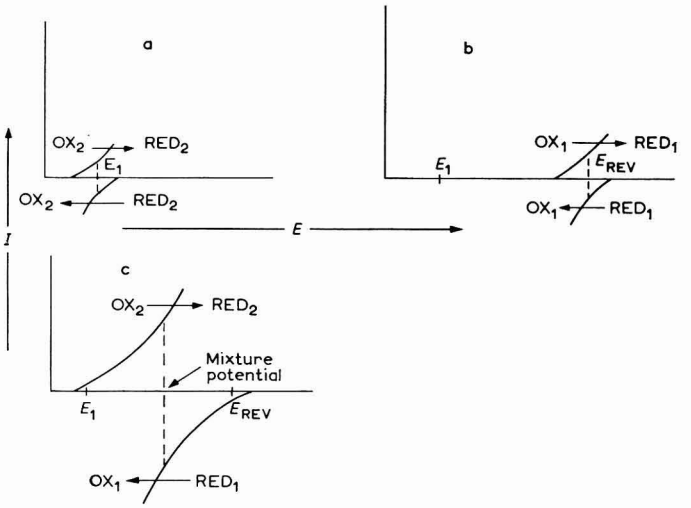

Fig. 5. Diagrammatic explanation of the first inflection illustrated in Fig. 3a.

The authors are indebted to Dr. DAVID PUGH for assistance in solving the diffusion equations.

SUMMARY

A new electroanalytical technique, closely related to current-cessation chronopotentiometry but derived by a consideration of the decay of the potential of the working electrode in coulometric titrations, is described. The potential range of applicability is suggested, and preliminary results suggest that the technique can be developed as a useful analytical tool. The theory of the method is treated at an elementary level. It is suggested that this method be termed Decay Chronopotentiometry.

REFERENCES

1 T. O. ROUSE, Ph.D. Thesis, University of Minnesota, 1961.
2 A. C. TESTA AND N. H. REINMUTH, *Anal. Chem.*, 33 (1961) 1324.
3 W. E. PALKE, C. D. RUSSELL AND F. C. ANSON, *ibid.*, 34 (1962) 1171.
4 W. A. ALEXANDER AND D. J. BARCLAY, *Analyst*, 90 (1965) 504.
5 P. DELAHAY, *New Instrumental Methods in Electro-Chemistry*, Interscience Publishers Inc., New York, 1954.
6 M. SPIRO AND A. B. RAVNO, *J. Chem. Soc.*, (1965) 87.

DOSAGE DU CADMIUM DANS LE NITRATE DE THORIUM PAR CHRONOAMPEROMETRIE LINEAIRE AVEC REDISSOLUTION ANODIQUE

K. A. KHASGIWALE
Analytical Division, A.E.E.T., Bombay (India)

R. MOLINA
Commissariat à l'Energie Atomique, S.E.A., Fontenay-aux-Roses, Hauts de Seine (France)
(Reçu le 2 février, 1966)

Le dosage d'impuretés comme le cadmium dans le thorium métal et ses sels présente un certain intérêt[1]. MENIS *et al.*[2] ont décrit une méthode polarographique directe pour le dosage du cadmium dans les solutions d'oxyde de thorium à pH 3 en milieu KCl et KCl–HCl comme électrolytes supports.

HIRANO *et al.*[3] ont étudié une méthode comprenant la séparation du cadmium dans des solutions de sels de thorium au moyen d'une résine échangeuse d'ions puis le dosage par polarographie à ondes carrées. En chronoampérométrie linéaire par redissolution anodique il est facile de séparer, concentrer et doser des traces très faibles d'impuretés en présence d'un grand excès d'ions non électroactifs à l'électrode utilisée. Nous avons étudié par cette méthode le dosage du cadmium dans les solutions de nitrate de thorium.

MONTAGE

C'est un montage classique à trois électrodes composé de:

(1) Une électrode auxiliaire de platine.

(2) Une électrode de référence Ag/AgCl en milieu KCl saturé.

(3) Une électrode indicatrice à goutte de mercure pendante.

Les jonctions électriques sont assurées par des compartiments munis de verre fritté et remplis d'un gel d'agar-agar au chlorure de potassium saturé. L'électrode à goutte pendante est fabriquée par la firme Metrohm ("équipement R.A."). Le remplissage de mercure est fait sous vide et les gouttes sont produites par le mouvement d'un piston mû par vis micrométrique. On peut obtenir ainsi des gouttes de surface reproductible à ± 0.07 mm^2 et qui restent stables pendant le temps nécessaire à la mesure. Nous avons utilisé un ensemble Solea-Tacussel constitué d'un potentiostat PRT 500L pour la stabilisation du potentiel et d'un pilote "Servovit" pour le balayage de potentiel. Le potentiel de l'électrode indicatrice par rapport à l'électrode de référence est vérifié à l'aide d'un millivoltmètre électronique Tacussel, type S6E.

Les courbes chronoampérométriques ont été tracées à l'aide d'un galvanomètre enregistreur type "GRSO Graphirac". Un agitateur magnétique tournant à 850 tours/min a été utilisé pour l'agitation durant la pré-électrolyse. Un barbotage d'argon pur préalablement saturé d'eau assurait le dégazage de la solution.

REACTIFS

Dans ce travail nous avons utilisé de l'eau bi-permutée et les réactifs "Prolabo" de pureté R.P. La préparation d'un électrolyte indifférent suffisamment pur pour nos essais présentait des difficultés. Seule l'électrolyse à potentiel contrôlé des électrolytes de base dans les conditions citées ci-dessous a permis d'obtenir un produit suffisamment pur.

Vol. de soln.	*Surface de la cathode de mercure*	*Potentiel d'électrolyse par rapport à Ag/AgCl*	*Temps d'électrolyse*
K_2CO_3, 4 *M*; 70 ml	28 cm^2	−1.4 V	12 h
KCl, 2 *M*; 70 ml		−1.5 V	12 h

Agitation mécanique 500 tours/min avec barbotage d'argon.

Les conditions opératoires de purification de KCl sont celles proposées par KEMULA *et al.*[4] Nous avons observé que la réduction des impuretés à ce potentiel s'accompagne d'une production d'ions OH^-. La réaction anodique étant l'oxydation des ions Cl^- (à une électrode de platine) et non la production d'ions H^+, le milieu devient basique et au bout d'une électrolyse de 12 h, le pH de la solution atteint la valeur 10. On constate alors une diminution de l'ordre de 70% de la hauteur du pic de Cd^{2+} pour une concentration donnée (inférieure à la limite de précipitation de l'hydroxyde pour cette valeur du pH). Pour expliquer ce phénomène on peut penser à la formation d'un complexe hydroxyde du type $CdOH^+$ (pK = 5.52) présentant une faible constante de diffusion*.

Pour les applications analytiques on doit donc ramener le pH vers une valeur de 7. Nous utilisons pour cela de l'acide chlorhydrique purifié par distillation isobare[5].

MODE OPÉRATOIRE

10 ml d'électrolyte support purifié comme il est indiqué plus haut, sont soumis à un barbotage d'argon avec agitation magnétique durant 20 min. Après l'arrêt du barbotage d'argon on forme une goutte de mercure de surface déterminée, puis on fixe la valeur du potentiel pour procéder à la pré-électrolyse durant un temps donné. Ce temps écoulé on arrête l'agitation et on attend durant 30 sec la cessation de tout mouvement convectif (temps de *repos*), le potentiel de l'électrode étant toujours stabilisé à la valeur initiale. Les temps sont mesurés à l'aide d'un chronomètre. A la fin du temps de repos on déclenche le balayage de potentiel vers les valeurs positives. Le même mode opératoire a été suivi pour les solutions étalons de cadmium et de nitrate de thorium seul, puis pour leur mélange.

CONCLUSIONS

Deux courbes types obtenues avec le nitrate de thorium seul et additionné d'une quantité connue de cadmium sont représentées Fig. 1. La Fig. 2 montre les courbes

* Le même phénomène est observé pour Cd^{2+} et In^{3+} en polarographie à impulsions (Mme BRIGAUDEAU, communication personnelle).

d'étalonnage obtenues pour le cadmium avec des concentrations variables de carbonate de potassium. Le Tableau 1 rassemble quelques résultats obtenus avec le nitrate de thorium dans K_2CO_3, 0.2 *M* et KCl, 1 *M* + HCl, 0.01 *M*, seul et avec addition de cadmium étalon.

Les courbes de la Fig. 2 montrent que la variation de la concentration de l'électrolyte support a un effet plus prononcé que dans le cas de la polarographie classique.

TABLEAU 1

Volume de solution, 10 ml. Surface de la goutte pendante, 2.72 mm². Pré-électrolyse: potentiel, 0.850 V par rapport à Ag/AgCl; agitation, 850 tours/min. Temps de repos, 30 sec. Vitesse de balayage, 0.8 V/min. Potentiel du pic correspondant à Cd(II), 0.590 V. 1 cm = 0.01 μA.

Electrolysé (h)	*Pré-électrolyse (min)*	*Electrolyte support*	h_p *(cm)*
12	5	0.2 *M* K_2CO_3 + 0.01 μg/ml Cd	4.2
			4.4
			4.4
12	5	0.2 *M* K_2CO_3 + 0.002 *M* Th(IV)	0.4*
			0.4
			0.4
			0.4
12	5	0.2 *M* K_2CO_3 + 0.002 *M* Th(IV) + 0.01 μg/ml Cd	4.7
			4.2
6	½	0.2 *M* K_2CO_3 + 0.02 μg/ml Cd	2.5
			2.6
			2.7
			2.2
6	½	0.2 *M* K_2CO_3 + 0.01 *M* Th(IV)	1.4*
			1.5
			1.5
6	½	0.2 *M* K_2CO_3 + 0.01 *M* Th(IV) + 0.02 μg/ml Cd	2.8
			2.2
			2.5
			2.8
			2.0
12	½	*M* KCl + 0.01 *M* HCl + 0.01 *M* Th(IV) + 0.1 μg/ml Cd(II)**	7.2
			7.5
			6.0
			7.5
			7.2
			6.5
			6.8

* Ces valeurs correspondent à la teneur en Cd(II) de l'électrolyte support.
** i_p = 0.0695 μA (0.1 μg/ml Cd(II) seul dans le même électrolyte support = 0.075 μA).

Il est possible de l'interpréter par la variation du mode de transport du cadmium avec la concentration de cet électrolyte support. Dans les solutions très concentrées le transfert du cadmium se fait presque totalement par un mécanisme de diffusion. Mais, lorsque la concentration de l'électrolyte indifférent décroît la migration du cadmium devient plus importante et pour un temps de pré-électrolyse donné, on atteint les concentrations plus importantes dans la goutte de mercure, donc des pics plus élevés lors de la redissolution. Cet effet n'est pas très prononcé dans

le cas de KCl. STURM[6] a remarqué des phénomènes identiques dans le cas de la polarographie à ondes carrées par redissolution anodique de Zn(II) en milieu HCl–KCl.

Les résultats montrent qu'il est possible de procéder à un dosage direct du cadmium dans le nitrate de thorium dans les deux milieux K_2CO_3 et KCl–HCl avec une dispersion de l'ordre de 14% pour des quantités de l'ordre de 8 p.p.m. de cadmium dans le thorium.

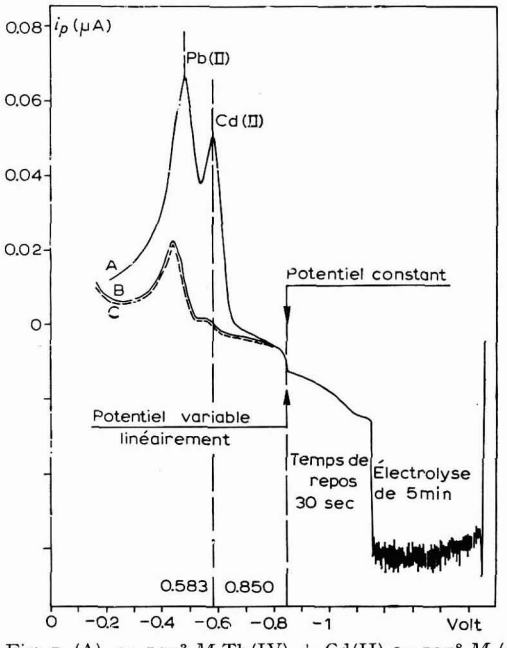

Fig. 1. (A), $2 \cdot 10^{-3}$ *M* Th(IV) + Cd(II) $9 \cdot 10^{-8}$ *M* (0.69 μg/ml); (B), $2 \cdot 10^{-3}$ *M* Th(IV); (C), électrolyte support.

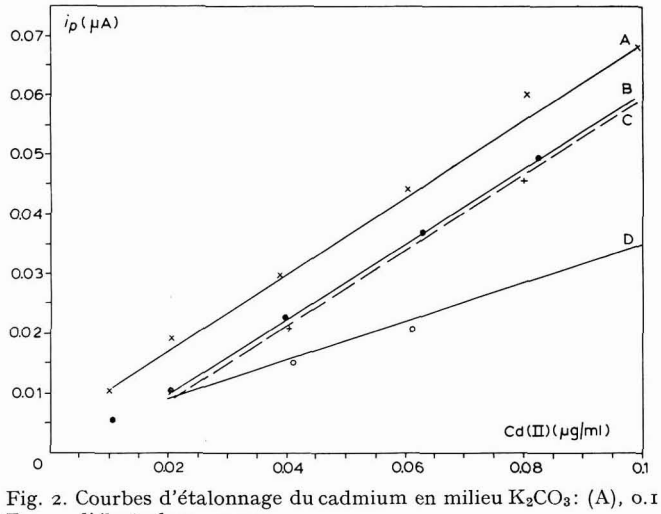

Fig. 2. Courbes d'étalonnage du cadmium en milieu K_2CO_3: (A), 0.1; (B), 0.2; (C), 0.5; (D), 1 *M*. Temps d'électrolyse, 30 sec.

REMERCIEMENTS

K.A.K. remercie vivement l'A.S.T.E.F. pour l'octroi d'une bourse de stage de spécialisation.

Ses remerciements vont également aux autorités du Commissariat à l'Energie Atomique pour les possibilités qui lui ont été offertes, ainsi que pour l'autorisation de publier cette partie du travail effectué durant son stage.

RÉSUMÉ

La chronoampérométrie linéaire par redissolution anodique a été appliquée au dosage du cadmium dans des solutions de nitrate de thorium pur en milieu K_2CO_3 et KCl–HCl comme électrolytes supports.

L'effet de la concentration de l'électrolyte support sur le courant d'oxydation est indiqué.

SUMMARY

Linear chronoamperometry by anodic stripping has been applied to the determination of cadmium in solutions of thorium nitrate with K_2CO_3 or KCl–HCl as supporting electrolyte.

The effect of supporting electrolyte concentration on the oxidation current is discussed.

BIBLIOGRAPHIE

1 C. J. Rodden, *Talanta*, 6 (1960) 12–13.
2 O. Menis, T. C. Rains, D. L. Manning, G. Goldstein et I. B. Rubin, *U.S. At. Energy Comm.*, TID-7568, Part 1, 1959, p. 157.
3 S. Hirano, A. Mizuike et Y. Iida, *Bunseki Kagaku*, 11 (1962) 1127; *cf. C.A.*, 58 (1963) 2834.
4 W. Kemula, E. Rakowska et Z. Kublik, *J. Electroanal. Chem.*, 1 (1959–1960) 205.
5 H. Irving et J. J. Cox, *Analyst*, 83 (1958) 526.
6 F. von Sturm et H. Ressel, *Proc. Austral. Conf. Electrochemistry, Sydney, 1963*, Pergamon Press, Oxford, p. 318.

A MERCURY-DROP SYNCHRONIZATION DEVICE

JAMES R. LUCK AND FRANK MILLS
Temperature Controls Group, Honeywell Inc., Minneapolis, Minn. 55408 (U.S.A.)
(Received January 24th, 1966)

INTRODUCTION

Since its introduction some 20 years ago, the technique of differential polarography has been studied by numerous workers. Although their results have been publicized in reputable journals the method has not gained wide acceptance, due mainly to the cumbersome equipment needed.

Initially, two independent polarographic cells were arranged to operate as nearly as possible in synchronization and the differential current was recorded[1-4]. The difference in frequency between the two capillaries registered as a beat or beaded-string effect superimposed on the polarogram. To eliminate the problem of dropping-electrode synchronization, the use of two streaming mercury electrodes was suggested, although not widely accepted[3,6]. At the time it was said, "If it were possible to synchronize the drop formation exactly at the two electrodes this would be an elegant, generally useful technique. Actually, however, such synchronization is virtually impossible."[5].

Probably the most progressive methods of drop synchronization were those reported by BARKER AND FAIRCLOTH[7], AIREY AND SMALES[8], and STAUNTON[9]. In all cases, a mechanical timing device caused a switch to actuate solenoids which dislodged drops from both capillaries concurrently. Other workers applied the same methods to oscillographic polarography[10-12].

Although many improvements in method and apparatus have appeared, the differential polarographic technique has not reached its greatest potential. Perhaps the major reason is the cumbersome, inflexible equipment used. The authors' goal was to develop a more attractive, simple and flexible differential polarographic accessory to perform the synchronization. The application of modern electronics provided reliable synchronization with easily adjusted frequency without the use of motors with cams and levers.

EQUIPMENT

Any appropriate polarographic cells can be used. Matching capillaries are obtained by breaking one capillary in half and using the mating broken ends as the drop exits. Cell assemblies and capillary-mercury stands are arranged in the usual manner. Each capillary is supplied with a solenoid or relay electromechanical drop-dislodgement device (Fig. 1). A 400-Ω, 24-V direct-current relay is modified by removing the contacts and installing a length of piano wire positioned to tap the capillary when the

coil is energized. The capillary is supported loosely by holding the plastic mercury tubing in a thermometer clamp.

Capillaries are adjusted so that their free-fall frequencies are nearly identical and slightly less than the desired frequency. Thus a very small mechanical impulse is sufficient to dislodge a drop, and solution stirring is kept to a minimum. Also, the mercury drop area is most reproducible when taken late in its normal life. The positions of the piano-wire hammers are adjusted to achieve simultaneous drop dislodgement. This is easily achieved since the hammers strike very quickly.

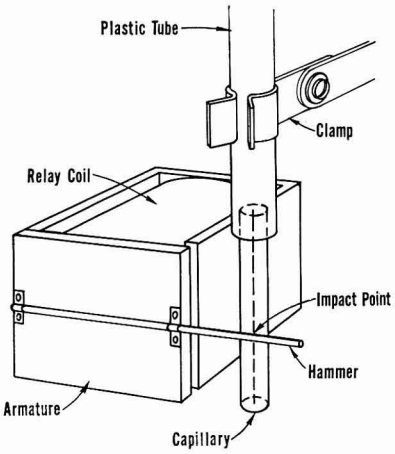

Fig. 1.

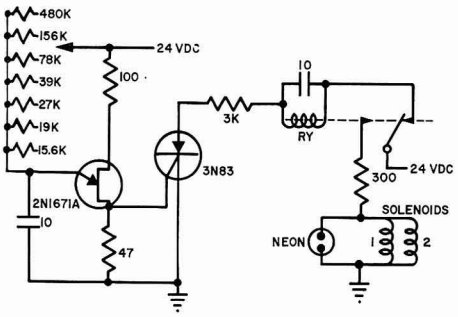

Fig. 2.

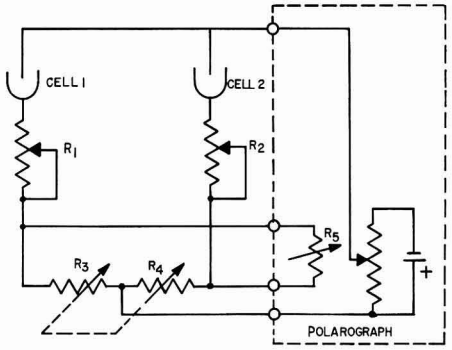

Fig. 3.

Both solenoids are actuated by a solid-state oscillator (Fig. 2). The frequency is adjustable. Frequencies of 0.33, 1, 2, 4, 6, 8 and 10 cycles/sec are obtained with the components given.

The two capillaries, actuated by the oscillator-solenoids, operate in perfect synchronization. The frequency is adjustable in steps to allow controlled variation of drop time. The frequency is reproducible since it is governed by stable components of the resistance-capacitance network of the oscillator circuit.

Application of the differential accessory is practically the same for all types of recording polarographs. A Wheatstone bridge is established using the sensitivity resistor of the polarograph as the measuring or central leg (Fig. 3). Two legs are matched stepwise with the sensitivity resistor. The last two legs are the polarographic cells with their zero-adjustment resistors. The installation requires that the lead from the sensitivity resistor to the applied potential bridge be opened in the polarograph.

To adapt a recording polarograph for use with the accessory, cut the lead from the sensitivity shunt network (R_5) to the applied voltage bridge (a switch may be inserted for quick change from standard polarography to differential polarography if desired). Determine the resistance values of the precision resistors in the sensitivity shunt of the polarograph. Build two duplicates (R_3 and R_4) of this shunt network on a two-wafer switch. The resistances of the external adjustable resistors must always be equal and also of the same value as the sensitivity resistor (R_5) in the polarograph. The zero-adjustment potentiometers (R_1 and R_2) are selected to allow the output to be zeroed under any experimental conditions.

APPLICATIONS

The apparatus has been used for diffusion-current compensation and interfering-wave elimination. Also, it may be used in derivative polarography by the Heyrovsky technique[3], strobe polarography, and some forms of single-sweep oscillographic polarography. Amperometric titrations may be performed to determine the concentration of an electrode reactive substance by adding a known amount of that substance to the reference cell until current cancellation. Normal polarograms using a single dropping electrode operating at the rapid controlled rate, may be obtained with time saving and an improved resolution.

SUMMARY

A simple solid-state oscillator has been developed for triggering electromechanical drop-dislodgement devices. The simplicity, versatility and reproducibility of the device recommend it for use in any polarographic laboratory. It should encourage the use of the valuable differential method.

REFERENCES

1 G. F. Reynolds, *Chem. & Ind. London*, (1953) 971.
2 G. W. C. Milner, *The Principles and Applications of Polarography*, Longmans, London, 1957, p. 118.
3 H. Schmidt and M. von Stackelberg, *Modern Polarographic Methods*, Academic Press, New York, 1963.
4 G. Semerano and L. Riccoboni, *Gazz. Chim. Ital.*, 72 (1942) 297–304.
5 I. M. Kolthoff and J. J. Lingane, *Polarography*, 2nd ed., Interscience, New York, 1952, pp. 331–332.
6 J. Heyrovsky, *Chem. Listy*, 40 (1946) 222–224.
7 G. C. Barker and R. L. Faircloth, *J. Polarog. Soc.*, 1 (1958) 11–16.
8 L. Airey and A. A. Smales, *Analyst*, 75 (1950) 287–304.
9 J. J. J. Staunton, U.S. Pat. 2689330, September, 1954.
10 W. Kemula, S. Brzoztowski and K. Butkiewicz, *Chem. Anal., Warsaw*, 3 (1958) 489–494.
11 C. I. Mooring, *Polarograph. Ber.*, 6 (1958) 63–65.
12 H. M. Davis and H. I. Shalgosky, *Advances in Polarography, Proceedings of the Second International Congress, Cambridge, 1960*, pp. 618–627.

RECONSIDERATION OF THE GALVANOSTATIC DOUBLE-PULSE METHOD

D. J. KOOIJMAN AND J. H. SLUYTERS
Laboratory of Analytical Chemistry, State University, Utrecht (Netherlands)
(Received February 3rd, 1966)

Fast electrode processes can be studied only by relaxation methods. In these methods, the electrode processes should be perturbed with signals of high frequency or short time in order to minimize concentration polarization.

One of the limitations encountered in the study of electrode kinetics with the galvanostatic single-pulse method is the influence of the double-layer capacitance at short pulse lengths. To remove this limitation, GERISCHER AND KRAUSE[1] developed the galvanostatic double-pulse method. The first pulse which is of higher amplitude, i_1, than the second pulse, primarily charges the double-layer capacitance to the overvoltage required by the current density, i_2, of the second pulse; *i.e.*, the overvoltage–time curve should start with a horizontal tangent at the beginning of the second pulse. Thus the current, passing the cell, is entirely faradaic at that moment. The value i_1/i_2 must be found by trial and error.

A mathematical analysis of the method, limited to cell responses of small amplitude, has been given by DELAHAY *et al.*[2]. They correct for the concentration polarization occurring within the time, t_1, of the first pulse. However, they do not consider the errors caused by the experimental difficulty of observing whether or not the cell response starts with a horizontal tangent at time t_1. In the present paper we shall show that this difficulty seriously limits the double-pulse method.

THEORY

According to DELAHAY *et al.*[2], the voltage–time relation for the response of an electrode process, that is perturbed by a double-pulse current (Fig. 1), is:

$$\begin{aligned}\eta(t) = {} & \frac{i_1}{C_d(\gamma-\beta)}\Big[\gamma/\beta^2(\exp\beta^2 t\,\mathrm{erfc}\,\beta\sqrt{t} + 2\beta\sqrt{\frac{t}{\pi}} - 1) \\ & - \beta/\gamma^2(\exp\gamma^2 t\,\mathrm{erfc}\,\gamma\sqrt{t} + 2\gamma\sqrt{\frac{t}{\pi}} - 1)\Big] \\ & + \frac{i_2-i_1}{C_d(\gamma-\beta)}\Big[\gamma/\beta^2(\exp\beta^2(t-t_1)\,\mathrm{erfc}\,\beta\sqrt{t-t_1} + 2\beta\sqrt{\frac{t-t_1}{\pi}} - 1) \\ & - \gamma/\beta^2(\exp\gamma^2(t-t_1)\,\mathrm{erfc}\,\gamma\sqrt{t-t_1} + 2\gamma\sqrt{\frac{t-t_1}{\pi}} - 1)\Big] \qquad (1)\end{aligned}$$

and if $\left(\frac{\mathrm{d}\eta}{\mathrm{d}t}\right)_{t=t_1} = 0$, then

$$\frac{i_2}{i_1} = 1 - \frac{1}{\gamma-\beta}[\gamma \exp \beta^2 t_1 \operatorname{erfc} \beta \sqrt{t_1} - \beta \exp \gamma^2 t_1 \operatorname{erfc} \gamma \sqrt{t_1}] \tag{2}$$

in which

$$\beta + \gamma = \frac{i_0}{nF}\left(\frac{1}{C_O{}^*\sqrt{D_O}} + \frac{1}{C_R{}^*\sqrt{D_R}}\right) \quad \text{and} \quad \beta\gamma = \frac{nFi_0}{RTC_d}.$$

The interpretation of eqn. (1) is difficult. Therefore we shall simplify it assuming that $t_1 \to 0$ and $i_1 t_1/C_d \to \eta_0$. Equation (1) then reduces to:

$$\eta(t) = \frac{\eta_0}{\gamma-\beta}[\gamma \exp \beta^2 t \operatorname{erfc} \beta \sqrt{t} - \beta \exp \gamma^2 t \operatorname{erfc} \gamma \sqrt{t}]$$
$$+ \frac{i_2}{C_d(\gamma-\beta)}\left[\gamma/\beta^2(\exp \beta^2 t \operatorname{erfc} \beta \sqrt{t} + 2\beta \sqrt{\frac{t}{\pi}} - 1)\right.$$
$$\left. - \beta/\gamma^2(\exp \gamma^2 t \operatorname{erfc} \gamma \sqrt{t} + 2\gamma \sqrt{\frac{t}{\pi}} - 1)\right] \tag{3}$$

The condition, $(d\eta/dt)_{t=0} = 0$, yields

$$i_2 = \beta\gamma C_d \eta_0 \tag{4}$$

If $i_2 = A\beta\gamma C_d \eta_0$, the curve will not start with a horizontal tangent, and for $A < 1$ the curve will exhibit a minimum at a time t_m, see Fig. 2. Obviously i_2 should be adjusted so that this minimum has just disappeared. This means that $\Delta\eta$ must be distinct for a small deviation of i_2 from the correct value.

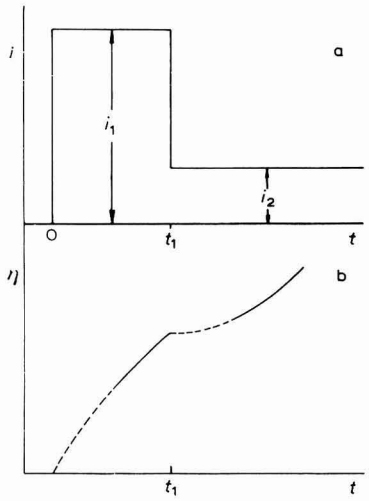

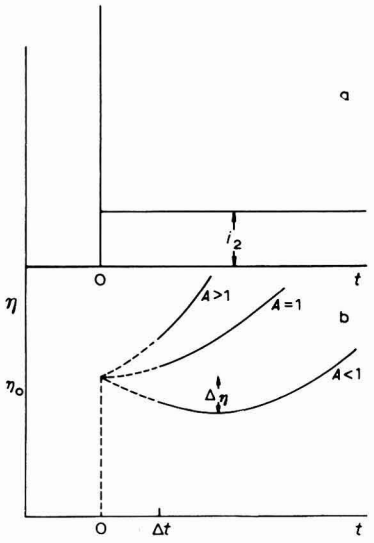

Fig. 1. (a), Shape of a double-pulse current; (b), cell response having a horizontal tangent at time t_1. The dashed parts of the curve indicate that in these regions the response is obscured by transients.

Fig. 2. (a), Double-pulse current with an infinitely short first-pulse length; (b), cell response having a horizontal tangent at time $t = 0$. The dashed part of the curve indicates the region, Δt, which is obscured by transients.

The values t_m and $\Delta\eta$ can be obtained by expansion in series of the exponential and error functions in eqn. (3) for small values of t:

$$\eta(t) = \eta_0 \left[1 - (1-A)\beta\gamma t + \frac{4}{3\sqrt{\pi}} \beta\gamma(\beta+\gamma)t\sqrt{t} \right] \tag{5}$$

$$\frac{d\eta}{dt} = 0 \quad \text{yields} \quad t_m = \frac{\pi}{4}\left(\frac{1-A}{\beta+\gamma}\right)^2 \tag{6a}$$

and

$$\frac{\Delta\eta}{\eta_0} = -\frac{\pi}{12}(1-A)^3 \frac{\beta\gamma}{(\beta+\gamma)^2} \tag{6b}$$

These equations are valid only if $\beta\gamma t < 1$ and $(\beta+\gamma)t^{\frac{1}{2}} < 1$. These conditions will be checked afterwards.

From Fig. 2 it can be seen that, in order to observe a minimum in the cell response, $\Delta\eta/\eta_0$ must have a finite value. Moreover t_m must be larger than Δt, the time during which the cell response is obscured by transients.

THE VALUES OF Δt AND $\Delta\eta$

Even with good electronic design, transients, due to finite time constants of cables and the cell in the circuit, will be observed at the initial part of the potential–time curve. We have found experimentally that these transients have been damped only after 0.4 μsec. Consequently, t_m must be larger than 0.4 μsec. Not only transients will contribute to Δt, but also the rise and decay times of the pulse-generators and the response time of the oscilloscope recording the overvoltage–time curve. If the ohmic drop in the cell is compensated by means of a bridge circuit of DELAHAY[3], the value of Δt will be generally larger than 1 μsec, as a differential oscilloscope with relatively poor rise time must be used. Elsewhere[4] we have described a set-up for the compensation of the ohmic drop in which an asymmetric fast response oscilloscope can be used. In that case Δt will be about 0.4 μsec.

The value of $\Delta\eta$ first depends on the line-width of the trace on the screen of the oscilloscope, generally $\Delta\eta/\eta \geqslant 0.01$. However, if high exchange current densities are measured, the compensation of the ohmic drop will be more important. If *e.g.* the miscompensation of the ohmic drop for the second pulse is 0.05 mV, the first part of the curve, from 0 to t_1, will be shifted an amount $(i_1 - i_2)/i_2 \cdot 0.05$ mV with respect to the second part of the curve, $t > t_1$. As a result, $\Delta\eta$ must be larger than 0.01 η in order to observe a minimum in the cell response. If the influence of a miscompensation of the ohmic drop is also taken into account, a value of $\Delta\eta/\eta_0 \geqslant 0.02$ seems reasonable.

SCOPE OF THE DOUBLE-PULSE METHOD

Inserting $t_m \geqslant 0.4$ μsec and $\Delta\eta/\eta_0 \geqslant 0.02$ in eqns. (6a) and (6b), one obtains:

$$\left.\begin{array}{lll} \text{for } A = 0.9: & \beta + \gamma \leqslant 140 & \text{and } \beta\gamma \geqslant 76(\beta+\gamma)^2 \\ A = 0.8: & \beta + \gamma \leqslant 280 & \beta\gamma \geqslant 9.6(\beta+\gamma)^2 \\ A = 0.5: & \beta + \gamma \leqslant 700 & \beta\gamma \geqslant 0.61(\beta+\gamma)^2 \end{array}\right\} \tag{7}$$

Taking the following reasonable values: $n = 2$, $T = 300$ °K, $D_{ox} = D_R = 10^{-5}$ $cm^2 sec^{-1}$, $C_d = 25 \cdot 10^{-6}$ Fcm^{-2} and $C_{ox}^* = C_R^* = C^*$, one can calculate the limits of k_{sh} and i_0, which should not be exceeded if accuracies of 10, 20 and 50% are required, respectively, see Table 1.

TABLE 1

A	C^* (mole cm^{-2})	i_0 (A cm^{-2})	K_{sh} (cm sec^{-1})
0.9	10^{-7}	$\leqslant 44 \cdot 10^{-6}$	$\leqslant 2.2 \cdot 10^{-3}$ (10%)
	$5 \cdot 10^{-7}$	$\leqslant 1.1 \cdot 10^{-3}$	$\leqslant 1.1 \cdot 10^{-2}$
	$2.5 \cdot 10^{-6}$	$\leqslant 27 \cdot 10^{-3}$	$\leqslant 5.4 \cdot 10^{-2}$
	$10 \cdot 10^{-6}$ and higher	—	$\leqslant 2.2 \cdot 10^{-1}$
0.8	10^{-7}	$\leqslant 350 \cdot 10^{-6}$	$\leqslant 1.7 \cdot 10^{-2}$ (20%)
	$5 \cdot 10^{-7}$	$\leqslant 8.8 \cdot 10^{-3}$	$\leqslant 8.8 \cdot 10^{-2}$
	$2.5 \cdot 10^{-6}$ and higher	—	$\leqslant 4.4 \cdot 10^{-1}$
0.5	10^{-7}	$\leqslant 5.2 \cdot 10^{-3}$	$\leqslant 0.26$ (50%)
	$4 \cdot 10^{-7}$ and higher	—	$\leqslant 1$

It should be noted that the error in the measured i_0 or k_{sh} is a systematic one. The measured value for the exchange current density or rate constant is always too low.

A numerical examination* of eqn. (1) revealed that even if $t_1 > 0$, the same limits, as tabulated above, are valid provided that the correction for concentration polarization, occurring within time t_1, is performed with sufficient accuracy. This may be difficult if the rate constant, k_{sh}, is large, as the extrapolation procedure proposed by DELAHAY[2] *et al.*, is not always allowed.

DETERMINATION OF THE EXCHANGE CURRENT DENSITY FOR THE Hg/Hg^{2+} ELECTRODE REACTION IN 1 M $HClO_4$

The Hg/Hg^{2+} electrode has been investigated by means of several relaxation methods and by different authors. IMAI AND DELAHAY[5] reported for 1 mM Hg_2^{2+}, an exchange current of 12 Acm^{-2}, measured with the faradaic rectification method. SLUYTERS-REHBACH AND SLUYTERS[6] conclude from a complex plane analysis that i_0 must be larger than 450 mA cm^{-2} for 1 mM Hg_2^{2+}. BIRKE AND ROE[7] measured with the galvanostatic single-pulse method an i_0 of about 350 mA cm^{-2}. The following data are reported from the galvanostatic double-pulse method.

C^* (mM)	i_0 (mA cm^{-2})		
	Delahay[2]	*Gerischer*[1]**	*Our data*
2	420	350	700
1	250	200	400
0.5	180	120	200
0.2	75		80
0.1			35

* Table of exp x^2 erfc x are tabulated by FADDEYEVA AND TERENT'EV[9].
** These values are corrected for concentration polarization occurring within the first pulse.

The results obtained with the different relaxation methods are inconsistent. As regards the double-pulse method, it can be shown by means of eqn. (7) (in which, for C_d, the values published by SLUYTERS-REHBACH AND SLUYTERS[8] are substituted) that the reported data contain errors larger than 50%. Therefore one may conclude that the Hg/Hg_2^{2+} electrode reaction behaves reversibly with respect to the double-pulse method. The inconsistency between our data for 1 mM and 2 mM Hg_2^{2+} and those of DELAHAY AND GERISCHER can be explained by assuming that their value of Δt was larger than ours.

CONCLUSIONS

The galvanostatic double-pulse method has no advantage over the single-pulse method, as the experimental conditions to be fulfilled in order to measure high exchange current densities, cannot be realized. For the same reason, the values of i_0 for the Hg/Hg_2^{2+} electrode reaction measured with the double pulse method, published previously and in this paper, have no meaning.

SUMMARY

A critical examination is made of the voltage response of a cell when a double-pulse current is applied. The limitations of the double-pulse method for studying fast electrode reactions are considered and it is shown that the maximum value of the heterogeneous rate constant measurable with this method is about 0.5 cm sec^{-1}. In this case the error will be 20%.

REFERENCES

1 H. GERISCHER AND M. KRAUSE, *Z. Physik. Chem. N.F.*, 10 (1957) 264.
2 H. MATSUDA, S. OKA AND P. DELAHAY, *J. Am. Chem. Soc.*, 81 (1959) 5077.
3 T. BERZINS AND P. DELAHAY, *J. Am. Chem. Soc.*, 77 (1955) 6448.
4 D. J. KOOIJMAN AND J. H. SLUYTERS, *Electrochim. Acta*, submitted.
5 H. IMAI AND P. DELAHAY, *J. Phys. Chem.*, 66 (1962) 1108.
6 M. SLUYTERS-REHBACH AND J. H. SLUYTERS, *Rec. Trav. Chim.*, 83 (1964) 983.
7 R. L. BIRKE AND D. K. ROE, *Anal. Chem.*, 37 (1965) 451.
8 M. SLUYTERS-REHBACH AND J. H. SLUYTERS, *Rec. Trav. Chim.*, 83 (1964) 987.
9 V. N. FADDEYEVA AND N. M. TERENT'EV, *Tables of the probability integral for complex argument*, 1954; Engl. translation, Pergamon Press, Oxford, 1961.

CONTROLLED-POTENTIAL OXIDATION OF ALIPHATIC AMIDES

JERRY F. O'DONNELL* AND CHARLES K. MANN**
Department of Chemistry, Florida State University, Tallahassee, Florida 32306 (U.S.A.)
(Received March 3rd, 1966)

SCHNEIDER[1] studied the electrochemical behaviour of amides and observed that electrolysis of pure formamide led to the formation of cyanuric acid, a cyclic trimer of cyanic acid. No mechanism was suggested. COUCH[2] studied the electrolysis of various formamides, acetamides and propionamides, both as pure liquids and with 10% aqueous sulfuric acid. He confirmed the production of cyanuric acid from formamides at the anode. Electrolysis of other amides yielded higher molecular-weight products. For example, 2,6-diformyl-2,6-diaza-4-oxaheptane was obtained from N,N-dimethylformamide. The mechanisms for these reactions were not discussed.

In studying the Kolbe reaction, ROSS, FINKELSTEIN AND PETERSON[3] found that the addition of N,N-dimethylamides during the reaction of formate or acetate greatly decreased the formation of gas and resulted in the formation of N-acyloxyl-N-methylamides (I). Three mechanisms are suggested for these reactions. Two of these involve initial formation of the acyloxyl radical at the electrode, with subsequent reaction of the radical with amide. The third suggested mechanism involves direct anodic reaction of amide in a two-electron process to produce the carbonium ion (II).

$$\underset{(I)}{R-CO-N(CH_3)CH_2OCOR} \qquad \underset{(II)}{RCON(CH_3)\overset{+}{C}H_2}$$

By observing the potential at which reaction took place with and without the amide, they showed that the third mechanism is very probable for acetate oxidation, but impossible for the formate oxidation.

We describe here the detailed examination of the anodic oxidation of a variety of primary, secondary and tertiary amides in acetonitrile solution at a platinum electrode. On the basis of product analysis, experiments involving controlled-potential coulometry and cyclic voltammetry, and a consideration of the effect of water concentration, a mechanism is presented.

EXPERIMENTAL

Reagents

MeCN was purified according to the procedure previously described[4]. A similar procedure was used for isobutyronitrile. $NaClO_4$ was recrystallized from 95% ethanol, dried in a vacuum oven and stored over P_2O_5. When rigorous exclusion of

* Present address: Pittsburgh Plate Glass Company, Chemical Division, Corpus Christi, Texas 78408.
** To whom reprint requests should be addressed.

water was desired, $NaClO_4$–MeCN solutions were percolated through a 15-mm × 15-cm bed of freshly activated BaO which was connected by ground joints to a previously purged electrolysis cell. Water could not be detected in these solutions by thermal conductivity gas chromatography (< 0.005%).

Commercially-available amides were used when possible; otherwise, they were synthesized from the appropriate amine and acyl chloride. Amides were checked for purity by gas chromatography[5]. The principal contaminant was water, which was removed from liquid amides by repeated evaporation with methylene chloride. Solid amides were recrystallized from 50:50 acetone:chloroform.

Apparatus

Electrochemical experiments were performed using a Ag/0.10 *M* $AgClO_4$–MeCN reference electrode. The reference solution made contact to the electrolysis solution through an asbestos fiber sealed in a glass probe. Reference electrodes were periodically referred to aqueous S.C.E. in separate measurements.

Cyclic voltammetry experiments were performed on platinum micro-electrodes at about 10 V/sec sweep rates using the apparatus previously described[6]. A conventional three-electrode electronic potentiostat was used for exhaustive controlled-potential electrolysis. An H-style cell with a 35 × 80-mm anode compartment and a 15 × 80-mm cathode compartment was used, with a 15 × 45-mm platinum-gauze anode and chromel cathode. Solutions were 0.2 *M* $NaClO_4$, 2–5 m*M* in amide for cyclic voltammetry, and 8–10 m*M* for exhaustive electrolysis.

Coulometry was carried out using a nitrogen–hydrogen coulometer as described by LINGANE[7]. Current during exhaustive electrolysis was recorded by monitoring *IR* drop across a suitably placed resistor in series with the electrolysis cell.

Electrolyzed solutions were analyzed for acid by titration[8] and for volatile compounds by hydrogen flame and thermal conductivity gas chromatography. Identifications were made by trapping from the chromatograph and comparing with i.r.- and NMR-spectra of valid samples. Head space over the anode compartment was examined volumetrically for gaseous products, with negative results.

RESULTS AND DISCUSSION

Cyclic voltammetry showed in all cases a one-step irreversible oxidation. Peak potentials for amides are sharply divided into three classes, according to the number of N-alkyl substituents. Primary amides are oxidized in the region of 2.0 V *vs.* S.C.E. Voltammetry peaks are not resolved from background with $NaClO_4$ or Me_4NBF_4 supporting electrolyte. Secondary amides show peaks at about 1.8 V *vs.* S.C.E.; tertiary amides show peaks from 1.22–1.51 V *vs.* S.C.E. Exhaustive electrolyses were carried out at 1.35 V for tertiary, 1.60 V for secondary and 1.85 V *vs.* S.C.E. for primary amides.

On integrating current in exhaustive electrolysis, all three classes showed one electron/amide molecule, within experimental error. Oxygen had no effect on this; similarly, water concentrations below 0.10 *M* with secondary and tertiary amides, and below 0.05 *M* with primary amides, had no effect on coulometry.

The titration of product mixtures revealed one equivalent of moderately strong acid/mole of starting amide. Results were the same for all three classes of amides. The

i.r. spectra of product mixtures were identical with spectra of protonated starting amide. When product mixtures were neutralized with $NaHCO_3$, and the solvent removed in vacuum, amides could be identified in the residue. The oxidation products of a number of amides in dry MeCN are shown in Table 1.

TABLE 1

OXIDATION PRODUCTS OF CERTAIN ALIPHATIC AMIDES IN DRY ACETONITRILE

Amide	E_p	n	% *Recovery of*:	
			Original amide	$(CH_2CN)_2$
N,N-dimethylacetamide	1.32	0.99	95	85
N-methylacetamide	1.81	0.98	92	90
N,N-dipropylpropionamide	1.26	0.98	90	83
Acetamide	—	0.98	96	94
Propionamide	—	0.99	99	87
Butyramide	—	0.98	98	91

E_p = cyclic voltammetry peak potential in volts *vs.* S.C.E.
n = number of electrons lost/amide molecule in overall electrode reaction.
% Recovery figures based on theoretical amount from mechanism.

We suggest that these results indicate that the anodic reaction of tertiary amides in dry MeCN is substantially as follows:

$$\mathrm{RCON(CH_2R')_2} \rightarrow \underset{\text{(III)}}{\mathrm{RCO\dot{N}(CH_2R')_2^+}} + e^- \tag{1}$$

$$\mathrm{III} + \mathrm{CH_3CN} \rightarrow \mathrm{RCONH(CH_2R')_2^+} + \cdot\mathrm{CH_2CN} \tag{2}$$

$$2 \cdot \mathrm{CH_2CN} \rightarrow \mathrm{(CH_2CN)_2} \tag{3}$$

When the reaction is run in isobutyronitrile, the products are protonated amide and methacrylonitrile. We suggest that the amide ion radical abstracts a hydrogen atom from the solvent to produce the tertiary radical, which disproportionates to form methacrylonitrile and isobutyronitrile.

With small concentrations of water, the reactions of secondary and tertiary amides are more complicated. The electron count and acid recovery are not changed. Plots of log current *vs.* time for exhaustive electrolysis, which are linear with dry solvents indicating simple kinetics, are non-linear with wet systems. Reaction products change with water content, as shown in Table 2. The recoveries of succinonitrile and protonated starting amide decrease as the recoveries of protonated dealkylated amide and of the corresponding aldehyde increase with increasing water concentration.

We suggest that in addition to reactions (1)–(3), the following also take place:

$$\mathrm{III} \rightleftharpoons \mathrm{R\overset{+}{C}ON(CH_2R')=CHR'} \leftrightarrow \underset{\text{(IV)}}{\mathrm{RCON(CH_2R')\overset{+}{C}HR'}} + \mathrm{H^+} + e^- \tag{4}$$

$$\mathrm{IV} + \mathrm{H_2O} \rightarrow \mathrm{R\overset{+}{C}ONH_2(CH_2R')} + \mathrm{R'CHO} \tag{5}$$

$$\mathrm{RCON(CH_2R')_2} + \mathrm{H^+} \rightarrow \mathrm{RCONH(CH_2R')_2^+} \tag{6}$$

We are supposing that the initial ion radical, III, can react in two ways: by

TABLE 2

EFFECT OF WATER ON REACTION PRODUCTS

Amide	*% Recovery of:*			
	Tertiary amide	*Secondary amide*	*RCHO*	*$(CH_2CN)_2$*
N,N-dimethylacetamide				
Water = 0 m*M*	95	0	trace	85
7	70	23	19	22
45	55	40	32	trace
119	47	49	45	0
N,N-dipropylacetamide				
Water = 35 m*M*	58	32	26	trace
119	44	44	53	0
N,N-dipropylpropionamide				
Water = 0 m*M*	90	7	5	83
7	81	12	10	55
35	59	35	32	5
119	49	49	38	0
N-methylacetamide				
Water = 0 m*M*		92	5	90
35		81	14	27
119		76	21	0
N,N-diamylacetamide				
Water = 119 m*M*	45	52	49	
N,N-diethylbutyramide				
Water = 119 m*M*	44	45	36	
N-propylacetamide				
Water = 119 m*M*			31	

abstraction of a hydrogen atom from the solvent as in reaction (2) or by loss of a second electron and a proton to form the carbonium ion, IV. Since the presence of water determines which path is taken, reaction (4) is taken to be reversible. In dry solvents, reaction of III is faster than any available reaction of IV. With sufficient water, IV reacts rapidly enough to cause the two-electron carbonium ion path to predominate. With intermediate water concentrations, both paths would be important. Although reactions (2) and (4) require two electrons, coulometry on wet systems shows just one electron/molecule of amide because an extra molecule is consumed in reaction (6).

For secondary amides, we suggest an entirely similar mechanism resulting in formation of protonated secondary and primary amides. The extent of dealkylation is controlled by water concentration in the same way. It may be noted that only one dealkylation can take place with a tertiary amide, not withstanding the fact that secondary amides are reactive. This follows because the products are, in all cases, protonated and therefore unreactive. We occasionally found small amounts of acetamide in wet reaction mixtures. This is attributed to hydrolysis of MeCN rather than to a second dealkylation, since propionamide was never found in wet tertiary propionamide reaction products.

Reactions (1) and (2) are the same as those suggested by ROSS *et al.*[3] to explain the effect of tertiary amides in the Kolbe reaction. We suggest that anodic oxidation is a generally applicable route with secondary and tertiary amides either to the ion radical *via* a one-electron process, or to the α-carbonium ion *via* a two-electron process. Choice of reaction paths and the identity of the final product will be determined by the relative availability of substances capable of reacting with radicals or with acids. Thus if a base, *e.g.*, water or acetate, is available to react with the carbonium ion, then the two-electron process may be favored. With no base present but with a compound capable of reacting with radicals, *e.g.*, MeCN or isobutyronitrile, the one-electron process is favored. That we observe dealkylation while ROSS *et al.* do not, follows because the product of reaction of the carbonium ion with the base, water, happens to be unstable, while the product of reaction with the base, acetate, is stable. It should be possible to vary the products by controlling the radical trap or base present during the reaction.

In connection with an investigation of this type, it is interesting to compare the electrochemical oxidation with chemical oxidations. SHARKEY AND MOCHEL[13] showed that photo-oxidation of N-pentylhexanamide formed valeraldehyde, valeric acid and caproic acid. Reactions of a variety of oxidizing agents with tertiary amines have been studied and found to cause dealkylation and formation of the appropriate aldehyde. Among these are ClO_2[10], N-bromosuccinimide[11], $Pb(OAc)_4$[12], HNO_2[13] and $Hg(OAc)_2$[14]. In all these cases, there is an obvious similarity between chemical and electrochemical oxidation of aliphatic nitrogen. In the reaction of $Hg(OAc)_2$, formation of the α-carbonium ion, corresponding to IV, is suggested[14].

When the chemical oxidation of primary amide is considered, however, similarity between chemical and electrochemical results is not evident. BAUMGARTEN AND STAKLIS[15] have found that primary amides react with $Pb(OAc)_4$ to form isocyanates in a reaction similar to the Hoffman rearrangement. By contrast, we find only protonated starting material; we observe the one-electron radical process.

The $Pb(OAc)_4$ oxidation is a base-catalyzed two-electron process which results in formation of $Pb(OAc)_2$, two molecules of AcOH and the postulated nitrene intermediate. Reaction of the primary amide is similar to that for secondary amide in that the one-electron electrochemical process is observed in the absence of base. It differs in forming the nitrene diradical on $Pb(OAc)_4$ oxidation, rather than the carbonium ion, because there is no carbon alpha to the nitrogen on which to form a carbonium ion. If a base were available that did not itself react at the potentials required for primary amide oxidation, it is possible that a two-electron electrochemical reaction would also be observed.

ACKNOWLEDGEMENT

Support in the form of Research Grant GM-10064 from the United States Public Health Service and of a research fellowship for JERRY F. O'DONNELL from the National Aeronautics and Space Administration is gratefully acknowledged.

SUMMARY

A systematic study of the electrochemical oxidation of primary, secondary and

tertiary aliphatic amides at platinum electrodes in aprotic solvents is reported. Results of product analyses, coulometry and cyclic voltammetry are presented. A mechanism is proposed which involves two different paths to stable products. One of these involves a one-electron reaction with subsequent radical reaction. The other involves a two-electron process with subsequent reaction with base. Examples of both types are presented for secondary and tertiary amides. Only the one-electron process has been observed electrochemically with primary amides. Comparison of chemical and electrochemical oxidations is discussed.

REFERENCES

1 V. H. SCHNEIDER, *Ber.*, 56 (1923) 2640.
2 D. E. COUCH, *Electrochim. Acta*, 9 (1964) 327.
3 S. D. ROSS, M. FINKELSTEIN AND R. C. PETERSON, *J. Am. Chem. Soc.*, 86 (1964) 4139; *J. Org. Chem.*, 31 (1966) 128.
4 J. F. O'DONNELL, J. T. AYRES AND C. K. MANN, *Anal. Chem.*, 37 (1965) 1161.
5 J. F. O'DONNELL AND C. K. MANN, *Anal. Chem.*, 36 (1964) 2097.
6 C. K. MANN, *Anal. Chem.*, 37 (1965) 326.
7 J. J. LINGANE, *Electroanalytical Chemistry*, Interscience, New York, 1958, p. 216.
8 K. K. BARNES AND C. K. MANN, *Anal. Chem.*, 36 (1964) 2502.
9 P. A. S. SMITH AND H. G. PARS, *J. Org. Chem.*, 24 (1959) 1325.
10 D. H. ROSENBLATT, A. H. HAYES, JR., B. H. HAMSON, R. A. SHEATY AND K. K. MOORE, *J. Org. Chem.*, 28 (1963) 2790.
11 S. DUNSTAN AND H. B. HENBEST, *J. Chem. Soc.*, (1957) 4905.
12 N. J. LEONARD AND M. A. REBENSTORF, *J. Am. Chem. Soc.*, 67 (1945) 49.
13 W. H. SHARKEY AND W. E. MOCHEL, *J. Am. Chem. Soc.*, 81 (1959) 3000.
14 N. J. LEONARD, A. S. HAY, R. W. FULMER AND V. W. GASH, *J. Am. Chem. Soc.*, 77 (1955) 439.
15 H. E. BAUMGARTEN AND A. STAKLIS, *J. Am. Chem. Soc.*, 87 (1965) 1141.

DETERMINATION OF ALIPHATIC AMIDES BY CONTROLLED-POTENTIAL COULOMETRY

JERRY F. O'DONNELL AND CHARLES K. MANN
Department of Chemistry, Florida State University, Tallahassee, Florida 32306 (U.S.A.)
(Received March 3rd, 1966)

The analysis of amides in the presence of other nitrogen compounds that make the classical Kjeldahl and Dumas techniques inapplicable has been the subject of considerable investigation in recent years. In general, the methods that have been developed are based on the titration of the amide in some medium which enhances its basicity, or on conversion of the amide to another class of compound by chemical means. The titration of amides in acetic anhydride was investigated by WIMER[1], and titration of amides in acetic acid was studied by HIGUCHI *et al.*[2]. However, titrations are in general not specific and are subject to interferences from other weakly basic compounds. POST AND REYNOLDS[3] have reported a method, based on the titration of primary amides with calcium hypobromite, which is applicable to primary amides. The method of MITCHELL AND ASHBY[4] involving reaction with 3,5-dinitrobenzoyl chloride can be applied only to primary amides. SIGGIA AND STAHL[5] employed reduction with lithium aluminum hydride, a method with which nitriles interfere. In a later paper, SIGGIA *et al.*[6] dealt with the problem of nitrile interferences by employing alkaline hydrolysis in which the amide hydrolyzes at a much faster rate than the nitrile, but this method has the disadvantage of requiring a total nitrogen determination by Kjeldahl or Dumas if both amides and nitriles are present.

We have found, using cyclic stationary electrode voltammetry, that aliphatic amides can be oxidized at a platinum electrode in acetonitrile (MeCN) solution. The difference in the peak potentials of the three types of amides indicated that it should be possible to oxidize selectively a mixture of amides by controlled-potential electrolysis. This forms the basis of the method reported here. The method offers good precision, is sensitive, and many other classes of compounds either do not interfere or may be removed by pre-electrolysis at lower potential.

EXPERIMENTAL

The apparatus and reagents used have been described previously[7].

Procedure

Fill the cell with 0.2 *F* $LiClO_4$ in MeCN. Position the electrodes and electrolyze at 1.9 V *vs.* S.C.E. until current becomes constant. With the cell described above, the background current is about 200 μA.

On completion of pre-electrolysis, introduce the sample containing 0.2–2 mmoles of amide. Complete the electrolysis at a potential appropriate to the sample, as discussed below. From the coulometer readings, calculate the composition of the sample on the basis of one electron/molecule.

RESULTS AND DISCUSSION

Results of the examination of the oxidation of aliphatic amines have been reported previously[8]. It was found that the voltammetric peak potentials varied in a rational way with the inductive effects of substituents. The result was that while the order of increasing difficulty in oxidation was tertiary-secondary-primary, the effect of changing individual substituents on tertiary and secondary compounds was sufficiently great to cause an overlapping of the potential range for oxidation of these classes of compounds.

The oxidation of aliphatic amide requires a considerably higher potential than for aliphatic amines because of the electron-withdrawing power of the carbonyl group. Effects of substituent changes are much less noticeable than with amines. We have examined eighteen amides by cyclic voltammetry and controlled-potential coulometry. The acyl groups varied from acetyl to stearyl, and N-substituents varied from methyl to hexyl. We find that the potentials for oxidation fall in three distinct groups: primary at about 1.86 V *vs.* S.C.E., secondary at 1.60 V and tertiary at about 1.35 V *vs.* S.C.E. In this group of compounds, the separation of types is large enough and the spread of potentials within a type small enough, to permit analysis of mixtures of aliphatic amides by type by performing electrolyses at 1.3, 1.5 and 1.85 V *vs.* S.C.E. Successive electrolyses can be performed on a single solution. Analyses of secondary

TABLE 1

SUMMARY OF THE COULOMETRIC DETERMINATION OF ALIPHATIC AMIDES

Amide taken	*Concn. (mM)*	*Contaminant introduced*	*Concn. (mM)*	*Amide* recovery (%)*	*Relative standard deviation (%)*
N,N-dimethylacetamide	4.52	None		99.0	0.2
N,N-dimethylformamide	5.69	None		97.0	0.2
N,N-dimethylpropionamide	31.2	None		103.0	
N,N-dipropylpropionamide	3.91–10.0	None		98.0	0.2
N,N-dimethylbutyramide	27.2	None		100.6	
N-methylacetamide	7.50–15.0	None		98.0	0.2
Acetamide	8.30–24.5	None		98.0	0.2
Propionamide	4.78–36.7	None		98.0	0.6
Butyramide	4.19–16.8	None		98.0	0.2
N,N-dimethylacetamide	4.53	Acetaldehyde	5.8	101.9	0.5
N,N-dimethylacetamide	4.53	Acetone	5.7	99.5	0.9
N,N-dimethylacetamide	4.53–9.16	Methanol	10.3	99.2	0.7
N,N-dimethylacetamide	4.53	*n*-Propylamine	5.1	99.3	
Propionamide	4.34	Water	139	93.3	
Propionamide	5.66	*n*-Propylamine	5.1	98.4	
N,N-dimethylacetamide	4.58	None		99.4	0.5
Acetamide	5.16			100.6	1.0
N,N-dimethylpropionamide	5.43	None		100.8	2.7
Propionamide	4.34			98.4	1.5
N,N-dimethylacetamide	4.58	None		98.1	2.3
N-methylacetamide	4.16			97.5	0.4
N,N-dimethylacetamide	4.58	*n*-Propylamine	5.1	98.2	
M-methylacetamide	4.16			98.6	

* Based on 1 F/mole.

and tertiary amides require 2–3 h and primary amides, 5–7 h. Initial currents range from 50–100 mA; final currents are usually about 0.4 mA.

The results of determinations of simple aliphatic amides are presented in Table 1. These data pertain to analyses of one to three replicate solutions. Where more than one analysis is represented, average values are given and an estimate of relative standard deviation is included. These experiments (with the cell described above) involved 0.26–2.1 mmole of amide in 65 ml of anode solution. It is possible to scale down the apparatus to an anode volume of 5 ml without making significant changes in conditions. This would permit reduction of sample size to about 0.02 mmole without much sacrifice of accuracy or precision.

The following types of compounds are unreactive under the conditions of this determination and have been found experimentally not to interfere: alcohol, aliphatic aldehyde, aliphatic ketone, saturated hydrocarbons, aliphatic nitriles, aliphatic nitro, aliphatic epoxide, aliphatic ether, aliphatic ester, quaternary ammonium ion.

Aliphatic amines react under these conditions but the interference can be avoided by pre-electrolysis at 1.0 V *vs.* S.C.E. This procedure was used to obtain the results in Table I in which *n*-propylamine is added. Propylamine was chosen because it is typical of primary amines and represents the worst case of interference by simple amines.

A number of types of compounds are known to be electroactive under these conditions. These include carboxyl, carboxylate, sulfide, sulfoxide, mercaptan, aromatic amine, aromatic amide, aromatic hydrocarbon, alkene, alkyne and phenol. In the case of aromatic amide, benzamide and similar compounds are oxidized with difficulty and would interfere with the determination of primary aliphatic amides but not with the determination of secondary or tertiary amide. When nitrogen carries an aromatic substituent, the compound is easily oxidized and undergoes a reaction involving more than one electron/molecule.

The necessity of carrying out this determination in fairly dry acetonitrile limits the number of inorganic compounds that can be present, because of solubility problems. Lithium, sodium and quaternary ammonium perchlorates and tetrafluoroborates are readily soluble and do not interfere. Nitrate and halides are oxidized under these conditions. Magnesium ion interferes when present in large concentration. Molecular oxygen has no effect on the determination.

ACKNOWLEDGEMENT

Supported in part by Research Grant GM-10064 from the U.S. Public Health Service. J.F.O. thanks the National Aeronautics and Space Administration for assistance in the form of a research fellowship 1963-66.

SUMMARY

The determination of a number of aliphatic amides in acetonitrile–$LiClO_4$ solution by controlled-potential oxidation at a platinum anode has been studied. The method gives an average precision of about 1% over a range of sample size from 0.2–2.0 mmoles. Mixtures of different types of amides can by analyzed for the amount of each type. Alcohols, aldehydes, ketones and nitriles do not interfere; amines interfere but may be removed by pre-electrolysis at lower potential.

REFERENCES

1 D. C. WIMER, *Anal. Chem.*, 30 (1958) 77.
2 T. HIGUCHI, C. H. BARNSTEIN, H. GHASSEMI AND W. E. PEREZ, *Anal. Chem.*, 34 (1962) 400.
3 W. R. POST AND C. A. REYNOLDS, *Anal. Chem.*, 37 (1965) 1171.
4 J. MITCHELL, JR. AND C. E. ASHBY, *J. Am. Chem. Soc.*, 67 (1945) 161.
5 S. SIGGIA AND C. R. STAHL, *Anal. Chem.*, 27 (1955) 550.
6 S. SIGGIA, J. G. HANNA AND N. M. SERENCHA, *Anal. Chem.*, 36 (1964) 227.
7 J. F. O'DONNELL AND C. K. MANN, *J. Electroanal. Chem.*, 13 (1967) 157.
8 C. K. MANN, *Anal. Chem.*, 36 (1964) 2424.

SOLUBILITY PRODUCT OF SILVER HALIDES IN MOLTEN ALKALI PERCHLORATES

MARIO FIORANI, G. GIORGIO BOMBI AND GIAN-ANTONIO MAZZOCCHIN
Istituto di Chimica Analitica dell' Università, Padova (Italy)
(Received November 29th, 1965)

INTRODUCTION

The use of fused alkali perchlorates as solvents has hitherto received very little attention. To our knowledge, the only investigations reported concern the double-layer capacity of the mercury–electrolyte interface[1] in molten $LiClO_4$–$NaClO_4$, and the solubility of water[2] and the formation of chloride complexes of lead and cadmium[3], in molten $LiClO_4$.

The thermal stability and the phase diagrams of alkali perchlorates have been reported in a number of papers by MARKOWITZ and co-workers (see *e.g.*, ref. 4). Some of their results are given in Table 1. From these data it appears that $LiClO_4$, both alone and in mixtures with $NaClO_4$ or $KClO_4$, can be used as a solvent over a relatively wide temperature range.

TABLE 1

MELTING POINTS AND DECOMPOSITION TEMPERATURES OF ALKALI PERCHLORATES

Salt or mixture	*Melting point*	*Temp. of rapid decomp.*	*Ref.*
$LiClO_4$	247°	438°	4
$NaClO_4$	468°	525°	4
$KClO_4$	580°	580°	4
$LiClO_4$ (72.5 mole %)–$NaClO_4$ (eutectic)	208°	higher than for pure $LiClO_4$	5
$LiClO_4$ (76.0 mole %)–$KClO_4$ (eutectic)	207°		5

It is well known that silver halides are sparingly soluble in molten alkali nitrates, and since it seemed likely that their behaviour would be similar in molten alkali perchlorates, we undertook the study of the reaction

$$AgX_{(s)} \leftrightarrows Ag^+ + X^- \qquad (1)$$

in molten $LiClO_4$–$NaClO_4$ (mole ratio 3:1), with X = Cl, Br and I. Known amounts of halide ions were titrated by adding silver ions, and the course of the titration was followed potentiometrically with a silver electrode.

EXPERIMENTAL

Lithium and sodium perchlorates were prepared from reagent-grade carbonates and $HClO_4$, and recrystallized twice from water as the trihydrate and the monohydrate, respectively. $LiClO_4 \cdot 3\ H_2O$ (m.p. 95°)[6] was melted in a flask and kept under reduced pressure until no more water was collected in a dry-ice trap in the vacuum line. As the water content of the melt decreased, the temperature was raised in order to keep the content of the flask, liquid. The salt was finally poured onto a stainless-steel plate and stored over P_2O_5. $NaClO_4 \cdot H_2O$ (m.p. 130°)[6] was slowly heated without fusion in a vacuum oven; in order to avoid excessive packing, the salt was frequently ground. Progress in water elimination was controlled by collecting the water on dry-ice as for $LiClO_4 \cdot 3\ H_2O$. The powdered, anhydrous salt was stored over P_2O_5. The water content of both $LiClO_4$ and $NaClO_4$, determined by Karl Fisher titration, was always less than 0.5%. Since the ultimate product of the decomposition of alkali perchlorates is chloride ion[7], the chloride content of the salts was determined. The method used was a modification of that described by GORDON[8]; perchlorate samples with a chloride content greater than about 10^{-4} mole.kg^{-1} were discarded.

Reagent-grade sodium halides and $AgNO_3$ were dried at 120° before use.

The apparatus employed in the preliminary measurements was the same as previously described[9]; subsequently, a cell without a sintered-glass disk and equipped with a cover of the type shown in Fig. 1 was used. This allowed the cell to be evacuated

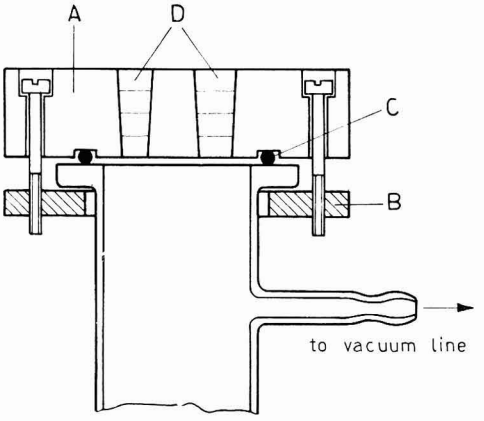

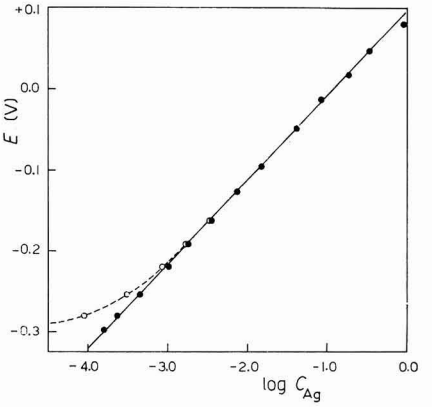

Fig. 1. Top of titration cell. (A), Plexiglass cover; (B), brass ring; (C), O-ring; (D), T holes of various diameters to accommodate electrodes, thermocouple, etc.

Fig. 2. Nernst plot for the silver–silver ion electrode at 535.0°K.

during the fusion of the solvent, thus enabling a further reduction of the water content of the melt. Potential differences were measured either with a Knick 35 pH-meter or with a Solartron LM 1420 digital voltmeter. The temperature was controlled within ±0.3°.

The validity of the Nernst equation for the silver–silver ion couple in molten perchlorates was tested by measuring the potential of a silver electrode immersed in a $LiClO_4$–$NaClO_4$ melt after the addition of various amounts of silver nitrate.

In all experiments, the reference electrode was a silvered-platinum plate immersed in a $LiNO_3-KNO_3$ molten mixture containing about 10^{-2} mole.kg^{-1} of $AgNO_3$[9], separated from the perchlorate solution by a G4 sintered-glass disk. This electrode was frequently standardized against a silver electrode immersed in a perchlorate melt of known Ag^+ content; all potential values were then referred to the standard silver electrode (SSE) (1 mole.kg^{-1} Ag^+ in 3:1 $LiClO_4-KClO_4$).

Since titrations with electrolytically-produced silver ions were successful in molten nitrates[9,10], this technique was initially employed, using as a solvent pure $LiClO_4$ and working at about 255°. In this case, however, it was found that silver electrodes underwent corrosion at an appreciable rate, so that low results were always obtained in the titrations. Moreover the Pyrex cells were rapidly attacked with the formation of characteristic, spider web-like, etchings and became useless after a few hours in service. The rate of attack on the glass was much reduced by using the 3:1 $LiClO_4-NaClO_4$ mixture as solvent. However, the corrosion of silver remained significant, so that continuous electrolytic production of silver ions was found to be unfeasible.

The titrations were then carried out by introducing, successively into the solution, weighed portions of $AgNO_3$; in order to minimize the harmful effect of corrosion of the indicator electrode, the latter was kept out of the solution and immersed only at the time of the measurements.

Some of the runs for the determination of the solubility product of silver bromide were carried out by adding known amounts of NaBr to a melt saturated with AgBr.

While solutions containing chloride or bromide ions were quite stable, and the equivalence point of the titrations was always in agreement with the quantity of halide initially introduced, the iodide solutions were rapidly oxidized (with production of iodide fumes) above 250°. Even at lower temperatures, some oxidation was evident, so that the quantity of iodide found at the equivalence point was always lower than the quantity introduced. By keeping the runs as short as possible, the iodide losses were reduced to between 1 and 20% depending on the temperature.

RESULTS AND DISCUSSION

The Nernst plot for the silver–silver ion electrode in molten $LiClO_4-NaClO_4$ at 535°K is given in Fig. 2. The potential values are referred to an arbitrary origin, *i.e.*, a particular reference electrode. The experimental points at concentrations below about 10^{-3} mole.kg^{-1} (open circles in Fig. 2) fall to the left of the straight line that can be drawn through the points referring to higher concentrations. This is probably due to the presence at the surface of the electrode, of a small concentration of silver ions produced by corrosion. From the value of the electrode potential before the first silver nitrate addition, and from the approximate straight line referred to above, this concentration can be calculated to be about $1.6 \cdot 10^{-4}$ mole.kg^{-1}. If the experimental points are corrected by adding this term to all the concentration values (full circles in Fig. 2), a good straight line is obtained over the whole concentration range (except near 1 mole.kg^{-1}). The least-squares slope of this line is 105.1 ± 0.4 mV (Nernst value, 106.1 mV). From the fact that the electrode behaves ideally for silver ion concentrations up to about 0.3 mole.kg^{-1}, it can be inferred that the presence in the solution of

nitrate ions (introduced as $AgNO_3$) does not interfere, at least up to the same concentration value.

When the data obtained in the precipitation titrations is used to calculate solubility-product values, the possibility of complex formation between silver- and halide-ions must be taken into account; it can, however, be supposed that the deviations from ideality are entirely due to complex formation, as is known to be the case for nitrate melts containing silver- and halide-ions[11]. With this assumption, the activity values for silver calculated from e.m.f. data can be identified with the concentration of free silver ions.

The following symbols will be used:

$C_{Ag}{}^0$, $C_X{}^0$ total number of g-ions of silver and halide added to 1 kg of solvent;

$\Delta = C_X{}^0 - C_{Ag}{}^0$;

$C_{AgX}{}^0$ number of moles of silver halide precipitated from 1 kg of solvent;

C_{Ag}, C_X concentrations of free silver and halide ions;

C_{ij} concentration of complex $Ag_jX_i{}^{(j-i)+}$;

$\beta_{ij} = \dfrac{C_{ij}}{C_{Ag}{}^j \cdot C_X{}^i}$ overall stability constant of complex $Ag_jX_i{}^{(j-i)+}$;

$K_{so} = C_{Ag} \cdot C_X$ solubility product of AgX.

The conservation of silver and halide ions gives:

$$C_{Ag}{}^0 = C_{AgX}{}^0 + C_{Ag} + \sum_{i,j} jC_{ij}$$

$$C_X{}^0 = C_{AgX}{}^0 + C_X + \sum_{i,j} iC_{ij}$$

Eliminating $C_{AgX}{}^0$, one obtains

$$\Delta = C_X - C_{Ag} + \sum_{i,j} (i-j)C_{ij}$$

$$= \frac{K_{so}}{C_{Ag}} - C_{Ag} + \sum_{i,j} (i-j)\beta_{ij} K_{so}{}^i C_{Ag}{}^{(j-i)} \qquad (2)$$

Since all the β_{ij} values for which $j-i=n$ appear grouped together in the coefficient of the term $C_{Ag}{}^n$, and since K_{so} does not appear alone in any term of the right-hand side of eqn.(2), it follows that the value of K_{so} cannot be obtained from this kind of measurement, unless the β_{ij}-values are known. This situation is very similar to that arising when solubility measurements are employed to obtain stability constants[12]: if polynuclear complexes are present, neither the stability constants nor the solubility product can be calculated from solubility data only.

In the absence of measured values of β_{ij} for silver-halide complexes in molten perchlorates, it has been necessary to postulate that in the concentration range prevailing in our experiments, the concentrations of complexes other than the ion pair,

AgX, (see below) are small relative to C_{Ag} and C_X. Equation (2) then becomes*

$$\Delta = \frac{K_{so}}{C_{Ag}} - C_{Ag}\ ; \qquad K_{so} = C_{Ag}(\Delta + C_{Ag}) \tag{3}$$

The influence of the presence of the simpler complexes, AgX_2^-, AgX and Ag_2X^+, on the values of K_{so} calculated from the simplified eqn. (3) will now be discussed.

When these complexes are taken into account, eqn. (2) becomes:

$$\Delta = \frac{K_{so}}{C_{Ag}}(1 + \beta_{2,1}K_{so}) - C_{Ag}(1 + \beta_{1,2}K_{so})$$

As has been pointed out [14,15], the ion pair, AgX, does not interfere with the calculations. The presence of the complex AgX_2^- alone ($\beta_{2,1} \neq 0$, $\beta_{1,2} = 0$) would lead to a titration curve, the shape of which is in accordance with eqn. (3), but the value of the constant obtained would be $K_{so} \times (1 + \beta_{2,1}K_{so})$ instead of K_{so}. It follows that, contrary to TIEN AND HARRINGTON's statement[14], the presence of AgX_2^- cannot be

TABLE 2

TITRATIONS OF CHLORIDE

Run	*T* (°K)	$C_{Cl^0} \cdot 10^2$ (*mole.kg*$^{-1}$)	$C_{Ag} \cdot 10^2$ (*mole.kg*$^{-1}$)	$-E$ *vs. SSE* (*mV*)	$K_{so} \cdot 10^7$ (*mole*^{2}*.kg*$^{-2}$)
1	493.8	1.564	0.197	445.6	3.865
			0.286	442.1	3.924
			0.376	439.9	3.842
			0.470	437.9	3.709
			0.579	433.4	3.717
			0.684	428.6	3.719
			1.521	326.4	4.138
				mean: 3.84 ± 0.04[a]	
5	537.1	1.829	0.393	412.0	19.76
			0.509	407.5	20.05
			0.640	403.5	19.74
			0.873	393.0	20.07
			1.036	385.5	19.74
			1.108	381.0	19.91
			1.352	360.0	21.75
				mean: 20.1 ± 0.3[a]	

[a] Uncertainties expressed as standard deviations

excluded on the basis of the constancy of the apparent solubility product obtained by applying eqn. (3). On the other hand, if $\beta_{1,2} \neq 0$, the shape of the titration curve is modified, and the presence of the Ag_2X^+ complex can be argued (provided its formation constant is large, and the data accurate enough) from the fact that the values of K_{so} obtained from eqn.(3) decrease with decreasing Δ.

* Equation (3) has been employed to obtain the solubility products of silver halides in nitrate melts by several authors[9,13,14]. On the basis of the results of BLANDER *et al.* the use of this equation (in nitrate melts) appears justified for bromide and iodide[15], but less satisfactory for chloride[16].

Since the K_{so}-values for silver chloride and bromide computed from experimental data by means of eqn. (3) do not, on the whole, show systematic trends (see typical results in Tables 2 and 3), it can be concluded that the presence of Ag_2X^+ has no relevant effect on the K_{so}-values. Furthermore, since in nitrate melts $\beta_{2,1}$ has the same order of magnitude as $\beta_{1,2}$, the assumption that even the presence of the complex AgX_2^- does not seriously affect the values of K_{so}, appears reasonable.

TABLE 3

TITRATIONS OF BROMIDE

Run	*T* (°K)	$C_{Br}^0 \cdot 10^3$ (*mole.kg*$^{-1}$)	$C_{Ag}^0 \cdot 10^3$ (*mole.kg*$^{-1}$)	$-E$ *vs. SSE* (*mV*)	$K_{so} \cdot 10^{10}$ (*mole*^{2}*.kg*$^{-2}$)
9	490.0	1.831	0.032	647.5	3.945
			0.244	645.5	3.649
			0.356	643.0	3.598
			0.724	632.5	3.463
			1.125	613.0	3.505
			1.327	598.0	3.575
			1.495	579.0	3.741
			1.610	557.5	4.117
				mean:	3.70 ± 0.08[a]
18	530.5	6.321	0.477	654.5	35.44
			0.629	653.0	35.67
			0.970	651.0	35.04
			1.549	647.5	33.73
			2.444	638.5	33.37
			3.382	624.5	34.37
			4.623	597.5	35.87
				mean:	34.8 ± 0.4[a]

[a] Uncertainties expressed as standard deviations.

The interpretation of the data obtained in the iodide titrations is made very uncertain by the aforementioned oxidation of iodide. It can easily be seen that in the general case in which the titrated substance, X, disappears from the solution in the course of the titration, if the calculations are carried out by using for C_X^0, the initial value, the values of K_{so} obtained at the beginning of the titration are near the true value but become larger than this value on approaching the equivalence point. On the other hand, if the value used for C_X^0 is that obtained from the experimental equivalence point, the values of K_{so} are initially lower than the true value, but approach it on approaching the equivalence point. However, it should be pointed out that the values of K_{so} calculated near the equivalence point are subject to greater uncertainty due to the errors in locating the equivalence point; in the present case, owing to the small number of experimental points, these errors could be relatively large.

K_{so}-values for silver iodide were calculated both from the *initial* C_I^0 and from the *equivalence point* C_I^0; according to the above discussion, the *best* K_{so}-value for each titration was then obtained by taking the mean between the first value calculated from the *initial* C_I^0 and the last (or the one before last) value calculated from the *equivalence point* C_I^0. It is difficult to estimate the accuracy of these K_{so}, but we

believe there is no doubt they are at least of the correct order of magnitude. The data for two runs are given as an example in Table 4.

In Figs. 3–5 are plotted the data referring to a run each for chloride, bromide and iodide; the points are experimental, and the curves were calculated from the

TABLE 4

TITRATIONS OF IODIDE

Run	*T* (°K)	$C_I^0 \cdot 10^3$ (*mole.kg*$^{-1}$)		$C_{Ag}^0 \cdot 10^3$ (*mole.kg*$^{-1}$)	$-E$ *vs. SSE* (*mV*)	$K_{so} \cdot 10^{14}$ (*mole*^{2}*.kg*$^{-2}$)	
		(*a*)	(*b*)			(*c*)	(*d*)
23	4.959	4.315	3.94	0.266	1064.5	6.167*	5.596
				0.574	1059.0	6.479	5.830
				0.940	1053.0	6.726	5.979
				1.393	1045.0	7.022	6.120*
				2.128	1024.5	8.492	7.036
					mean of the asterisked values:		6.1
26	512.4	4.351	3.37	0.722	1035.0	24.04*	17.54
				1.097	1019.5	30.62	21.39
				1.445	1012.5	32.05	21.23
				1.952	992.5	41.60	24.59*
				2.577	955.5	71.10	31.78
					mean of the asterisked values:		24

K_{so}-values in column (c) were calculated from the initial C_I^0 (column (a)), while K_{so}-values in column (d) were calculated from the *equivalence point* C_I^0 (column (b)).

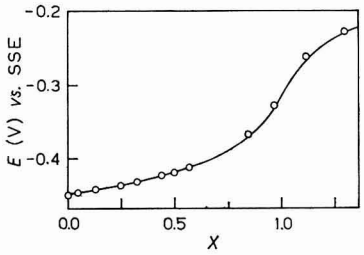

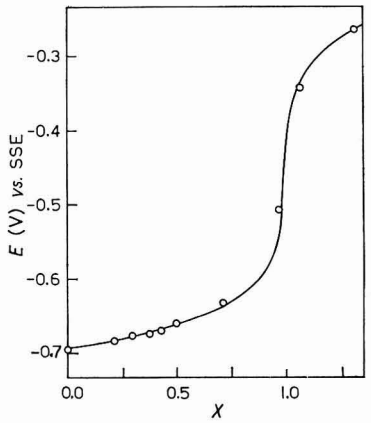

Fig. 3. Titration curve of chloride (run 3). $T = 523.0$°K; $C_{Cl}^0 = 2.257 \cdot 10^{-2}$ mole.kg^{-1}; $X = C_{Ag}^0/C_{Cl}^0$.

Fig. 4. Titration curve of bromide (run 15). $T = 521.1$°K; $C_{Br}^0 = 8.895 \cdot 10^{-3}$ mole.kg^{-1}; $X = C_{Ag}^0/C_{Br}^0$.

K_{so}-values obtained from the same runs. The agreement is reasonably good and confirms, for chloride and bromide, the absence of large effects due to formation of the complex, Ag_2X^+.

The values of pK_{so} for the three halides are plotted *vs.* the reciprocal of the temperature in Fig. 6; the straight lines drawn in this figure were obtained by the

least-squares method and have the following equations*:

AgCl $pK_{so} = -2.12 + (4.22 \pm 0.15) \cdot 10^{-3}/T$

AgBr $pK_{so} = -2.35 + (5.76 \pm 0.23) \cdot 10^{-3}/T$

AgI $pK_{so} = -4.21 + (8.65 \pm 0.39) \cdot 10^{-3}/T$

The values of pK_{so} at 250° and of ΔH^0 are given in Tables 4 and 5 together

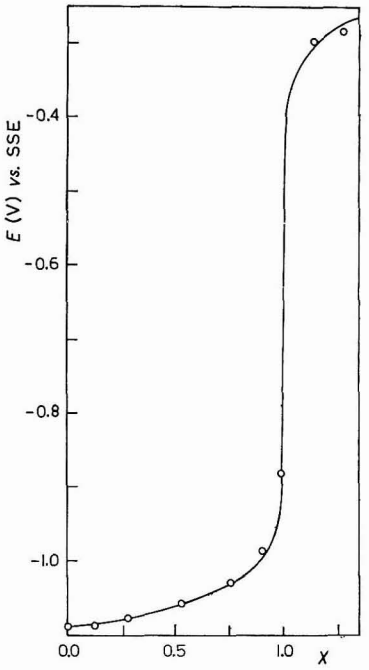

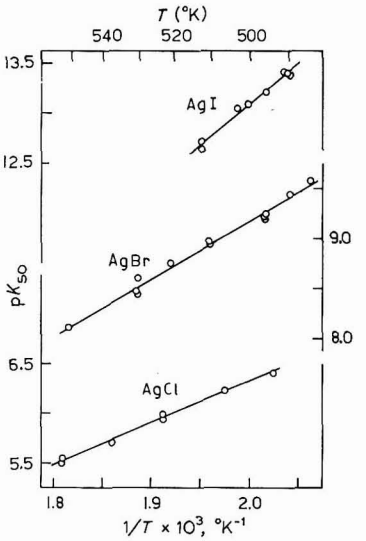

Fig. 5. Titration curve of iodide (run 22). $T = 491.5°K$; $C_I^0 = 5.78 \cdot 10^{-3}$ mole.kg^{-1} (from equivalence point); $X = C_{Ag}^0/C_I^0$.

Fig. 6. pK_{so} *vs.* $1/T$ for silver halides.

with literature values of the corresponding data for nitrate melts. From Table 4 it can be seen that, while in nitrate melts a change in the solvent cation has only a relatively small influence on the solubility products, the change from nitrate to perchlorate has a marked effect, the solubility products all being smaller in the latter solvent. This fact is in accord with the larger size and lower polarizability of the perchlorate anion as compared with the nitrate; however, since the nature of the solvent anion should influence, to a first approximation, only the activity of the solute cation, the difference between the pK_{so}-values in nitrate and perchlorate could be expected to be roughly constant when passing from chloride to bromide and iodide, which is not the case. The ΔH^0 for AgCl is practically the same in nitrates and perchlorates (Table 5), while there is an increasing difference for AgBr and AgI. This trend reflects that of the pK- (and ΔG^0-) values, since the ΔS^0 of the dissolution processes appear to have similar values in both solvents.

* The uncertainties of the slopes are expressed as standard deviations.

TABLE 5

pK_{so} FOR SILVER HALIDES[a] IN NITRATE AND PERCHLORATE MELTS AT 250°

Solvent	*AgCl*	*AgBr*	*AgI*	*Ref.*
$LiNO_3-KNO_3$	5.31[b]	7.13[b]	8.69[b,c]	14
$LiNO_3-KNO_3$	5.84[b]	—	—	17
$NaNO_3-KNO_3$	5.28	7.12	9.73	13
$NaNO_3-KNO_3$	—	7.01	9.79	15
KNO_3	5.37[b]	—	—	16
$LiClO_4-NaClO_4$	5.94[d]	8.65[d]	12.3[d]	this work

[a] Concns. expressed as molalities; to obtain pK_{so}-values with concns. expressed as mole fractions, add 2.12 for $LiNO_3-KNO_3$, 2.06 for $NaNO_3-KNO_3$, 1.99 for KNO_3 and 1,91 for $LiClO_4-NaClO_4$. [b] Extrapolated value. [c] This value is probably low[9]. [d] The standard deviations of the pK_{so}-values are 0.01, 0.02 and 0.04 (at 250°) for AgCl, AgBr and AgI, respectively.

TABLE 6

ΔH^0 FOR THE DISSOLUTION OF SILVER HALIDES IN NITRATE AND PERCHLORATE MELTS (IN KCAL.MOLE^{-1})

Solvent	*AgCl*	*AgBr*	*AgI*	*Temp.*	*Ref.*
$LiNO_3-KNO_3$	19.5	23.2	28.4	172°	14
$LiNO_3-KNO_3$	18.9[a]	26.1[a]	32.1[a]	158°	17, 18
$NaNO_3-KNO_3$	18.30	21.30	29.35	250°	13
$NaNO_3-KNO_3$	—	22.4	27.9	250°	15
KNO_3	19.2	—	—	350°–436°	16
$LiClO_4-NaClO_4$	19.3 ± 0.7[b]	26.3 ± 1.0[b]	39.6[c]	see Tables 2–4	This work

[a] From calorimetric measurements. [b] Uncertainties expressed as standard deviations. [c] The standard deviation of ΔH^0 for silver iodide is 1.8 kcal.mole^{-1}; however, owing to the small temperature range and to the uncertainty in the evaluation of the K_{so}-values, the true uncertainty is certainly larger than this value.

ACKNOWLEDGEMENT

The authors thank Prof. L. RICCOBONI for helpful discussion and suggestions.

This work was supported by the Italian Council of Research (Consiglio Nazionale delle Ricerche).

SUMMARY

The validity of the Nernst equation for the silver–silver ion electrode in molten $LiClO_4-NaClO_4$ (3:1 mole ratio) was tested.

The precipitation of silver halides from the same melt was studied by potentiometric titration; the solubility products and the heats of dissolution were determined.

REFERENCES

1 J. E. B. RANDLES AND W. WHITE, *Z. Elektrochem.*, 59 (1955) 666.
2 F. R. DUKE AND A. S. DOAN, JR., *Iowa State Coll. J. Sci.*, 32 (1958) 451.
3 F. R. DUKE AND W. W. LAWRENCE, *J. Phys. Chem.*, 63 (1959) 2087.
4 M. M. MARKOWITZ AND D. A. BORYTA, *J. Phys. Chem.*, 69 (1965) 1114.

5 M. M. MARKOWITZ, D. A. BORYTA AND R. F. HARRIS, *J. Phys. Chem.*, 65 (1961) 261.
6 *Handbook of Chemistry and Physics*, 44th ed., The Chemical Rubber Publishing Co., Cleveland, Ohio, 1962, p. 596 and 654.
7 M. M. MARKOWITZ, *J. Inorg. Nucl. Chem.*, 25 (1963) 407.
8 H. T. GORDON, *Anal. Chem.*, 24 (1952) 857.
9 G. G. BOMBI, M. FIORANI AND G. A. MAZZOCCHI, *J. Electroanal. Chem.*, 9 (1965) 457.
10 H. S. SWOFFORD, *Anal. Chem.*, 37 (1965) 610.
11 J. BRAUNSTEIN, M. BLANDER AND R. M. LINDGREN, *J. Am. Chem. Soc.*, 84 (1962) 1529.
12 F. J. C. ROSSOTTI AND H. ROSSOTTI, *The Determination of Stability Constants*, McGraw-Hill, New York, N.Y., 1961, p. 189.
13 S. N. FLENGAS AND E. RIDEAL, *Proc. Roy. Soc. (London)*, A233 (1956) 443.
14 H. T. TIEN AND G. W. HARRINGTON, *Inorg. Chem.*, 2 (1963) 369.
15 M. BLANDER AND E. B. LUCHSINGER, *J. Am. Chem. Soc.*, 86 (1964) 319.
16 M. BLANDER, J. BRAUNSTEIN AND M. D. SILVERMAN, *J. Am. Chem. Soc.*, 85 (1963) 895.
17 J. JORDAN, J. MEIER, E. J. BILLINGHAM, JR. AND J. PENDERGRAST, *Anal. Chem.*, 32 (1960) 651.
18 J. JORDAN, J. MEIER, E. J. BILLINGHAM, JR. AND J. PENDERGRAST, *Nature*, 187 (1960) 318.

SHORT COMMUNICATIONS

Pulse polarographic determination of cadmium in silver bromide

A common procedure for the determination of cadmium in the presence of silver requires a separation and several extraction steps[1] and is somewhat lengthy and tedious. A simple, rapid, and accurate determination is possible using pulse polarography. The large current from the previous reduction of silver does not interfere in the cadmium determination. Thus, pulse polarography can be used to considerable advantage in the analysis of cadmium (as well as many other dopants) in silver bromide. Provided that the concentration of the impurity or dopant is not lower than 0.05–0.1 mole%, several ions can be determined simultaneously, accurately, and easily using the pulse polarograph. As an illustration, the determination of approximately 0.1 mole% cadmium bromide in silver bromide is described.

The pulse polarograph used was designed in this laboratory but any commercial instrument can be used[2]. The chemicals were reagent grade and were used without further purification. The cadmium bromide doped silver bromide was a single crystal obtained commercially.

Initially, potassium cyanide was used to dissolve the silver bromide and act as a supporting electrolyte but this had two disadvantages. The cadmium wave in dilute (*i.e.*, 0.1 *M*) potassium cyanide solution is irreversible which seriously restricts the peak height that can be obtained in the nominal cadmium concentration range[2]. The

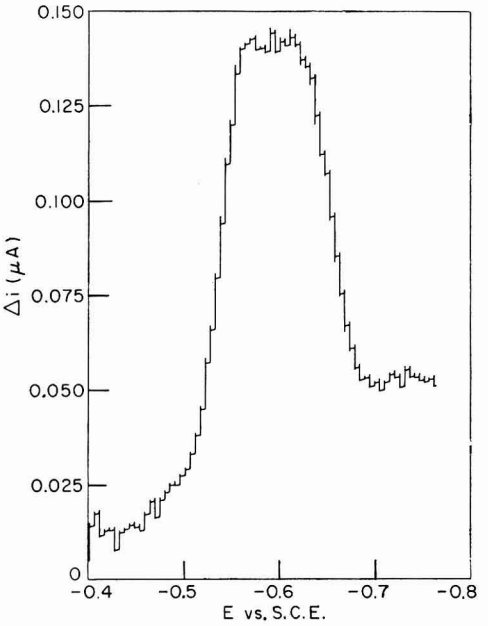

Fig. 1.

wave can be made more reversible by significantly increasing the potassium cyanide concentration. In 6 M potassium cyanide, the slope of the wave is very close to the theoretical value. However, the high concentration of potassium cyanide introduces impurities that interfere with the cadmium wave. The second disadvantage is that the diffusion current of the silver ion reduction in the potential range over which cadmium is reduced is somewhat irregular even in the presence of gelatin. This gives rise to considerable noise in the cadmium peak.

Potassium thiocyanate was found to be the best supporting electrolyte for the determination. Silver bromide is easily soluble, cadmium gives a well-defined, reversible peak[3,4] and the diffusion current of silver ion is regular and well defined, even in the absence of gelatin, in the potential range in which cadmium is reduced. A typical curve is shown in Fig. 1 for $2 \cdot 10^{-6}$ M cadmium ion and 10^{-3} M silver ion in 10% potassium thiocyanate solution. The difference current is represented by the horizontal lines and each line represents an average reading for two successive drops.

In the procedure, approximately 25–50 mg of sample were accurately weighed and dissolved in 10% potassium thiocyanate with heating, if necessary, to effect solution. The cooled sample was then diluted to the mark in a volumetric flask with 10% potassium thiocyanate. The sample size and final dilution volume were adjusted so that the concentration of cadmium was in the range $8 \cdot 10^{-7}$–$8 \cdot 10^{-6}$ M. The sample was put in the polarographic cell, oxygen was removed, and the voltage was scanned from -0.5 to -0.7 V using a pulse amplitude of 100 mV. The peak height of the curve obtained was compared with the linear calibration graph which was prepared by treating pure silver bromide in the same manner as above, and adding aliquots of a standard cadmium solution. A number of other ions could be determined simultaneously in the solution using appropriate calibration.

TABLE 1

Sample	*Mole% Cd (colorimetry)*	*Mole% Cd (pulse polarography)*
A	0.31	0.29
C	0.23	0.22

Although the colorimetric procedure is tedious, two samples were analyzed by this technique to obtain comparative results. Table 1 shows that the results of the two methods compare favorably. The greater ease of determination and the faster analysis time for the pulse polarographic procedure are important advantages.

North American Aviation Science Center,
Thousand Oaks, California 91360 (U.S.A.)

E. P. PARRY
T. H. JOHNSTON
H. J. GOLDNER

1 E. B. SANDELL, *Colorimetric Metal Analysis*, Interscience, New York, 3rd. ed., 1959, p. 358.
2 E. P. PARRY AND R. A. OSTERYOUNG, *Anal. Chem.*, 37 (1965) 1634.
3 J. W. GRENIER AND L. MEITES, *Anal. Chim. Acta*, 14 (1956) 482.
4 D. N. HUME, O. D. DEFORD AND G. C. B. CAVE, *J. Am. Chem. Soc.*, 73 (1951) 5323.

Received April 26th, 1966

Hydrogen oxidation on platinum

MAKOWSKI, HEITZ AND YEAGER[1] established that hydrogen oxidation on platinum in purified acid solutions was a reaction of the first order, whereas FRUMKIN AND AIKASYAN[2–5] found it to be a reaction of zero order. To judge by the maximum value of the currents observed, the electrodes of MAKOWSKI, HEITZ AND YEAGER were markedly more active than those of FRUMKIN AND AIKASYAN. In the work of FRUMKIN AND AIKASYAN, the reaction order was determined by an unusual method, *viz.*, from the nature of the dependence of the current density, i_M, corresponding to the maximum on the i,φ curve (φ-potential), upon the rev./sec of the rotating disk electrode (m); we thought it necessary, therefore, to verify the result obtained using a direct method, *i.e.*, determining the dependence of the current density upon the partial pressure of hydrogen p_{H_2}. However, this method soon showed that the results of FRUMKIN AND AIKASYAN were not always reproducible; depending on uncontrollable factors, either the first- or zero-order of the reaction was obtained. Only quite recently have we been able to work out a technique to obtain at will, electrodes on which the reaction would proceed either by one or other mechanism[6]. We used Hilger spectroscopical platinum and N HCl and N HBr solutions purified by cathodic polarization on platinum wire for 24 h, followed by purification for 3–4 h on platinized platinum in a hydrogen atmosphere. If the pre-treatment of platinum was confined to the usual procedures (mechanical cleaning by emery paper, cleaning by concentrated HCl, washing with distilled water, multiple alternate anodic–cathodic polarization — the anodic polarization being carried out for 30 sec at a potential of 1.2 V in N HCl and at 0.8 V in N HBr, the cathodic polarization — for 1 min using a current of 3 mA/cm^2), the reaction order observed was close to the first order (0.85), the activity of the electrodes being much higher than in the investigation of FRUMKIN AND AIKASYAN and probably as high as that observed by MAKOWSKI, HEITZ AND YEAGER (in N HCl the maximum current at 100 rev./sec was 4 mA/cm^2, the limiting kinetic current *ca.* 10 mA/cm^2). However, if before activation the electrode had been subjected to a prolonged (altogether 8 h) cathodic reduction with a current of 3 mA/cm^2 in N HCl, a reproducible reaction order close to zero order (0.01) was observed. This reaction order was retained also after subsequent activations of the electrode by alternate anodic–cathodic polarization. In this case, the value of the limiting kinetic current decreased, approaching those observed by FRUMKIN AND AIKASYAN. Figure 1 shows the zero reaction order for an electrode pre-treated in such a manner in N HCl. The same result was obtained in N HBr. Naturally, with decreasing hydrogen partial pressure, the current density in the diffusion region diminishes in proportion to the H_2 pressure, the value of the limiting kinetic current remaining, however, unchanged. Zero reaction order follows also from the shape of the $i_M - \sqrt{m}$ curve. In our opinion, the following conclusions can be drawn from the above experiments which were quite reproducible and will be described in more detail elsewhere[6]:

1. The determination of the reaction order from the nature of the current density dependence upon rev./sec gives results concordant with the determination from the dependence upon hydrogen partial pressure.

2. The reaction of hydrogen oxidation can proceed both by the first and zero order depending on the pre-treatment of the platinum surface.

3. The transition to zero order does not appear to be connected with insufficient purification of the solution. This is evident from the high current values observed in the same solutions on the electrodes not subjected to intensive cathodic reduction.

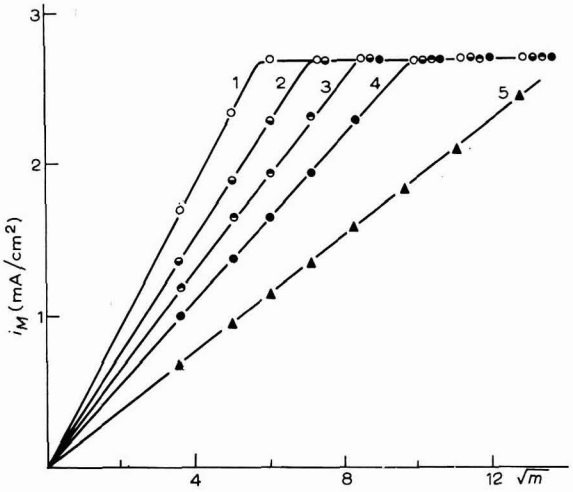

Fig. 1. Dependence of the maximum rate of hydrogen oxidation on $\sqrt{m}$ at different hydrogen partial pressures. p_{H_2} (atm.): (1), 1.0; (2), 0.8; (3), 0.7; (4), 0.58; (5), 0.41. Reduced electrode in N HCl, m = rev./sec.

As regards the factors determining the transition from the first to the zero order of the reaction, they can at present be considered in a hypothetical manner only. It is possible that initially strongly-bound adsorbed oxygen was present on the surface of smooth platinum used by us (this hindered the adsorption of halogen ions) and that the zero order is typical of a surface on which anion adsorption occurs without difficulty. Some results of FRUMKIN AND AIKASYAN had already indicated that the anion adsorption has a greater effect upon the reaction of H_2 oxidation than oxygen adsorption[4,5]. In the experiments of MAKOWSKI, HEITZ AND YEAGER such strongly-bound oxygen could have resulted from a treatment of the platinum surface with an acid permanganate solution. But this is only a hypothesis and we do not claim to have determined in a general form the conditions of the transition from the first to the zero order. In particular, the vigorous cathodic treatment employed by us was not made use of in the experiments of FRUMKIN AND AIKASYAN when observing a zero order.

If we wish to explain the transition to the zero order, we must assume that the inhibiting action of the anion adsorption primarily affects a step of the overall process of H_2 ionization which follows the initial step of the H_2 molecule adsorption. This might be, for example, the step of the surface migration of H_{ads} from the sites on which H_2 chemisorption occurs, to those on which H_{ads} is ionized[3,5].

Moscow State University, Moscow, USSR

A. FRUMKIN
V. SOBOL
A. DMITRIEVA

1 M. P. MAKOWSKI, E. HEITZ AND E. YEAGER, *J. Electrochem. Soc.*, 113 (1966) 204.
2 E. AIKASYAN AND A. FRUMKIN, *Dokl. Akad. Nauk SSSR*, 100 (1955) 315.
3 A. FRUMKIN AND E. AIKASYAN, *Izv. Akad. Nauk SSSR, Otd. Khim. Nauk*, 202 (1959).
4. E. AIKASYAN, *Zh. Fiz. Khim.*, 33 (1959) 1016.
5. A. FRUMKIN, *Advances in Electrochemistry*, edited by P. DELAHAY, Interscience, New York, 1963, p. 287.
6 V. SOBOL, A. DMITRIEVA AND A. FRUMKIN, *Elektrokhimiya*, in press.

Received May 14th, 1966

A potentiometric end-point in coulometric titrations

A recent short paper[1] gave a potentiometric method for determining the end-point in a constant-current coulometric titration by plotting the potential of the working electrode *vs.* a reference electrode 10 sec after the interruption of the generating current at intervals during the electrolysis. This note seeks to explain—at least qualitatively— the essential theory of the method. The case when the working electrode is an anode is examined; an analogous discussion holds when the electrode is a cathode.

Consider the coulometric titration of red_1 by ox_2 electrogenerated from red_2. As i_{app}, the generating current, is greater than i_d, the limiting diffusion current of red_1, the potential of the working electrode will be determined by the ox_2/red_2 couple. When the current is interrupted, the potential of the electrode will decay to the zero-current potential of the system which will be determined by the ox_1/red_1 couple prior to the end-point, and the ox_2/red_2 couple after it—assuming both electrode reactions to be reversible. If the potential measurements are taken after sufficiently long decay times, and these readings are plotted against electrolysis time, a normal potentiometric titration curve will result.

The nature of the decay process was examined using the circuit described previously (*loc. cit.*) but using an oscilloscope to observe the potential between the working and reference electrodes. Examples of the type of decay curve obtained during the titration of iron(II) (red_1) by electrogenerated cerium(IV) (ox_2) after various electrolysis times are shown in Fig. 1. The decay is observed to consist of two parts—a plateau, the extent of which is much greater at low iron(II) concentrations than at high, followed by a rapid exponential drop.

The shape of these curves can be explained by assuming that on interrupting the current there is an amount, S, of ox_2 concentrated at the electrode and that there is also a concentration gradient of red_1 at the electrode. The time taken to attain equilibrium at the electrode will be governed by mass transfer of ox_2 from, and red_1 to, the electrode—assuming the reaction between ox_2 and red_1 to be instantaneous. When the bulk concentration of red_1 (C_{red_1}) is relatively high, S will be small as ox_2 will be used up virtually as fast as it is produced. The decay of the potential under these conditions will be determined only by the diffusion of red_1 through the Nernst diffusion layer (thickness, δx), and assuming a step function concentration of red_1, it can

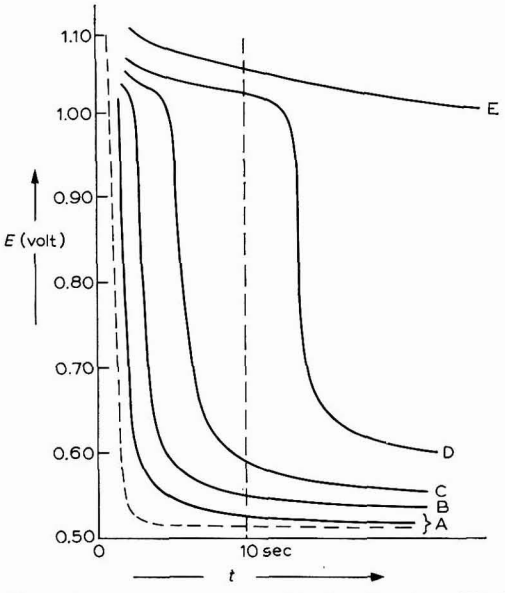

Fig. 1. Decay curves obtained in the titration of Fe(II) with Ce(IV) at 10-mA generating current. The theoretical end-point is after 7.25 min of electrolysis; t is the time in seconds after interruption of the current. Electrolysis time after which the decay was observed: (A), 1.00; (B), 5.00; (C), 7.00; (D), 7.20; (E), 7.40 min. The potential was measured *vs.* a calomel electrode. The broken curve is that calculated from eqn. (1) taking δx as 10^{-3} cm and D_1 as 10^{-5} cm²/sec at an iron(II) concn. corresponding to an electrolysis time of 1 min.

be shown (see Note*) that:

$$C_{\mathrm{red}_1}{}^0 = C_{\mathrm{red}_1} \operatorname{erfc} \frac{\delta x}{\sqrt{4D_1 t}} \tag{1}$$

where $C_{\mathrm{red}_1}{}^0$ = concentration of red$_1$ at the interface,
erfc = complement of the error function,
D_1 = diffusion coefficient of red$_1$,
t = decay time.

Substitution of values of the concentration of red$_1$ at the electrode calculated from (1) in the Nernst equation yields an exponential decay curve in agreement with the experimental results. The dotted line in fig. 1 shows the calculated results.

When the bulk concentration of red$_1$ is small, however, S will not be negligible and the concentration of ox$_2$ at the electrode will have to be considered. It can be shown also (see Note) that:

$$C_{\mathrm{ox}_2}^0 = S(\pi D_2 t)^{-\frac{1}{2}} \tag{2}$$

Note. Assuming semi-infinite linear diffusion, eqns. (1) and (2) are solutions of Fick's diffusion equations for the boundary conditions:

(1) Concn. of red$_1$ = C_{red_1}, $x < 0$, $t \geqslant 0$ (x measured towards electrode from face of diffusion layer)
Concn. of red$_1$ = 0, $x > 0$, $t = 0$, and assuming reflection at the electrode where $x = \delta x$;
(2) Amount of ox$_2$ at electrode at $t = 0$ is S (x' measured from the electrode)
Amount of ox$_2$ at $x' > 0$ at t = 0 is 0;

and are obtainable from standard texts, *e.g. Diffusion*, by JOST.

where $C_{ox_2}^0$ = concentration of ox_2 at the electrode, and D_2 = diffusion coefficient of ox_2. Combining eqns. (1) and (2):

$$C_{red_1}{}^0 = C_{red_1} \operatorname{erfc} \frac{\delta x}{\sqrt{4D_1 t}} - S(\pi D_2 t)^{-\frac{1}{2}} \tag{3}$$

It will be observed from eqn. (3) that the concentration of red_1 at the electrode will be zero until:

$$C_{red_1} \operatorname{erfc} \frac{\delta x}{\sqrt{4D_1 t}} > S(\pi D_2 t)^{-\frac{1}{2}} \tag{4}$$

The inequality (4) explains the plateau at low concentrations of red_1; S decreases as C_{red_1} increases. Since it is impractical to assess S for a stirred solution, this could not be verified by calculation. A report on further investigations on unstirred solutions is in the press[2].

In very dilute solutions of iron(II), *i.e.*, as the end-point was approached, the extent of the plateau corresponded to a time greater than 10 sec (Fig. 1)—this resulted in premature end-points being observed, and this is the probable explanation of the slightly low results reported in the previous communication (*loc. cit.*) using this end-point method. Table I gives a comparison of titrations using different decay times prior to the taking of potentiometric readings.

TABLE 1

COMPARISON OF THE RESULTS FOR THE TITRATION OF 4.35×10^{-5} EQUIVALENTS OF IRON(II) WITH ELECTROGENERATED CERIUM(IV) AT DIFFERENT DECAY TIMES

Working current approximately 10 mA.

Decay time (sec)	*Titration time (min) (Replicates)*	*Theoretical titration time*
10	7.16, 7.18, 7.18	7.25
30	7.23, 7.22, 7.23	7.25
60	7.24, 7.25, 7.25	7.25

From this table it is clear that better results may be obtained by using a 60-sec decay time as the end-point of the titration is approached.

Department of Pure and Applied Chemistry,
University of Strathclyde, Glasgow (Scotland)

W. A. ALEXANDER
D. J. BARCLAY

1 W. A. ALEXANDER, D. J. BARCLAY AND A. MCMILLAN, *Analyst*, 90 (1965) 504–506.
2 W. A. ALEXANDER AND D. J. BARCLAY, *J. Electroanal. Chem.*, 13 (1967) 137.

Received March 22nd, 1966

Propylene carbonate: a versatile solvent for electrochemistry and EPR

Propylene carbonate (4-methyldioxolone-2) has been employed widely as a solvent for various synthetic polymers and as a reaction medium. The majority of the common solvents are miscible in all proportions with propylene carbonate (PC) and it readily dissolves many organic compounds, and some inorganic salts. Its low vapor pressure, high dielectric constant (69.0 at 23°), relatively low toxicity and high chemical stability make it ideal as an ionizing solvent that can be handled with ease. These properties suggest its use as an electrochemical solvent, and upon further investigation one finds that it possesses marked advantages over the commonly used non-aqueous electrochemical solvents, *viz.* acetonitrile, N,N-dimethylformamide (DMF), and dimethylsulfoxide (DMSO). In addition to those properties listed previously, PC is not hygroscopic to any great extent and is non-corrosive. An excellent technical bulletin put out by Jefferson Chemical Company[1] covers a good deal of the known literature on the physical and chemical properties, previous applications and potential uses of this solvent. The use of propylene carbonate in electrochemistry has been limited to studies of conductivities[2,4–6] and some polarographic and impedance measurements[3,7]. It has not been previously employed as a solvent for EPR studies.

Experimental

Purification is a simple matter and subsequent decomposition is negligible. Distillation at reduced pressure[4] was carried out twice with collection of the middle 60%-fraction only. For most work, a single distillation would probably suffice. A distillation temperature of 120–130° was found to be quite satisfactory. Above 200° appreciable decomposition occurs[8], and traces of acids or bases will promote degradation to propylene oxide, propionaldehyde, allyl alcohol and carbon dioxide[1]. After distillation, the solvent was stored over molecular sieves in a nitrogen atmosphere.

The supporting electrolyte used, tetraethylammonium perchlorate (TEAP), was prepared from tetraethylammonium bromide and lithium perchlorate. The crude product was recrystallized seven times from water.

The instrumentation employed for cyclic voltammetry and chronopotentiometry has been described elsewhere[9,10] and the EPR spectra were obtained with a Varian V-4500, X-band spectrometer with 100-kc field modulation.

Results and discussion

The potential limits for practical voltammetry in PC are similar to those of acetonitrile. At platinum, one has a working range of +1.7 to −1.9 V (*vs.* SCE) and the cathodic limit at mercury (hanging drop electrode) extends to −2.5 V. The background current at platinum is exceptionally low (see Fig. 1). A relatively high solution resistance can be overcome by using a supporting electrolyte concentration of 0.25 *M*.

The primary advantage of PC as an electrochemical solvent is its high viscosity (1.67 centistokes at 38°). This means that natural convection should be greatly diminished relative to a solvent like acetonitrile. Table 1 shows a comparison of transition times for a well-behaved reversible one-electron oxidation, that of 5,10-dihydro-5,10-dimethylphenazine (4 m*M* in both cases), in both acetonitrile and PC.

The working electrode was a horizontally-oriented Beckman platinum button (No. 39273). It can be seen that $i\tau^{\frac{1}{2}}$ is constant (to within 2%) for PC out to transition times of 45–50 sec, while the $i\tau^{\frac{1}{2}}$ product begins a rapid increase in the range 10–13

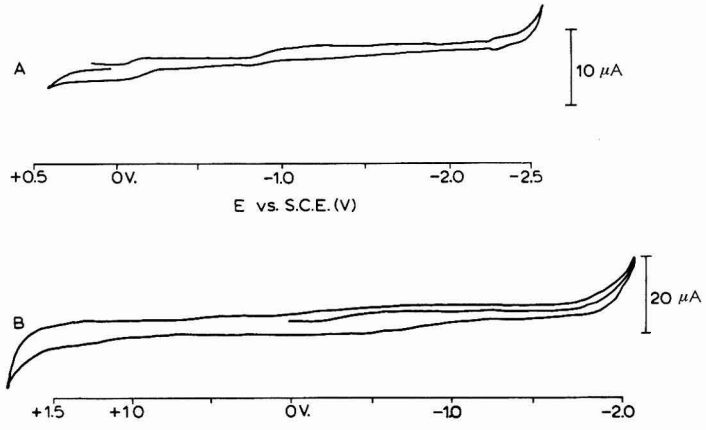

Fig. 1. Background scans showing potential limits in propylene carbonate. Potentials are in volts *vs.* aq. SCE. (A), Mercury hanging drop electrode; (B), platinum button electrode. Scan rate, 7.8 V/min; electrode area, 0.22 cm^2.

TABLE 1

COMPARISON OF CONSTANCY OF $i\tau^{\frac{1}{2}}$ IN ACETONITRILE AND PROPYLENE CARBONATE

Acetonitrile			*Propylene carbonate*		
i (μA)	*τ (sec)*	$i\tau^{\frac{1}{2}}$	*i (μA)*	*τ (sec)*	$i\tau^{\frac{1}{2}}$
168	4.34	350	80.5	2.48	127
142	6.18	353	74.1	2.85	127
111	9.94	350	70.8	3.22	127
107	10.7	350	63.5	4.02	127
98.9	12.8	354	56.1	5.21	128
95.7	13.7	354	49.5	6.63	127
90.3	15.7	357	42.4	8.96	127
87.7	16.9	360	36.7	12.1	128
83.0	18.9	361	33.0	14.8	127
80.8	20.0	362	30.7	17.4	128
76.8	22.8	367	27.2	22.2	128
72.6	25.6	368	23.8	29.4	128
67.7	30.4	373	21.2	37.2	129
63.6	36.6	385	19.0	46.6	130
62.3	38.2	386	17.2	57.8	130
61.1	40.8	391			

sec in acetonitrile. Since there are no chemical complications involved, an increase in the $i\tau^{\frac{1}{2}}$ product signals the onset of natural convection. This considerably extends the working range for such techniques as reverse-current chronopotentiometry and cyclic chronopotentiometry. This extended time interval is also valuable for studying variations of $i\tau^{\frac{1}{2}}$ as a function of increasing current density to detect kinetic processes associated with electrochemical reactions. This decrease in convection is also significant

in the recording of $it^{\frac{1}{2}}$ decay curves and for slow cyclic and linear-scan voltammetry.

As a solvent for EPR, PC possesses marked advantages, especially for *in situ* generations of organic radicals. Because of its high dielectric constant and excellent solvating properties, in some cases it is a better solvent for cation radicals than acetonitrile. Some cation radicals (*e.g.*, benzidines) that precipitate out in acetonitrile and show poorly defined spectra are soluble in PC. An appreciable increase in resolution is realized. Since convection in PC is so limited, *in situ* generations in the thin portion of an EPR cell are practically exhaustive, *i.e.*, homogeneous exchange (parent-radical electron transfer) is minimized. On the other hand, one would expect PC to retard tumbling in solution and hence increase the probability of anisotropic broadening. So far this has not been observed. The increase in resolution one obtains *in situ* in going from acetonitrile to PC is quite marked in some cases (see Fig. 2).

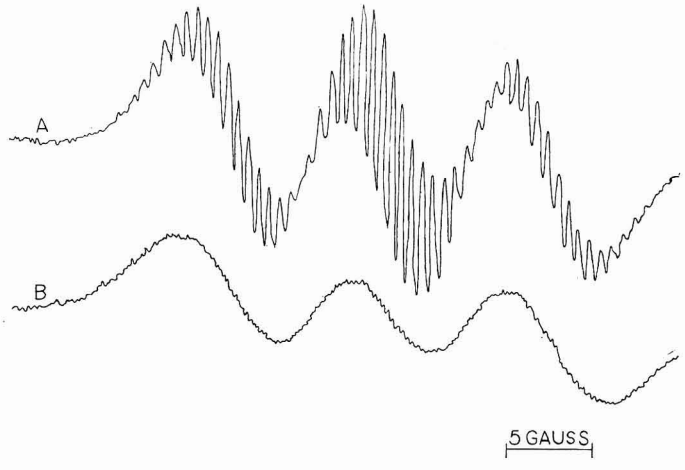

Fig. 2. EPR spectra of $5 \cdot 10^{-4}$ *M* *p*-trianisylamine, generated *in situ* with a platinum-gauze electrode. (A), Spectrum in propylene carbonate; (B), spectrum in acetonitrile.

A similar improvement was noted for anion radicals. For the compounds studied in this laboratory, radical stability appears to be comparable to that in acetonitrile. For the standard EPR technique of external electrochemical generation of radical species[11], PC was found to be an adequate solvent.

Acknowledgements

The support of the General Research Fund of the University of Kansas is gratefully acknowledged.

Department of Chemistry,
University of Kansas,
Lawrence, Kans. 66045 (U.S.A.)

ROBERT F. NELSON
RALPH N. ADAMS

1 *Propylene Carbonate*, technical bulletin, Jefferson Chemical Company, P. O. Box 303, Houston 1, Texas (USA).
2 R. E. MEREDITH AND C. W. TOBIAS, *J. Electrochem. Soc.*, 108 (1961) 286.

3 L. S. MARCOUX, K. B. PRATER, B. G. PRATER AND R. N. ADAMS, *Anal. Chem.*, 37 (1965) 1446.
4 P. L. KRONICK AND R. M. FUOSS, *J. Am. Chem. Soc.*, 77 (1955) 6114.
5 L. Y. CHOW AND R. M. FUOSS, *J. Am. Chem. Soc.*, 80 (1958) 1095.
6 R. M. FUOSS AND E. HIRSCH, *ibid.*, 82 (1960) 1013.
7 R. PARSONS, personal communication.
8 C. E. LEVIN AND A. L. SHAPIRO, *Khim. Prom.*, 41 (1965) 264.
9 J. R. ALDEN, J. Q. CHAMBERS AND R. N. ADAMS, *J. Electroanal. Chem.*, 5 (1963) 152.
10 D. HAWLEY AND R. N. ADAMS, *ibid.*, 8 (1964) 163.
11 R. N. ADAMS, *ibid.*, 8 (1964) 151.

Received February 4th, 1966

BOOK REVIEWS

Organic Polarographic Analysis by P. ZUMAN, Pergamon Press, Oxford, London, New York and Paris, 1964, x+313 pages, 50s.

This book has been written specifically to call the attention of organic chemists to the potentialities available to them in polarographic techniques. Nevertheless, the first three chapters would form an excellent first introduction for anyone wishing to learn how to use a polarograph. The phenomena are clearly and simply described and the practical details are fully explained. The following six chapters are specifically organic, illustrating the wide variety of associated techniques, and there are, in chapter VIII, a number of practical applications which may be useful in themselves or as models for the development of new applications. This part of the book is well filled with detailed practical instructions which should convince the prospective organic polarographer of the real usefulness of the technique. The book concludes with two chapters on physical organic chemistry, one on the measurement of rates and equilibria, and one on the relation to structure of organic molecules. The latter is the region where much recent progress has been made and Dr. ZUMAN himself is one of those who has made great contributions here. Consequently it is a little disappointing that this chapter has been kept so short. It is clear that this is to avoid unbalancing the book and also because the material is readily available elsewhere. It might also be regretted that no electrodes other than mercury are discussed and that the approach concentrates firmly on classical polarography, but again this is undoubtedly justified at present; these techniques are those most likely to be of practical use to the organic chemist without excessive development problems. Finally, it must be noted that the book concludes with a useful literature survey and an excellent index.

ROGER PARSONS, University of Bristol

Thermodynamics of Irreversible Processes, by PIERRE VAN RYSSELBERGHE, Hermann and Blaisdell Publishing Company, Paris and New York, 1963, 165 pages, $7.50.

Despite its title, nearly one third of this monograph is devoted to an exposition of classical thermostatics, admittedly orientated towards the discussion of irreversible processes, but touching only marginally on the topics that are usually regarded as forming the domain of irreversible thermodynamics. I do not intend this remark as an adverse criticism; on the contrary, I think no one will make much progress in irreversible thermodynamics without a very clear understanding of the basic ideas of thermostatics, which is not guaranteed by an ability to manipulate the van 't Hoff isochore and the like. As the author points out, the monograph follows the lines that De Donder's school have developed; in particular, *affinity* and *degree of advancement* figure largely. But at the same time, the treatment does not differ too widely from those developed by other schools and should not present any difficulty to the reader unfamiliar with De Donder's methods.

The book is intended as an introduction to the subject, and the discussion of various classes of irreversible processes is necessarily brief. But it ranges quite widely and will give the reader an insight into the applications of irreversible thermodynamics in a number of different fields. It should prove useful, although I am sorry to see that Professor VAN RYSSELBERGHE has not succeeded in developing a really simple, neat and tidy symbolism. Most, if not all, writers on this subject are open to the same criticism; perhaps the problem is insoluble.

On three minor points the book may be misleading. The first arises in the introduction of temperature and entropy. We find (p. 19) a mention of "the empirical temperature T", and a little later (p. 22) dQ/T is an exact differential; no mention of the Kelvin scale. The second relates to thermodynamic forces and Onsager reciprocity; it is not made clear (*e.g.*, p. 71) that the forces must be correctly defined if the reciprocity relations are to hold in their usual form. Finally, in the treatment of diffusion (p. 128), the solvent is assumed ... "to have a uniform chemical potential". In general this assumption is not true in diffusion processes, nor is it required in discussing them.

J. N. AGAR, University of Cambridge

VOL. 13 NO. 1/2 JOURNAL OF ELECTROANALYTICAL CHEMISTRY AND INTERFACIAL ELECTROCHEMISTRY JANUARY 1967

CONTENTS

continued on the next page

PRINTED IN THE NETHERLANDS